Discovery and characterization of Pun1p, a putative component of the yeast fertilization synapse

Dissertation

zur Erlangung des akademischen Grades des Doktors der Naturwissenschaft

(Dr. rer. nat.)

Vorgelegt der Fakultät Chemie und Chemische Biologie der Technischen Universität Dortmund

Angefertigt am Max-Planck-Institut für molekulare Physiologie in Dortmund

Vorgelegt von

Sheila Kemunto Mainye

1st referee: Prof. Dr. Stefan Raunser

Department of Structural Biochemistry, Max- Planck- Institute of Molecular Physiology, Dortmund;

Faculty of Chemistry and Chemical Biology, Technical University Dortmund.

2nd referee: Prof. Dr. Roland Winter

Department of Physical Chemistry,

Faculty of Chemistry and Chemical Biology, Technical University Dortmund.

Date of submission: 02.06.2021

Formal declaration

The work described in this dissertation was carried out between March 2017 and May 2021 under the guidance of Dr. Matias Hernández at the Max-Planck-Institute of Molecular Physiology, Dortmund.

I hereby declare that I carried out the work independently and did not use any aid, other than the ones mentioned.

Eidesstattliche Erklärung

Die vorliegende Arbeit wurde in der Zeit von März 2017 bis Mai 2021 am Max-Planck-Institut für Molekulare Physiologie in Dortmund unter der Anleitung von Dr. Matias Hernández durchgeführt.

Hiermit erkläre ich, dass ich die vorliegende Arbeit selbstständig und nur mit den angegebenen Hilfsmitteln angefertigt habe.

Dedication

I dedicate this work to my late grandparents.

Table of Contents

List of abbreviations

APS	ammonium persulfate
Arg	arginine
ATP	Adenosine- 5'- triphosphate
bp	base pairs
Ca^{2+}	Calcium ions
CHK	check
Cys	cysteine
DH	Dbl-homology
DMSO	dimethyl sulfoxide
DNA	deoxyribonucleic acid
dNTP	deoxynucleoside triphosphate
DTT	dithiothreitol
E. coli	*Escherichia coli*
EDTA	ethylenediaminetetraacetate
EGTA	Ethylene-bis(oxyethylenenitrilo)tetraacetic acid
ER	endoplasmic reticulum
et al	et alii
G	Glycine
GDP	guanosine diphosphate
GEF	guanine nucleotide exchange factor
GFP	green fluorescent protein
GTP	gaunine triphosphate
HEK	Human embryonic kidney
HEPES	2-[4-(2-hydroxyethyl) piperazine-1-yl] ethane sulfonic acid
Hgr	HAP2-GCS1 related
HIS	histidine
HOG	high osmolarity glycerol
HRP	horseradish peroxidase
kb	kilo base pairs
KDa	kilo daltons
L	Leucine
LEU	leucine
Lys	lysine
M	molar
MAPK	mitogen activated protein kinase
Met	methionine
min	minutes
mM	milli molar
mNG	mNeonGreen
MW	molecular weight
PBS	phosphate buffered saline
PCR	polymerase chain reaction

PH	pleckstrin homology
Phe	phenyl alanine
RT	room temperature
SD	Standard deviation
sec	seconds
TBS	tris buffered saline
TBST	tris buffered saline-tween
TEMED	tetramethylethylenediamene
Tris	tris(hydroxymethyl)-aminomethane
Trolox	(S)-6-Hydroxy-2,5,7,8-tetramethylchromane-2-carboxylic acid
URA	uracil
W	tryptophan
WT	wild type

1 ABSTRACT

1.1 Abstract

Cell-cell fusion is a fundamental process in sexual reproduction and development but the mechanisms mediating and regulating this process are only now beginning to be uncovered. Despite recent progress in identifying key players in the plant and protist kingdoms, large gaps remain in other Eukaryotic lineages, including fungi. The cell fusion in the mating of the yeast *Saccharomyces cerevisiae* therefore presents itself as an ideal system to understand the molecular mechanisms underlying cell fusion in fungi. In an effort to identify novel components of the yeast fusion machinery and associated regulators, this thesis reports on the discovery and characterization of a membrane protein that negatively regulates the fusion of the plasma membrane (PM) which resembles tight junction claudins found in mammals.

A proteomics analysis of pheromone-regulated membrane proteins revealed that components of the MCC/eisosomes, a specialized furrow-like, membrane domain important for PM organization, were preferentially down-regulated during the pheromone response. An exception was Pun1p, a four-pass membrane-spanning protein with a conserved claudin motif, which was up-regulated in response to pheromone and was targeted to the transient junction established between two mating cells. Whereas deletion of *PUN1* and its paralogs presented mild fusion defects, its function was distinctly revealed in a sensitized *prm1Δ* null background, where high-copy expression of *PUN1* resulted in a partial inhibition of cell fusion. Further examination of the Pun1p inhibition activity in *prm1Δ* mutants revealed that *PUN1* expression had no effect on lysis or formation of cytoplasmic bubbles, two *prm1Δ* phenotypes that occur after the cell wall (CW) has been remodeled. Instead, *PUN1* expression inhibited fusion by enhancing the formation of a flat PM interface between two cells. However, contrary to previous reports, further analysis revealed that in a proportion of these mating pairs, the flat PM interface was structurally stabilized without any underlying CW material, suggesting the arrest occurred at a stage after CW remodeling via an unknown mechanism. Notably, the Pun1p inhibition activity was dosage and concentration-dependent and was enhanced with increasing concentration of Pun1p molecules across the mating junction, indicating additive functional *trans*- interactions. Analysis of the mechanistic basis of Pun1p activity revealed a claudin-like activity as a Pun1p mutant version of the conserved claudin motif lost its inhibitory activity. Additionally, the mutant protein exhibited localization defects and was modified at the monomeric level. Together, these results suggest that Pun1p is expressed in mating conditions and localized at the mating junction where it interacts with other unknown proteins to promote the formation of a PM junction-like structure similar to mammalian claudin-mediated tight junctions. The PM junction-like structure would function as a fusion fidelity checkpoint that negatively regulates PM fusion in the event of a compromised fusion machinery.

Finally, the identification of Pun1p as a novel component of the fusion machinery prompted further characterization of the mating junction by employing a Horseradish Peroxidase (HRP)-based proximity labeling approach. Using a HRP-Fus1p recombinant protein as a proof of principle, specific HRP-mediated labeling was observed at the shmoo tip of polarized cells, consistent with the pheromone-dependent localization of Fus1p. Although the ultimate objective of characterizing the labelled proteins was not plausible during the course of this thesis, these initial findings demonstrate the feasibility of this approach in yeast studies and its applicability in elucidating the molecular architecture of other similar junctions, a structure which we here refer to as a fertilization synapse.

1.2 Zusammenfassung

Die Zell-Zell-Fusion ist einer der grundlegenden Prozesse der sexuellen Reproduktion und der Entwicklung von Organismen, doch die verantwortlichen molekularen Mechanismen und deren Regulation sind bisher nur unzureichend erforscht. Während viele der wichtigsten Faktoren bei Pflanzen und Protisten bereits identifiziert wurden, liegt bei anderen Eukaryoten wie Pilzen noch Vieles im Dunkeln. Die Zellfusion während der Paarung der Hefe *Saccharomyces cerevisiae* stellt ein ideales System dar, um die allgemeinen molekularen Grundlagen der Zellfusion in Pilzen zu untersuchen. Im Zuge der Identifizierung neuer Komponenten der Fusions-Maschinerie und der mit ihr assoziierten Faktoren charakterisiere ich in dieser Dissertation ein Membranprotein das mit Claudinen in Tight Junctions von Säugern ist und die Fusion der Plasmamembran (PM) negativ beeinflusst.

Eine Proteomik-Analyse von Pheromon-regulierten Membranproteinen zeigte, dass Bestandteile des MCC/Eisosoms, eines spezialisierten, an eine Furche erinnernden und für die Organisation der Plasmamembran wichtigen Membranbereichs, zum Großteil durch Pheromone herunterreguliert werden. Eine Ausnahme davon war Pun1p, ein integrales Membranprotein mit vier Transmembransegmenten und einem konservierten Claudin-Motiv, welches durch Pheromone hochreguliert und zur vorrübergehend ausgebildeten Kontaktstelle zwischen zwei sich paarenden Zellen lokalisiert wurde. Während die Deletion von *PUN1* und seiner Paraloge zu schwachen Fusionsdefekten führte, wurde seine Funktion in einem sensibilisierten *prm1Δ* null Hintergrund offensichtlich, wo eine Überexpression von *PUN1* zu einer teilweisen Hemmung der Fusion führte. Eine tiefere Untersuchung der inhibitorischen Aktivität von Pun1p in *prm1Δ*-Mutanten zeigte, dass die Expression von *PUN1* die Lyse oder die Ausbildung von zytoplasmatischen Ausstülpungen nicht beeinflusst, welche beides *prm1Δ*-Phänotypen sind die auftreten nachdem die Zellwand (ZW) umgeformt wurde. Stattdessen inhibierte die Expression von *PUN1*, indem die Ausbildung einer flachen PM-Grenzfläche zwischen beiden Zellen verstärkt wurde. Allerdings ergab eine weitergehende Untersuchung, im Widerspruch zu vorherigen Berichten, dass die flache PM-Grenzfläche bei einem Teil der sich kreuzenden Zellpaare strukturell ohne Mitwirken von ZW-Material stabilisiert wurde. Dies deutet darauf hin, dass der Arrest erst nach der Umformung der ZW durch unbekannte Mechanismen ausgelöst wurde. Interessanterweise war die Inhibition durch Pun1p abhängig von der Dosis und Konzentration, und wurde durch ansteigende Konzentration von Pun1p über die Paarungs-Kontaktfläche hinweg verstärkt, was auf additive und funktionale *trans*-Wechselwirkungen hindeutet. Eine mechanistische Analyse der Aktivität von Pun1p ergab, dass das Protein ähnlich der Claudine wirkt da die Mutation des Claudin-Motivs den inhibitorischen Effekt verhindert. Zusätzlich war das mutierte Protein falsch lokalisiert und vermutlich auch nicht korrekt posttranslational modifiziert. Insgesamt deuten diese Ergebnisse darauf hin, dass Pun1p unter Paarungs-Bedingungen exprimiert und an den Paarungs-Kontaktflächen lokalisiert ist, wo es mit anderen bislang unbekannten Proteinen zusammen die Ausbildung einer PM-Kontaktflächen-ähnlichen Struktur verursacht die den Claudin-mediierten Tight Junctions in Säugern ähneln. Diese PM-Kontaktflächen-ähnliche Struktur würde als Kontrollpunkt für die korrekte Fusion dienen und die PM-Fusion verhindern falls die Fusions-Maschinerie kompromittiert ist.

Schließlich führte die Identifikation von Pun1p als Bestandteil der Fusionsmaschinerie auch zu einer tieferen Charakterisierung der Paarungs-Kontaktfläche durch eine Meerrettichperoxidase (HRP)-basierte Nähenbestimmung. Als Machbarkeitsbeweis konnte im Fall eines rekombinanten HRP-Fus1-Proteins eine spezifische HRP-verursachte Markierung in der Shmoo-Aubsuchtung beobachtet werden, was sich mit der Pheromon-abhängigen Lokalisation von Fus1p deckt. Und obwohl das abschließende Ziel, die Charakterisierung der markierten Proteine, im Rahmen dieser Arbeit nicht erreicht werden konnte, zeigen diese vorläufigen Ergebnisse die Durchführbarkeit des Ansatzes in Hefe-Studien und seine Anwendbarkeit zur Aufklärung der molekularen Architektur von anderen ähnlichen Verbindungen, einer Struktur die als Befruchtungs-Synapse bezeichnet wird.

2 Introduction

2.1 Cell-cell fusion: a ubiquitous process

Cell-cell fusion is a fundamental biological process that occurs throughout eukaryotic development. Gamete fusion during fertilization defines the onset of life while fusion of somatic cells such as myoblasts, trophoblasts and macrophages facilitates the formation of muscle fibers, placenta syncytia and osteoclasts, respectively (reviewed by [1], [2], [3], [4]). Cell fusion events also occur during viral infections and intracellular trafficking between organelles ([5], [6]). The fusion of two or more cells is a multi-step process that involves cell-cell recognition and adhesion, cytoskeletal rearrangements and removal of the intervening material or extracellular matrix such as cell wall or protoplast to allow close plasma membranes (PMs) apposition. Once the PMs appose, activation of the fusogenic machinery mediates PM fusion and lipid mixing resulting in fusion pore formation and cytoplasmic content mixing upon fusion pore expansion ([3], [7]).

Notably, the rate-limiting step of all fusion events is the merging of two PMs. Preceding membrane merger, adhesion molecules closely appose the fusing membranes to an atomic distance of about 20 nm. As the fusing membranes approach a distance of below 10nm, high energy barriers including: (i) high membrane repulsive 'hydration force' and expulsion of the water molecules that exist between the apposed membranes, (ii) displacement of membrane proteins towards the periphery, (iii) membrane deformations and lipid bilayer rearrangements, must be surmounted in order for the membranes to fuse ([3], [8], [9]). Consequently, membrane merger does not occur spontaneously but instead, specialized proteins known as fusogens lower these high energy barriers to metastable transition states that favor fusion ([5], [6], [10]). Interestingly, apart from the extensively studied virus-cell and intracellular vesicle fusion events, very few *bona fide* fusogens have been identified and characterized. Importantly, a molecular understanding of gamete fusion in mammals and fungi and the fusogens that mediate this fundamental process remain elusive. Additionally, the regulatory mechanisms that prevent unwanted cellular fusion are not well defined.

2.1.1 Plasma membranes fuse via a hemifusion stalk intermediate formation

As mentioned, the merging of two membranes is the defining step of all fusion events. PM fusion is generally proposed to occur via two mechanisms: (i) direct PM fusion through the formation of a proteinaceous fusion pore or, (ii) fusion through a hemifusion intermediate ([11], [12]). The highly studied membrane fusion events of viral infections and intracellular vesicular trafficking have led to the understanding that PM fusion mainly occurs via a hemifusion intermediate ([12], [13], [14], [15], [16], [17]). Following close membrane apposition and destabilization by the activity of fusogens, apposed outer leaflets of the bilayers merge while the distal inner non-contacting leaflets remain separate, forming a fusion stalk (**Figure 1**). Subsequent lipid mixing and expansion of the fusion stalk results in formation of an intermediate structure called the hemifusion diaphragm (HD). The HD minimizes the area of membrane apposition and results in a corresponding decrease in the repulsive forces. Finally, fusion of the inner leaflets results in formation of a fusion pore lined by the fused lipid bilayers ([12], [14], [16], [17], [18]). Once the fusion pore is formed, high protein concentrations at the fusion zone mediate fusion pore expansion ([12]). Consistently, low protein concentrations due to proteolysis or protein inactivation results in dissociation of the hemifusion intermediate ([13], [17], [19]).

For PM fusion to occur, the membrane lipid composition and the respective lipid molecular shapes are important determinants of the bilayers' propensity to bend and fuse ([18]). Lipids such as phosphatidylcholine (PC) that contain equal polar heads and hydrophobic tails adopt a cylindrical shape. As a result, they tend to form flat to slightly negative curvature monolayers upon assembly. On the other hand, lipids such as phosphatidylethanolamine (PE), oleic acid (OA) and diacylglycerol (DAG) that contain larger hydrophobic tails when compared to their polar head groups adopt a cone-like shape upon association. Consequently, they form negative curvatures that splatter in the direction of the hydrophobic tails, a phenomenon that favors membrane bending and hemifusion intermediate formation ([12], [16], [18]). On the contrary, lysophosphatidylcholine (LPC) and polyphosphoinositides are characterized by large polar heads and small hydrophobic tails and are often termed as inverted cones. These tend to spontaneously form positive curvatures upon association, a phenomenon that favors membrane bending while inhibiting hemifusion stalk formation ([14], [20], [21]). Intriguingly, LPC favors pore formation when present on the distal

leaflets of fusing membranes, suggesting that positive curvature is critical during pore formation particularly at the edges (**Figure 1**) ([12], [21], [22]).

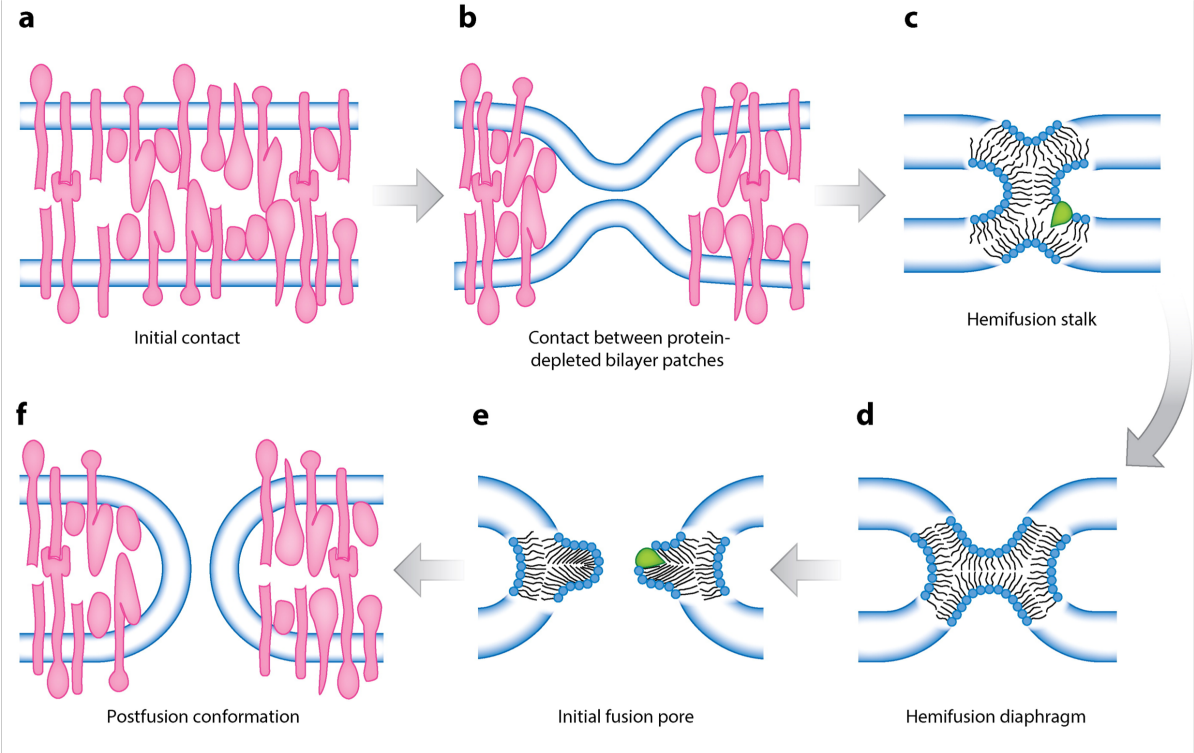

Figure 1: PM fusion proceeds via a hemifusion stalk intermediate formation. (**a**) PM fusion begins when the fusing membranes make the initial contact. The membranes are composed of lipid bilayers (blue lines depict lipid heads) as well as integral and peripheral membrane proteins (pink shapes). (**b**) Fusogens mediate a closer PM apposition and displace membrane proteins towards the periphery. (**c**) Fusion of outer bilayer leaflets results in formation of a hemifusion stalk intermediate. (**d**) As the hemifusion stalk expands, it creates a hemifusion diaphragm (HD) that minimizes the area of PM apposition and lowers the bilayer repulsive force. (**e**) Fusion of the distal leaflets leads to formation of an initial fusion pore, (**f**) that expands allowing cytoplasmic mixing and completion of the fusion process. The molecular shape of lipids determines the propensity of bilayer deformation. Lipids such as lysophosphatidylcholine (LPC) spontaneously form inverted cone-shapes (green) and do not favor hemifusion stalk intermediate formation. When present in the distal leaflet, LPC fits the fusion pore positive curvature and promotes pore opening. Adapted from: ([23]).

Therefore, with the existing understanding of PM fusion, it is generally acceptable that a *bona fide* fusogenic machinery, whether a single protein or a protein complex, mediates fusion by dehydrating the bilayer polar head groups, promoting hemifusion intermediate formation and pore formation and expansion ([3]). Indeed, Influenza virus Hemagglutinin HA2 subunit and the SNARE proteins are the two extensively characterized *bona fide* fusogens ([5], [6]). Recent advances have led to the identification of additional fusogens, a few of which have been discussed below. These include the developmental fusogens EFF-1 and AFF-1 that mediate fusion in *Caenoharbditis elegans*, Myomerger and Myomixer that facilitate myoblast fusion and the Syncytin-1 protein involved in placenta trophoblast fusion ([10], [24], [25], [26], [27], [28]). Hitherto, HAP2/GCS1 is the only known fusogen and mediates gamete fusion in plants, algae and protists ([29]). However, the absence of HAP2/GCS1 in vertebrates and fungi suggests the presence of an alternative gamete fusogenic machinery in these organisms. Whether these machineries are composed of single or multiple proteins is currently unknown. Furthermore, it remains elusive whether the molecular mechanisms of fusion are similar across the different organisms.

2.2 *Bona fide* fusogens

2.2.1 Virus-cell fusion: Influenza Hemagglutinin (HA)

The fusion of enveloped viruses with host target cells is one of the highly characterized membrane fusion events. Enveloped viruses such as Influenza, HIV and Ebola infect host cells via surface glycoproteins expressed on the viral envelopes. Occasionally, these surface glycoproteins also mediate cell fusion of infected cells with non-infected cells resulting in viral propagation and virulence ([30], [31]). During membrane fusion, viral glycoproteins perform the fusogenic activity of bringing the membranes into close apposition and overcoming the energy barriers associated with membrane deformation, hemifusion stalk formation and fusion pore formation and expansion ([32]). While some viruses such as retroviruses require only one glycoprotein, others such as the paramyxoviruses and herpesviruses require multiple glycoproteins, and the concerted efforts facilitate membrane fusion ([30]). In addition, various viruses require different fusion triggers often involving ligand binding such as low pH, host cell receptor binding, presence of a co-receptor on the host cell surface or a combination of both. However, in viruses such as HIV, Hepatitis or the Sendai virus, fusion can occur on the cell surface and at neutral pH ([5], [30], [32]). Regardless of the trigger mechanism, the fusogenic glycoproteins undergo a conformational change from the native prefusion to a fusion-competent state, a process commonly referred to as 'priming'.

The fusion of the Influenza virus with host target cells is one that is best understood mechanistically. It involves a trimeric-hairpin, spring-loaded model of fusion, although compelling evidence suggests that most viruses generally adopt a similar model ([33], [34], [35], [36], [37]). Infection of target cells by the Influenza virus is facilitated by the Hemagglutinin (HA) glycoprotein, of which about 300-500 225kDa trimeric HA spike proteins exist on the viral cell surface ([38], [39]). HA is secreted as a precursor protein HA0 which undergoes a post-translational cleavage in the trans-Golgi network (TGN) or in the endocytic vesicles to yield two subunits, HA1 and HA2 ([40], [41], [42], [43]). The HA1 contains a sialic-acid binding domain linked via a disulfide bond to the three-chain alpha helical coiled coil of the HA2 subunit (**Figure 2A**). The three-chains of the alpha helical coiled coil are spread apart from the three-fold axis, generating a pocket in which the N-terminal hydrophobic fusion peptide is inserted ([40], [43], [44]). Upon receptor-binding via HA1 to the sialic acid moiety on target cell glycoproteins, the virus is taken up into endosomes where endosomal maturation results in a pH shift to an acidic pH ([42], [45]). The acidic pH triggers an irreversible conformational change on HA1 head resulting in exposure of the HA2 N-terminal hydrophobic fusion peptide and subsequent activation of membrane fusion ([36], [46], [47], [48]).

The hydrophobic fusion peptide, about 20-25 residues and connected to the helix via a loop, then assembles into a metastable, homo-trimeric pre-hairpin intermediate that inserts into the target membrane (**Figure 2A**) ([5], [49]). The folding back of the inserted trimeric pre-hairpin into an energetically stable hairpin structure pulls the target membrane towards the viral envelope, resulting in the close apposition of the two membranes. The collapse of the pre-hairpin and the continuous anchoring of the HA2 C-terminus on the viral membrane results in distortion of the two membranes, thus lowering the energy barrier ([37], [42], [50]). However, recent cryotomography structural studies suggest that the target membrane is highly deformed as opposed to viral membrane, generating a dimpled, open-mouthed lipid funnel with the viral membrane at the base ([51], [52]). Consistently, the phosphatidylcholine (PC) curvature of the distal endosomal membrane leaflet, and the dimpled lipid funnel of the target membrane may insert into the viral membrane, favoring the merging of the outer leaflets of the bilayers to form a hemifusion intermediate stalk (**Figure 2A**) ([21], [52], [53], [54]). Further endosome maturation results in weakening of the protective viral matrix layer and opening of the hemifusion intermediate stalk to form a fusion pore. As HA2 undergoes further refolding, it stabilizes the open pore state, allowing the fusion pore to dilate and permit viral content release ([51], [55], [56]).

Indeed, the general fold and structure of the viral glycoproteins in the pre and post-fusion conformations has led to the classification of viral fusogens into three main classes namely: class I fusogens characterized by an alpha-helix fold, class II fusogens containing a β-sheet fold, and class III fusogens that contain a mix of both class I and class II ([40]). Finally, the ability of HA to induce syncytia formation in heterologous cells confirms that it is a *bona fide* fusogen ([57], [58]).

2.2.2 Intracellular vesicle trafficking: SNARE proteins

Eukaryotic exocytosis events such as neurotransmitter release at the neuronal synapses, and the yeast secretory and vacuolar pathways involve the fusion of intracellular and extracellular membranes ([59], [60], [61], [62]). The fusion of exocytic vesicles with target membranes is mediated by several proteins including members of the soluble N-ethylmaleimide-sensitive factor (SNF) attachment protein receptor (SNARE) protein family, Rab proteins as well as the Sec1/Munc-18 (SM) related proteins ([61], [63], [64], [65]). The highly characterized SNARE proteins include the synaptic vesicle-associated Synaptobrevins/VAMPs (v-SNAREs or R-SNAREs) and the target membrane-associated Syntaxin 1 and Synaptosome-associated protein of 25kDa (SNAP-25) (t-SNAREs or Q-SNAREs) involved in synaptic fusion events ([6], [61], [66]). In yeast intracellular trafficking, the v-SNARE homologs include Snc1 and Snc2 proteins, while the heterodimer composed of Sec1 and Sso1/2 proteins represents the t-SNARE homolog ([67], [68]). The Syntaxin and Synaptobrevin families are characterized by the presence of a single SNARE motif flanked by a variable N-terminus and a C-terminal transmembrane region necessary for membrane anchorage as well as mediating protein-protein interactions. The SNARE motif, consisting of approximately 60 residues, mediates the assembly of SNARE proteins into SNARE complexes necessary in fusion ([61], [69], [70]). On the other hand, the t-SNARE SNAP-25 consists of two SNARE motifs separated by a cysteine-rich sequence and lacks the transmembrane regions. The post-translational attachment of palmitoyl lipids to the cysteine residues facilitates its anchorage to the membranes ([71], [72]).

During neuronal vesicular transport and membrane tethering via the Rab proteins, the three SNARE proteins undergo conformational changes and assemble in *trans* in a 1:1:1 stoichiometry ratio via their SNARE motifs, forming highly stable ternary helical core complex ([64], [65], [73], [74], [75], [76]). The four SNARE motifs, each from Synaptobrevin 2 and Syntaxin 1a and two from SNAP-25, assemble into a four-helical bundle about 12nm long, with the individual helices twisted parallel to each other ([65], [75], [77], [78]). The N- to C-terminal zippering assembly exerts a pulling force on the interacting membranes resulting in close membrane apposition to ~8 nm distance (**Figure 2B**) ([79], [80]). Additionally, their transmembrane domains assemble into homotypic and heterotypic oligomeric complexes, further contributing to the complex stability ([77], [81]). The SNARE assembly results in the formation of a hemifusion stalk intermediate. Indeed, mutations in the SNARE complex result in a block in fusion with the membranes arresting at defined hemifusion intermediate stages ([17], [82], [83]).

Therefore, similarly to the viral fusogens, the SNAREs mediate fusion by undergoing the initial steps of membrane tethering and activation of the fusogenic machinery. Conformational changes and foldback of the fusogenic machinery exert a pulling force on the membranes resulting in close membrane apposition and subsequent hemifusion intermediate formation. Notably, the two classes of fusogens do not require external energy to drive fusion. Instead, the respective protein folding generates sufficient energy to closely appose the two membranes and drive fusion ([8]). However, contrary to the irreversible viral membrane fusion mechanism, the SNARE core complexes can undergo dissociation in an ATP hydrolysis-dependent manner to allow recycling of the SNARE proteins ([62]). Consequently, the downstream events of distal membrane leaflets mixing, and pore formation are suggested to proceed via unknown proteins. Presence of transient and reversible fusion pores that can undergo numerous cycles of opening and closing has been reported in exocytosis events, suggesting the existence of fusion pore intermediates ([84], [85]). Additionally, intracellular trafficking requires the presence of SNAREs in both membranes (t-SNAREs and v-SNARES) as opposed to viral fusion that is unilaterally mediated by the viral glycoproteins (**Figure 2B**). Nonetheless, both the SNAREs and the viral fusogens are sufficient to induce fusion in vitro, suggesting that they are *bona fide* fusogens ([86]).

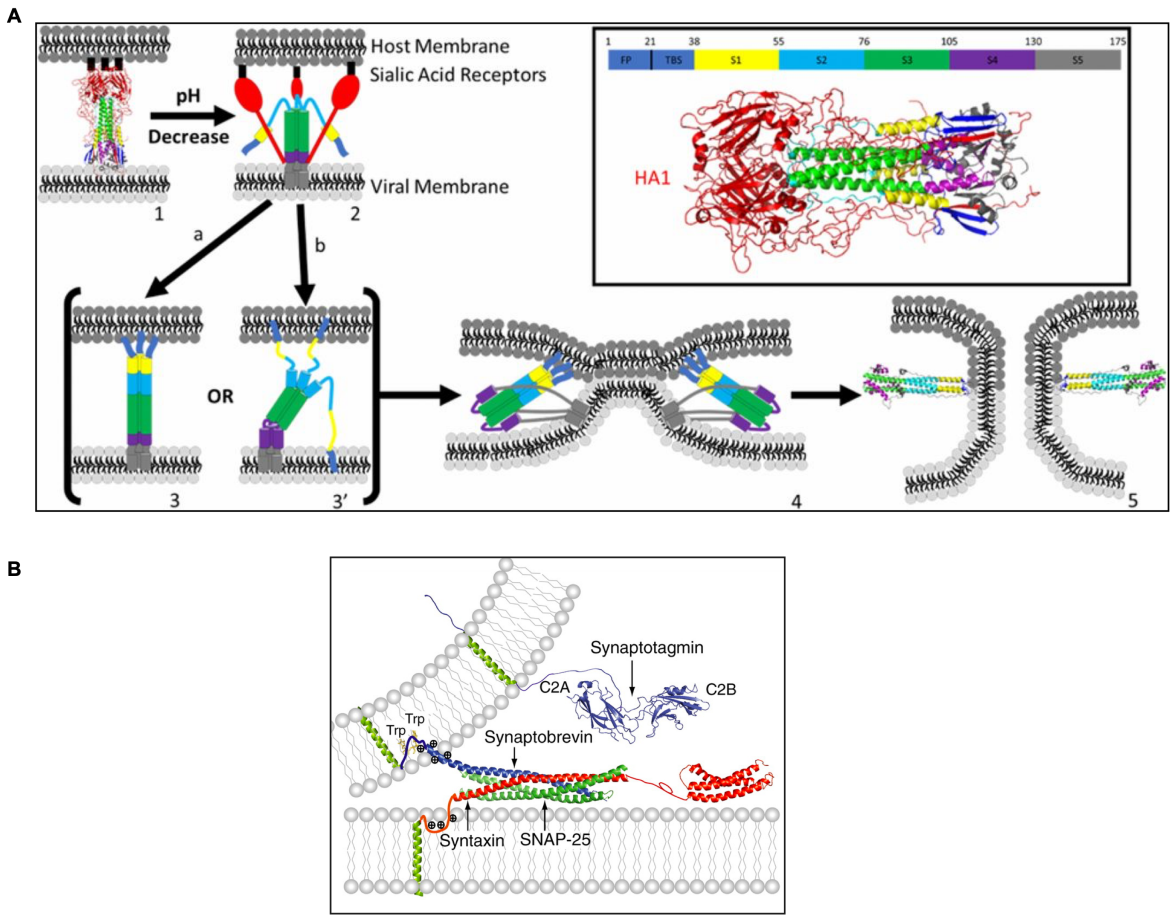

Figure 2: Proposed 'spring-loaded' model of HA-mediated membrane fusion and the SNARE proteins. (**A**) Prefusion HA structure at neutral pH (PDB 1HGF). Viral binding to the host membrane occurs via the HA1 (red) interaction with sialic acid moieties resulting in viral uptake into endocytic vesicles. A pH change in the endosome triggers a conformational change resulting in the swinging away of the HA1 domain and exposure of the HA2 N-terminal hydrophobic fusion peptide (FP) (dark blue) to the host membrane. A fully or partially extended homo-trimeric pre-hairpin intermediate is formed and inserts into the host membrane. A foldback of the inserted trimeric pre-hairpin into an energetically stable hairpin structure pulls the host membrane towards the viral envelope, resulting in the close PM apposition, promoting hemifusion stalk formation and ultimate pore formation. (**B**) Model of a *trans*-SNARE complex comprising of the v-SNARE Synaptobrevin and the t-SNAREs Syntaxin and SNAP-25. The four SNARE motifs assemble into a four-helical bundle that upon zippering, exerts a pulling force on the interacting membranes resulting in close membrane apposition, and promoting hemifusion stalk formation and pore opening. Figures adapted from ([87], [88]).

2.2.3 Placental trophoblast fusion and syncytia formation: Syncytins

The mammalian placenta is a vital organ for embryo implantation and development. It is composed of cytotrophoblasts, endoderm and extraembryonic mesoderm cells. The cytotrophoblasts form part of the outer epithelial cells while the endoderm and extraembryonic mesoderm cells form the inner cell mass (ICM) ([89]). Consequently, the cytotrophoblasts physically connect the embryo to the uterus. During pregnancy, embryo maturation requires the fusion of trophoblasts to form a thin multinucleated syncytiotrophoblast layer or syncytium that constitute the materno-fetal interface ([24], [90]). The syncytium not only establishes an immuno-tolerant environment necessary for fetal development, but also provides an exchange surface for fetal and maternal vascular connections. Additionally, syncytiotrophoblasts promote tissue remodeling and specific hormone synthesis and secretion necessary for overall fetal growth and development ([89], [91], [92], [93]).

The presence of retroviral elements in the placenta led to the identification of the fusogenic protein Syncytin-1 ([24], [94]). The human *syncytin* gene, flanked by 5' and 3' long terminal repeat regions

(LTR), encodes an envelope protein of the human endogenous retrovirus family W (HERV-W) ([90], [24], [95]). Syncytin-1 is mainly expressed in placental syncytiotrophoblasts although fewer syncytin-1 transcripts have also been detected in other reproductive tissues including the endometrium, ovary and testis ([24], [96], [97], [98]). Its placental expression is regulated by increased DNA demethylation of 5' LTR cytosines in the CpG island and elevated cyclic adenine monophosphate (cAMP) levels ([99], [100], [101], [102]). Interestingly, syncytin-1 transcripts have also been detected in various cancers including endometrial, ovarian and breast cancer, where syncytin-1 is proposed to mediate cell proliferation ([100], [103], [104]).

Similarly to other viral envelope proteins, Syncytin-1 is expressed as a precursor protein of ~75kDa. Upon post-translational cleavage in the *trans*-Golgi, Syncytin-1 yields a surface (SU) subunit and a transmembrane (TM) subunit ([90], [105]). The two subunits subsequently associate via a disulfide bond forming a SU-TM complex that is trafficked to the cell surface. At the cell surface, the SU subunit mediates receptor recognition by interacting with the Type D mammalian retrovirus receptor, a ubiquitously expressed sodium-dependent neutral amino acid transporter type 2 (ASCT2), present on the target membrane ([90], [94]), [106], [107]). The SU-receptor interactions result in conformational changes on the TM subunit necessary for its activation. The fusion peptide on the N-terminus of the TM subunit interacts with the target membrane and promotes fusion, analogous to the highly characterized unilateral viral fusion ([94]). Additionally, the two heptad repeats present on the TM subunit have been implicated in the fusion process while its C-terminus possesses a fusion inhibitory activity, similar to the fusion inhibitory R-peptide reported in Murine leukemia virus (MLV) ([90], [108]). Importantly, Syncytin-1 mediates both homotypic cytotrophoblast fusion in the human trophoblastic choriocarcinoma BeWo cell line as well as heterotypic fusion in a variety of cell lines including HeLa, COS, 293 cells and TE671 human cells, corroborating its fusion sufficiency ([24], [94]).

A second protein Syncytin-2 encoded by HERV- FRD-1, mediates cytotrophoblasts fusion in humans ([109], [110]). In contrast to syncytin-1, Syncytin-2 mediates fusion in different cell types. It portrays a unique, highly fusogenic activity in feline and other human cell lines, and to a lesser extent in HeLa cells ([109]). These differences therefore suggest that Syncytin-2 uses a different receptor to the Syncytin-1 type D mammalian retrovirus receptor. Nevertheless, Syncytin-2 possesses the canonical retroviral envelope protein characteristics including the SU and TM subunits and an immunosuppressive domain in TM subunit whose activity protects the fetus from maternal immune responses ([109], [111]). Intriguingly, recent studies have implicated Syncytins in osteoclast development and myoblast fusion in mice, confirming their fusogenic activity ([112], [113], [114]).

Overall, the discovery of the Syncytin proteins is a clear indication of opposite evolutionary dynamics involving the positive selection of viral genes that are beneficial to the human host as opposed to viruses acquiring beneficial genes from their hosts ([24]). Indeed, a placenta-specific Syncytin-Ory1 protein has been identified in rabbits and mediates syncytiotrophoblast formation ([115]). Similarly, Syncytin- A and Syncytin- B, although phylogenetically unrelated to Syncytin-1 and Syncytin-2 and use different surface receptors, mediate cytotrophoblast fusion in mice ([116]). These data thus suggest the evolutionary acquisition and conservation of the endogenous retroviral protein across different organisms.

2.2.4 Developmental fusion family proteins: EFF1 and AFF-1

Cellular development in the nematode *Caenorhabditis elegans* (*C. elegans*) involves the fusion of various cells such as those of the hypodermis, pharynx and vulva to generate multinucleated cells and initiate syncytia formation. About one third of *C. elegans* somatic nuclei are present in syncytial cells that arise from cell-cell fusion events ([25], [117], [118]).

Two fusion family (FF) proteins, Epithelial Fusion Failure (EFF-1) and Anchor Fusion Failure (AFF-1), mediate *in vivo* cell-fusion processes in *C. elegans* ([25], [26]). EFF-1 is a type 1 integral membrane glycoprotein that mediates fusion of epidermal and vulval epithelial cells ([10], [25], [119]). The full-length EFF-1 contains an extracellular N-terminus and a cytoplasmic C-terminus although additional isoforms arising from alternative splicing exist ([25]). The N-terminus is characterized by an extracellular hydrophobic peptide (EHP) comparable to that of viral fusogens

and is crucial for EFF-1 fusogenicity ([25], [120]). Additionally, the N-terminus contains a putative phospholipase A_2 (PLA_2) aspartic acid active sites region. Although previously presumed to mediate membrane lipid digestion during fusion events, recent mutagenesis studies have revealed that the PLA_2 sequence is dispensable in the fusion process ([25], [120]). AFF-1 on the other hand mediates fusion of anchor cells to form the uterine-vulval tube as well as pharyngeal muscles. AFF-1 expression is regulated by the transcription factor FOS-1 and its fusogenic activity is temporally limited to small membranes ([26]). Despite the different fusion action sites, EFF1- and AFF-1 share a general protein structure characterized by a glycosylated ectodomain containing eight conserved disulfide bonds and a TGF-β-type 1 Receptor-like fold ([25], [26]). These structural similarities are suggestive of conserved fusion mechanisms ([26], [121]). Indeed, FF proteins are functionally conserved across nematodes and FF orthologs have been detected in other species such as chordates, protists and arthropods ([119], [121], [122], [123]).

Notably, EFF-1-mediated fusion is homotypic and restricted only to EFF-1 expressing cells. For these cells to fuse, EFF-1 must be expressed on both fusion partners at relatively and mutually high levels, suggesting a bilateral EFF-1 fusion mechanism ([120], [123], [124]). Prior to fusion, EFF-1 is transiently localized at the apical edges of fusion competent cells ([120], [125]). The C-terminus of the extracellular domain mediates protein-protein interactions necessary for the formation of EFF-1 protein complexes at the cell surface ([120], [123]). Interestingly, loss of the extracellular hydrophobic peptide results in protein mislocalization, suggesting that this domain is necessary for correct protein translocation but not protein oligomerization ([120]). Indeed, EFF-1 is secreted in both monomeric and trimeric forms, in which the trimeric form is structurally similar to class II viral fusogens (**Figure 3**) ([126]). Similarly to SNAREs and viral fusogens, both FF proteins mediate fusion via hemifusion intermediate formation as demonstrated by reversible inhibition of EFF-1 mediated fusion by the hemifusion-inhibiting lipid, lysophosphatidylcholine (LPC) ([12], [123]). It has been proposed that monomeric, metastable EFF-1 molecules across the apposed membranes undergo an irreversible trans-oligomerization stage to form a stable post-fusion trimer. Analogous to the viral hairpin formation, EFF-1 trans-trimerization results in a conformational change of the ectodomain, subsequently bringing the TM segments into close proximity. These changes deform the apposed membranes to facilitate membrane merger and distal leaflet fusion ([12], [123], [126]). Once the two membranes fuse, a fusion pore is formed at the adherens junction-containing cell apex. The pore then expands towards the basal direction while displacing the junction components and internalizing the apposed membranes ([117]). Upon fusion completion, EFF-1 is removed from the contact site in a Dynamin and Rab5 GTPase-dependent endocytosis to prevent excessive ectopic fusion ([125]).

The ectopic expression of EFF-1 on nematode cells that do not normally fuse results in fusion. Additionally, the ability of EFF-1 to induce fusion in heterologous cells confirms its fusion sufficiency as a *bona fide* fusogen ([10], [120], [121], [123]). Similarly, AFF-1 can fuse heterologous cells and confer infectivity to pseudo-viruses expressing surface AFF-1 instead of the VSVG surface protein ([121]). Interestingly, EFF-1 can form heterotypic interactions with AFF-1 to promote fusion in heterologous cells ([121], [127]). However, despite their high fusion potency, the two FF proteins do not interact *in vivo*. Moreover, EFF-1 expression and localization is highly regulated, indicative of a regulated developmental fusion process that possibly involves the formation of barriers between adjacent cells to prevent non-specific fusion ([119], [121]). Indeed, EFF-1 overexpression results in unspecific fusion ([119]). Deletion of EFF-1 leads to fusion failure in epidermal and vulval epithelial cells although upstream events such as cellular differentiation and pattern formation remain unaffected ([25]).

In conclusion, EFF-1 shares some fusion characteristics with viral fusion peptides and SNAREs such as fusion via a hemifusion intermediate and formation of protein complexes. However, its activity is distinct in that it requires EFF-1 expression on both mating types. This phenomenon not only highlights the possible *trans* homotypic interactions of EFF-1 molecules, but also presents an additional regulatory mechanism to prevent unwanted fusion events.

2.2.5 Gamete fusion: HAP2/ GCS1

The Hapless 2/Generative Cell Specific 1 (HAP2/GCS1) protein is the only known gamete fusogen that mediates fusion in evolutionary distant organisms such as *Arabidopsis thaliana*, *Chlamydomonas reinhardtii*, *Tetrahymena thermophila*, *Dictyostelium discoideum* and the parasites of the genus Plasmodium and Leishmania ([29], [128], [129], [130], [131], [132], [133]). HAP2 is however absent in vertebrates and fungi. Similarly to *C. elegans* EFF-1, HAP2/GCS1 is a type 1 membrane glycoprotein characterized by a N-terminal signal peptide, a large ectodomain containing the conserved HAP2/GCS1 family H/G domain and a cytoplasmic C-terminal tail ([134]). The H/G-containing ectodomain is required for proper protein localization to the plasma membrane while the cysteine motifs in the cytoplasmic domain are critical for protein targeting to the fusion site. The cytoplasmic domain is also responsible for HAP2 fusogenicity ([135]).

The high structural similarity of HAP2 to class II viral fusogens and EFF-1 implicates HAP2/GCS1 as a class II fusogen (**Figure 3**) ([126], [127], [136], [137], [138]). However, in contrast to EFF-1, HAP2/GCS1 expression and activity varies across the different species. Whereas HAP2/GCS1 is expressed in male gametes in *A. thaliana*, *C. reinhardtii* and *P. falciparum*, it is expressed in all mating types of the seven-sexed isogamous ciliate *T. thermophila* ([29], [129], [130], [131], [132]). In *T. thermophila*, HAP2 is localized at the mating junction and is implicated in stabilizing the mating pair as well as mediating membrane pore formation ([129]). In the green alga *C. reinhardtii*, HAP2 is necessary during fertilization between the *plus* and *minus* gametes. While FUS1, expressed in the *plus* gametes, mediates prefusion attachment of the mating structures to approximately a 10 nm gap, HAP2 is localized to the membrane surface of the *minus* gamete and facilitates membrane fusion ([29], [139]). Similarly in the malaria parasite Plasmodium, P48/45 protein complex functions in the preceding gamete adhesion step whereas HAP2 is localized along the length of the male gamete and mediates gamete membrane fusion ([29], [140]). Notably, HAP2 gene deletion in both organisms results in membrane fusion failure and a subsequent block in fertilization, but gamete adherence remains unaffected ([29], [134]). In the slime mold *D. discoideum*, HAP2/GCS1 orthologs HgrA and HgrB are expressed in the mating types I and II that correspond to the male gametes but are absent in the female mating type III strain ([128]). HgrA and HgrB are localized to the gamete membrane and mediate gamete fusion. It is unclear whether the two proteins form a fusogenic complex or can function individually. Nonetheless, cells deleted of either gene are unable to complete conjugation, indicating that HgrA and HgrB are indispensable in the membrane fusion process ([128]).

In *A. thaliana*, HAP2/GCS1 is expressed in mature sperms and is present in intracellular vesicles. Following sperm-egg interactions, HAP2/GCS1 is released from the intracellular vesicles and distributed at the sperm surface before being localized to the fusion zone ([29], [141]). HAP2/GCS1 mediates correct pollen tube guidance to the ovules, and *hap2Δ* mutants exhibit disordered pollen tube growth within the ovary hampering sperm cells from reaching the ovules. In cases where the pollen tube is correctly targeted to the ovules, HAP2/GCS1 mediates membrane merger events between the egg and the central cell with the two sperm cells, hence is necessary for fertilization. Additional studies implicate HAP2/GCS1 in seed formation ([131], [132], [133]). Interestingly, *hap2Δ* mutants undergo normal sperm development and exhibit wild type-like transport within the pollen tube ([132]). Similarly to *C. elegans* EFF-1, cells expressing HAP2/GCS1 fuse via hemifusion intermediates formation ([127]). In addition, the *A. thaliana* HAP2 can fuse heterologous cells confirming its fusogenic activity. However, fusion in heterologous systems requires the presence of HAP2/GCS1 in both fusing cells, supporting a HAP2/GCS1 bilateral fusion mechanism ([127]). Furthermore, *A. thaliana* HAP2 and *C. elegans* EFF-1 can form heterotypic *trans*-interactions and mediate fusion, suggesting a possible direct protein interaction and similar fusion mechanisms ([127]).

Altogether, these studies indicate that while the different organisms employ species-specific proteins for upstream events including gamete adhesion, HAP2 remains a conserved fusogen that mediates membrane merger. This strongly suggests that HAP2 may be an ancient fusogen and that divergence at upstream events could be a mechanism to meet evolutionary needs. Additionally, the structural as well as functional similarities between class II viral fusogens, EFF-1 and HAP2/GCS1 further reinforce a possible common ancestry of the three classes of proteins that have evolutionarily diverged. Indeed, these proteins have recently been categorized as Fusexins

due to their ability to promote fusion both in gametes as well as somatic cells ([127], [136], [137]). Nevertheless, the proposed bilateral HAP2 membrane fusion mechanism does not reconcile with the *in vivo* data in which HAP2/GCS1 is exclusively expressed in the sperm cell. The HAP2 receptors or HAP2/GCS1-like interactors expressed on the egg surface thus remains elusive. Furthermore, it remains unclear whether these supposed receptors and/or interactors constitute possible trigger mechanisms for HAP2, considering its similarity to class II viral fusogens.

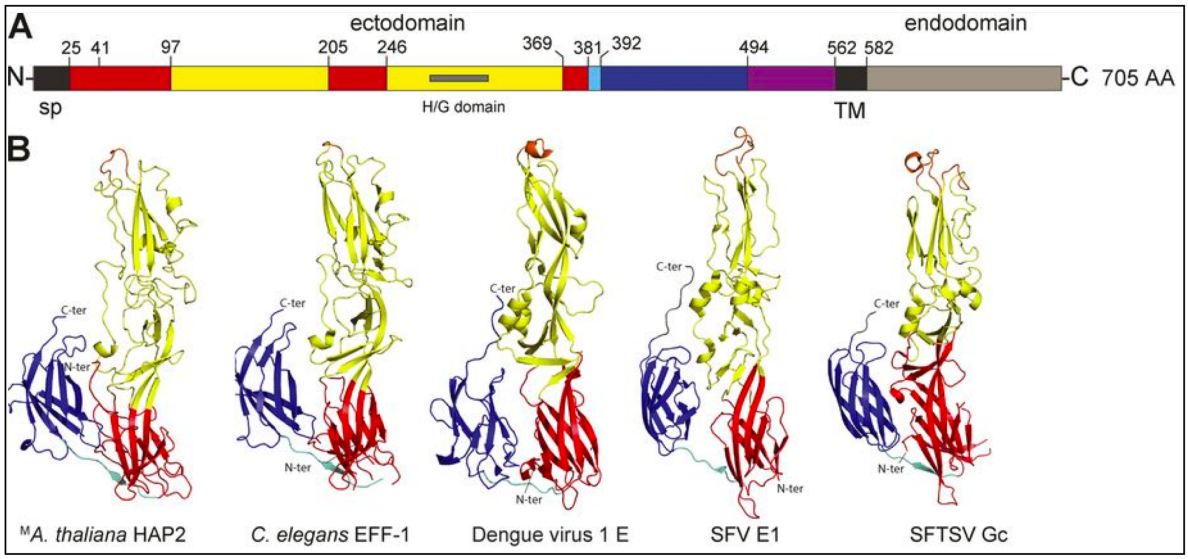

Figure 3: The *A. thaliana* HAP2 and *C. elegans* EFF-1 ectodomains are structurally similar to class II viral fusogens. (**A**) *A. thaliana* HAP2 is a type 1 membrane protein with an N-terminal signal peptide (sp), a large ectodomain that consists of a H/G domain, a short transmembrane region (TM) and a cytoplasmic endodomain. (**B**) *A. thaliana* HAP2 and *C. elegans* EFF-1 (PDB 4OJC) ectodomains are structurally similar to class II viral fusogens of Dengue virus E glycoprotein (PDB 4GSX), Semliki Forest virus (SFV) E1 glycoprotein (PDB 1RER) and severe fever with thrombocytopenia syndrome virus (SFTSV) glycoprotein Gc (PDB 5G47). The overall fold of the three domains: β-barrel domain 1 (D1) (red), a β-stranded domain II (DII) (yellow), and an Ig-like C2-set topology module (DIII) (blue) is similar to that of class II viral fusogens. The domain color code is also depicted in (**A**). Notably, the structural similarities are applicable to entire HAP2/GCS1 family. Figure adapted from ([127]).

2.2.6 Sperm-oocyte fusion: Known effector proteins

The cellular fusion of a sperm and egg (oocyte) to generate a diploid zygote during fertilization signals the onset of life and the introduction of genetic diversity. During *in vivo* fertilization, the sperm cell characterized by a nucleus and acrosome-containing head, a mitochondria-containing midpiece and a motile tail, swims through the uterus into the oviduct. Once in the oviduct, the sperm encounters the egg, a large cell surrounded by a transparent glycoprotein protective matrix known as the Zona pellucida (ZP) ([142], [143]). The invention of *in vitro* fertilization has facilitated the dissection of fertilization into four major steps: (a) acrosome reaction during which the acrosome membrane fuses with the sperm membrane releasing enzymes and other surface ligands, (b) sperm penetration of the ZP and its localization into the perivitelline space surrounding the egg, (c) sperm cell binding and adherence to the oolemma, the egg microvillar membrane, (d) fusion of the sperm and egg to allow genetic material mixing (**Figure 4**) ([144], [145]). Once fertilization is complete, the oolemma and ZP undergo changes in their biochemical composition that block the entry of additional sperms thus preventing polyspermy ([146], [147], [148]). While fertilization remains a fundamental process in eukaryotic life, a comprehensive molecular understanding of the proteins involved sperm-egg recognition, adhesion and fusion is lacking. In the recent past, extensive gene knock-out (KO) studies in mice have revealed essential factors in fusion but the *bona fide* fusogen remains elusive.

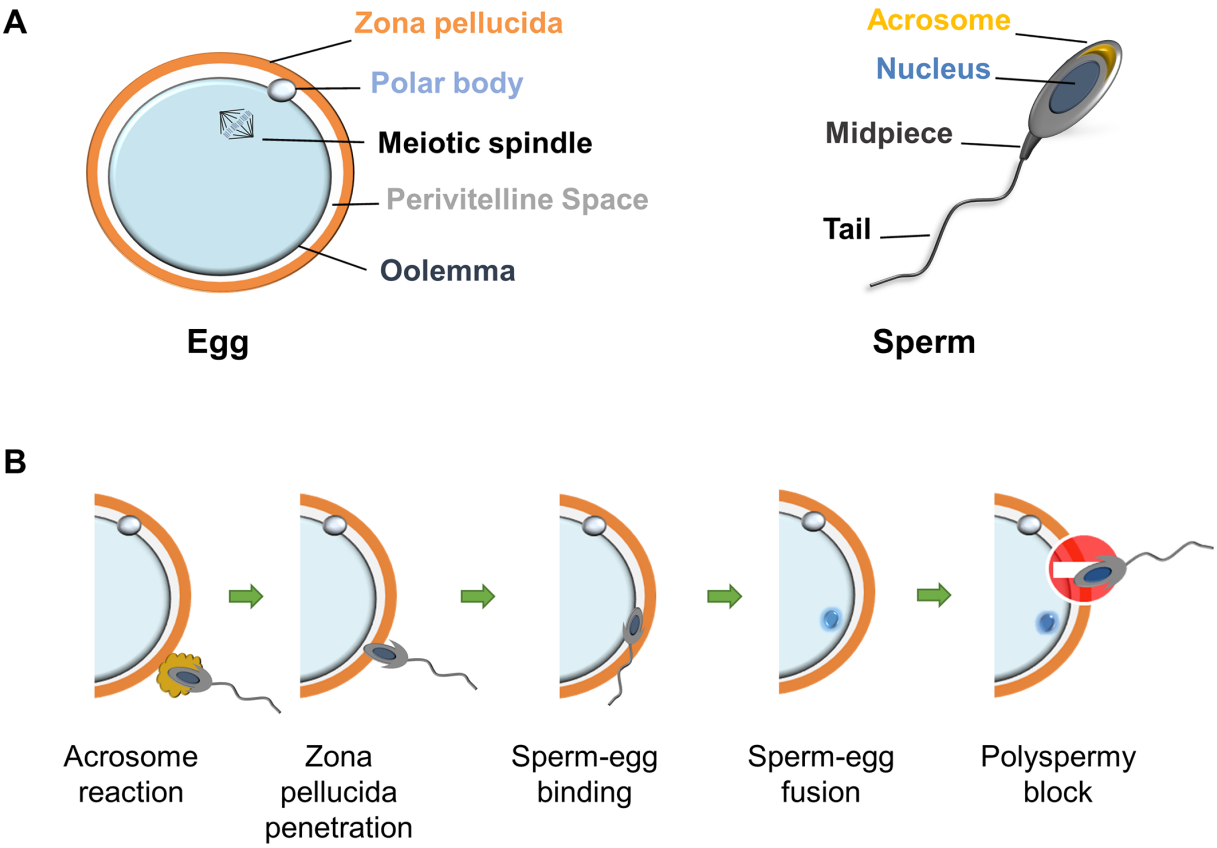

Figure 4: Mammalian sperm-egg fusion is a multi-step process. (**A**) Schematic of the mammalian gametes. The female egg is significantly larger than the sperm cell and consists of the outermost protective zona pellucida (ZP), a perivitelline space, and an oolemma lined with microvilli except at the polar body to prevent sperm binding at this region. (**B**) Sperm-egg fusion is characterized by a sperm acrosome reaction and release of enzymes and proteins that facilitate ZP penetration. In the perivitelline space, the acrosome-reacted sperm cell adheres to the oolemma after which PM fusion permits diploid zygote formation and fertilization. A fertilized egg induces polyspermy block by altering its oolemma and ZP. Adapted from ([149]).

2.2.6.1 Fertilin

Fertilin is a sperm plasma membrane protein that belongs to the ADAM (a disintegrin and metalloprotease) family proteins involved in cellular adhesion and protease functions ([150], [151], [152]). In mature sperm cells, fertilin exists as a heterodimer composed of α (ADAM1b) and β (ADAM2) subunits, two integral glycoproteins with putative fusogenic peptide-like and integrin binding sequences ([152], [153]). In spermatogenic cells, the α- and β-subunits are secreted as precursor proteins consisting of six ADAM domains: a pro-domain, a metalloprotease, a disintegrin, a cysteine-rich, a transmembrane and a cytoplasmic domain. During sperm cell maturation, the pro- and metalloprotease domains are proteolytically cleaved resulting in mature subunits comprised of the disintegrin domain at the N-termini. Fertilin is proposed to mediate sperm-egg attachment and adhesion via the interactions between the disintegrin domain of the β-subunit and the egg integrin receptor, resulting in egg activation ([154], [155]). While loss of the β-subunit does not affect sperm morphology, motility and acrosome reaction, it results in the concomitant decrease in the α-subunit concentration possibly due to free α-subunit degradation. Additionally, the ADAM2 mutant sperms have a reduced egg ZP binding and adherence capacity as well as reduced sperm migration to the oviduct. Interestingly, egg activation remains unaffected and the ADAM2 KO mice remain fertile ([156]). On the other hand, ADAM1b KO mice are fertile and express sperms with normal morphology, motility as well as migration to the oviduct. ADAM1b mutants are able to bind

to the egg ZP and fuse with ZP-free eggs suggesting that fertilin is necessary in mediating sperm-egg adhesion but not the egg activation and fusion steps ([156], [157]).

2.2.6.2 IZUMO1 and JUNO

Another essential fusion factor in sperm-egg fusion is Izumo1, a type 1 membrane protein with an extracellular Immunoglobulin (Ig) domain ([158]). There are four sperm-associated Izumo proteins (Izumo1-Izumo4), all of which share high N-terminal sequence homology ([159]). Izumo1 is localized at the inner and outer acrosome membranes of acrosome-intact sperm cells. Upon acrosome reaction, Izumo1 is translocated to the equatorial segment of the sperm plasma membrane and the entire post-acrosomal region, suggesting that its function is exerted downstream of acrosome reaction ([158], [160]). Once localized at the surface, Izumo1 recognizes Juno, a monomeric glycosylphosphatidylinositol (GPI)- anchored folate receptor 4 (Folr4) protein localized at the egg surface (**Figure 5**) ([147], [161]). The Izumo1-Juno interaction induces Izumo1 to dimerize and undergo a conformational change. By possibly interacting with other unknown proteins, the dimerized Izumo1 mediates membrane pulling and tight apposition to facilitate fusion ([159], [162]). Indeed, recent structural studies have revealed the putative interaction model between Izumo1 and Juno, and is conserved across different mammalian species ([147], [163], [164], [165]). Eggs lacking Juno mature normally but are unable to undergo fertilization. Instead, they accumulate sperms in the perivitalline space implicating Juno in the fusion process ([147], [166]). Sperms obtained from *Izumo1Δ* KO mice can carry out normal acrosome reaction and penetration into the egg ZP. Interestingly, the sperm cells fail to undergo fusion, implicating Izumo1 in sperm-egg fusion ([158], [160]). Heterologous expression of Izumo1 results in enhanced adhesion to the egg surface, suggesting a gamete adhesion function ([162], [167]). Interestingly, heterologous expression of both Izumo1 and Juno in non-fusing HEK293 cells does not result in syncytia formation despite their extended cellular adhesion ([147]). It is therefore proposed that the Izumo1-Juno interaction mediates gamete recognition and adhesion rather than fusion. Consequently, the interaction of the two proteins is crucial in overcoming the membrane hydration repulsive forces, a major barrier in cell-cell fusion processes. Upon sperm-egg fusion and completion of fertilization, Juno is translocated into extracellular vesicles, possibly to prevent polyspermy ([147]).

2.2.6.3 CD9

Cluster of **D**ifferentiation 9 (CD9) is a tetraspanin, four-pass membrane protein expressed on the egg microvillar membrane in addition to other body tissues such as blood, epithelia and neuronal cells ([168], [169]). In the egg membrane, CD9 associates with other membrane proteins including integrin α6β1, α3β1, α5β1 and the GPI-anchored protein EWI-2 ([170], [171], [172], [173]). Similarly to other tetraspanins, CD9 is capable of forming both homotypic and heterotypic interactions resulting in the formation of multimolecular complexes enriched at the tetraspanin-enriched microdomain (TEM) ([174]). As a result, CD9 has been proposed to interact with other proteins and mediate cell adhesion, motility and signaling by accumulating other sperm receptors into nanodomains to facilitate sperm binding ([175], [176], [177]). Indeed, CD9 interacts with CD81, another egg membrane tetraspanin that is localized to tetraspanin-rich domains and is also necessary for fusion ([174], [178]).

During fertilization but preceding fusion, CD9 is localized at the sperm-egg contact site and is thus proposed to mediate membrane reorganization into a fusion-competent state ([175], [179]). Its localization at the contact site is dependent on sperm head oscillations underneath the egg membrane that are generated by the flagellum beating ([180]). These oscillations are suggested to last for about 2-3 minutes until the sperm's equatorial zone is perpendicularly oriented to the egg membrane to facilitate receptor binding and membrane fusion ([180], [181]). Indeed, CD9 is localized at the microvilli-rich region of the egg membrane where it regulates microvilli structure and dynamics to favor tight membrane interactions and fusion (**Figure 5**) ([175], [182]). Interestingly, egg microvilli have been implicated in fusion. Additionally, sperm binding and fusion preferentially occurs at the microvilli-rich region as opposed to the microvilli-devoid region ([175]). More recent studies have further implicated CD9 in regulating the re-localization of GPI-anchored proteins such as Juno from the microvilli-devoid, chromosome-containing actin-cap region to the microvilli-rich region. This protein sequestration facilitates local Juno clustering to enhance binding

avidity while preventing the sperm from binding at the microvilli-devoid region, thus ensuring coordinated gamete fusion ([147], [183]). Egg cells lacking CD9 show abnormal microvilli shape and distribution along the egg membrane and a subsequent reduction in fusion ([168], [172]). Consequently, CD9 KO eggs show reduced fertility despite normal ovulation and egg maturation ([168], [172], [184]). Interestingly, *cd9Δ* KO cells exhibit normal sperm penetration of the ZP and binding at the oolemma but end up accumulating at the perivitalline space, confirming that CD9 is essential in the latter stage of cell fusion ([168], [172]). Once fusion is complete, CD9 is immediately translocated away from the microvilli-rich, sperm-contact site. This re-localization suggests that CD9 function is exerted at the fusion step and that it facilitates oolemma membrane architecture reorganization to prevent polyspermy ([147], [181]).

2.2.6.4 SPACA6

The Sperm ACrosome membrane-Associated protein 6 (SPACA6) is another recently identified protein indispensable in sperm-egg fusion. SPACA6 is an immunoglobulin-like, single-pass transmembrane protein expressed in the sperm cell and detected at the equatorial segment of the sperm head (**Figure 5**) ([185], [186]). Similarly to IZUMO1, SPACA6 is first localized at the acrosomal cap but undergoes relocation to the equatorial segment following acrosome reaction ([158], [185], [187]). Additionally, sperms deleted of *spaca6Δ* portray normal morphology and motility and retain their ability to penetrate the egg ZP. However, these cells have a block in fusion characterized by the accumulation of sperms in the perivitelline space ([185], [187]). Interestingly, contrary to IZUMO1, heterologous expression of SPACA6 does not enhance sperm adhesion to the egg membrane, suggesting that SPACA6 is not involved in gamete adhesion ([162], [185]). Indeed, IZUMO1 is correctly localized at the equatorial segment in *spaca6Δ* KO cells further confirming that the two proteins are not functionally redundant. Therefore, despite their structural similarities, SPACA6 and IZUMO1 are functionally different although both proteins are necessary in the fusion process. Recent studies propose that SPACA6 and Izumo1 interact to form a complex that in turn recruits the fusogenic machinery, although experimental evidence is pending ([187]).

2.2.6.5 TMEM95, SOF1, FIMP and SPACA4

The TransMEMbrane protein 95 (TMEM95) is a single-pass transmembrane protein localized at the acrosome membrane, equatorial segment and the connecting piece of the sperm cell. Upon acrosome reaction, TMEM95 is shed from the acrosome suggesting that it possibly functions at the acrosome reaction step. *Tmem95Δ* KO mice exhibit absolute block in fusion implicating TMEM95 in sperm-egg fusion ([188], [189]).

The Sperm-Oocyte Fusion required 1 protein (SOF1) is a sperm protein expressed in immature spermatozoon but is post-translationally modified during sperm maturation. SOF1 contains the conserved 'LLLL and CFN (L or S) AS' motif, although the functional relevance of these domains remains unknown. *Sof1Δ* KO sperm cells are sterile and do not fuse with WT oocytes, although the fusion defect can be rescued via SOF1 transgenic expression ([149], [187]).

The Fertilization Influencing Membrane Protein (FIMP) is a single-pass membrane protein encoded by the testis-specific *4930451I11Rik* gene on mouse chromosome 7 ([190]). While 4930451I11Rik protein is expressed as two isoforms namely the transmembrane (TM) isoform and the secreted form, only the TM form (FIMP) is implicated in fusion ([190]). FIMP is localized to the equatorial segment of sperm head after acrosome reaction. *FimpΔ* KO cells exhibit partial fusion defects that can be restored by expressing the FIMP membrane isoform ([187], [190]).

Similarly to the aforementioned SPACA6, TMEM95, SOF1 and FIMP KO sperm cells are morphologically normal and undergo acrosome reaction and ZP penetration. However, they display a fusion defect characterized by sperm accumulation at the perivitelline space and binding to the oolemma. Notably, the KO cells do not exhibit a gamete binding defect. Furthermore, IZUMO1 expression and localization is not impeded in respective gene KOs, suggesting that these proteins function downstream of the IZUMO1-JUNO complex formation, or that they are part of an IZUMO1-independent fusion pathway ([185], [187], [188]).

SPACA4, also known as sperm acrosomal membrane-associated protein 14 (SAMP4), is a GPI-

anchored glycoprotein that belongs to the Ly-6/urokinase-type plasminogen activator receptor (uPAR) superfamily ([149], [191]). SPACA4 is localized at the inner acrosomal membrane following acrosome reaction, and a SPACA4 antibody inhibits fusion thus implicating SPACA4 in the fusion process ([191]). Despite the limited understanding of SPACA4 function, its structural homology to Bouncer, an egg surface protein that mediates sperm-egg recognition and binding in zebrafish, suggests that SPACA4 may play a similar role in mammalian fertilization ([149], [192]).

Intriguingly, heterologous expression of IZUMO1 but not SPACA6, TMEM95, FIMP and SOF1 proteins, enhances binding of ZP-free eggs with HEK293T cells, suggesting that IZUMO1 facilitates membrane adhesion. However, the fact that none of these proteins enhances fusion of ZP-free eggs with HEK293T cells implies that they are essential but not sufficient components of the fusogenic machinery. Additionally, these findings point to the existence of additional and uncharacterized sperm factors that are necessary in the sperm-oocyte fusion process ([187]). Consequently, a comprehensive characterization of the molecular mechanisms of mammalian gamete fusion and the *bona fide* gamete fusogenic machinery are still lacking.

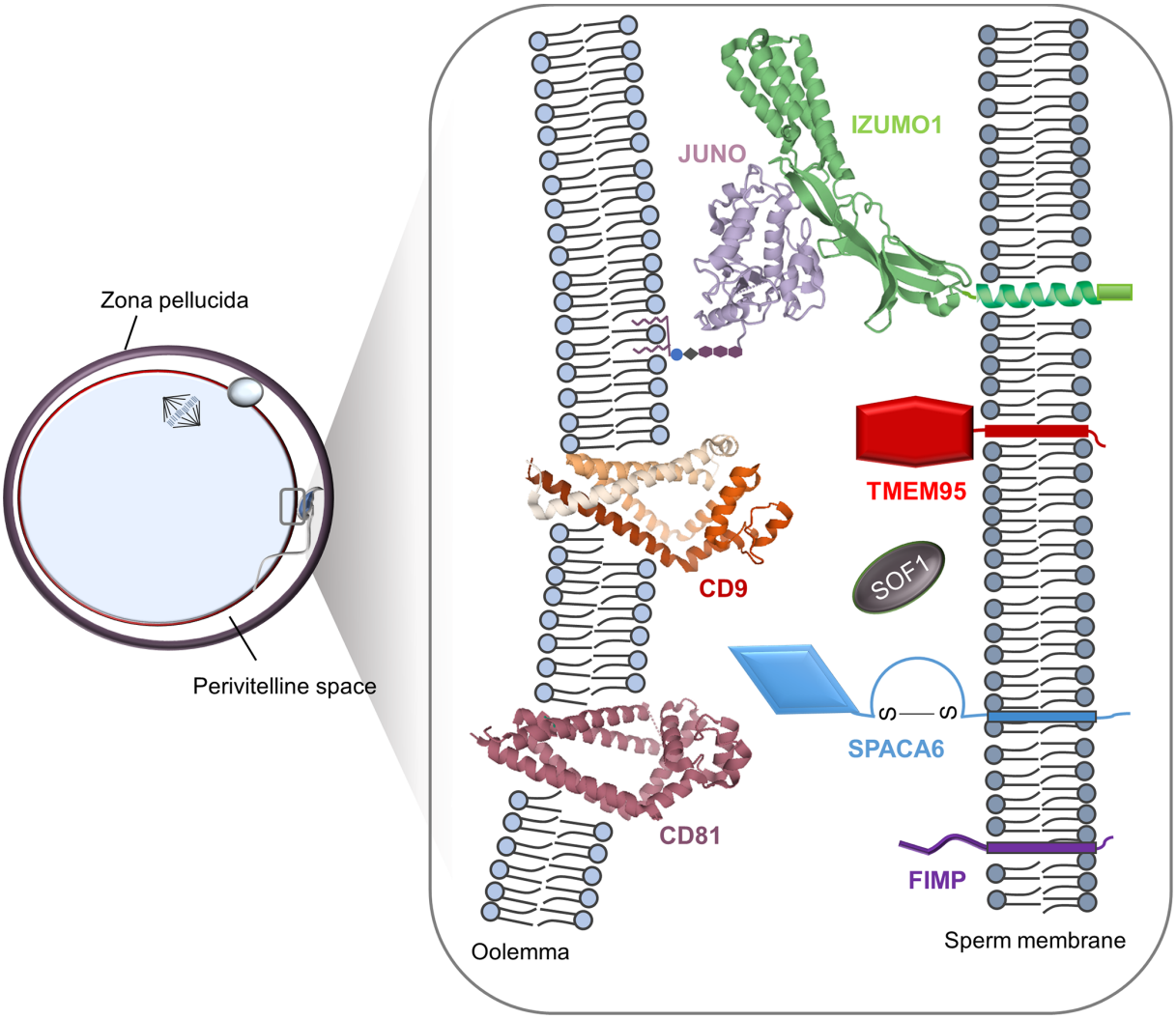

Figure 5: Several effector proteins are involved in the mammalian sperm-egg fusion process. The tetraspanins CD81 and CD9 and the IZUMO1 receptor JUNO, are present on the egg membrane. Sperm cell-specific proteins include the GPI-anchored IZUMO1 involved in sperm-egg adhesion, the single-pass transmembrane proteins FIMP, TMEM95 and the immunoglobulin-like SPACA6. SOF1 is a putative secreted protein, while SPACA4 and Fertilin are not depicted in the schematic. Except for IZUMO1-JUNO complex and Fertilin, all the other sperm-specific proteins supposedly operate downstream of sperm-egg adhesion but are not *bona fide* fusogens. Adapted from: ([149]).

In conclusion, extensive research in the recent past has led to a better understanding of the molecular mechanisms of cell-cell fusion. In addition to viral fusogens and the SNARE proteins, developmental fusogens such as Syncytins, Myomaker and Myomerger-Minion involved in myoblast fusion and the EFF1-1 and AFF-1 fusion proteins have been identified and characterized ([10], [24], [25], [26], [27], [28]). Furthermore, effector proteins such as the transmembrane protein macrophage fusion receptor (MFR) and its putative ligand CD47 and CD44 have been identified and implicated in macrophage fusion ([193], [194], [195]). On the other hand, HAP2/GCS1 that mediates fusion in plants and protists, is the sole gamete fusogen that has been characterized ([29]). In concert with the absence of HAP2/GCS1 in vertebrates and fungi, no mammalian or fungal gamete fusogen has been yet identified. Instead, effector proteins necessary in sperm-oocyte fusion and in yeast mating have been reported, suggesting that gamete fusion is a highly regulated process involving an interplay of different molecules.

Notably, the structural and functional similarities between HAP2/GCS1, EFF-1 and viral class II fusogens not only suggest a possible common ancestry of both gamete and somatic fusogens, but also similarities between somatic and gamete fusion events across different organisms ([127]). Consequently, the genetic simplicity of a yeast cell provides a suitable model organism to understand the late cell-fusion events of the otherwise complex process of mammalian fertilization. Indeed, yeast cells, *Saccharomyces cerevisiae* or *Schizosaccharomyces pombe,* can undergo mating analogous to the mammalian sperm-oocyte fusion. Similarly to sperm-oocyte fusion, haploid yeast cells fuse to generate a stable diploid zygote. Intriguingly, both the mammalian and the fungal *bona fide* gamete fusogen(s) as well as a molecular understanding of PM fusion in both organisms remain unknown. These current gaps in understanding fungal gamete fusion inspired the focus of this thesis. By employing the mating process of budding yeast (*S. cerevisiae*), this thesis focuses on understanding the late cell-fusion events as well as the underlying regulatory mechanisms, with a particular focus on identifying the positive and negative regulators of PM fusion.

2.3 Mating in *Saccharomyces cerevisiae*: a model organism

Haploid *S. cerevisiae* cells exist as either *MAT***a** or *MATα* mating types, that fuse to generate a diploid zygote. Mating in *MAT***a** and *MATα* haploid cells is initiated by secretion of mating type-specific pheromones (***a***-factor and *α*-factor) and expression of *STE2* and *STE3* surface receptors, respectively. Each receptor is coupled to a heterotrimeric G protein consisting of Gα, Gβ and Gγ subunits encoded by *GPA1*, *STE4* and *STE18* genes respectively, and a downstream Mitogen Activated Protein (MAP) kinase cascade. In the *MAT***a** cell for instance, binding of the *α*-factor to the Ste2p cell surface receptor activates the heterotrimeric G protein stimulating a GDP to GTP exchange on the Gα subunit. This results in the dissociation of the Gα subunit from the Gβγ complex. The free Gβγ complex is released into the cytoplasm where it binds to the scaffold protein Ste5p ([196], [197]). The new Gβγ-Ste5p complex is subsequently recruited to the PM and the Ste5p-membrane localization is dependent on its N-terminal amphipathic helix, its two membrane binding domains and a PH domain ([198], [199]). Cdc24p, a Cdc42p guanine exchange factor (GEF), has also been implicated in mediating the Gβγ-Ste5p complex membrane re-localization ([200], [201]).

At the membrane, Ste5p interacts with a p21-activated kinase (PAK) Ste20p, that functions as an effector protein of the GTPase Cdc42p. GTP-bound Cdc42p is necessary in activating Ste20p, resulting in downstream stimulation of the MAPK pathway ([202]). Simultaneously, Ste5p binds the MAPK cascade components while undergoing a conformational change that prevents cascade inhibition ([203], [204], [205]). Coupled with GTP hydrolysis and subsequent phosphorylation steps on serine/threonine-proline (S/TP) phosphorylation sites, Ste20p activates a MAP kinase kinase kinase (MAPKKK) Ste11p that in turn activates the MAP kinase kinase (MAPKK) Ste7p. By phosphorylation, Ste7p activates Fus3p and Kss1p, two partially redundant MAP kinases (MAPK) (**Figure 6**) ([206]). Though both MAP kinases can sufficiently activate the transcription factor Ste12p, Fus3p activation results in mating-specific gene activation while Kss1p results in activation

of genes involved in filamentous growth ([207]). In particular, Fus3p-dependent Ste12p phosphorylation results in its release from Dig1p and Dig2p proteins that function as negative regulators of Ste12p ([208]). In addition, Fus3p has been implicated in cell cycle arrest by phosphorylating cyclin-dependent kinase (Cdk) inhibitor Far1p which interacts with and inhibits G1-cyclin/Cdk1, necessary for the initiation of cell cycle. This inhibition results in cells arresting at the G1 phase, hence promoting downstream pheromone signaling ([209], [210], [211]). Fus3p also phosphorylates components of the polarisome to promote polarized growth ([212]). The activated transcription factor Ste12p subsequently binds to the pheromone response elements (PREs) of mating genes, resulting in pheromone-dependent transcription of mating genes [213].

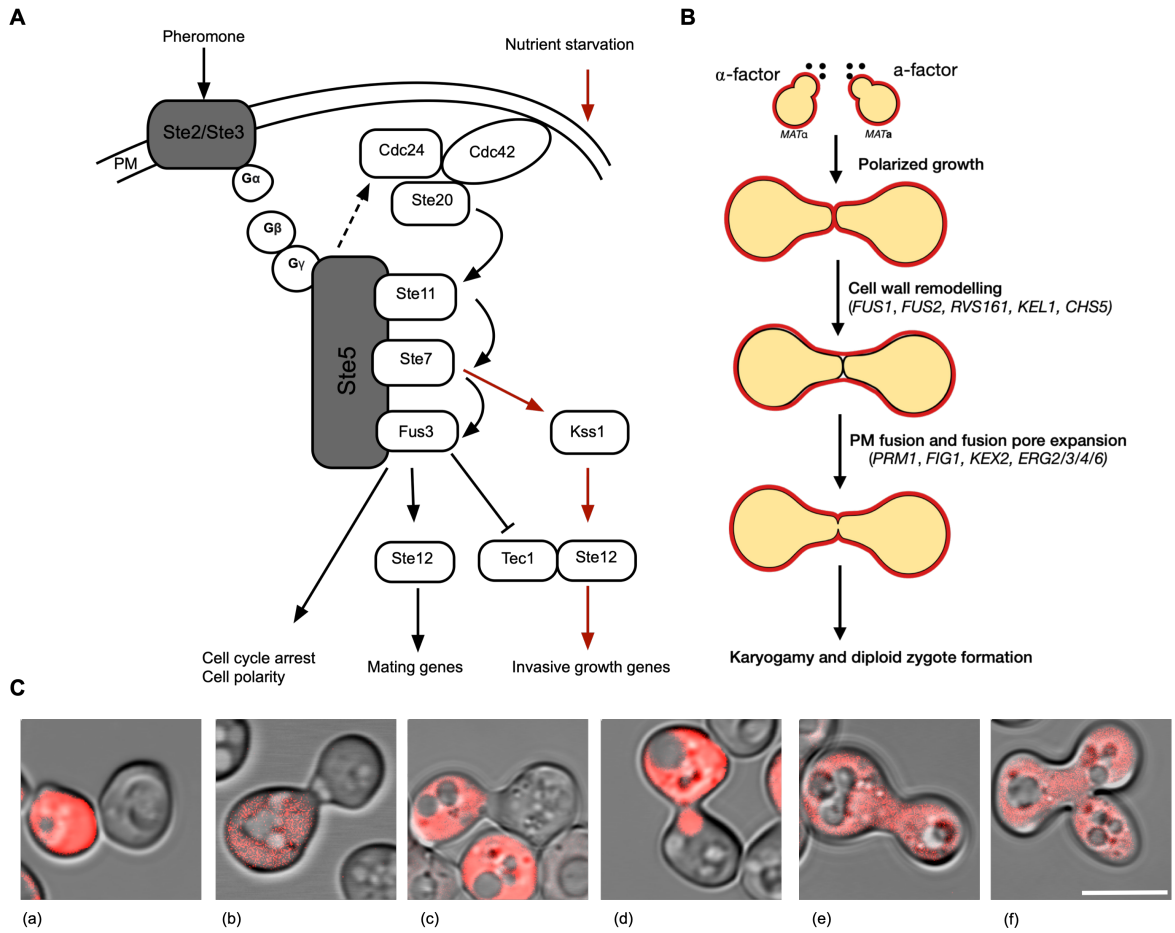

Figure 6: Model of the MAPK pathway and the multi-step fusion process of haploid *S. cerevisiae* cells. (**A**) Components of the MAPK pathway are shared between the mating (black arrows) and the invasive growth (red arrows) program. The MAPK Fus3p and Kss1p determine the specificity of each program. Dashed arrow depicts the recruitment of the Gβγ-Ste5p complex to the plasma membrane (PM). (**B**) During mating, haploid *MAT***a** and *MATα* cells respond to pheromone signaling by undergoing polarized growth towards the mating partners forming shmoos, cell wall remodeling (depicted in red) to allow PM apposition (depicted in black). PM fusion and pore formation and expansion permits cytoplasmic mixing and karyogamy to form a diploid zygote that re-enters the cell cycle. Figure modified from ([214]). (**C**) Representative images of the mating process (a-f). The *MATα* cell is expressing the cytoplasmic marker Pgk1p-mCherry. Upon pheromone response, haploid cells in a mating mixture polarize towards each other. Once contact is established, the cells remodel their CW to allow PM apposition. PM fusion is characterized by transfer of the cytoplasmic marker Pgk1p-mCherry into the *MAT***a** cell. Fusion pore expansion results in cytoplasmic mixing and karyogamy to generate a diploid zygote. Scale bar= 5 µm.

2.3.1 Polarisome activation and Shmoo formation

Haploid yeast cells undergo polarized growth during budding and in response to pheromones. In both instances, Cdc42p functions as a polarization regulator whose activity is regulated by Cdc24p and the GTPase activating proteins Bem3p, Rga1p and Rga3p ([215], [216], [217]). Cell polarity is therefore determined by the specific recruitment and localization of Cdc42p and Cdc24p to the cell cortex. Additionally, by associating with the plasma membrane, Bem1p positively regulates Cdc42p localization at the cell cortex ([218], [219]). In response to mating pheromones, polarized growth is characterized by cellular growth towards the mating partner and along the pheromone gradient, forming distinct pear-shaped mating projections often referred to as 'shmoos' ([220] [221]). The localization of Cdc42p and Cdc24p thus forms the shmoo tip, a precursor cell-cell contact site and mating zone. Shmoo tip selection is dependent on the scaffold protein Far1p ([222]). During pheromone response, Far1p interacts with Cdc24p in the nucleus, forming a Far1p-Cdc24p complex. This complex subsequently interacts with the Gβγ at the cell cortex, resulting in the recruitment of Cdc42p and Bem1p from the bud site towards the direction of the pheromone gradient ([205], [209], [223]). Indeed, *far1Δ* mutants form shmoos that are localized at the bud site instead of towards the mating partner. However, in the presence of isotropic pheromone concentrations, haploid cells activate the 'default pathway' that results in cells mating randomly with both pheromone-producing and non-producing cells. Intriguingly, the putative bud sites become the shmoo tip sites ([224]).

Furthermore, Fus3p and Cdc42p activate Bni1p, a formin that regulates cytoskeleton reorganization and cell polarization ([212], [225]). The Bni1p-dependent actin nucleation at the pheromone response site therefore functions as a mating pathway effector and promotes polarized growth ([225]). Indeed, shmoos are characterized by an asymmetrically reorganized cytoskeleton that is oriented towards the shmoo tip while the nucleus and most organelles accumulate at the base of the shmoo tip ([226]). Additionally, Bni1p interacts with polarisome components Spa2p and Pea2p, and together mediate polarized growth at the shmoo tip ([227]). Furthermore, proteins necessary in mating such as agglutinins and Fus1p co-localize with actin at the shmoo tip. The polarisome machinery is therefore implicated in vesicle transport necessary for trafficking of CW synthases and hydrolases to the mating zone as well as trafficking PM proteins for fusion. Indeed, *spa2Δ* and *pea2Δ* mutants are defective in proper shmoo formation and fail to cluster vesicles at the shmoo tip ([225], [227], [228]).

Upon cell-cell contact, cell adhesion between the *MAT***a** and *MATα* cells is mediated by the surface-expressed **a**- and *α*-agglutinins, encoded by *AGA1/2* and *SAG1* genes, respectively ([229]). The **a**-agglutinin is a highly O-glycosylated glycoprotein composed of two subunits, the anchorage subunit Aga1p and the binding subunit Aga2p, linked by two disulfide bonds. The anchorage subunit Aga1p is GPI-anchored to the CW via its C-terminus while the binding subunit Aga2p is exposed on the CW exterior ([229], [230], [231]). The *α*-agglutinin on the other hand contains an immunoglobulin-like, highly flexible N-terminus and a highly glycosylated GPI-anchored C-terminus ([232], [233]). Interaction between complementary agglutinins on opposite mating types occurs in a 1:1 stoichiometry ratio via the surface exposed N-termini and occurs with high affinity and specificity ([233], [234]). Indeed, agglutinin mutants portray reduced mating efficiency due to reduced cell adhesion ([229], [235]). Importantly, the interaction between the complementary agglutinins establishes an irreversible cell-cell contact that defines the onset of cell wall (CW) remodeling. The mating cells subsequently undergo a highly regulated CW remodeling step giving rise to PM apposition.

2.3.2 Cell Wall remodeling: A pre-requisite for PM fusion

2.3.2.1 Fus1p and Fus2p

Yeast cells grow in a hypo-osmotic environment. The CW thus serves as an additional protective layer to the PM against external osmotic pressure that would otherwise result in cell lysis ([236], [237]). However, during mating, cells must remodel their CWs to allow PM contact and fusion while avoiding lysis. Following pheromone signaling, polarized growth and agglutination, the two cells generate a unified CW around the mating pair. The on-time and localized CW degradation at the contact sites (shmoo tips) allows the two PMs to closely appose and later fuse. Early genetic

studies led to the identification of Fus1p as a key regulator of CW remodeling ([238], [239]). Fus1p is an O-glycosylated type 1 membrane protein whose expression in either mating type is pheromone-dependent. The N-terminal O-glycosylation as well as a Chs5p-dependent secretory pathway results in a polarized localization of Fus1p to the shmoo tip and to the fusion zone in mating pairs (**Figure 7A** and **7B**) ([239]). Indeed, at its C-terminus, Fus1p interacts with GTP-bound Cdc42p and Chs5p to facilitate its secretion in response to pheromone signaling. In addition, Fus1p contains a C-terminal Src homology 3 (SH3) domain and a proline-rich peptide. The SH3 domain mediates Fus1p interaction with Bni1p to promote polarized growth and secretion. On the other hand, the proline-rich peptide mediates a direct interaction with Sho1p, an osmo-sensor of the HOG-MAPK pathway. This interaction facilitates down-regulation of the HOG pathway and glycerol synthesis in favor of the fusion pathway. Consistently, deletion of *SHO1* suppresses the *fus1Δ* -associated fusion defects ([240]). At the mating projection, Fus1p partitions into ergosterol-sphingolipid rafts that arise from PM reorganization in response to pheromone signaling. By partitioning into lipid rafts, Fus1p is retained at the zone of cell fusion (ZCF) or mating junction until the fusion process is complete ([241]).

Functionally, Fus1p facilitates the localization of secretory vesicles at the mating junction. The vesicles presumably carry CW hydrolases and synthases that facilitate CW thinning and regeneration, respectively. Additionally, the secretory vesicles are proposed to carry other components of the fusion machinery including PM proteins that mediate PM fusion. This allows the on-time delivery of the secreted fusion machinery to the fusion site ([228],[242]). Notably, vesicle clustering at the mating junction is as important as vesicle localization. Spa2p, a component of the polarisome, coordinates vesicle clustering ([228], [243]). Indeed, wild type (WT) mating pairs contain secretory vesicles that localize and cluster at the mating junction across regions of CW thinning prior to PM fusion ([228], [244], [245]). Inhibiting secretion arrests fusion, confirming the necessity of polarized secretion in late mating events ([242]). Consistently, *fus1Δ* mutants fail to degrade the intervening CW material at the mating junction and ~70% of *fus1Δ* mutants portray no vesicle clustering. On the other hand, *spa2Δ* mutants display dispersed vesicles (**Figure 7C**) ([228]).

Fus2p, a membrane-associated protein, is another CW remodeling effector protein. In mitotic cells, Fus2p remains localized in the nucleus. In response to pheromone signaling, Fus2p is translocated to the cytoplasm where it interacts with Rvs161p via its C-terminal Rvs161 binding domain (RBD). Rvs161p is an Amphiphysin-like protein that binds and stabilizes membrane curvature. The two proteins form a banana-like helical heterodimer that is transported to the shmoo tip via actin polymerization and Myo2p pathway ([246], [247]). Whereas the Fus2p C-terminal is crucial for Rvs161p interaction and its localization to the shmoo tip, Fus2p correct localization is also dependent on the Rvs161p membrane interaction. Lysine mutations of Rvs161p that abolish membrane interaction result in Fus2p mislocalization ([248]). However, recent findings have shown that the Fus2p C-terminus is not sufficient for its mating junction localization. A C-terminally truncated form of Fus2p (Fus2p 1-650) is correctly localized at the mating junction similar to the WT protein. Interestingly, this truncated form remains mis-localized in polarized cells suggesting that additional factors such as components of the polarisome are essential in correct protein localization in polarized cells but not at the junction ([249]). Consistently, polarized cells are characterized by positive membrane curvature at the shmoo tip. This morphology would likely favor the Fus2p-Rvs161p interaction that is dependent on the Fus2p C-terminus ([250]). In addition, it is speculated that Fus2p-Rvs161p heterodimer interacts with secretory vesicles in the cytoplasm via the vesicle curved membranes. These vesicles are then transported along the Myo2p-actin pathway to the shmoo tip where the complex interacts with Fus1p, a possible scaffold protein. Retention of the Fus2p-Rvs161p heterodimer at the shmoo tip is thus dependent on Fus1p and actin-dependent pathways. Abolishment of both pathways results in total protein mislocalization ([250]).

Fus2p mislocalization can be suppressed by overexpression of the redundant Kelch-domain proteins Kel1p/ Kel2p ([251], [252]). In pheromone treated cells, Kel1p localizes at the shmoo tip and is required for correct Fus2p localization ([248]). In mitotic cells, Kel1p interacts with Bud14p and Kel2p in regulating Bni1p activity in actin assembly ([248]). Intriguingly, Fus2p is mis-localized in *fus1Δkel1Δkel2Δ* mutants that are treated with Latrunculin A, a compound that depolymerizes actin. This suggests that Kel1p and Kel2p redundantly function via the actin-dependent and Fus1p-

dependent pathways ([248], [252]). It remains unclear how Kel1p interacts with Fus1p to promote Fus2p localization. However, the fact that Fus1p is necessary in secretory vesicle trafficking in polarized cells would imply that mutating *FUS1*, *KEL1* and *KEL2* genes affects both actin assembly necessary for secretory vesicle traffic and localization at the shmoo tip. On the other hand, residual Fus2p localization in *fus1Δkel1Δkel2Δ* mutants implies the presence of a third unknown redundant pathway ([248]).

In mating pairs, Fus2p not only binds Rvs161p but also recruits Cdc42p to the mating junction ([238], [253]). The Fus2p Dbl-homology domain interacts with activated GTP-bound Cdc42p via the Cdc42p rho-insert domain and focuses the G protein to the mating junction. It is postulated that the GTP-bound Cdc42p binds the Rvs161p-Fus2p heterodimer to promote fusion by catalyzing the exocytotic release of hydrolases into the mating junction that in turn promote CW degradation ([228], [246], [250]). Consistently, mutations of the Cdc42p rho-insert domain result in loss of Cdc42p-Fus2p interaction but do not affect the localization of Fus2p to the shmoo cortex or center of mating junction in prezygotes or unfused mating pairs. However, a point mutation on Cdc42p i.e. Cdc42-138 abolishes Fus2p binding hence decreased mating efficiency. Interestingly, Kel1p overexpression suppresses the Cdc42-138 mating defect, but is dependent on Fus2p ([248]). This suggests that Kel1p likely stabilizes the Cdc42-138 mutant, facilitating its interaction and function with Fus2p. While the Cdc42p focus localization at the mating junction is Fus2p-dependent, Cdc42p localizes at the shmoo tip independently of Fus2p ([249]). The contradicting Cdc42p-Fus2p interactions at the shmoo tip and mating junction are likely due to the differences in membrane curvature. While the shmoo tip is characterized by a positive membrane curvature that favors Rvs161p binding, cell-cell contact results in formation of a flat interface between the mating partners. Consequently, the flat interface results in a loss of membrane curvature and this would facilitate Cdc42p binding and focus at the mating junction ([249]).

Bilateral matings of the *fus2Δ* and *rvs161Δ* mutants i.e. (*MAT***a** *fus2Δ* x *MATα fus2Δ* or *MAT***a** *rvs161Δ* x *MATα rvs161Δ*) exhibit normal vesicle localization and clustering, but *rvs161Δ* mutants display elevated levels of vesicle accumulation at the mating junction (**Figure 7C**). This elevated vesicle accumulation likely results from a block in endocytosis ([228]). Indeed, Rvs161p has been implicated in regulating actin cytoskeleton organization and endocytosis ([254]). The *fus2Δ* and *rvs161Δ* mutants also exhibit electron-dense plaques and membrane invaginations at the mating junction. These plaques and invaginations are proposed to arise from the materials deposited by secreted vesicles due to Fus1p and Spa2p activities ([228], [246]). These findings therefore support the hypothesis that Fus1p and Fus2p function in parallel pathways, with the respective double mutants displaying stronger fusion defects than single mutants. Kel1p has been previously reported to partially suppress the *fus2Δ* mutations via Kel1p binding and inefficiently localizing Cdc42p to the shmoo tip ([248]). Alternatively, the partial suppression could be due to an unknown pathway, redundant to Fus2p, that is activated only upon Kel1p overexpression. Indeed, Kel1p overexpression also suppresses mating defects associated with deletions of *SPA2* ([255]).

Nonetheless, bilateral matings of *fusΔ* mutants display several other phenotypes. First, they contain extended regions of cellular apposition suggesting that the partner cells have been in close contact without fusion for a long time (**Figure 7C**). Secondly, *fusΔ* single deletion mutants display partial *fusΔ* zygotes characterized by partial PM fusion that permits karyogamy despite the presence of CW material at the mating junction. This suggests a leaky phenotype in which localized CW breakdown and PM fusion occurs while most of the CW at the cell-cell contact site remains intact. Consistently, remnant CW material at the mating junction is observed in partial *fusΔ* zygotes. Cytoplasmic mixing and nuclear fusion can still take place in such prezygotes resulting in budding off of diploid daughter cells ([228]). Notably, this leaky phenotype is proposed to result from functional redundancy of Fus1p and Fus2p such that the presence of one protein can functionally compensate for the other, albeit less effectively ([228], [238]). On the other hand, full *fusΔ* mutants are characterized by the presence of double CW material at the mating junction and a complete block in PM fusion. These mutants are often referred to as early prezygotes due to fact that fusion is arrested in an earlier CW remodeling step. Interestingly, majority of the full *fusΔ* zygotes do not transition to partial *fusΔ* zygotes over extended periods of mating. Instead, both mating partners may re-enter the cell cycle and through budding, produce haploid daughter cells called cytoductants ([220], [228]). Recent studies further postulate that CW degradation at the cell-cell contact site is driven by the contact-dependent increased concentration of CW degrading enzymes

due to reduced diffusion ([256]). However, this is likely insufficient to drive fusion and additional factors such as membrane curvature and localization of Cdc42p to the mating junction may be additional necessary regulators of CW remodeling and PM fusion.

2.3.2.2 Chs5p

During mating, cells alter and synthesize new CW and PM material in order to accommodate the asymmetric polarized growth. In particular, the shmoo CW is characterized by increased chitin deposition at the subapical portion ([257]). Chitin constitutes an important structural component of the yeast CW ([258]). Moreover, treatment of WT cells with Calcofluor, a substance that binds to chitin and alters its structure, strongly reduces mating in these cells, suggesting that chitin participates in the mating process ([259]). During pheromone response and mating, chitin synthase III (CSIII) encoded by *CHS3/4/5* and *CHS6* genes, is responsible for chitin synthesis ([258], [260],[261]). Although other Chitin synthases including CSI and CSII encoded by *CHS1* and *CHS2* respectively, exist, only CSIII is required during mating ([261], [262]). Intriguingly, expression of Chs1p but not Chs3p is highly pheromone-dependent ([258], [263]). Chs3p is mainly localized at cortical sites of polarized growth as well as cytoplasmic patches ([260]). These patches co-localize with a Chitin-synthase related protein 5 (Chs5p) and are affected by Myo2p mutations, suggesting that the cortical localization of Chs3p is mediated by Chs5p and the actin cytoskeleton ([260]).

Chs5p is a neurofilament-like protein that forms part of the exomer complex. This complex mediates export of proteins such as Chs3p from the Golgi to the PM ([259]). Chs5p is constitutively expressed in vegetative and mating cells indicating its general role in chitin synthesis. During pheromone treatment, *chs3Δ* mutants portray a defect in chitin synthesis implying that Chs3p is the CHSIII catalytic subunit while Chs5p functions as a regulator of the CHSIII-mediated chitin synthesis ([259]). Indeed, *chs5Δ* null mutants display reduced chitin levels at the shmoos in addition to an aberrant shmoo morphology. Strikingly, *chs5Δ* null mutants exhibit a reduced fusion efficiency with mutant cells accumulating *fusΔ*-like prezygotes at the mating junction. Notably, the *chs5Δ* mutants display no cytoplasmic mixing as observed in the partial *fusΔ* mutants, suggestive of a complete CW remodeling defect ([259]). Mating crosses between *fus1Δfus2Δ* mutants and *chs5Δ* mutants display enhanced fusion defects as compared to *fus1Δfus2Δ* mutants crossed to WT cells. The former crosses have a 0.2% frequency of diploid formation and no tri-lobated zygotes are formed ([259]). This indicates that Chs5p activity requires the activity of Fus1p and/or Fus2p. Indeed, overexpression of either *FUS1* or *FUS2* can partially rescue the *chs5Δ* mating phenotype. On the contrary, *CHS5* overexpression does not rescue the *fus1Δfus2Δ* mating defect and overexpression of the MAPK *FUS3,* does not rescue the *chs5Δ* phenotype ([259]). Overall, these findings point to the functional similarities among the Fus1p, Fus2p and Chs5p and imply that *CHS5* does not function redundantly to *FUS1* and/or *FUS2*. Nevertheless, Chs5p possibly functions downstream of Fus3p but upstream of Fus1p and Fus2p such that overexpression of the either Fus1p or Fus2p can rescue an upstream effect.

While it remains unclear how Chs5p facilitates fusion, one model proposes that the protein is involved in the secretory transport of Chs3p as well as transport of other components of the fusion machinery to the PM. Indeed, Chs5p cytoplasmic patches co-localize with Kex2p, a late Golgi-protease that has been implicated in fusion ([260], [264], [265]).

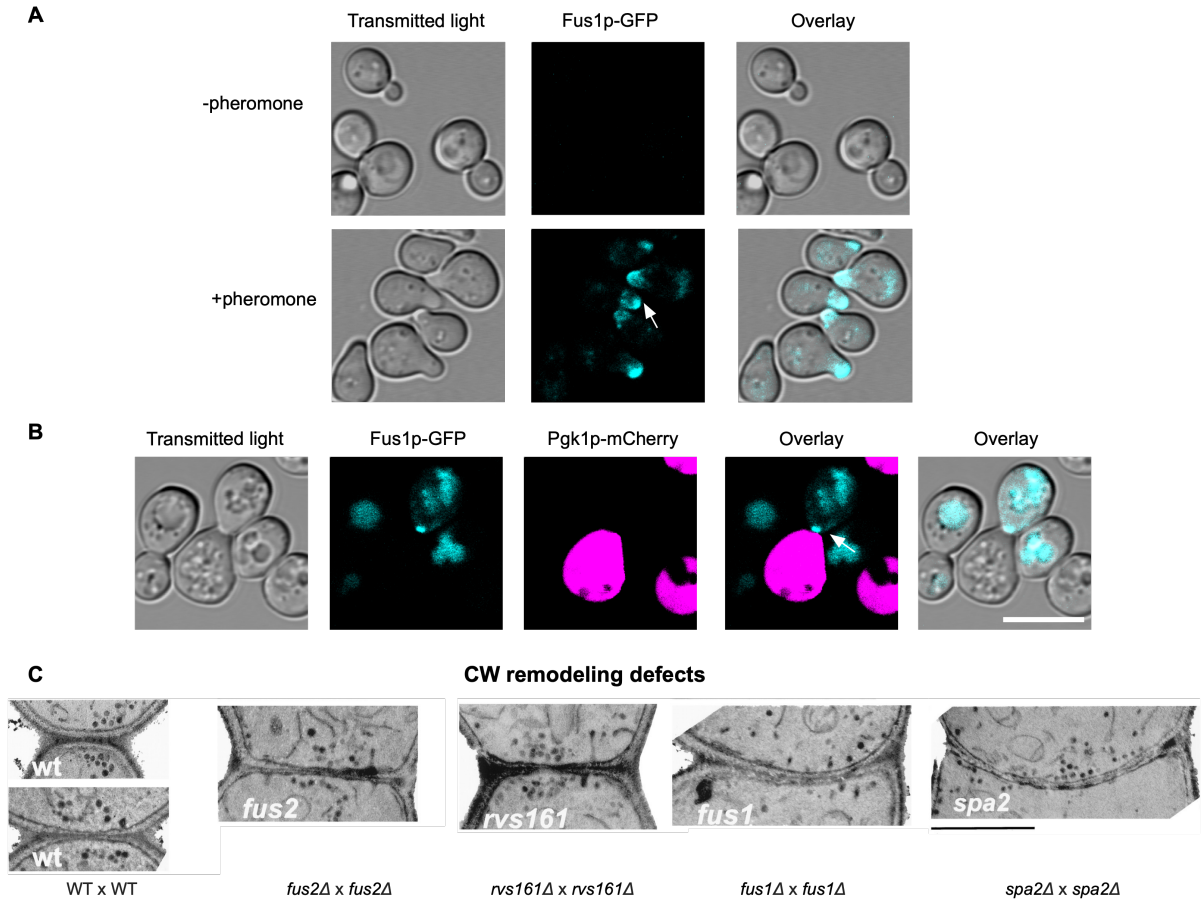

Figure 7: Representative images of mutants exhibiting CW remodeling defects. (**A**) Expression of the CW remodeler Fus1p is pheromone dependent. Fus1p is expressed only upon pheromone treatment and is localized at the shmoo tip. (White arrow shows the Fus1p shmoo tip localization). (**B**) Fus1p is localized at the mating junction of an unfused mating pair in which PM fusion has not occurred (no Pgk1p-mCherry transfer to the mating partner). Fus1p is localized as a distinct puncta at the mating junction. Scale bar= 5 µm. (**C**) Electron micrographs of representative images of CW remodeling defects. Bilateral matings of respective CW remodeling mutants and their defects in vesicle accumulation at the mating junction. In comparison to WT mating pairs, *fus2Δ* and *rvs161Δ* mutants exhibit CW remodeling defects characterized by vesicle accumulation at the mating junction. These vesicles are lacking in *fus1Δ* mutants while they appear dispersed in *spa2Δ* mutants. Note the extended zones of cell-cell contact especially in the *fus1Δ* and *spa2Δ* mutants. Figure 7C modified from ([228]).

2.3.3 PM fusion

Following CW remodeling, the two PMs are closely apposed and separated by an ~8 nm gap ([266]). The membranes then rapidly fuse generating a fusion pore that upon expansion, permits cytoplasmic content mixing ([267]). The presence and activity of various membrane proteins as well as the PM composition facilitate an efficient PM fusion process.

2.3.3.1 Prm1p: An important component of the PM fusion machinery

Prm1p, a highly Pheromone-Regulated Membrane protein (PRM), is the first protein implicated to have a direct role in PM fusion ([266]). Identified through a reverse genetics approach, Prm1p is a 115kDa glycoprotein consisting of 4 trans-membrane domains (TMDs) with 14 N-glycosylation sites ([268], [269]). Prm1p exists as a disulfide-linked homodimer with 4 cysteine residues present in the extracellular loops. Cys_{120} in loop1 and Cys_{545} in loop2 are indispensable for disulfide crosslinks formation and are necessary for the Prm1p fusion activity. Prm1p expression is pheromone-dependent and the protein localizes at the mating junction before PM fusion. During PM fusion, Prm1p is retained at the junction after which it is translocated to the vacuoles once the mating

process is completed ([268]). Interestingly, Prm1p homologs in *Schizosaccharomyces pombe* and *Candida albicans* are necessary for fusion, suggesting a functional conservation across different fungal species ([270]).

Consistent with its localization pattern, bilateral matings of *prm1Δ* mutants (*MAT***a** *prm1Δ* x *MATα prm1Δ*) exhibit a significant reduction in fusion with mutants displaying various phenotypes. First, *prm1Δ* mutants have a delayed fusion due to an initial reduction in the fusion pore permeance ([271], [267]). Secondly, they display a partial fusion defect with ~40-60% of cells fusing successfully ([266], [271]). Of the fusion arrested mating pairs, ~20% lyse. The lysis is PM contact-dependent as demonstrated by reduced lysis in *prm1Δfus1Δ* mutants and a complete elimination of lysis in *prm1Δfus1Δfus2Δ* triple mutants ([269]). Consistent with delayed fusion, *prm1Δ* mating pairs contain cytoplasmic fingers or bubbles characterized by a PM-enclosed cytoplasm of one cell pushing into the other mating partner (**Figure 8**) ([266], [269], [272]). The cytoplasmic fingers vary between 1- 4 µm long. Notably, formation of cytoplasmic fingers precedes both fusion and lysis with the two events occurring with similar kinetics ([271]). It is therefore likely that the fingers are formed due to a delay in PM fusion after a completed CW remodeling step ([269]). Consequently, these arrested mating pairs are generally referred to as late prezygotes because they are formed once CW remodeling is complete. Occasionally, prezygotes containing fingers may proceed to fusion when rescued by a Prm1p-independent pathway. Indeed, such have been reported in WT mating pairs suggesting that finger formation likely occurs during a delay in PM fusion. However, in *prm1Δ* mating pairs, most late prezygotes are arrested with cytoplasmic fingers confirming that it is an end point phenotype that cannot proceed to fusion ([269]).

Furthermore, *prm1Δ* prezygotes with fingers can either lyse immediately or continue to project into the partner cell depending on the direction of the osmotic gradient. Fingers mostly emanate from the cell with a higher osmotic pressure but do not necessarily lead to lysis as most cells with fingers do not lyse. Notably, the cell invaded with the long fingers lyses earlier than the invading cell, suggesting a possible exerted mechanical force on the invaded cell that facilitates its lysis. Interestingly, it has been reported that the invading cell can survive by reorienting its growth axis and attempting to bud or mate with another partner. Lysis events involving micro-fingers have also been reported. These occur within the same time in both cells, and similarly to the *prm1Δ*-dependent lysis, cannot be rescued by osmotic balance ([269], [272]). It is therefore unlikely that the osmotic pressure from both cells alone can drive fusion in WT cells. Instead, it would possibly ensure a closer PM apposition but still require the action of the fusion machinery to bring about complete fusion ([269]). Similarly to other fusion genes, matings between *prm1Δ* mutants and WT cells fuse normally, indicating that Prm1p can sufficiently perform its function when present in one mating partner.

Overall, these studies highlight the necessity of Prm1p in the PM fusion step. The presence of unfused mating pairs indicate that the fusion machinery is indeed dysregulated in *prm1Δ* mutants. Nonetheless, the fact that about 50% of the cells with *prm1Δ* mutations successfully fuse suggests that the Prm1p is not the *bona fide* fusogen. Alternatively, Prm1p is a fusogen but there exists a Prm1p-like protein that is functionally redundant to Prm1p, such that absence of one results in the activation of the other. This is however unlikely since *prm1Δ* mutants attempt to fuse but lyse. Prm1p could therefore be involved in priming the PMs for fusion by stabilizing the fusion machinery. Once a stable fusogenic machinery is engaged, cells proceed to fusion. Indeed, the well-studied viral fusogens such as HA fuse the membranes via its amphipathic fusion peptide that contains intrinsic membrane destabilizing properties ([40]). Arguably, the observed lysis in the *prm1Δ* mutants could result from a mis-regulated membrane destabilizing fusion machinery ([269]). For the unlysed and fused cells, it is likely that the same machinery is quickly rescued by a Prm1p-independent redundant pathway.

2.3.3.2 Fig1p: The role of Ca^{2+} ions in PM fusion

Following the identification of *FUS* genes, a subsequent screen of pheromone-regulated genes led to the identification of Factor-Induced genes (FIG) *FIG1*, *FIG2*, *FIG3*/*KAR5* and *FIG4*. While the bilateral matings of respective *FIG* gene deletion mutants exhibited a decrease in mating efficiency, bilateral matings of *fig1Δ*, *fig2Δ*, and *fig4Δ* displayed abnormal cell polarization and zygote morphologies. The *fig3* mutants on the other hand displayed nuclear fusion defects, consistent with

a role in karyogamy ([273]). Of interest is Fig1p whose gene deletion mutants display a cell fusion defect characterized by cytoplasmic fingers, similar to those observed in *prm1Δ* mutants ([271], [273]).

Fig1p is a pheromone induced tetra-spanning membrane protein with two extracellular loops (ECL1 and ECL2) and cytoplasmic N and C-termini. Remarkably, Fig1p contains the conserved claudin-like GLWxxC(8-10 aa)C consensus motif at its ECL1, suggesting possible structural similarities with mammalian claudins ([273], [274]). The Fig1p GxxGxC(8-20 aa)C claudin-like motif has also been reported in the *Schizosaccharomyces pombe* Dni1p and Dni2p proteins that have been implicated in fission yeast fusion ([275], [276]). The conserved cysteine residues are particularly necessary in mediating protein function and stability. This similarity to mammalian claudins has therefore led to the classification of Fig1p, Dni1p and Dni2p as fungal claudin-like proteins ([276]). Interestingly, the claudin-like motif has also been reported in the tetra-spanning *SUR7*-family proteins consisting of the paralogous proteins Sur7p, Fmp45p, Ynl194cp and Pun1p ([277], [278]). Fig1p localizes at the shmoo tip in pheromone treated cells as well as the mating junction. Once PM fusion is complete, Fig1p localizes at the neck of the mating bridge after which it is translocated to the vacuoles once the mating process is complete. Functionally, Fig1p has been implicated in cell polarization and regulation of the low affinity Ca^{2+} influx system (LACS) that is necessary for maintaining cell viability against high pheromone doses ([271], [273], [279]).

Consistent with its localization profile, bilateral matings of *fig1Δ* mutants display ~20-25% fusion defect. Of the fusion arrested mating pairs, ~10% exhibit cytoplasmic fingers similar to those observed in *prm1Δ* mutants, and ~6% lyse (**Figure 8**) ([271]). Similarly to *prm1Δ* mutants, the *fig1Δ* unilateral defects are less severe compared to the bilateral defects. Depletion of extracellular Ca^{2+} ions results in a slight enhancement of the *fig1Δ* fusion defect and the cells fuse with ~60% fusion efficiency. Surprisingly, bilateral matings of *prm1Δfig1Δ* mutants display a significant fusion defect with ~10% fusion efficiency and the majority of the cells remain unfused but do not proceed to lysis. However, upon Ca^{2+} depletion, a significant number of mating pairs lyse with enhanced lysis observed in *prm1Δfig1Δ* mutants as compared to *prm1Δ* mutants. Addition of extracellular Ca^{2+} rescues lysis in both categories of mutants ([271]). The lack of enhanced fusion defect upon Ca^{2+} ions depletion in *fig1Δ* mutants rules out the likelihood of direct involvement of Ca^{2+} ions in PM fusion. However, the fact that the enhanced cell lysis phenotype in *prm1Δfig1Δ* mutants is rescued by extracellular Ca^{2+} ions demonstrates; (i) the role of Ca^{2+} ions in membrane repair, (ii) corroborates the possible Prm1p role in stabilizing the membrane. It is therefore likely that Fig1p regulates Ca^{2+} ions uptake that is necessary in maintaining membrane fidelity throughout the fusion process. However, the absence of membrane repair in *fig1Δ* mutants points to the presence of additional factors that regulate membrane fidelity even in the absence of Ca^{2+} ions. Additionally, the fact that Ca^{2+} ions supplementation only rescues lysis in *prm1Δfig1Δ* and *prm1Δ* mutants likely indicates that the Ca^{2+}-dependent membrane repair mechanism is activated upon *PRM1* gene deletion.

As previously mentioned, Fig1p portrays structural similarities to mammalian claudins that reside and regulate tight junction permeability and barrier function ([280], [281]). It is therefore plausible that, in addition to its role as an extracellular Ca^{2+} uptake regulator, Fig1p exerts a structural role at the mating junction. Prior to PM fusion, Fig1p possibly facilitates the tight membrane apposition, an indispensable step in PM fusion, while acting as a membrane barrier that prevents leakage of molecules into the intercellular space ([274], [282]). In addition, the presence of cytoplasmic fingers in *fig1Δ* mutants suggests a possible role of Fig1p in maintaining a proper CW and membrane organization during the mating process ([271]). Indeed, the Fig1p structural homologs *S. pombe* Dni1p has been implicated in a similar function ([275]). Finally, deletion of *FIG1* abolishes LACs that is required in mating conditions ([273], [279]). Indeed, the activity of the polarization machinery as well as the CW remodelers (Fus1p and Fus2p) is Ca^{2+}-dependent. It is therefore plausible that *fig1Δ* mutants exhibit altered intracellular Ca^{2+} ion levels that in turn affect the overall activity of other proteins ([273], [282]).

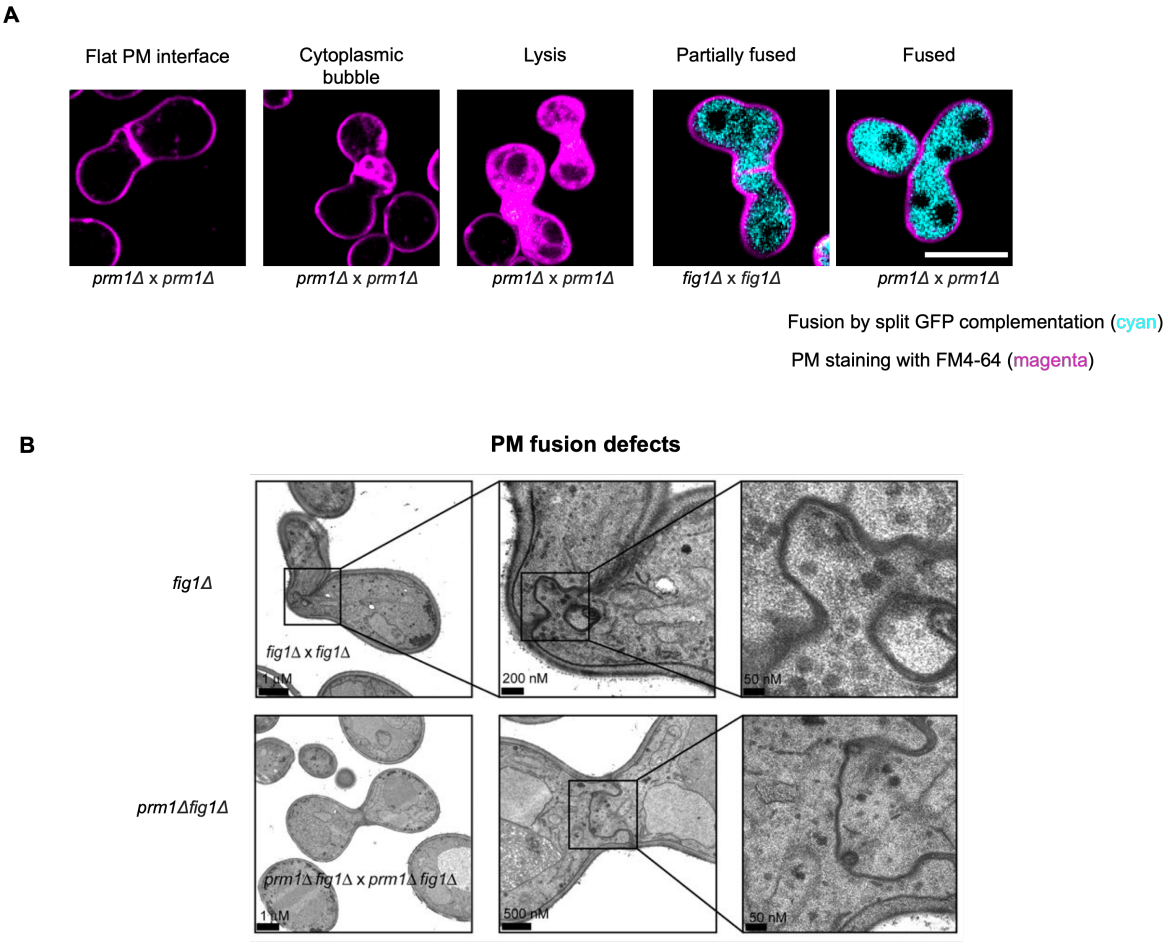

Figure 8: Representative images of PM fusion defects in *prm1Δ* and *fig1Δ* mutants. (**A**) Bilateral matings of *prm1Δ* and *fig1Δ* mutants result either in fusion or arrest as unfused mating pairs with a flat PM interface, cytoplasmic bubbles or undergo lysis. A flat PM interface is proposed to indicate an early prezygote with an intervening CW material. Mating pairs that form cytoplasmic bubbles or lyse are referred to as late prezygotes because they form after the CW has been degraded. The partially fused phenotype is observed in *prm1Δ* and *fig1Δ* mutants and suggests PM fusion and pore formation while degradation of the intervening CW is incomplete. Scale bar= 5 µm. (**B**) Electron micrographs of the cytoplasmic bubble formation phenotype. Bilateral matings of *fig1Δ* and *prm1Δfig1Δ* mutants result in PM fusion arrest and formation of cytoplasmic bubbles with no intervening CW material. Figure 8B modified from ([271]).

2.3.3.3 Kex2p: An unknown Kex2p substrate(s) interacts with Prm1p

Kex2p (Killer Expression defective 2) is a Ca^{2+}-dependent Golgi-resident endopeptidase that cleaves protein sequences at a dibasic Lys-Arg sites and Arg-Arg sites ([264], [283]). Kex2p consists of a N-terminal domain homologous to the subtilisin family of serine proteases, a trans-membrane domain and a highly acidic C-terminus ([284]). Kex2p is localized in multiple, discrete cytoplasmic patches that correspond to late Golgi. However, Kex2p is not incorporated into secretory vesicles suggesting that it is a Golgi resident protein ([264]). Its closely related protein, Kex1p, is a Golgi-associated exopeptidase that functions after the Kex2p protease activity. Kex1p processes the C-terminus of the generated N-terminal fragment, removing the Lys or Arg sequences ([285], [286]).

In addition to cleaving the M_1 killer toxin, Kex2p is involved in the proteolytic cleavage of prepro- *α*-factor to a mature pheromone ([284]). Its role in *MAT***a** cells had however remained elusive until a genetic screen to identify enhancers of *prm1Δ* phenotype was carried out ([272]). Mating crosses between *MAT***a** *kex2Δ* mutants and WT *MATα* cells display a slight fusion defect that can be suppressed by osmotic support. This suggests a possible *kex2Δ*-induced CW stress similar to that

observed in other CW remodeling mutants such as *fus1Δ* and *fus2Δ* ([228]). However, mating crosses between *MAT***a** *kex2Δ* mutants and *MATα prm1Δ* mutants display a 2-fold decrease in the fusion efficiency. Interestingly, a 4-fold decrease in fusion efficiency occurs when *MAT***a** *kex2Δprm1Δ* mutants are crossed to *MATα prm1Δ* mutants. These findings suggest that the *kex2Δ* fusion defect is unilateral and that *KEX2* deletion enhances the *prm1Δ* fusion defect particularly when in *trans* to the *prm1Δ* mutation. Notably, the *kex2Δ* fusion arrested pairs display extracellular membrane-bounded cytoplasmic blebs that are CW embedded and separated from both PMs by ~8 nm width ([272]).

It is therefore plausible that a synergistic interaction between *KEX2* and *PRM1* exists with the likelihood that Kex2p acts on an unknown substrate that is part of the fusion complex with Prm1p. Deletion of both genes especially in *trans* greatly affects PM fusion, suggesting that Kex2p or its unknown substrate acts on the same step as Prm1p in the PM fusion process. Therefore, for efficient fusion to take place, either protein should be present in at least one mating partner. However, the Kex2p and Kex1p substrate(s) and how it interacts with Prm1p during PM fusion remains eluded. Finally, the fact that a small percentage of cells (~15%) fuse in *kex2Δprm1Δ* bilateral matings suggests the presence of unidentified factors that promote PM fusion ([272]).

2.3.3.4 Ergosterol genes: The PM sterol composition affects fusion

The yeast PM is ergosterol and sphingolipid rich and has a high sterol-protein and sterol-phospholipid ratio when compared to other membranes. Phosphatidylserine (PS) is the most abundant glycerophospholipid constituting ~34% ([287], [288], [289]). Furthermore, the yeast PM is characterized by an asymmetrical composition that is comprised of phosphatidylserine (PS), phosphatidylethanolamine (PE) and phosphatidylinositol (PI) in the inner leaflet, and sterols and sphingolipids in the outer leaflet of the lipid bilayer ([287], [290]). The membrane lipid composition plays an integral role in determining membrane fluidity, thickness, curvature and permeability ([291]). The high ergosterol content and PM protein composition have particularly been implicated in determining membrane flexibility ([292]). Additionally, the interactions between PM sterol and sphingolipid long acyl chains often result in formation of liquid-ordered phase membrane microdomains referred to as lipid rafts ([293]).

Upon pheromone induction and polarized growth, the yeast PM undergoes reorganization. In particular, the PM alters its composition by increasing the ergosterol content while maintaining its phospholipid content ([241]). These PM changes result in the clustering of proteins and lipids raft microdomains at the shmoo tip. Indeed, proteins such as Fus1p have been shown to associate with lipid rafts, thus contributing to its polarized secretion and retention at the shmoo tip ([241]). Ergosterol biosynthesis is a multi-step process whose final steps are dependent on the biosynthesis enzymes encoded by the *ERG2*, *ERG3*, *ERG4, ERG5* and *ERG6* genes. Interestingly, the respective proteins Erg2p, Erg3p, Erg4p and Erg6p have all been implicated in PM fusion ([291], [294], [295]).

Firstly, Erg2p, Erg3p and Erg6p are necessary in the recruitment of the scaffold protein Ste5p, a key protein in the activation the MAPK pathway, to the PM. Secondly, consistent with the formation of lipid rafts that facilitate protein clustering at the mating junction, all the four proteins promote fusion independently of Prm1p. Indeed, bilateral matings of respective *erg2Δ*, *erg3Δ* and *erg6Δ* mutants result in delayed fusion, increased accumulation of early prezygotes with intervening CW material, late prezygotes in which the intervening CW material has been removed, and also haploid cells that do not engage with the opposite mating type cell. Notably, bilateral matings of *erg6Δ* mutants not only portray a delay in fusion, but mating pairs undergo lysis, albeit a small proportion, suggesting an Erg6p role in PM fusion. Interestingly, Prm1p is normally expressed and localized to the mating junction of these mutants, suggesting that the Erg proteins and Prm1p function in independent pathways ([291]). Consistently, deletion of *PRM1* in *erg3Δ* and *erg6Δ* mutants results in an additive phenotype, with bilateral matings of *erg3Δprm1Δ* and *erg6Δprm1Δ* mutants mainly accumulating late prezygotes and little to no fusion. In these double mutants, fusion can be partially restored upon expression of Prm1p from a strong promoter, indicating the fusion dependency on Prm1p ([291]). Intriguingly, increasing the mating duration and a higher pheromone response in

erg3Δ and *erg6Δ* mutants can partially rescue the fusion defect, suggesting a delayed initiation of the fusion process.

Similarly, *erg4Δ* mutants are defective in CW remodeling step with the bilateral matings exhibiting a 4-fold increase in fusion defects than the unilateral matings ([294]). Additionally, the *erg4Δ* mutants are defective in shmoo and mating pair formation with <10% of cells forming shmoos. Contrary to the pheromone signaling defect observed in other *ergΔ* mutants, the *erg4Δ* shmoo and mating pair formation defect is as a result of the accumulation of an intermediate sterol, ergosta-5,7,22,24(28)-tetraenol, that functions as the Erg4p substrate. Compared to ergosterol, ergosta-5,7,22,24(28)-tetraenol is characterized by an additional double bond in its sterol aliphatic chain that may contribute to increased PM rigidity. Consequently, *erg4Δ* mutants fail to properly remodel their cell shape and form shmoos in response to pheromone ([294]). This defect can however be rescued by ergosterol supplementation, suggesting that the shmoo formation is largely ergosterol-dependent. Surprisingly, protein and lipid polarization remain unaffected in *erg4Δ* mutants, indicating that polarizations events likely occur via distinct ergosterol-independent mechanisms and are not necessarily facilitated by shmoo formation. Notably, removal of the Erg4p sterol intermediate restores fusion of *erg4Δ* mutants to WT levels, further corroborating that the *erg4Δ* mating defects are majorly due to ergosta-5,7,22,24(28)-tetraenol accumulation. In concordance with other *ergΔ* mutants, deletion of *PRM1* enhances the *erg4Δ* fusion defect, indicative of an additive phenotype. This therefore suggests that Erg4p and Prm1p operate in distinct steps in the mating pathway ([294]).

Taken together, these findings demonstrate the importance of a proper PM sterol composition during mating. Indeed, pheromone signaling may depend on a proper PM balance between ergosterol and sphingolipids. In particular, shmoo formation and fusion is largely dependent on PM ergosterol composition. While protein and lipid secretion and polarization may remain unaffected in *ergΔ* mutants, it is plausible that protein retention at the mating junction is ergosterol-dependent. Consistently, sphingolipids and ergosterol are reportedly crucial for protein delivery particularly in the secretory pathway as well as their retention at the PM. Affecting their synthesis and by proxy balance, may thus affect protein targeting and PM, a phenomenon that is crucial in the mating pathway ([241], [296]). Alternatively, the Ergosterol biosynthesis proteins could be important co-factors or interactors to proteins necessary in the fusion process such that their absence results in altered protein dynamics. Indeed, Erg4p has been suggested to interact with the PAK kinase Ste20p necessary in MAPK pathway signaling cascade initiation ([295]). Lastly, the overall lipid bilayer properties and propensity to fuse are dependent on both the sterol and glycerophospholipids composition and structure. This has indeed been depicted in SNARE proteins and viral fusion peptides studies ([297], [298], [299]).

2.3.3.5 PM fusion: A present day enigma

All these findings point to the direct involvement of Prm1p in the PM fusion step. Fig1p, Kex2p, Erg3p, Erg4p and Erg6p all seem to mainly enhance the *prm1Δ* mating defect. In particular, the lysis events observed in *prm1Δ* mutants strongly suggest a Prm1p role in stabilizing the fusion complex. However, the residual fusion observed in *prm1Δ* mutants implies genetic redundancy in the fusion pathway and the presence of a Prm1p-independent pathway. In addition, unilateral mutations often present minor fusion defects as compared to the bilateral mutations. This indicates that gene expression on one mating type is sufficient in carrying out the protein function across the mating junction. In the case of Prm1p, this can be argued that expression of the tetra-spanning protein on one mating partner sufficiently spans and engages both membranes while stabilizing the fusion machinery. Indeed, the fact that Prm1p exists as a homodimer would suggest that each Prm1p dimer simultaneously interacts with two binding partners on identical binding sites, resulting in a cooperative binding of the fusion machinery to sufficiently fuse the two bilayers ([268]). However, how the Prm1p-stabilized fusion machinery carries out PM fusion remains to be investigated. Another hypothesis is that Prm1p functions as an activator of fusion competence that tethers the two membranes before the fusogen/fusogenic complex is engaged. By inserting its hydrophobic extracellular loop into the apposed membrane, hydrophobic interactions between the Prm1p hydrophobic extracellular loop and the membrane lipids would favor membrane curvature and subsequent fusion ([268]).

Finally, studies on *bona fide* fusogens such as the viral fusogens, SNAREs, EFF-1 and HAP2 have led to the general conclusion that fusion proceeds through formation of a hemifusion intermediate ([21], [83]). Whether a similar stepwise fusion process occurs during yeast PM fusion and whether fusion involves one or more proteins is yet to be unraveled. Notably, while the proteins highlighted above can be classified as components of the yeast fusion machinery, the identity of the fusogen/fusogenic complex remains elusive. Further studies are required to elucidate not only the *bona fide* fusogen, but also the molecular mechanism of yeast PM fusion and pore formation.

2.3.4 Fusion Pore formation and expansion

Once PM fusion occurs, an initial nascent pore forms with a burst and constantly expands to allow content mixing. Interestingly, formation of multiple nascent pores has been previously reported, but it remains unclear how many fusion pores are formed during the PM fusion process ([267]). Additionally, It is unknown whether Prm1p is directly or indirectly involved in fusion pore opening. Nonetheless, once a nascent pore (s) is formed, pore expansion allows the transition from a nanometer-size to a micrometer range that permits cytoplasmic content mixing. So far, the CW remodeler Fus1p has been implicated in fusion pore expansion. Consistently, Fus1p is retained at the mating junction once PM fusion is complete, suggesting its possible role in facilitating fusion pore expansion ([267]). Additionally, the continuous pore expansion is indicative of a continuous CW remodeling process to accommodate the expanding zygote. Indeed, cell-fusion associated vesicles remain localized at the newly formed pore, and /or close to the peripheral CW remnants until karyogamy ensues ([228]). Vesicle clustering and accumulation of CW remnant material at the mating junction in pre-karyogamy zygotes thus indicates the retention of the fusion machinery at the mating junction during pore expansion. Consistently, once karyogamy has taken place, vesicle clustering disappears and rare CW remnants are observed ([228]). It is therefore plausible that Fus1p not only facilitates vesicle clustering during pore expansion, but also anchors the Fus2p-Rvs161p and Cdc42p complex necessary in vesicle exocytosis and release of CW remodeling enzymes and components of PM fusion machinery. Vesicle clustering would thus result in increased local concentration of CW hydrolases and fusion machinery that facilitates local CW removal and continuous PM fusion. Indeed, the Fus2p-Rvs161p and Cdc42p complex has been implicated in vesicular exocytosis at the mating junction. Both Fus2p and Cdc42p co-localize at the mating junction and to the remnant CW after PM fusion ([228], [248], [249], [250]). Furthermore, the complex would facilitate pore expansion mainly due to the preference of Rvs161p for curved membranes generated during this process ([247], [254]). A similar observation has been reported in syncytium formation whereby overexpression of the curvature generating protein (CGP) GRAF1 that contains a BAR (Bon/amphiphysin/Rvs) domain promotes syncytium formation ([300]). Finally, *prm1Δ* mutants portray a reduced fusion pore permeance and expansion, suggesting a possible involvement of Prm1p in pore formation and expansion ([267]). All in all, these findings demonstrate the multi-functionality of the yeast mating proteins across the different steps of the mating pathway.

2.3.5 Regulation of the yeast mating pathway

Despite its importance in ensuring genetic recombination and diploid cell formation, the yeast mating process is a risky, energy-demanding process that requires a high degree of regulation at various levels. Firstly, pheromone secretion and response leads to activation of the MAPK signaling pathway. High levels of pheromone are required to ensure a sustained pheromone response ([220] [221]). Once the MAPK signaling pathway has been activated, the cell must simultaneously inhibit the invasive growth pathway that shares the MAPK components with the mating pathway (**Figure 6**). Activation of the mating-responsive genes results in polarized growth towards the mating partner and along the pheromone gradient. Once cell-cell contact is established, localized CW degradation must be carefully regulated to avoid undesired cell lysis. As previously discussed, membrane merger does not occur spontaneously but rather involves the activity of specialized proteins that constitute the fusion machinery. Additionally, a proper lipid bilayer composition is required to ensure PM fusion. The final level of regulation occurs during karyogamy. However, this level is beyond the scope of this thesis and will not be discussed. Nonetheless, it is apparent that yeast cells regulate the mating process to ensure fusion fidelity and generation of diploid zygotes.

2.3.5.1 Regulation of the MAPK signaling pathway: Mating versus invasive growth

The MAPK signaling pathway is not specific to the mating program. Instead, its components are shared with the invasive growth program upon nutrient starvation. Major upstream components such as the MAPK kinase kinase Ste11p, MAPK kinase Ste7p, and the two MAPK Fus3p and Kss1p are shared amongst the two programs (**Figure 6A**). In addition, the transcription factor Ste12p, that is directly activated by Fus3p or Kss1p, is required in both programs ([301], [302]). During pheromone response, Ste12p binds to gene specific pheromone response elements (PRE) resulting in expression of mating-responsive genes. However, during invasive growth, Ste12p activity is executed indirectly via activation of Tec1p transcription factor. Tec1p binds at Tec1-binding site (TCS) elements of invasive growth genes resulting in expression of genes necessary in invasive growth ([301], [302], [303]). Intriguingly, Tec1p transcription is dependent on pheromone presence and upstream MAPK signaling, consistent with the fact that *TEC1* contains numerous Ste12p-binding PRE elements at its promoter region ([303], [304]).

Compelling evidence indicates that program specificity is brought about at the level of the MAPK: Fus3p versus Kss1p. The physical occlusion model suggests that: in the presence of a mating partner and the downstream activation of the MAPK pathway, Fus3p negatively regulates the invasive growth program by sterically occluding Kss1p from undergoing phosphorylation. As a result, mating-responsive genes are activated. Consistently, Kss1p activates the invasive growth-responsive genes only when phosphorylated (**Figure 6A**) ([207], [214]). Additionally, pheromone signaling in *fus3Δ* mutants results in increased levels of Kss1p phosphorylation and activation of invasive growth genes ([305], [306], [307]). Interestingly, a small proportion of Kss1p has been shown to undergo phosphorylation during pheromone response. However, this phosphorylation does not activate the invasive growth program, suggesting the existence of additional suppressive mechanisms ([305], [308]). A second model proposes the existence of two separable and distinct MAPK cascades. However, this model remains irreconcilable with existing studies, suggesting the possibility that the degree of Fus3p and Kss1p phosphorylation dictates downstream program activation.

A second level of program specificity occurs at Tec1p phosphorylation. Upon pheromone treatment, Fus3p has been implicated to negatively regulate Tec1p-dependent invasive growth gene expression via Tec1p phosphorylation. Tec1p phosphorylation promotes its degradation, subsequently downregulating invasive growth gene expression (**Figure 6A**) ([214], [306], [307], [309]). The Fus3p-mediated suppression of Tec1p-dependent genes can however be rescued in *fus3Δ* mutants, further corroborating the finding that Fus3p downregulates Tec1p activity as well as its downstream targets ([214]).

Finally, Ste12p and by proxy Tec1p are suggested as possible contributors of program specificity. The specific binding of Ste12p at gene-specific PRE elements results in expression of mating responsive genes. Similarly, binding of Tec1p at TCS elements of invasive growth genes both in presence and absence of Ste12p, results in expression of invasive growth genes ([303]). It is therefore apparent that expression of pheromone-responsive genes is inhibited during invasive growth, and similarly no invasive growth genes are activated during pheromone response ([310], [311]).

2.3.5.2 Regulation of CW remodeling via the cell wall integrity (CWI) pathway

The yeast CW contributes to cellular shape and offers mechanical stability against environmental stress such as heat, drugs and polarization during budding or shmoo formation. The CWI pathway functions in repairing CW damage that may arise during normal cellular growth. The CWI pathway consists of five mechano-sensors; Wsc1p, Wcs2p, Wsc3p, Mid2p and Mtl1p. All five proteins consist of a single transmembrane domain and extracellular N-termini and small cytoplasmic C-termini ([312], [313], [314], [315]). By connecting with the CW polysaccharides or proteins, the extracellular N-terminus senses the CW changes and transduces the signal via the PM into the cytoplasm. While the Wsc1p and Wsc3p employ their N-terminal cysteine-rich lectin binding domain (CRD/WSC), Mid2p and Mtl1p contain a conserved N-glycosylated asparagine residue ([316], [317]). Their cytoplasmic C-termini mediate the CWI signaling pathway via interactions with

downstream effectors such as the GDP/GTP exchange proteins (GEPs) Rom2p and Rom2p, and the master regulator Rho1p ([318], [319]). Rho1p,a Cdc42p-related Rho-GTPase, subsequently activates the sole protein kinase C (Pkc1p), resulting in downstream activation of the CWI- MAPK cascade consisting of *BCK1*/*SLK1*, *MKK1*/*2* and *MPK1*/*SLT2* ([320], [321], [322]). Activation of the CWI- MAPK cascade subsequently activates the transcription factor Rlm1p that regulates the expression of CWI pathway genes involved in CW biosynthesis and cell cycle ([323], [324]). In addition to activating Pkc1p, Rho1p directly regulates CW β-glucan biosynthesis by activating the β-glucan synthase enzyme. Consistently, Pkc1p is localized at CW remodeling sites such as regions of polarized growth. However, upon CW damage, Pkc1p is re-localized to sites of damage where it elicits a localized response ([320], [325]). Null mutations of *PKC1* or components of the CWI- MAPK pathway are defective in stress tolerance resulting in cell lysis. Interestingly, in mitotic cells, the lysis defect can be rescued by growing cells in osmotic stabilizers such as 1M sorbitol ([314], [315]).

During pheromone response and mating, polarized growth is characterized by increased CW remodeling. To avoid lysis, mating cells activate the CWI pathway, but this activation is carefully regulated to permit fusion while preventing cell lysis. In mating cells, Wsc1p and Mid2p are the main mechano-sensors and the *mid2Δ* null mutants result in mating-induced death ([313], [314], [326]). The mating-induced death is due to unregulated fusion characterized by premature CW removal at the shmoo tip ([327]). Surprisingly, while the mating-induced death cannot be rescued by osmotic stabilizers, *mid2Δ* mutations can be suppressed by extracellular calcium supplementation, similarly to the calcium transporter *mid1Δ* mutations ([328]). Indeed, Mid2p contains a calcium binding domain, suggesting its possible calcium regulatory role during mating ([329]). Additionally, expression of a hyperactive Pkc1p (*PKC1*-R398P) that negatively regulates fusion can suppress the *mid2Δ* mutations ([330]). Consistent with a negative regulatory role of the CWI pathway, the *mid2Δ* mutations are suppressed by deletions of the CW remodelers *FUS1*, *FUS2*, *CDC42* and *RVS161*, suggesting that the two pathways function antagonistically. Indeed, in concert with the premature CW removal observed in *mid2Δ* mutants, all the four proteins (Fus1p, Fus2p, Cdc42p and Rvs161p) are localized at the shmoo tip or to the tip cortex in the case of Cdc42p, and to the mating junction where they promote CW removal ([228], [238], [248]). Furthermore, loss of *MID2* or *WCS1* suppresses the *fus1Δ* or *fus2Δ* fusion defect, indicating that that upstream components of the CWI pathway negatively regulates fusion ([327]).

It is therefore proposed that during mating, careful regulation of CW remodeling is achieved via a Mid2p-dependent localization of Cdc42p ([327]). To prevent unwanted CW removal before cell-cell contact is established, Mid2p facilitates the Cdc42p localization to the shmoo tip cortex, preventing it from co-localizing with the Fus2p-Cdc42p complex that would otherwise promote CW removal ([249]). Once cell-cell contact is established, Cdc42p is re-localized to a focus at the mating junction where it interacts with the Fus2p- Rvs161p complex. The interaction of the three proteins consequently activates the exocytosis of CW hydrolases- containing vesicles that promote localized CW removal ([327]). This re-localization is indeed down-regulated in the presence of the hyperactive Pkc1p, further corroborating that the CWI pathway prevents Cdc42p focus at the mating junction ([327], [330]).

All in all, the CWI pathway constitutes the only characterized pathway that negatively regulates fusion at the CW remodeling and possibly PM fusion steps. It is plausible that yeast cells employ other unknown regulatory mechanisms particularly at the PM fusion step. Importantly, for fusion to take place, a careful balance between CW removal and biosynthesis must be achieved.

2.4 Aim of this thesis

Cell-cell fusion remains a fundamental process in mammalian sexual reproduction and development. During fertilization, the sperm and egg merge their PMs to permit cytoplasmic mixing, nuclear fusion and generation of a diploid zygote. PM merger is an energetically demanding event that is mediated by specialized proteins known as fusogens ([3], [82]). Hitherto, the *bona fide* mammalian gamete fusogen remains elusive. Similarly in budding yeast *Saccharomyces cerevisiae*, haploid *MAT***a** and *MATα* cells fuse to generate a diploid zygote. The two cells secrete mating type-specific pheromones and express surface receptors to initiate the mating process. Binding of the pheromones to the receptors activates the MAPK signaling pathway leading to cell cycle arrest in the G1 phase and transcription of mating responsive genes ([331]), [330]). The cells undergo polarized growth along the pheromone gradient and towards the mating partner, generating mating projections or shmoos ([220]). Once cell-cell contact is established, the mating pair remodels its intervening CW giving rise to close PM apposition to ~8 nm distance ([228], [238]). This close PM apposition creates a short-lived and spatially-limited mating junction herein referred to as the "Fertilization Synapse". The two PMs then rapidly fuse generating a fusion pore which upon expansion, permits cytoplasmic content mixing and nuclear fusion.

So far, a handful of proteins that constitute the fertilization synapse have been identified. They include the CW remodelers Fus1p, Fus2p, Rvs161p, Cdc42p, Chs5p, and the proteins implicated in PM fusion such as Prm1p, Fig1p, Kex2p, Erg3p, Erg4p and Erg6p ([228], [271], [266], [294]). Notably, the *bona fide* fusogen or fusogenic complex is still unknown. The paucity of fertilization synapse constituents and lack of a detailed understanding of the molecular mechanism of yeast PM fusion formed the basis of this thesis. I aimed to employ two independent yet interrelated approaches to identify and characterize novel putative components of the yeast fusion machinery. Firstly, a completed proteomic analysis of yeast PM proteins upregulated during pheromone treatment identified ~20 pheromone-upregulated proteins with unknown functions in yeast mating. Working with the hypothesis that components of the yeast fusion machinery are both pheromone-upregulated and localized at the mating junction, I first focused on characterizing the localization profile of these proteins in pheromone-treated and mating conditions. Pun1p, a *SUR7*-family membrane protein with no known function in yeast mating, was highly expressed and localized at the mating junction ([277]). To determine whether Pun1p is a putative component of the fertilization synapse, I aimed at characterizing the expression and localization profile of Pun1p in mating conditions. The presence of Pun1p at the mating junction prior to CW remodeling and PM fusion, as well as its junction retention during PM fusion hinted that it is a novel constituent of the fertilization synapse. By employing gene deletion and gene overexpression approaches, this thesis aimed at further characterizing the function of Pun1p in mating conditions.

Secondly, generation of the temporal and spatially-limited fertilization synapse precedes PM fusion. Consequently, late intracellular and intercellular protein-protein interactions necessary for PM fusion likely to occur at the synapse. Determination of the synapse constituents thus provides a novel approach to identify putative components of the yeast fusion machinery. This thesis therefore aimed at developing a Horseradish peroxidase (HRP)-mediated proximity labeling approach coupled to mass spectrometry to identify novel putative constituents of the fertilization synapse ([332], [333]). As proof of principle, HRP- Fus1p recombinant protein was used to demonstrate the feasibility of this approach in pheromone-treated cells. The ultimate objective of this approach was to characterize the identified proteins via a variety of bioinformatics, proteomics, biochemistry and molecular genetics tools in order to fully elucidate their putative roles in yeast mating. Notably, this approach presents a novel means of mapping the yeast mating junction and may provide clues on the components of the yeast PM fusion machinery.

3 Materials and Methods

3.1 Materials and Instrumentation

3.1.1 Chemicals and buffers

Table 1 : Chemicals used in this thesis

Chemical	Manufacturer
Acetic acid	AppliChem
Acetone	Sigma-Aldrich
Acrylamide 4K-Solution (30%)	PanReac AppliChem
Agar	EMD Millipore Corp
Agarose	Invitrogen
Alpha factor	GenScript or synthesized in house
Ammonium sulfate	Carl Roth GmbH
Ampicillin	Gerbu
Bacto- Peptone	Difco
Beta Mercapto-ethanol	SERVA Electrophoresis GmbH
Biotin- AEEA-Phenol	Iris BioTech
Bromophenol blue	SERVA Electrophoresis GmbH
Coomassie Briiliant Blue R250	BioNol Feinchem.GmbH
D-Sorbitol	Sigma-Aldrich
Dimethyl sulfoxide (DMSO)	SERVA Electrophoresis GmbH
dNTPs	ThermoScientific
Dried skimmed milk powder	Sigma-Aldrich
EDTA	Sigma-Aldrich
EGTA	Sigma- Aldrich
Ethanol	J.T. Baker
Floro Orotic Acid monohydrate (5-FOA)	Formedium
G418 disulphate	Sigma-Aldrich
Glass beads	Carl Roth GmbH
Glycine	Carl Roth GmbH
HCl	VWR Chemicals
HEPES	SERVA Electrophoresis GmbH
Hydrogen peroxide	Carl Roth GmbH
Hygromycin	Formedium
Isopropanol	Sigma-Aldrich
KCl	Sigma-Aldrich
Lithium acetate	Sigma-Aldrich

Luminol solution	GE Healthcare
Methanol	Sigma-Aldrich
MgCl2	Sigma-Aldrich
Mowiol	Synthesized in-house
Na_2HPO_4	Sigma-Aldrich
NaCl	Sigma-Aldrich
NaF	Sigma-Aldrich
$NaH_2PO_4.H_2O$	Sigma-Aldrich
$NaHCO_3$	Sigma-Aldrich
NaN_3	AppliChem
NaOH	J.T. Baker
Nonidet-40 (NP-40)	Sigma-Aldrich
Nourseothricin	Sigma-Aldrich
PEG 3350	Sigma-Aldrich
Phenylmethylsulfonyl fluoride (PMSF)	Sigma-Aldrich
PIC	Sigma-Aldrich
Ponceau stain	Sigma-Aldrich
Potassium Chloride	J.T. Baker
Sodium ascorbate	Sigma-Aldrich
Sodium azide	SERVA Electrophoresis GmbH
Sodium dodecyl sulfate (SDS)	Sigma-Aldrich
Sodium Hydroxide	Carl Roth GmbH
TEMED	Carl Roth GmbH
Trichloroacetic acid (TCA)	Sigma-Aldrich
Tris	Carl Roth GmbH
Triton X-100	Carl Roth GmbH
Trolox	Santa Cruz Biotechnologies
Tween-20	Bio Rad
Yeast Extract	Formedium
YeastMaker ^{TM} Carrier DNA	Takara

Table 2: General buffers used in this thesis

General Buffers	Composition
4X SDS-PAGE sample buffer	250 mM Tris, 100 mM DTT, 6% SDS, 40% glycerol, 0.02% Bromophenol blue
Blocking solution	5% (w/v) milk powder, filled up with TBS
Coomassie Staining solution	0.15% Coomassie Brilliant Blue R-250, 12% acetic acid, 44% ethanol
Coomassie Destaining solution	50% (v/v) methanol, 10% (v/v) acetic acid filled up with ddH20
Spheroplasting buffer	20 mM HEPES, 1M Sorbitol
Lysis buffer	50 mM Tris, pH=8, 150 mM NaCl, 2 mM EDTA
PBS	137 mM NaCl, 2.7 mM KCl, 10 mM Na_2HPO_4, 1.7 mM NaH_2PO_4, pH=7.5
PEG solution	100 mM LiOAc, 10 mM Tris–HCl pH=8, 1 mM EDTA/NaOH pH=8, 40% PEG3350
Quenching solution	10 mM Sodium azide, 10 mM Sodium ascorbate, 5 mM Trolox
SDS Running buffer	25 mM Tris, 192 mM Glycine, 0.28% SDS
SORB	100 mM LiOAc, 10 mM Tris–HCl pH=8, 1 mM EDTA/NaOH pH=8, 1 M Sorbitol
TAE buffer	40 mM Tris, 20mM Acetate, 1mM EDTA, pH=8.6
TAF buffer	20 mM Tris-HCl pH=7.4, 20 mM NaN_3, 20 mM NaF in PBS
TBS	150 mM NaCl, 10 mM Tris, pH=7.5
TBST	150 mM NaCl, 10 mM Tris, pH=7.5, 0.025 % (v/v) Tween-20,
Transfer buffer	192 mM Glycine (15 g), 25 mM Tris (3 g), 0.04% SDS (0.4 g), 20% MeOH 200 mL, filled up with ddH_2O to 1L

3.1.2 Media

Table 3: Media used in this thesis

Media	Composition
LB	200 mM NaCl (10 g), 1% (w/v) bacto-tryptone (10 g), 0.5% (w/v) yeast extract (5 g), filled up with ddH_2O to 1L, pH=7.0
SC	6.7 g Yeast nitrogen base without amino acids (YNB), 590 mg Amino acids (AA) Mix, 40 mL sterile 50% Glucose (w/w)
SD	6.7 g Yeast nitrogen base without amino acids (YNB), defined Amino acids (AA), 40 mL sterile 50% Glucose (w/w)
SOC	10 mM NaCl (0.58 g), 2.5 mM KCl (0.19 g), 10 mM $MgCl_2$ (0.95 g), 20 mM glucose (3.6 g), 0.5% (w/v) yeast extract (5 g), 1% (w/v) Bacto-tryptone (10 g), filled up with ddH_2O to 1L, pH=7.0

YPD	1% (w/v) 10 g yeast extract, 2% (w/v) 20 g Bacto-Peptone, 2% (w/v) dextrose (glucose) 40 mL sterile 50% Glucose (w/w), filled up with ddH_2O to 1L

3.1.3 Commercial kits and disposables

Table 4: Commercial kits and disposables

Name	Manufacturer
Graduated pipettes (5, 10, 25, 50 mL)	Sarstedt
MF Millipore Membrane Filter, 0.45 µm	Sigma- Aldrich
Micropipette tips 10, 200, 1250 µL	nerbe plus
Microscope glass slides	KnittelGlass and Diagonal
Mini-PROTEAN TGX Stain-Free Gels	Bio Rad
Nitrocellulose membrane	GVS North America
Parafilm	Pechiney Plastic Packaging
Plastic Erlenmeyerflasks	Corning
QIAGEN Gel Extraction Kit	Qiagen
QIAGEN Plasmid MiniPrep	Qiagen
Reaction tubes (0.5, 1.5, 2.0 mL)	Eppendorf
Reaction tubes (15, 50 mL)	Falcon
SERVALight Polaris HRP Substrate kit	SERVA Electrophoresis GmbH
Trans-Blot Turbo Transfer pack	Bio Rad
Whatman Filter paper No.4	GE Healthcare

3.1.4 Enzymes, dyes and antibodies

Table 5: List of enzymes, dyes and antibodies

List of enzymes, dyes and antibodies	Manufacturer
BamH1	New England BioLabs
Dpn1, FastDigest	Thermo Scientific
Gibson assembly Master mix	New England BioLabs
DreamTaq DNA Polymerase	Thermo Fisher Scientific
Kpn1	New England BioLabs
Nhe1	New England BioLabs
Phusion Hot start flex DNA polymerase	New England BioLabs
Phusion High Fidelity 2x Master Mix	New England BioLabs
PNGase F	Sigma Aldrich

Sac1	New England BioLabs
Sal1	New England BioLabs
T4 DNA Ligase	New England BioLabs
Zymolyase 100T	US Biological Life Sciences
1 kb DNA Ladder	Thermo Fisher Scientific
100 bp plus DNA Ladder	Thermo Scientific
6X Loading dye	Thermo Fisher Scientific
PageRuler Prestained Protein ladder	Thermo Scientific
Calcofluor white	Sigma-Aldrich
Concanavalin A Tetramethylrhodamine (ConA- Tet)	Thermo Fisher Scientific
Concanavalin A, Alexa Fluor 647 conjugate (ConA-AF 647)	Thermo Fisher Scientific
FM4-64	Molecular Probes/Invitrogen
PageRuler Prestained Protein Ladder	Thermo Scientific
Streptavidin Alexa Fluor 647 conjugate	Life Technologies
SYBR Red	New England BioLabs
Anti-actin antibody Nb100 (mouse)	Sigma-Aldrich
Anti-HA antibody (mouse)	Sigma-Aldrich
Anti-mouse IgG2-HRP conjugate (goat)	BioRad
Anti-mouse IgM-HRP conjugate (rabbit)	BioRad
Anti-V5 antibody (mouse)	Invitrogen

3.1.5 Plasmids

Table 6: Plasmids used in this thesis

Plasmid	Parent	Genotype	Reference
pRS425		LEU2 2µ ampR	[334]
pRS426		URA3 2µ ampR	[334]
pRS315		LEU2 CEN ampR	[334]
pRS316		URA3 CEN ampR	[334]
pAS01	pRS426	prADH1-URA3 2µ ampR	Anson Shek
pAS07	pRS426	prADH1-*PRM1* 2µ *URA3*	Anson Shek
pAS23	pRS425	prADH1-LEU2 2µ ampR	Anson Shek
pMAM56		pFA6a-mCherry-natNT2	([335])
pYM14		pFA6a-KanMX4	([335])
pMS131		pFA6a-mNeonGreen-KanMX4	Michal Skruzny
pFA6a-HIS3MX6		pFA6a-HIS3MX6 ampR	[336]
pFA6a-URA3		pFA6a-URA3 ampR	[337]
pAS64	pRS316	mNeonGreen *CEN URA3*	Anson Shek
pFA6-natNT2		pFA6-natNT2 ampR	([335])
HA-nHRP-klURA3-cHRP		pMK-RQ KanR	This work
pSKM01	pRS426	prADH1-*PUN1* 2µ *URA3*	This work
pSKM02	pRS426	prPUN1-*PUN1* 2µ *URA3*	This work
pSKM03	pRS316	prADH1-*PUN1 CEN URA3*	This work

pSKM04	pRS316	prADH1-*PUN1*-V5 *CEN URA3*	This work
pSKM05	pRS316	prADH1-*PUN1*-mNeonGreen *CEN URA3*	This work
pSKM06	pRS316	prPUN1-*PUN1*- CEN URA3	This work
pSKM07	pRS425	prADH1-*SUR7* 2µ *LEU2*	This work
pSKM08	pRS426	prADH1-*SUR7* 2µ *URA3*	This work
pSKM09	pRS426	prSUR7-*SUR7* 2µ *URA3*	This work
pSKM10	pRS316	prADH1-*PUN1* G74AL75AW76A *CEN URA3*	This work
pSKM11	pRS316	prADH1-*PUN1* G74AL75AW76A-V5 *CEN URA3*	This work
pSKM12	pRS316	prADH1-*PUN1* G74AL75AW76A-mNeonGreen *CEN URA3*	This work
pSKM13	pRS316	prADH1-*PUN1* C79S *CEN URA3*	This work
pSKM14	pRS316	prADH1-*PUN1* C79S-V5 *CEN URA3*	This work
pSKM15	pRS316	prADH1-*PUN1* C90S *CEN URA3*	This work
pSKM16	pRS316	prADH1-*PUN1* C90S-V5 *CEN URA3*	This work
pSKM17	pRS316	prADH1-*PUN1* C79SC90S *CEN URA3*	This work
pSKM18	pRS316	prADH1-*PUN1* C79SC90S-V5 *CEN URA3*	This work
pSKM19	pRS316	prADH1-*PUN1* C79SC90S-mNeonGreen *CEN URA3*	This work
pSKM20	pRS316	prADH1-*PUN1* L75AW76A *CEN URA3*	This work
pSKM21	pRS316	prADH1-*PUN1* G74AL75AW76A+C79SC90S *CEN URA3*	This work
pSKM22	pRS316	prADH1-*PUN1* G74AL75AW76A+C79SC90S-V5 *CEN URA3*	This work
pSKM23	pRS316	prADH1-*PUN1* G74AL75AW76A+C79SC90S-mNeonGreen *CEN URA3*	This work

3.1.6 Yeast and bacterial strains

Table 7: Yeast strains used in this thesis

Strain	Parent	Genotype	Source
BY4741	S288C	*MAT**a** his3Δ1 leu2Δ0 met15Δ0 ura3Δ0*	[338]
BY4742	S288C	*MATα his3Δ1 leu2Δ0 lys2Δ0 ura3Δ0*	[338]
MATa YKO	BY4741	*MATa his3Δ1 leu2Δ0 met15Δ0 ura3Δ0, geneΔ::KanMX*	[339]
MATα YKO	BY4742	*MATα his3Δ1 leu2Δ0 lys2Δ0 ura3Δ0, geneΔ::KanMX*	[339]
PSAY 981 *MATα* N-GFP	BY4742	*MATα ura3Δ0 his3Δ1 leu2Δ0 lys2Δ0, NeGFP-TRP1-NatMX4 (p1371)*	Pablo Aguilar
PSAY 982 *MAT*a N-GFP	BY4742	*MAT**a** ura3Δ0 his3Δ1 leu2Δ0 lys2Δ0, NeGFP-TRP1-NatMX4 (p1371)*	Pablo Aguilar
PSAY 983 *MAT*a C-GFP	BY4742	*MAT**a** ura3Δ0 his3Δ1 leu2Δ0 lys2Δ0, CeGFP-LEU2 (p1370) Δlys1::KanMX-pTEF2-mCherry*	Pablo Aguilar
PSAY 984 *MATα* C-GFP	BY4742	*MATα ura3Δ0 his3Δ1 leu2Δ0 lys2Δ0, CeGFP-LEU2 (p1370) Δlys1::KanMX-pTEF2-mCherry*	Pablo Aguilar
FUS1-GFP	BY4741	*MAT**a** FUS1-GFP::HIS3MX6*	([340])
YIL108W-GFP	BY4741	*MAT**a** YIL108W-GFP::HIS3MX6*	([340])
YHR097C-GFP	BY4741	*MAT**a** YHR097C-GFP::HIS3MX6*	([340])

YJL049W-GFP	BY4741	*MAT**a** YJL049W-GFP::HIS3MX6*	([340])
YNR065C-GFP	BY4741	*MAT**a** YNR065C-GFP::HIS3MX6*	([340])
YNR066C-GFP	BY4741	*MAT**a** YNR066C-GFP::HIS3MX6*	([340])
YIL108W-GFP	BY4741	*MAT**a** YIL108W-GFP::HIS3MX6*	([340])
4E5 *ORC2*-TAP-URA3	BY4741	*MAT**a** lys2Δ0 ura3Δ0 ho::LYS2 leu2::hisG TRP ARG4 pch2::URA3:pPCH2(300bp):3HA-*	Heinz Neumann
SKM001	PSAY 983	*MAT**a** ura3Δ0 his3Δ1 leu2Δ0 lys2Δ0, CeGFP-LEU2*	This work
SKM001	PSAY 983	*MATα ura3Δ0 his3Δ1 leu2Δ0 lys2Δ0, CeGFP-LEU2*	This work
ASG7-mNG	BY4741	*MAT**a** ASG7-mNG::KanMX4*	This work
FIG1-mCherry	BY4741	*MATa PUN1-mNG::KanMX4 FIG1-mCherry::natNT2*	This work
FIG1-mNG	BY4741	*MAT**a** FIG1-mNG::KanMX4*	This work
FMP45-mNG	BY4741	*MAT**a** FMP45-mNG::KanMX4*	This work
ISC1-mNG	BY4741	*MAT**a** ISC1-mNG::KanMX4*	This work
PGK1-mCherry	BY4742	*MAT**a** PGK1-mCherry::natNT2*	This work
PIL1-mCherry	BY4741	*MAT**a** PUN1-mNG::KanMX4 PIL1-mCherry::natNT2*	This work
PIL1-mNG	BY4742	*MATα PIL1-mNG::KanMX4*	This work
PRM5-mNG	BY4741	*MAT**a** PRM5-mNG::KanMX4*	This work
PUN1-mCherry	BY4742	*MATα PUN1-mCherry::natNT2*	This work
PUN1-mNG	BY4741	*MAT**a** PUN1-mNG::KanMX4*	This work
SUR7-mCherry	BY4742	*MATα SUR7-mCherry::natNT2*	This work
SUR7-mNG	BY4741	*MAT**a** SUR7-mNG::KanMX4*	This work
YNL058C-mNG	BY4741	*MAT**a** YNL058C-mNG::KanMX4*	This work
YNL194C-mNG	BY4741	*MAT**a** YNL194C-mNG::KanMX4*	This work
YPR170W-B-mNG	BY4741	*MAT**a*** YPR170W-mNG::KanMX4	This work
fig1Δ	PSAY 981	*MATα fig1Δ::hphNT1, NeGFP-TRP1-NatMX4*	This work
fig1Δ	PSAY 983	*MAT**a** fig1Δ::hphNT1, CeGFP-LEU2 (p1370) Δlys1::KanMX-pTEF2-mCherry*	This work
fig1Δpun1Δsur7Δfmp45Δ	PSAY 981	*MATα pun1Δ::hphNT1 fig1Δ::KanMX4 sur7Δ::HIS3 fmp45Δ::URA3, NeGFP-TRP1-NatMX4*	This work
fig1Δpun1Δsur7Δfmp45Δ	PSAY 983	*MAT**a** pun1Δ::hphNT1 fig1Δ::KanMX4 sur7Δ::HIS3 fmp45Δ::URA3, CeGFP-LEU2 (p1370)*	This work
isc1Δ	PSAY 981	*MATα isc1Δ::hphNT1, NeGFP-TRP1-NatMX4*	This work
isc1Δ	PSAY 983	*MAT**a** isc1Δ::hphNT1, CeGFP-LEU2 (p1370) Δlys1::KanMX-pTEF2-mCherry*	This work
pil1Δ	PSAY 981	*MATα pil1Δ::hphNT1, NeGFP-TRP1-NatMX4*	This work
pil1Δ	PSAY 983	*MAT**a** pil1Δ::hphNT1, CeGFP-LEU2 (p1370) Δlys1::KanMX-pTEF2-mCherry*	This work
prm1Δ	PSAY 981	*MATα prm1Δ::hphNT1, NeGFP-TRP1-NatMX4*	This work
prm1Δ	PSAY 983	*MAT**a** prm1Δ::hphNT1, CeGFP-LEU2 (p1370) Δlys1::KanMX-pTEF2-mCherry*	This work

prm1Δ	PSAY 983	*MAT**a** prm1Δ::hphNT1, CeGFP-LEU2 (p1370)*	This work
prm1Δprm5Δynl058cΔ	PSAY 981	*MATα prm1Δ::HIS3prm5Δ::hphNT1 ynl058cΔ::KanMX4, NeGFP-TRP1-NatMX4*	This work
prm1Δprm5Δynl058cΔ	PSAY 983	*MAT**a** prm1Δ::HIS3prm5Δ::hphNT1 ynl058cΔ::KanMX4, CeGFP-LEU2 (p1370)*	This work
prm1Δpun1Δ	PSAY 981	*MATα prm1Δ::hphNT1 pun1Δ::KanMX4, NeGFP-TRP1-NatMX4*	This work
prm1Δpun1Δ	PSAY 983	*MAT**a** prm1Δ::hphNT1 pun1Δ::KanMX4, CeGFP-LEU2 (p1370)*	This work
prm1Δsur7Δ	PSAY 981	*MATα prm1Δ::KanMX4 sur7Δ::HIS3, NeGFP-TRP1-NatMX4*	This work
prm1Δsur7Δ	PSAY 983	*MAT**a** prm1Δ::KanMX4 sur7Δ::HIS3, CeGFP-LEU2 (p1370)*	This work
prm5Δfus1Δ	PSAY 981	*MATα prm5Δ::hphNT1 fus1Δ::KanMX4, NeGFP-TRP1-NatMX4*	This work
prm5Δfus1Δ	PSAY 983	*MAT**a** prm5Δ::hphNT1 fus1Δ::KanMX4, CeGFP-LEU2 (p1370)*	This work
prm5Δynl058cΔ	PSAY 981	*MATα prm5Δ::hphNT1 ynl058cΔ::KanMX4, NeGFP-TRP1-NatMX4*	This work
prm5Δynl058cΔ	PSAY 983	*MAT**a** prm5Δ::hphNT1 ynl058cΔ::KanMX4, CeGFP-LEU2 (p1370)*	This work
pun1Δ	PSAY 981	*MATα pun1Δ::hphNT1, NeGFP-TRP1-NatMX4*	This work
pun1Δ	PSAY 983	*MAT**a** pun1Δ::hphNT1, CeGFP-LEU2 (p1370) Δlys1::KanMX-pTEF2-mCherry*	This work
pun1Δ	PSAY 983	*MAT**a** pun1Δ::hphNT1, CeGFP-LEU2 (p1370)*	This work
pun1Δfig1Δ	PSAY 981	*MATα pun1Δ::hphNT1 fig1Δ::KanMX4, NeGFP-TRP1-NatMX4*	This work
pun1Δfig1Δ	PSAY 983	*MAT**a** pun1Δ::hphNT1 fig1Δ::KanMX4, CeGFP-LEU2 (p1370)*	This work
pun1Δfig1Δsur7Δ	PSAY 981	*MATα pun1Δ::hphNT1 fig1Δ::KanMX4 sur7Δ::HIS3, NeGFP-TRP1-NatMX4*	This work
pun1Δfig1Δsur7Δ	PSAY 983	*MAT**a** pun1Δ::hphNT1 fig1Δ::KanMX4 sur7Δ::HIS3, CeGFP-LEU2 (p1370)*	This work
pun1Δfig1Δsur7Δfmp45Δynl194cΔ	PSAY 981	*MATα pun1Δ::hphNT1 fig1Δ::KanMX4 sur7Δ::HIS3 fmp45Δ::URA3 ynl194cΔ::LEU2, NeGFP-TRP1-NatMX4*	This work
pun1Δfig1Δsur7Δfmp45Δynl194cΔ	PSAY 983	*MAT**a** pun1Δ::hphNT1 fig1Δ::KanMX4 sur7Δ::HIS3 mp45Δ::URA3 ynl194cΔ::NatMX4, CeGFP-LEU2 (p1370)*	This work

pun1Δfus1Δ	PSAY 981	*MATα pun1Δ::hphNT1 fus1Δ::KanMX4, NeGFP-TRP1-NatMX4*	This work
pun1Δfus1Δ	PSAY 983	*MAT**a** pun1Δ::hphNT1 fus1Δ::KanMX4, CeGFP-LEU2 (p1370)*	This work
pun1Δfus1Δfus2Δ	PSAY 981	*MATα pun1Δ::hphNT1 fus1Δ::KanMX4 fus2Δ::HIS3, NeGFP-TRP1-NatMX4*	This work
pun1Δfus1Δfus2Δ	PSAY 983	*MAT**a** pun1Δ::hphNT1 fus1Δ::KanMX4 fus2Δ::HIS3, CeGFP-LEU2 (p1370)*	This work
pun1Δprm1Δsur7Δ	PSAY 981	*MATα pun1Δ::hphNT1 prm1Δ::KanMX4 sur7Δ::HIS3, NeGFP-TRP1-NatMX4*	This work
pun1Δprm1Δsur7Δ	PSAY 983	*MAT**a** pun1Δ::hphNT1 prm1Δ::KanMX4 sur7Δ::HIS3, CeGFP-LEU2 (p1370)*	This work
pun1Δsur7Δ	PSAY 981	*MATα pun1Δ::hphNT1 sur7Δ::KanMX4, NeGFP-TRP1-NatMX4*	This work
pun1Δsur7Δ	PSAY 983	*MAT**a** pun1Δ::hphNT1 sur7Δ::KanMX4, CeGFP-LEU2 (p1370)*	This work
FUS1-mNG	BY4741	*MAT**a** FUS1-mNG::KanMX4*	This work
FUS1-6HA	BY4741	*MAT**a** FUS1-6HA::KanMX4*	This work
HA-HRP-FUS1-6HA	BY4741	*MAT**a** HA-HRP-FUS1-mNG::KanMX4*	This work
HA-HRP-FUS1-mNG	BY4741	*MAT**a** HA-HRP-FUS1-mNG::KanMX4*	This work

Table 8: Bacterial strains used in this thesis

Organism	Name	Genotype
Escherichia coli	XL-10 Gold	TetRΔ(*mcrA*)183 Δ(*mcrCB-hsdSMR-mrr*)*173 endA1 supE44 thi-1 recA1 gyrA96 relA1 lac* Hte [F´ *proAB lacIqZΔM15 Tn10* (TetR) Amy CamR]
Escherichia coli	Omni-max	F' {proAB+laclq lacZΔM15 Tn10(TetR) Δ(ccdAB)} mcAr Δ(mrr--hsdRMS--mcrBC) φ80(lacZ)ΔM15 Δ(lacZYA--argF) U169 endA1 recA1 supE44 thi-1 gyrA96 reAl1 tonA

3.1.7 Primers

Table 9: List of primers used in this thesis

Primer	Sequence (5'-3')
ASG7 C' Tag pYM Fw	ACTCATAATATTTGTAGTTCTCCTATGTAAGAAAAGCCGTCGTACGCT GCAGGTCGAC
ASG7 C' Tag pYM Rev	GAAAGAGGCTGATATCATTTTCTGTCTTTAGATCTACCTAATCGATGAA TTCGAGCTCG

ASG7 C' Tag CHK Fw	TGGTTGGTGAATCTTTTAGC
FIG1 C' Tag pYM Fw	TAACTACTCTTCGGATTCATCTACATTGCATTCCAAAGTTCGTACGCTG CAGGTCGAC
FIG1 KO pYM Fw	AACAAACAAACAAACAAACAAAAAAAAAAAAAAAAAATGCGTACGCT GCAGGTCGAC
FIG1 C' Tag pYM Rev	ATCCGCTCAAAACTTATATGTTTATTTGAGGATAAAACTAATCGATGAA TTCGAGCTCG
FIG1 C' Tag CHK Fw	TCAAGCGTTGTCTTGAACATTTTG
FIG1 WT CHK Fw	TTCTTCTCATCGGCTGTTAC
FIG1 WT CHK Rev	TCAAAATGTTCAAGACAACG
FIG1 5‘ UTR CHK Fw	GCATTGCCTCTTTATTTGAC
FMP45 C' Tag pYM Fw	TGGGGATGGTGGTCTTGCCGGGCCAGTGACGGTACGCGACCGTACG CTGCAGGTCGAC
FMP45 C' Tag pYM Rev	AAAAATTAGGAAGTATTTTATGGTGATTATTTCCTTCCTAATCGATGAA TTCGAGCTCG
FMP45 KO URA3 Fw	AAGTAACAAGTAACACTAATCACTATAATCTACCGCTATGTCGGGGCT GGCTTAACTATG
FMP45 KO URA3 Rev	AAAAATTAGGAAGTATTTTATGGTGATTATTTCCTTCCTAGCGGTATTT TCTCCTTACGC
FMP45 C' Tag CHK Fw	TATGTGAAGGCCAGAAAGAC
FMP45 WT CHK Fw	TATTCTGTCAGGAGGCAGAG
FMP45 WT CHK Rev	GAAGGAAGGTAGCCAGAAAG
FUS1 C' Tag pYM Fw	TAGAGGCATTGTGCCTGGTGACTGTCTCCAAGAATACGACCGTACGC TGCAGGTCGAC
FUS1 KO pYM Fw	GAGCAGGATATAAGCCATCAAGTTTCTGAAAATCAAAATGCGTACGCT GCAGGTCGAC
FUS1 KO pYM Rev	AGGTATAGATTAAATGCGAACGTCAATATTATTTTCATCAATCGATGAA TTCGAGCTCG
FUS1 C' Tag CHK Fw	TGACTGCAATAAAAGCACTG
FUS1 WT CHK Fw	GATATAATGCCTGACGAACG
FUS1 WT CHK Rev	GCAATGGTTTAGAACGTGAC
FUS1 5‘ UTR CHK Fw	AACAGAACAATAACGGCAAC
FUS1 F1 Fw	TCTTTTGCTTCCATATTTACCATGTGG
FUS1 R1 Rev	AGCGTAGTCTGGAACGTCGTATGGGTACATTTTGATTTTCAGAAACTT GATGGC
FUS1 F2 Fw	GCTGGTGCTGGTGCTGGTGCAGTAGCAACAATAATGCAGACGACAAC AAC
FUS1 R2 Rev	GGATTTGAAATGGACACCGAATTCC
FUS1 CHK Fw	TTTGTTGTCAGTGATGCCTCAATCC
cHRP CHK Fw	CAGCTTCGCTAATAGCACACAAACC
nHRP CHK Rev	AATGCAATCTCAAAATAGAGGCAGC
ISC1 C' Tag pYM Fw	GGACGCGGAGCACCACCTGCAAACTTTCTTGAGCGAGAAACGTACGC TGCAGGTCGAC
ISC1 KO pYM Fw	TGCGCTTTCCGCGTAAAAAGGGAAAAAAAGCAGATATATGCGTACGC TGCAGGTCGAC
ISC1 KO Rev	GTAATTTTTTTACATATGCTAAAGAAAATCGATAATATCAATCGATGAA TTCGAGCTCG
ISC1 C' Tag CHK Fw	ACTCATGCACCCTTAACATC
ISC1 WT CHK Fw	ACAGAGATGTTCACGAGAGG
ISC1 WT CHK Rev	AACGCTGATACGGATACTTG
ISC1 5‘ UTR CHK Fw	CTGCTCTCTGGTGGTATTTG
PIL1 C' Tag pYM Fw	ACACCAGCAAAGTGAGTCTCTTCCCCAACAAACAACAGCTCGTACGC TGCAGGTCGAC

PIL1 KO pYM Fw	TGCAAAGTGAAGAATATATCAGCATCAAGTATATAGTATGCGTACGCT GCAGGTCGAC
PIL1 KO pYM Rev	TTTTTTTTGTTTCTAATAGATTGTTGATTTATTTTGATTAATCGATGAATT CGAGCTCG
PIL1 C' Tag CHK Fw	TTGCTTTAATCGCTGGTTAC
PIL1 WT CHK Fw	CAGCTTTAGGAGAAGTGCTG
PIL1 WT CHK Rev	AGCAGCTCTCAACTTTGACC
PIL1 5‘ UTR CHK Fw	GCGCTTGTCTTATAAAATTCC
PGK1 C' Tag pYM Fw	TAAGGAATTGCCAGGTGTTGCTTTCTTATCCGAAAAGAAACGTACGCT GCAGGTCGAC
PGK1 C' Tag pYM Rev	GAAAAAAATTGATCTATCGATTTCAATTCAATTCAATTTAATCGATGAAT TCGAGCTCG
PGK1 C' Tag CHK Fw	TGACAAGGAAGGTATTCCAG
PRM1 C' Tag pYM Fw	GGTAATTCTCCGATTACGTCTTCGCAAAGCCACCTTTGACCGTACGCT GCAGGTCGAC
PRM1 KO pYM Fw	AGGATGATTCCCTTTCGAATTTGTGAACGTTGATGATATGCGTACGCT GCAGGTCGAC
PRM1 KO pYM Rev	ATAGAGTTATGACGGAAAAAGTCTATCAACTAATTAATCAATCGATGAA TTCGAGCTCG
PRM1 C' Tag CHK Fw	ATGTGCCATTGAAAATAAGC
PRM1 WT CHK Fw	TTCCTCAATCAACGATAAGC
PRM1 WT CHK Rev	TCCAGAGCTTGATTTCATTC
PRM1 5‘ UTR CHK Fw	TTCCGATGATGCCTACATAC
PRM4 C' Tag pYM Fw	CAACTTGCTGGTAGAAAAAAAAGACATCCCTTCTAATTCTCGTACGCT GCAGGTCGAC
PRM4 C' Tag pYM Rev	TTAGCTGCGGCTGCTCGTCGATAGGAGTGATAACAAATTAATCGATGA ATTCGAGCTCG
PRM5 C' Tag pYM Fw	TTATCTCGAGCACATGCTGGAGGGGAAAGAACAGGATGAGCGTACGC TGCAGGTCGAC
PRM5 KO pYM Fw	GTTGAAAATAGAATAAATTGACACTCAAAACGCAAGAATGCGTACGCT GCAGGTCGAC
PRM5 KO pYM Rev	TGCTTAAAAAAAATATTGCAAAATATCATAAAAGTTTTTAATCGATGAAT TCGAGCTCG
PRM5 C' Tag CHK Fw	TAAGGATGAATCGGTGAAAG
PRM5 WT CHK Fw	TAACCACTTCCACTTCTTCG
PRM5 WT CHK Rev	CCGTAAAACTGGGTATGTTG
PRM5 5‘ UTR CHK Fw	TTTCTTAGCAGGGTTATTGC
PUN1 C' Tag pYM Fw	CATCTATGCGAACGCTCCAATTGAGGAAAAACCATTGATTCGTACGCT GCAGGTCGAC
PUN1 KO pYM Fw	GAAAAAAACAAACACATCATCGAAGGACGCTATAAGCATGCGTACGC TGCAGGTCGAC
PUN1 KO pYM Rev	ACACAAAAATTAATTAATAACCTTGCCTTTTTCAAATTCAATCGATGAAT TCGAGCTCG
PUN1 C' Tag CHK Fw	TGCCCGAAAAACTAAAAAG
PUN1 WT CHK Fw	ACATCCAATCATGTTCTTCG
PUN1 WT CHK Rev	ATGAGTAAGTGCCCAAACAC
PUN1 5‘ UTR CHK Fw	TCAGCCACACATTGACGTAC
PUN1 Endo Fw	AGATGAAACATGTGAAACCC
PUN1 Endo Rev	CCTTATATGGATGCCCTGAACATC
PUN1 AS01 Fw	ATGAGGAATTTTTTCACGTTATTTTTTGC
PUN1 AS01 Rev	TCAAATCAATGGTTTTTCCTCAATTGG

PUN1 C79S	CCTCATATATAAATATAGGGCTTTGGTCGTACTCTACAGTGGACTCCTCGCATAAC
PUN1 C79S Seq Fw	CGGCCTTCCTTCCAGTTACTTG
PUN1 AAA Fw	GGCCTGCCCTCATATATAAATATAGCTGCTGCGTCGTACTGTACAGTGGACTCCTCGC
PUN1 AAA Rev	TATATTTATATATGAGGGCAGGCCCAACGAAGATAGCGTAGCAGAACTCAAAGAAGG
PUN1 Seq Fw	GAGCAACGGTATACGGCCTTC
PUN1 C90S	CTCCTCGCATAACATCCAATCATCTTCTTCGCCTCACGGTATC
PUN1 C90S Seq Fw	CGGCCTTCCTTCCAGTTACTT
SUR7 C' Tag pYM Fw	TATAAGAAAATCACACGAGCGCCCGGACGATGTCTCTGTTCGTACGCTGCAGGTCGAC
SUR7 KO pYM Fw	AGAGACTAAGTATAGTAACGCATATCCGCACAATACTATGCGTACGCTGCAGGTCGAC
SUR7 KO pYM Rev	TATAAATATATATTACAAAGCGGAAAACTTGCGCCATTTAATCGATGAATTCGAGCTCG
SUR7 C' Tag CHK Fw	AGATGCTTTCAGAGATGGTG
SUR7 WT CHK Fw	TCCTTTACGTTTTGACTTGG
SUR7 WT CHK Rev	GTCAATATTGGGTCAGTTGC
SUR7 5‘ UTR CHK Fw	AAGAGAAAGCAAAGGGAGAG
SUR7 Endo Fw	GAATTGCAATTGTTTGTTTG
SUR7 Endo Rev	CAGCAGCCTTATAAATGGATTCGG
SUR7 ADH1 pAS01 Fw	ATGGTTAAGGTCTGGAATATAGTACTAC
SUR7 ADH1 pAS01 Rev	TTAAACAGAGACATCGTCCGGGCGCTC
YIL108W C' Tag CHK Fw	GTCGTCGCTTTTGATGTTAG
YHR097C C' Tag CHK Fw	GACGCTGAACCAACTACAAG
YJL049W C' Tag CHK Fw	TCAAAATAACCTCGCTCAAG
YNR065C C' Tag CHK Fw	ACGATGGGCTGATAGAAAAC
YNR066C C' Tag CHK Fw	TTTTCAAAAGGCACGTCTAC
YNL194C C' Tag pYM Fw	GGAACGCGTCTATACTGAACAGAATGTTCCTGTTGTATCACGTACGCTGCAGGTCGAC
YNL194C C' Tag pYM Rev	CTTTAATAATAAGGGAAAAAAAAGCCTCCTTTGCACCCTAATCGATGAATTCGAGCTCG
YNL194C KO LEU2 Fw	TAAGTATAACCTCATATATTTCCGTTTCTAATAATCAATGGGGCGCGTCAGCGGGTGTTG
YNL194C KO LEU2 Rev	CTTTAATAATAAGGGAAAAAAAAGCCTCCTTTGCACCCTAGCGGTATTTTCTCCTTACGC
YNL194C KO NAT Fw	TAAGTATAACCTCATATATTTCCGTTTCTAATAATCAATGCGTACGCTGCAGGTCGAC
YNL194C KO NAT Rev	CTTTAATAATAAGGGAAAAAAAAGCCTCCTTTGCACCCTAATCGATGAATTCGAGCTCG
YNL194C C' Tag CHK Fw	TCACGCTTTTCTTCATAACC
YNL194C WT CHK Fw	TTTTATTGGTTTCAGGCATC
YNL194C WT CHK Rev	TATGAAGAAAAGCGTGATCC
YNL194C 5‘ UTR CHK Fw	ATTTGGGAAGACGACAAAG
YNL058C C' Tag pYM Fw	GATGTTTTTGGATGATGTCCTGAATGGTAGAGAAATAATCCGTACGCTGCAGGTCGAC

YNL058C C' Tag pYM Rev	TAACCTGAACAACCATGTATCTTAGATGTCAGGGTATCTAATCGATGAATTCGAGCTCG
YNL058C C' Tag CHK Fw	ACCATTCAACCCAATTCAG
YNL058C WT CHK Fw	TATCGCTGGTCAGAAGAGAC
YNL058C WT CHK Rev	ACGACGAGACAAATAACTGG
YNL058C 5‘ UTR CHK Fw	GTATAGGGGAACCTGGTGAC
YPR170W-B C' Tag pYM Fw	AGTTTACCTAGCCAGAAGAAAACCTTCGATCGAGTTGCGTCGTACGCTGCAGGTCGAC
YPR170W-B C' Tag pYM Rev	TATTAATGCATTTGGTATTATCCTATTGGCTTCAAGACTAATCGATGAATTCGAGCTCG
YPR170W-B C' Tag CHK Fw	CCGTTGTATCCACTGGTAAG
pAS01 CHK Fw (AS132F)	TAAGTTGGGTAACGCCAGGG
AS194 CEN Rev	GTCATCACCGAAACGCGC
AS027 prADH1 Fw	CTCGTCATTGTTCTCGTTC
HA CHK Rev	AGAACCGGAGTCGACCTG
Hygromycin CHK Rev	CAGCTATTTACCCGCAGGAC
K.l URA3 CHK Fw	GAGGGTACTGTCGTTCCATTG
Kanamycin CHK Rev	CTGCAGCGAGGAGCCGTAAT
Kpn1-PUN1 Fw	CCGGGTACCATGAGGAATTTTTTCACGTTATTTTTTGC
LEU2 CHK Rev	CACCTGTAGCATCGATAGCA
M13 (49) Rev	GAGCGGATAACAATTTCACACAGG
M13(43) Fw	AGGGTTTTCCCAGTCACGACGTT
mNG CHK Rev	TCAATTCTTCGTAACCGTCG
natNT2 CHK Rev	TGGTGAAGGACCCATCCAG
S.kluyveri HIS3 CHK Rev	TAGCTTGGGAAGCTACATC
S2 Rev	GTCGACCTGCAGCGTACG
prSP6 Fw	ATTTAGGTGACACTATAGA
prT7 Rev	TAATACGACTCACTATAGGG
V5 Rev	CCGGAGCTCTTACGTAGAATCGAGACCGAGGAGAGGGTTAGGGATAGGCTTACCTTCGAACCGCGGGCCCGTCGACCCAATCAATGGTTTTTCCTCAATTGGA

3.1.8 Instrumentation

Table 10: Instruments used in this thesis

Instrument	Manufacturer
Agarose gel chamber	Bio Rad
Autoclave	SHP Laborklav 100-MV
BD Accuri C6 Plus Flow Cytometer	BD Biosciences
Centrifuge 5424	Eppendorf
Centrifuge 5810R	Eppendorf
ChemiDoc MP Imaging System	Bio Rad
Gel Doc XR System	Bio rad
Incubator, 30 °C	Memmert Peltier
Incubator, 37 °C	Memmert Peltier
Light Microscope	Kolleg SHB45

Magnetic stirrer RCT basic	Heidolph
Microwave Continent MW 800 G	IKA Labortechnick
Millipore Synergy	Millipore
Mini Protean II	Bio Rad
Mini Trans-Blot^{R} Cell	Bio Rad
pH Meter 761 Calimatic	Knick
Refrigerator, -20 ºC	LIEBHERR
Refrigerator, -80 ºC	Sanyo
Refrigerator, 4 ºC	LIEBHERR
Safety Hood	Waldner service
Shaker KS 130 Basic	IKA Labortechnick
Singer Micromanipulator	Singer Instruments MSM
Marianas Spinning Disk Confocal microscope	Intelligent Imaging Innovations
Thermomixer C	Eppendorf
Trans-Blot Turbo Transfer System	Bio Rad
UV/Vis- spectrophotometer ND-1000 NanoDrop	Peqlab Biotechnologie
Zeiss LSM 800 Confocal microscope	Carl Zeiss

Table 11: Common abbreviations for mixtures and reagents used in this thesis

Abbreviation	
YPD	Yeast Peptone Dextrose
SD-URA	Standard Defined-Uracil
SD-HIS	Standard Defined-Histidine
SD-LEU	Standard Defined-Leucine
SC	Standard Complete
LB	Lysogeny Broth
PBS	Phosphate Buffered Saline
PNGase F	Peptide-N-Glycosidase F
BP	Biotin- AEEA-Phenol
SORB	Sorbitol
PEG	Polyethylene Glycol
TAF	Tris-HCl (pH 7.4), NaN3, NaF in PBS
TCA	Trichloroacetic acid
ConA- 647	Concanavalin A, Alexa Fluor 647 conjugate
ConA-Tet	Concanavalin A Tetramethylrhodamine
SDS	Sodium dodecyl sulfate

3.2 Methods

3.2.1 Molecular biology

3.2.1.1 Polymerase Chain Reaction

Polymerase Chain Reaction (PCR) was used to amplify specific DNA fragments or introduce point mutations. DNA amplification was carried out using DreamTaq DNA polymerase (Thermo Scientific) or Phusion polymerase (New England BioLabs). A general PCR protocol outlined below was used and was modified according to specific needs.

Table 12: General composition of a 50 µL PCR reaction

1 µL	DNA template 200 ng
0.64 µL	Forward primer 0.5 µM (0.64 µM final concentration)
0.64 µL	Reverse primer 0.5 µM (0.64 µM final concentration)
1.2 µL	dNTP mix 12.5 mM (0.3 mM final concentration)
5 µL	10x DreamTaq buffer (1x final concentration)
0.5 µL	DreamTaq polymerase
	Fill up with ddH_2O

Table 13: General PCR protocol used in this thesis

Step	**Temperature**	**Time**	
Initial denaturation	95 °C	1 min	
	95 °C	15 sec	
Annealing	55 °C	30 sec	25-35 cycles
Extension	72 °C	30 sec/ kb	
Final extension	72 °C	5 min	
Hold	12 °C	∞	

3.2.1.2 DNA restriction digestion and ligation

Plasmids were generated either via restriction digestion and ligation or Gibson assembly. DNA restriction digestion and ligation was performed using commercially available restriction enzymes, following the manufacturer's instructions. For each reaction, 500 ng -1 µg of plasmid were mixed with 1 µL of restriction enzyme and 1x CutSmart Buffer in a 20 µL volume. The reaction was incubated at 37 ^{o}C for at least 1 h. Digested fragments were electrophoretically separated by agarose gel electrophoresis (1%) and the desired DNA extracted using the QIAGEN DNA gel extraction kit according to the manufacturer's instructions. Using about 20-50 ng vector DNA, ligation of the purified DNA fragments (vector and insert) was carried out in a 10 µL reaction volume using T4 DNA ligase and 1x T4 ligase buffer in a 3:1 insert to vector ratio. The ligation mixture was incubated on ice for 10 min before being transferred to 37^{o} C for at least 1 h. 1 µL of the ligation

mixture was then transformed into competent *E. coli* cells.

For plasmids generated via Gibson assembly, the desired DNA fragments were first designed such that the respective PCR amplicons would contain 20 bp of homology upstream and downstream of the vector restriction sites when joined to the linearized vector. A 50 µL PCR reaction was prepared using Phusion polymerase (New England BioLabs). Amplified DNA fragments were subsequently isolated by agarose gel electrophoresis (1%) and the desired DNA extracted using the QIAGEN DNA gel extraction kit according to the manufacturer's instructions. Linearized vector DNA was generated via restriction digestion as described above. For the Gibson assembly reaction, a 10 µL reaction containing 20-40 ng of linearized vector DNA mixed with the PCR products (inserts) in a 3:1 insert to vector ratio and 5 µL 2x Gibson assembly mix was prepared. The reaction was incubated at 50 °C for 20 min to 1 h depending on the number of inserts. 1 µL of the reaction was then transformed into competent *E. coli* cells.

3.2.1.3 Transformation of *E. coli* cells

Bacterial transformation was carried out by mixing 50 µL of desired competent *E. coli* cells with 1 µL of the ligation or Gibson assembly mixture reaction. The cells were incubated on ice for 15 min followed by a heat shock step at 42 °C for 90 sec. The cells were quickly transferred to ice and incubated for 2 min. Cells were then recovered by adding 1000 µL of pre-warmed LB or SOC medium and incubated at 37 °C for 1 h with shaking at 300 rpm. Cells were then harvested (10000 rpm for 1 min) and the supernatant discarded to a final volume of 100 µL volume. The cells were resuspended and plated on LB agar plates containing Ampicillin (100 µg/mL) antibiotic that corresponded to the plasmid-encoded antibiotic resistance marker to apply selection pressure. Cells were allowed to grow overnight at 37 °C.

3.2.1.4 Site-directed mutagenesis

To introduce point mutations, site- directed mutagenesis using single- step or sequential PCR amplification was carried out. For the single-step mutagenesis PCR, respective 30 µL PCR reactions were prepared by mixing 2 ng/µL of plasmid template DNA, 1.2 µM primer (20 µM stock), 1x Phusion High Fidelity 2x Master Mix (New England Biolab) and 1M DMSO (New England BioLab). Desired DNA fragments were amplified using the site- directed mutagenesis protocol 1 below. For the sequential PCR, a forward primer containing the mutated residues was designed. Additionally, each primer was designed to contain a template complementary region of about 60 °C and a second complementary region at the 5' end with an annealing temperature of <5 °C to that of the template complementary region. A 50 µL PCR reaction was prepared by mixing 10 ng/µL of plasmid template DNA, 1 µM of each primer and 1x Phusion High Fidelity 2x Master Mix (New England BioLab). The desired DNA fragments were amplified using the site-directed mutagenesis protocol 2 below. Once the PCR reactions were completed, template DNA was digested overnight with Dpn1 at 37 °C after which the respective PCR products were transformed into Omni-max *E. coli* cells as described above.

Table 14: SDM PCR protocol 1 used in this thesis

Step	**Temperature**	**Time**	
Initial denaturation	98 °C	1 min	
	98 °C	15 sec	
Annealing	51 °C	30 sec	28 cycles
Extension	72 °C	45 sec/ kb	
Final extension	72 °C	5 min	

Hold	12 °C	∞

Table 15: SDM PCR protocol 2 used in this thesis

Step	Temperature	Time	
Initial denaturation	98 °C	5 min	
	98 °C	15 sec	
Annealing	60 °C	30 sec	12 cycles
Extension	72 °C	30 sec/ kb	
Final extension	72 °C	5 min	
Denaturation	98 °C	15 sec	
Annealing	54 °C	30 sec	
Extension	72 °C	30 min	1 cycle
Final extension	72 °C	5 min	
Hold	12 °C	∞	

3.2.1.5 DNA preparation, separation and purification

Isolation of desired plasmid DNA was carried out by first amplifying the plasmid DNA. A bacterial clone was inoculated in 5 mL LB medium containing 5 µL Ampicillin (100 µg/mL) to apply selection pressure. The cells were incubated overnight at 37 °C, 200 rpm. The plasmid DNA was subsequently isolated using the QIAGEN plasmid isolation kit according to the manufacturer's instructions. To obtain desired amplified DNA fragments, PCR products were electrophoretically separated via agarose gel electrophoresis. 1% agarose gel was prepared in 1x TAE buffer and supplemented with 1x Sybr Red to stain the DNA. DNA bands of interest were excised and DNA extracted from the gel using the QIAGEN DNA Gel extraction kit according to the manufacturer's instructions. DNA concentrations were measured in a final 20 µL volume using the Nanodrop ND-1000.

3.2.1.6 DNA quantification and sequencing

The concentrations of double-stranded (ds) DNA were estimated using the Nanodrop ND-1000 instrument that is based on the DNA light absorbance at 260 nm wavelength. At 260 nm, an optical density (OD) of 1 corresponds to a dsDNA concentration of 50 ng/µL. DNA sequencing of all plasmids obtained was performed in order to confirm the success of the cloning strategy and the incorporation of desired mutations. Sequencing was performed by commercially available sequencing services (Microsynth SeqLab and EuroFins), all of which followed the Sanger dideoxyribonucleotide (ddNTP) chain termination method ([341]).

3.2.2 Yeast molecular biology

3.2.2.1 C-terminal gene tagging, epitope tagging and gene deletion

Two *S. cerevisiae* cell lines (*MAT***a** BY4741/ *MATα* BY4742) and (*MATα* PSAY 981/ *MAT***a** PSAY 983) derived from S288C were used [338]. C-terminal gene tagging and gene deletion was carried out in the BY and PSAY strains, respectively using gene specific primers as described by Janke ([335]). Briefly, gene-specific primer pairs were prepared using the Primers4Yeast platform (http://www.weizmann.ac.il/Primers-4-Yeast/). DNA amplification was carried out using Hot-Start Taq DNA polymerase (Thermo Scientific) or Phusion polymerase (New England BioLabs) in a general 50 µL reaction as described above. A general PCR protocol of 72 ^{o}C and 68 ^{o}C elongation temperature was used for C-terminal tagging and gene deletion, respectively. The conditions were nonetheless modified according to specific needs.

Table 16: PCR protocol for C-terminal tagging and gene deletion used in this thesis

Step	**Temperature**	**Time**	
Initial denaturation	95 °C	5 min	
	95 °C	30 sec	
Annealing	55 °C	30 sec	10 cycles
Extension	68- 72 °C	1 min/kb	
Final extension	72 °C	5 min	
Denaturation	98 °C	30 sec	
Annealing	55 °C	30 sec /cycle	20 cycles + 20 sec
Extension	68- 72 °C	1 min/kb	
Final extension	72 °C	5 min	
Hold	12 °C	∞	

3.2.2.2 Yeast transformation

Respective competent yeast cells were transformed as described by Knop with a few modifications ([342]). Competent yeast cells were prepared by inoculating a fresh yeast colony in 5 mL YPD medium. The cell culture was incubated at 30 ^{o}C, 220 rpm and cells grown overnight to saturation. The following day, the saturated culture was used to inoculate a fresh 50 mL culture that was grown overnight at 25 ^{o}C, 220 rpm to mid-log phase (roughly 9 x10^{6} cells/mL). Cells were subsequently harvested by centrifugation (5 min, 500g), washed once with 25 mL sterile water and once with 10 mL SORB. After the final wash, the supernatant was carefully decantedand the cell pellet resuspended in 360 µL SORB. The resuspended cells were mixed with 40 µL of 10 mg/mL Salmon sperm carrier DNA (Takara) and aliquoted into 60 µL portions for immediate use or storage at -80

°C. For transformation, 60 µL of competent cells were thawed and mixed with 20 µL of the purified PCR product. A six-fold volume of PEG solution was added (420 µL of PEG solution) and the cells incubated at RT for a minimum of 30 min. A 1/9 volume of DMSO was then added and the cells were incubated at 42 °C for 20 min. Cells were gently centrifuged at 3000 rpm, 3 min to remove the supernatant that would otherwise slow their growth once plated. Depending on the selection marker being used, the cell pellet was treated differently. In cases where cells were selected based on the antibiotic resistance marker, the cell pellet was carefully and gently resuspended in 3 mL YPD medium and incubated at 30 °C, 220 rpm for a minimum of 4 h to allow expression of the antibiotic resistance marker gene. Cells were thereafter centrifuged at 3000 rpm 3 min to remove the supernatant before resuspending the pellet in the final 100 µL. Cells were plated on a YPD plate containing the respective antibiotics: YPD + G418 (400 µg/mL), YPD + Hygromycin (300 µg/mL), YPD + Nourseothricin (100 µg/mL). In cases where cells were selected based on the auxotrophic selection marker, the cell pellet was directly resuspended in 100 µL of synthetic defined (SD) medium lacking the corresponding amino acid (SD-URA, SD-HIS, SD-LEU). The cells were then carefully spread on the corresponding selection plates. All plates were incubated at 30 °C until transformants appeared (approximately 3-4 days). In order to select for true positive transformants, random colonies from the respective selection plates were plated on fresh selection plates, after which a colony PCR was carried out to confirm correct gene tagging or deletion.

3.2.2.3 Colony PCR

In order to extract the genomic DNA for colony PCR, the glass bead Chelex 100 preparation (GC prep) method that makes use of the metal chelating resin, chelex, was used ([343]). Briefly, a small amount of cells from a fresh, single colony was resuspended in 100 µL of sterile 5% Chelex solution and about half the total volume of glass beads were added. The cells were vortexed at maximum speed for 4 min, 30 °C and then incubated at 100 °C for 3 min. Cells were centrifuged at a maximum speed of 13000 rpm for 1 min in order to pellet the cell debris. The supernatant containing genomic DNA was carefully transferred to a fresh tube and used immediately or stored at 4 °C.

Table 17: Composition of the 25 µL colony PCR reaction

4 µL	Genomic DNA
0.125 µL	Forward primer 0.5 µM (0.5 µM final concentration)
0.125 µL	Reverse primer 0.5 µM (0.5 µM final concentration)
0.4 µL	dNTP mix 12.5 mM (0.2 mM final concentration)
2.5 µL	10x DreamTaq buffer
0.25 µL	DreamTaq polymerase
	Fill up with ddH_2O

Table 18: PCR protocol for colony PCR used in this thesis

Step	**Temperature**	**Time**	
Initial denaturation	95 °C	5 min	
	95 °C	30 sec	
Annealing	55 °C	30 sec	35 cycles
Extension	72 °C	2 min	
Final extension	72 °C	5 min	
Hold	12 °C	∞	

3.2.2.4 Scarless gene tagging

In order to carry out a Horseradish peroxidase (HRP)-mediated proximity labeling at the extracellular fertilization synapse, a Scarless gene tagging technique was used to incorporate a yeast-codon optimized HRP sequence at the *FUS1* N-terminus without disrupting any upstream regulatory elements ([344]).

First, a split-HRP construct consisting of a N-terminus HA epitope tag, a TEV cleavage site and a *Kluyveromyces lactis* (*K.l*) *URA3* marker separating the two HRP fragments (nHRP amino acid 1-213, and cHRP amino acid 83-308) i.e., **HA-nHRP-*KlURA3*-cHRP**, was constructed (Invitrogen). To facilitate cassette integration into the *FUS1* locus upon homologous recombination, a two-step PCR was adopted. In the first PCR step, two *FUS1* homology arms (H1 and H2) containing 300 bp upstream and downstream of the ATG start codon that would flank the HRP construct were amplified using the PCR protocol shown below (**Table 19**). The H1 and H2 homology arms were subsequently used as megaprimers in the second PCR step using **HA-nHRP-*KlURA3*-cHRP** as the template DNA. The new PCR product consisting of H1-**HA-nHRP-*KlURA3*-cHRP**-H2 was then transformed into competent cells as described above and positive transformants selected by colony PCR. To excise the *K.l URA3* selection marker, the 5-FOA counter-selection approach was adopted ([345]). Synthetic complete (SC) media plates containing 5-FOA were prepared as described in GoldBio.com by mixing a 1:100 dilution of 100 mg/mL FOA in 100 mL SC media. Cells expressing the HRP-Fus1p recombinant protein and appropriate controls were grown in YPD media, at standard growth conditions (30 ºC, 220 rpm) to mid-log phase. Two serial dilutions of cultures were prepared (1:100 and 1:1000) after which 100 µL of each dilution was spread on a 5-FOA plate and the plates incubated at 30 ºC to allow cellular growth. Colonies that grew on 5-FOA plates represented clones in which the *K.l URA3* selection marker had been excised, allowing the two HRP fragments to reconstitute into a fully functional HRP. These were verified by colony PCR as described above.

Table 19: PCR protocol 1 for Scarless gene tagging used in this thesis

Step	**Temperature**	**Time**	
Initial denaturation	95 °C	5 min	
	95 °C	30 sec	
Annealing	55 °C	30 sec	40 cycles
Extension	72 °C	2 min	
Final extension	72 °C	5 min	
Hold	12 °C	∞	

Table 20: PCR protocol 2 for Scarless gene tagging used in this thesis

Step	Temperature	Time	
Initial denaturation	98 °C	30 sec	
	98 °C	10 sec	
Annealing	53 °C	30 sec	35 cycles
Extension	72 °C	2 min	
Final extension	72 °C	5 min	
Hold	12 °C	∞	

3.2.2.5 Generation of multiple gene deletion mutants by tetrad dissection and sporulation

The construction of double gene deletions of *PRM1*, *PUN1* and *PRM5* were carried out by first generating single *prm1Δ::hphNT1*, *pun1Δ::hphNT1* and *prm5Δ::hphNT1* deletions in the PSAY 983 and PSAY 981 as described above. Respective double gene deletions, in which one gene is replaced by the Kanamycin (KanMX) cassette that offers resistance to geneticin (G418) antibiotic, were generated by making use of the Yeast Knockout (YKO) collection of the *Saccharomyces* Genome Deletion Project (Euroscarf) ([346], [339]). To generate the double mutants, the mCherry-KanMX cassette present in the original PSAY 983 *MAT***a** strains (*prm1Δ, pun1Δ,* or *prm5Δ*) was first removed by crossing the PSAY 983 *MAT***a** strains with WT BY4742 *MATα* cells. The cells were crossed on a YPD plate and incubated at 30 ^{o}C overnight to allow sufficient mating. The resulting diploids were subjected to sporulation and tetrad-dissection following a standard sporulation protocol provided by **Dieter Shmidt** (Max Planck Institute for Biophysical Chemistry, Göttingen). Briefly, the diploids were inoculated in 5 mL sporulation medium (YP+ 2% Galactose) to induce sporulation and incubated overnight at 30 ^{o}C, 220 rpm. The following morning, cells were harvested by a short centrifugation at 2000 rpm, 3 min, and the pellet resuspended in the final 100 µL of medium. Cells were gently spread on a 1% K-acetate plate and incubated at 20 ^{o}C for 5-6 days to allow sporulation ([347]). Once enough asci had formed, a sufficient amount of cells were scrapped off the plate and resuspended in 250 µL distilled water. In order to allow asci digestion, cells were incubated with 50 µL of 2 mg/mL Zymolyase-100T at RT for 20 min. Digested cells were then spread in vertical streaks on one edge of a flat YPD plate. Using a Singer Micro-manipulator, the digested tetrads were carefully transferred onto the opposite edge of the YPD plate and dissected into individual spores according to the manufacturer's instructions. Dissected spores were allowed to germinate into individual haploid clones by incubating the cells at 30 ^{o}C for 2 days. The haploid clones were subsequently replica-plated onto selection media plates to select for haploids with a 2:2 segregation and that contained all the desired genotypes. In this case, *MAT***a** haploids that grew on a SD-LEU plate, a YPD+ Hygromycin (300 µg/mL) plate but failed to grow on a YPD+ G418 (400 µg/mL) plate represented the correct *MAT***a** deletion mutants with a c-GFP::LEU2 fragment and no mCherry-KanMX cassette, and were therefore used in subsequent steps.

Consistently, double *prm1Δpun1Δ* mutants were generated by crossing *prm1Δ::hphNT1* mutants with *pun1Δ::KanMX* from the YKO collection and subsequent sporulation and tetrad dissection as described above. Double gene deletion mutants of *PUN1* and *PRM5* were also generated by crossing the PSAY 981 and PSAY 983 *pun1Δ::hphNT1* and *prm5Δ::hphNT1* strains with selected gene KOs in the YKO collection of the BY4741 and BY4742 background. Triple mutants of *pun1Δfig1Δsur7Δ* and *prm1Δpun1Δsur7Δ* were generated by deleting *SUR7* in a double *pun1Δfig1Δ* and *prm1Δpun1Δ* backgrounds, respectively, via PCR using a *HIS3MX6* cassette as described above. Quadruple mutants of *pun1Δfig1Δsur7Δfmp45Δ* were generated by first deleting

FMP45 using a *URA3* auxotrophic marker via PCR in the PSAY 981 and PSAY 983 *pun1Δ::hphNT1* background, generating *pun1Δ::hphNT1 fmp45Δ::URA3* double mutants. The quadruple mutants were then generated by crossing the triple *pun1Δfig1Δsur7Δ* mutant with a double *pun1Δfmp45Δ* and selecting for haploids expressing the desired genetic combinations following sporulation and tetrad dissection. The quintuple mutants *pun1Δfig1Δsur7Δfmp45Δynl194cΔ* were generated by deleting *YNL194C* via PCR using a *LEU2* cassette in the PSAY 981 quadruple mutant background, and a Nourseothricin cassette in the PSAY 983 quadruple mutant background. All gene deletions were confirmed by colony PCR.

3.2.3 Quantitative cell biology assays

3.2.3.1 Pheromone response assays

Fresh colonies of *MAT***a** cells expressing fluorescent proteins were inoculated in 5 mL YPD medium and grown to saturation by incubating cells at 30 ^{o}C, 220 rpm. These cultures were used to prepare fresh secondary cultures in synthetic complete (SC) or synthetic defined (SD) medium and cells were grown overnight at 25 ^{o}C, 220 rpm. Once the cells had reached mid-log phase (OD600=0,6 corresponding to approximately 6x10^{6} cells/mL), they were washed once with water following a short centrifugation (3000 rpm, 3 min), before final resuspension in fresh medium. Cells were treated with synthetic α-factor (20 µM final concentration) and incubated at 30 ^{o}C, 220 rpm for 1.5 h. An additional 10 µM α-factor was added to replenish Bar1p protease-depleted pheromone and the cells incubated for an additional 1.5 h. Pheromone response was stopped by washing the cells once in fresh medium and once in 1 mL ice-cold TAF buffer (20 mM Tris-HCl pH 7.4, 20 mM NaN_3, 20 mM NaF). Cells were resuspended in the final 50 µL TAF buffer and stored at 4 ^{o}C until imaged.

3.2.3.2 Yeast mating assays

Standard mating assays were performed by inoculating fresh colonies of respective *MAT***a** cells and *MATα* in 5 mL YPD or synthetic defined (SD) medium. Cells were grown to saturation following overnight incubation at 30 ^{o}C, 220 rpm. Saturated cultures were subsequently used to inoculate fresh secondary cultures in desired medium and cells grown to mid-log phase (OD600=0,6 corresponding to approximately 6x10^{6} cells/mL). Equal amount of *MAT***a** and *MATα* cells were then mixed in a total of 5 mL YPD medium (approximately 5x10^{6} cells/mL), and cells vacuumed to 0.45 µm-pore size nitrocellulose filter disks (MF-Millipore). The filters, now containing concentrated cells, were incubated cell-side up on YPD plates and incubated at 30 ^{o}C and cells allowed to mate for 3.5 h unless specified. To stop the mating reactions, cells were scrapped off the filters and resuspended in 1 mL ice-cold TAF buffer by brief vortexing. Cells were then concentrated by centrifugation at 3000 rpm, 3 min, and final resuspension in the remaining 50 µL TAF buffer. Cells were stored at 4 ^{o}C until imaged.

3.2.3.3 GFP bimolecular fluorescence complementation (BiFC)- based flow cytometry fusion assay

In order to quantify cell- cell fusion, a quick and efficient multicolor flow cytometry assay based on GFP bimolecular fluorescence complementation (BiFC) was adopted as described by Salzman ([348]). This assay is based on the expression of non-fluorescent GFP fragments (NeGFP and CeGFP) fused to a leucine zipper dimerization domain, in the haploid *MATα* and *MAT***a** cells, respectively. Upon cell-cell fusion, complementation of the n-GFP and c-GFP fragments results in the formation of a fluorescent GFP protein whose fluorescence be detected and quantified ([349]). In order to identify mating pairs from a mating mixture, haploid *MATα* and *MAT***a** cells are first differentially stained with Concanavalin A (ConA)–fluorophore conjugates. The stained cells are mixed and allowed to mate for a period of 3.5 h at 30 ^{o}C after which the mating reactions are analyzed by a multicolor flow cytometer. By applying the required gating strategies, stained and unstained cell populations are differentiated, and mating pairs identified as a double-stained sub-population. Notably, fused mating pairs are identified as double-stained cells expressing GFP and can be distinguished from the unfused mating pairs i.e. double stained but GFP negative. The

fusion efficiency is subsequently quantified as a percentage of the GFP positive cells in the total double-stained sub-population (**Figure 9**).

Accordingly, haploid *MATα* and *MAT***a** cells harboring non-fluorescent NeGFP and CeGFP fragments, respectively, were grown to mid-log phase in YPD or selective medium as described above. Cells were harvested and washed once with 5 mL sterile water and a final resuspension in 2 mL 1x PBS. *MATα* and *MAT***a** cells were differentially stained with Concanavalin A (ConA)–fluorophore conjugate (Invitrogen) ConA-647 (1 µg/µL) and ConA-Tet (5 µg/µL) respectively and incubated at RT in the dark for at least 30 min. The cells were subsequently washed once with 5 mL sterile water to remove excess dyes before a final resuspension in 5 mL YPD medium. Equal amounts of *MATα* and *MAT***a** cells were mixed (approximately 2 x10^6 cells/mL) in a final volume of 5 mL YPD and vacuumed to 0.45 µm-pore size nitrocellulose filter disks (MF-Millipore). The filters, now containing concentrated cells, were incubated cell-side up on YPD or specified plates and incubated at 30 °C for 3.5 h, allowing the cells to mate. Mating pairs were scrapped off the filters and resuspended in 1 mL ice-cold TAF buffer by brief vortexing and were ready for flow cytometry analysis as described by ([348]). Briefly, using independent unstained and stained haploid cells as controls, a standard forward scatter (FSC) versus side scatter (SSC) cell gate was applied to remove debris and define the different stained and unstained sub-populations in a logarithmic scale. Haploid cells that formed mating pairs were subsequently identified as a double-stained sub-population in a ConA-647 versus ConA-Tet plot. From the double-stained sub-population, fused mating pairs expressing GFP following complementation of the NeGFP and CeGFP fragments were distinguished from unfused mating pairs using a SSC versus GFP plot. The respective fusion efficiencies were quantified as the percentage of the GFP positive cells in the total double-stained sub-population (**Figure 9**).

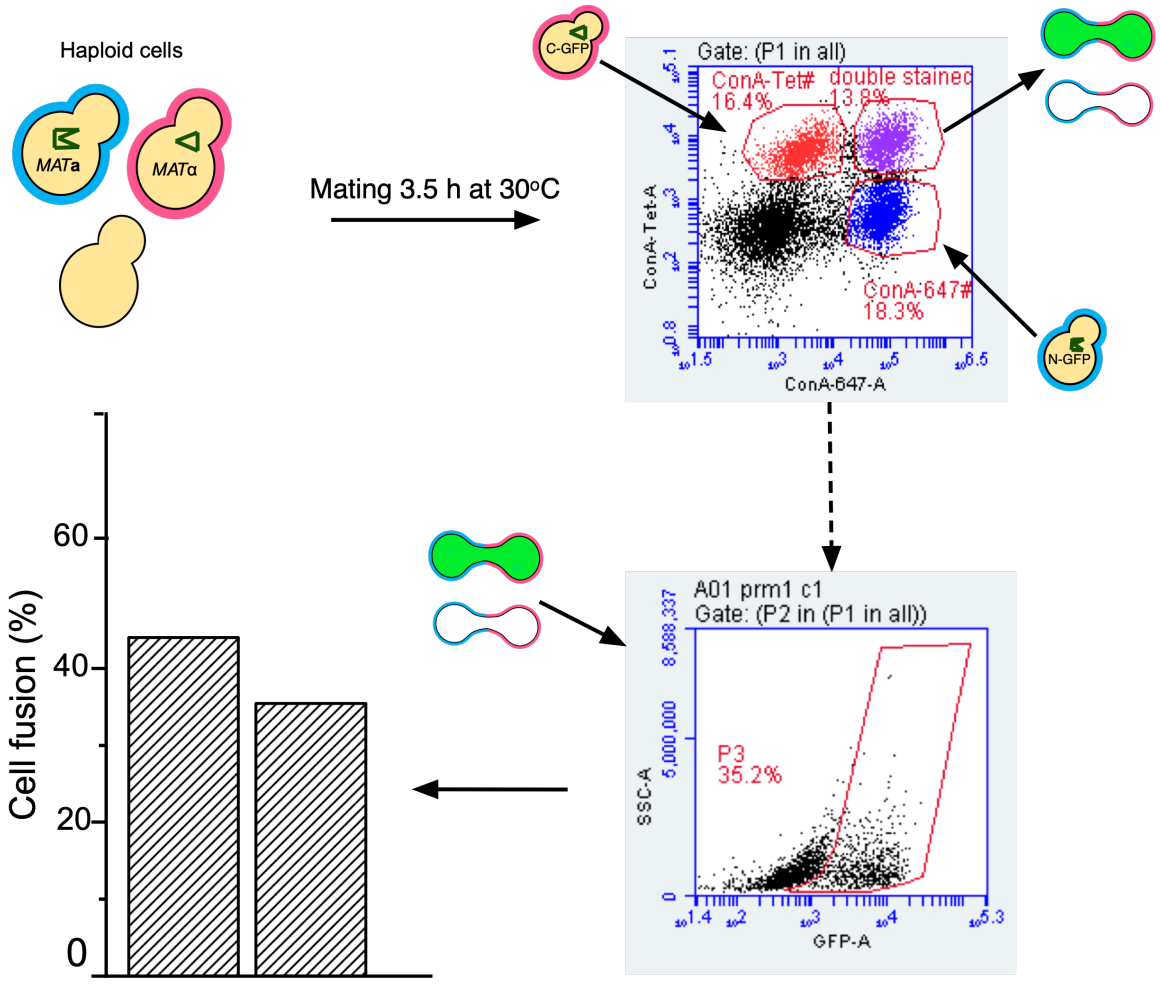

Figure 9: Schematic of the quantitative BIFC-based flow cytometry fusion assay. Haploid *MATα* and *MAT***a** cells

expressing NeGFP and CeGFP fragments are differentially stained with Concanavalin A (ConA)–fluorophore conjugates, ConA-647 and ConA-Tet. The stained cells are mixed and allowed to mate for 3.5 h at 30 ºC. The mating mixtures are analyzed by a multicolor flow cytometer that distinguishes the stained and unstained sub-populations using a FSC versus SSC plot. In a ConA-Tet versus ConA-647 plot, the double-stained sub-population represents stained haploid cells that have formed mating pairs. Of these, fused mating pairs are scored as double stained cells with GFP fluorescence following complementation of the NeGFP and CeGFP fragments. The percentage of GFP+ cells in the double-stained sub-population represents the fusion efficiency.

3.2.3.4 Calcium depletion and supplementation assays

Mating assays to determine the effect of calcium supplementation in the mating reactions were performed by first inoculating cells in 5 mL YPD or SD-URA medium supplemented with 1 mM $CaCl_2$. Cells were incubated overnight at 30 ºC, 220 rpm and grown to saturation. Respective secondary cultures were prepared in fresh 5 mL YPD or SD-URA supplemented with 1 mM $CaCl_2$ and grown to mid-log phase. Equal amounts of cells of each mating type were mixed in 5 mL YPD supplemented with 1 mM $CaCl_2$ with and vacuumed to a 0.45 µ nitrocellulose filter disks (MF-Millipore). The cells were allowed to mate as described above except that the YPD plates were supplemented with 1mM $CaCl_2$. On the other hand, the effect of calcium depletion on the mating process was assessed by growing cells in YPD or SD-URA medium (Formedium) using standard conditions both in the saturated and secondary cultures as described for standard quantitative yeast mating assays. However, mating was performed in Ca^{2+} depleted conditions by incubating the nitrocellulose filters on YPD supplemented with 20mM EGTA (Sigma-Aldrich). The cells were allowed to mate for 3.5 h and the mating reactions stopped by resuspending cells in TAF buffer as described above. The mating efficiencies of respective reactions were determined using the BiFC-based flow cytometry fusion assay.

3.2.3.5 CW and PM staining

In the event where CW and/or PM staining was necessary before imaging, cells were treated with different dyes upon resuspension in 1 mL ice-cold TAF buffer. Staining of the CW α-mannan was performed by mixing the cells with 5 µL of ConA-647 (1 µg/µL) dye and incubating the cells in the dark for at least 30 min. Cells were washed once with 1 mL ice-cold TAF buffer to remove excess dye before final resuspension in remaining 50 µL TAF buffer. Calcofluor white chitin staining was performed by mixing the cells with 1:100 dilution of 1 mg/mL Calcofluor white stain (Sigma-Aldrich). Cells were incubated at RT, in the dark for at least 5 min after which they were washed once with 1 mL sterile water and a final resuspension of the cell pellet in the remaining 50 µL water. When both stains were required, cells were first stained with ConA-647 (1 µg/µL) and thereafter Calcofluor white as described above with no washing step between the two staining events. PM staining with FM4-64 was performed on ice just before imaging as described by Grote ([350]). Briefly, 2 µL of cells (stained or unstained) were mixed with 2 µL of FM4-64 (Molecular Probes/Invitrogen, 4 mM final concentration). 1.8 µL of the stained cells were loaded onto a slide for imaging.

3.2.3.6 Fluorescence Microscopy

Cells expressing fluorescence proteins or stained cells were imaged with either confocal light microscopy (Zeiss LSM-800) or Marianas Spinning Disk confocal microscope (Zeiss). For the Zeiss LSM-800, single images were acquired either with a 63x Plan-Apochromat oil-immersion objective (NA=1.4) or 40x Plan-Apochromat water-immersion objective (NA=1.0). A 100X Plan-Apochromat oil-immersion objective (NA=1.4) was used for the Spinning Disk confocal microscope. Images for the quantification of cell fusion phenotypes were acquired with a 40x Plan-apochromat objective fitted with Airyscan. Desired laser channels as well as differential interface contract (DIC) were used to automatically acquire images from random image fields as identified using DIC optics. Time-lapse imaging was carried out as previously described by Grote with minor modifications ([350]). Briefly, mating mixtures were prepared as described above and cells allowed to mate for 35 min. Cells were concentrated by brief centrifugation (2000 rpm, 1 min) and 1.8 µL of cells carefully transferred onto agarose pads containing 1.8% agarose (Invitrogen) in synthetic complete (SC) medium. Coverslips were carefully placed on the cell suspension, avoiding formation of air

bubbles, and sealed with nail polish. Cells were imaged at 30 ºC for a minimum of 2 h.

3.2.4 Protein biochemistry

3.2.4.1 Yeast cell disruption and protein extraction

Disruption of cells and protein extraction varied slightly during different experiments, but a general protocol of glass bead cell lysis and alkaline-TCA protein precipitation is as described below. Fresh colonies were inoculated in 5 mL of desired medium and cells were incubated overnight at 30 ºC, 220 rpm and grown to saturation. The saturated cultures were then used to inoculate fresh 50 mL cultures or more in desired medium and cells were grown to mid-log phase. In cases where cells were directly subjected to lysis, cells were first harvested and washed with 0.5 volumes distilled water and once with 0.2 volumes ice-cold TAF buffer. Pellets were stored at -20 ºC or immediately subjected to cell lysis. In cases where cells were subjected to pheromone treatment conditions, the cultures were first washed with 0.5 volumes distilled water and cells subsequently resuspended in 50 mL fresh medium. Cultures were divided into two equal halves and one half was treated with pheromone as described above. All cultures were incubated for 3 h at 30 ºC, 220 rpm to allow pheromone response and expression of mating-responsive genes. Cells were subsequently harvested and washed as described above. For lysis, cell pellets were resuspended in Roedel-mix consisting of 2M NaOH and 1.25% β-mercaptoethanol and supplemented with 1 mM PMSF, 2x protease inhibitor cocktail (PIC, 1000x stock) consisting of antipain, aprotinin, leupeptin, chymostatin, pepstatin A and incubated on ice for 10 min. Lysis buffer and about half the final volume of 0.5 mm glass beads (Sigma-Aldrich) were added and the cells broken by vortexing at high speed for at least 10 min with 30 sec pause on ice after each minute. Once a sufficient amount of cells had lysed, cells were cleared of debris by a brief centrifugation at 3000 rpm, 3 min, 4 ºC. The cleared lysates were transferred to fresh tubes and proteins precipitated with TCA (30% final concentration) for 20 min on ice. The protein pellets were subsequently washed twice with 100% acetone, and the pellets dried at RT for 10 min. The protein extracts were ready for solubilization.

3.2.4.2 Protein de-glycosylation

In order to cleave N-linked glycans, cell lysates were first prepared by the alkaline-TCA method as described above. The protein pellets were subsequently resuspended in 100 µL distilled water supplemented with 10 mM DTT and 2% SDS. Proteins were denatured by heating the samples at 95 °C for 5 min. The denatured extracts were cooled at RT for 5 min after which the sample pH was brought to 7.5 with 0.5 M sodium phosphate buffer (pH 7.53). Samples were divided into two equal halves after which one half was treated with 50U/µL PNGase F (Sigma Aldrich) and 2% Nonidet P-40 (NP-40) detergent to prevent PNGase F inactivation by SDS. Samples were incubated overnight at 37 °C and the de-glycosylation reaction was stopped by adding 2x SDS sample buffer.

3.2.4.3 Sodium dodecyl sulfate-polyacrylamide gel electrophoresis (SDS-PAGE)

Protein extracts were dissolved in 2x SDS loading buffer and denatured by boiling at 95 ºC for 5 min unless specified. The denatured extracts were briefly centrifuged at max speed for 1 min and the clear supernatants were ready for loading onto SDS-polyacrylamide gel. Pre-cast 4-15% Mini-PROTEAN TGX Stain-Free Protein gels or self-prepared Laemmli SDS-PAGE discontinuous mini-gels were used during different experiments. Discontinuous mini-gels were cast according to the manufacturer's instructions (Bio-Rad, Munich, Germany). Briefly, the casting apparatus were properly assembled to allow no leaks during casting. About 80% volume of separating gel solution (see below composition for 10% gel) was loaded and overlaid with isopropanol to form a uniform level. The gel was allowed to polymerize at RT for about 20 min. The isopropanol was then removed and the stacking gel solution (see below composition for 4% gel) was added. Combs were immediately inserted, and the gel allowed to polymerize for about 20 min after which the gels were stored in damp paper clothes at 4 ºC. For protein separation according to size, Laemmli denaturing conditions were used ([351]). 10-15 µL of protein samples were loaded and 5 µL of PageRuler

Prestained protein ladder. Samples were separated under constant voltage of 110V for approximately 70 min or until the dye front had run out of the gel. Separated proteins were visualized either by Coomassie staining (see composition) or by Western blotting. For Coomassie staining, gels were incubated with the staining solution for 1 h at RT with gentle agitation. Optionally, staining was accelerated by shortly heating the gels in a microwave. Excess dye was removed by incubating the gels with the De-stain solution that de-stain the gels leaving only the stained protein bands.

Table 21: 10% SDS-PAGE gel composition

	Separating gel (10%)		**Stacking gel (4%)**	
Component	**Stock Concentration**	**Volume**	**Stock Concentration**	**Volume**
Water		4.1 mL		6.1 mL
Acrylamide	30%	3.3 mL	30%	1.3 mL
Tris-HCl		2.5 mL		2.5 mL
SDS	10%	100 µL	10%	100 µL
APS		10 µL		10 µL
TEMED	10%	32 µL	10%	100 µL

3.2.4.4 Western blot analysis

Following protein separation by SDS-PAGE, proteins were transferred to PVDF using the semi-dry Trans-Blot Turbo Transfer System (BioRad) (constant 2.5 A, 25 V, 7 min), or transferred to a nitrocellulose membrane via the wet transfer method in a Mini Trans-Blot^{R} Cell (BioRad) (constant 2.8 A, 2.40 h or constant 0.09 A, 16 h overnight). For the wet blot transfer, a transfer sandwich consisting of the nitrocellulose membrane sandwiched between two Whatman paper sheets was assembled in transfer buffer (20% (v/v) methanol, 25 mM Tris-HCl, pH 7.4, 190 mM glycine). The assembled sandwich was positioned in the Mini Trans-Blot^{R} Cell with the gel facing the cathode and the membrane facing the anode. Protein transfer was done at 4 ^{o}C with gentle agitation (300 rpm) to allow homogenous distribution of any heat generated during the transfer. In order to visualize the blots by immunodetection, membranes were first blocked with a blocking solution containing 5% fat-free milk in TBS-T for 1 h, at RT under gentle agitation. Membranes were subsequently incubated with primary antibodies in blocking solution at RT for 2 h or overnight at 4 ^{o}C with gentle agitation. The membranes were washed four times for at least 10 min with TBS-T and then incubated with HRP-conjugated secondary antibodies dissolved in blocking solution, for 1 h at RT. Membranes were washed five times with TBS-T, each wash lasting 5 min, before chemiluminescence detection using GE Healthcare chemiluminescence substrate and a BioRad imager.

3.2.4.5 HRP- Fus1p- mediated proximity labelling

In order to carry out HRP-Fus1p- mediated proximity labeling, BY4741 *MAT***a** cells expressing the recombinant protein were first treated with pheromones as described above. Once sufficient amount of cells had polarized and formed shmoos, cells were harvested and washed two times with fresh medium before final resuspension of the cell pellet in 100 mM $NaCO_3$ (pH 9.4) in presence of α-factor (5 µM) for 10 min at RT to loosen the CW. The subsequent steps were then performed at 4 ^{o}C to inhibit membrane transport. Cells were gently harvested and washed once with 1x PBS before resuspension and incubation in 900 µL of 200 µM of Biotin-AEEA-Phenol (in 1x PBS) for 2 min. After 2 min, 100 µL of 1 M Hydrogen peroxide (1 mM final concentration) was added to initiate the biotinylation reaction. After 1-2 min, the reaction was stopped by quickly spinning down the cells and adding 1 mL of the Quenching solution (10 mM Sodium azide, 10 mM

Sodium ascorbate, 5 mM Trolox in Spheroplasting buffer). The cells were then gently centrifuged and washed two times with the Quenching solution before a short incubation (1-2 min) in 1 mL TAF buffer. This short incubation in TAF buffer promotes the complete inhibition of any metabolic activity in the cell. The cells were then washed once with 1x PBS before a final resuspension in 1 mL 1x PBS. To initiate biotin staining, 2 µL of Streptavidin coupled to Alexa 647 (streptavidin Alexa 647 conjugate) was added and the cells were incubated for 60 min in the dark. Stained cells were subsequently washed twice in 1x PBS to remove unbound streptavidin before proceeding to imaging.

3.2.5 Bioinformatics analysis and visualization tools

DNA sequences of all yeast genes were obtained from the Saccharomyces Genome Database (SGD) website (https://www.yeastgenome.org). Gene-specific primers were designed in the Primers4Yeast platform (https://www.weizmann.ac.il/Primers-4-Yeast/). Plasmid design was performed using the SnapGene Viewer software while plasmid DNA sequence alignment was carried out using the SeqMan Pro tool of the DNASTAR software. Respective protein sequences were obtained from the UniProt website (uniprot.org). Membrane topology predictions were carried out using the TOPCONS server ([352]). Multiple sequence alignments were performed using the Clustal Omega server (EMBL-EBI) or the HHpred Bioinformatics tool in the MPI Bioinformatics Toolkit (https://toolkit.tuebingen.mpg.de/tools/hhpred) ([353]). The Phyre2 web server was used to predict the three-dimensional structure of proteins based on their sequences while the 'UCSF Chimera' program was used to compare protein structures ([354]). All microscopy images were processed using the Image J software while the SDS-PAGE and Western blot images were processed using the Image Lab (Bio-Rad) software. Figures in this thesis were created and modified with Graphic software or Microsoft PowerPoint.

3.2.6 Statistical analysis and significance testing

Generally, three different cultures were prepared from three different colonies of a single strain, and thus defined as biological triplicates. For the *PUN1* overexpression studies, all replicates represented different independent clones of each particular strain, and hence defined as biological replicates. The repeated mating experiments were performed independently from the same biological samples, but with each experiment subjected to similar experimental conditions and setup. Quantification of mating phenotypes was performed on three biological replicates, and a minimum of 150 mating pairs counted across all replicates. Microsoft Excel and Origin were used for statistical analysis and data presentation. Two-tailed paired t-test was used to compare groups of data. A P-value below 0.05 was considered statistically significant and was represented with two asterisks (**), while a P-value below 0.01 was represented with three asterisks (***) in a graph. Data that showed no statistical significance were indicated as "ns". Error bars generally represent standard error of the mean (SEM) unless indicated otherwise.

4 Results

4.1 A SILAC-based proteomics approach identifies differentially regulated membrane-associated proteins upon pheromone treatment

Yeast mating provides a genetically amenable model system to understand sexual cell-cell fusion. In *Saccharomyces cerevisiae*, the mating of *MAT***a** and *MATα* cells to produce a diploid zygote is analogous to the sperm-egg fusion process during fertilization. In both systems, a comprehensive molecular characterization of how the two cells merge their plasma membranes (PM) to facilitate cytoplasmic mixing and diploid zygote formation is lacking. In particular, the *bona fide* fusogen/fusogenic complex that directly mediates lipid bilayer fusion remains elusive. In *S. cerevisiae,* a handful of proteins involved in the critical stages of cell wall (CW) remodeling and PM fusion have been identified. Fus1p and Fus2p are two proteins necessary in the CW remodeling step ([228], [238], [253]). When either gene is deleted, early prezygotes that arrest at the CW remodeling step are formed ([228]). In the recent past, a reverse genetics approach identified Prm1p as a protein directly involved in the PM fusion step during yeast mating ([266]). Indeed, *prm1Δ* mutants arrest at the PM fusion step although ~50% of *prm1Δ* mating pairs still fuse. Other genes such as *KEX2*, *FIG1* and the ergosterol synthesis genes *ERG3*, *ERG4* and *ERG6* have also been implicated in PM fusion ([272], [291], [355], [356], [357]). However, their null mutants do not completely block fusion, suggesting the existence of additional players of fusion.

To identify additional players of PM fusion, work done by Matias Hernandez involved a comprehensive mass spectrometry-based analysis of changes in PM composition as the cell transitions from vegetative to mating-ready state (**Figure 10A**). To mimic the cellular transition from vegetative to mating-ready state, haploid *MAT***a** and *MATα* cells were treated with α-factor and **a**-factor, respectively. Treatment of both mating types with pheromone allowed the identification and characterization of the general as well as mating-type specific PM changes as the cell transitions to a mating-ready state. Notably, owing to the hypothesis that proteins involved in fusion are either integral membrane proteins or associated with the PM, membrane fractions were isolated and subjected to mass spectrometry (MS) analysis. Importantly, the stable isotope labeling by amino acids in cell culture (SILAC)-based MS proteomics analysis permitted a quantitative comparison of the abundance of individual protein peptides in vegetative and pheromone-treated cells. A total of 24 PM proteins were pheromone-upregulated in both mating types (**Table S1**). Of these, ~10 proteins were membrane proteins with known functions in yeast mating, thus validating this approach. These included Prm1p, Prm3p, Fig1p, Chs1p, Sst2p, Sag1p, *MAT***a**-specific Asg7p and the α-factor receptor Ste2p, as well as the MAP kinase Fus3p ([266]). The additional 14 proteins present in the pheromone-upregulation cluster had no known functions in yeast mating. Strikingly, the down-regulated protein cluster was mainly represented by eisosome-associated proteins except for one protein, Pun1p. Consistently, these down-regulated proteins showed high mean intensities, suggesting high protein levels in vegetative cells.

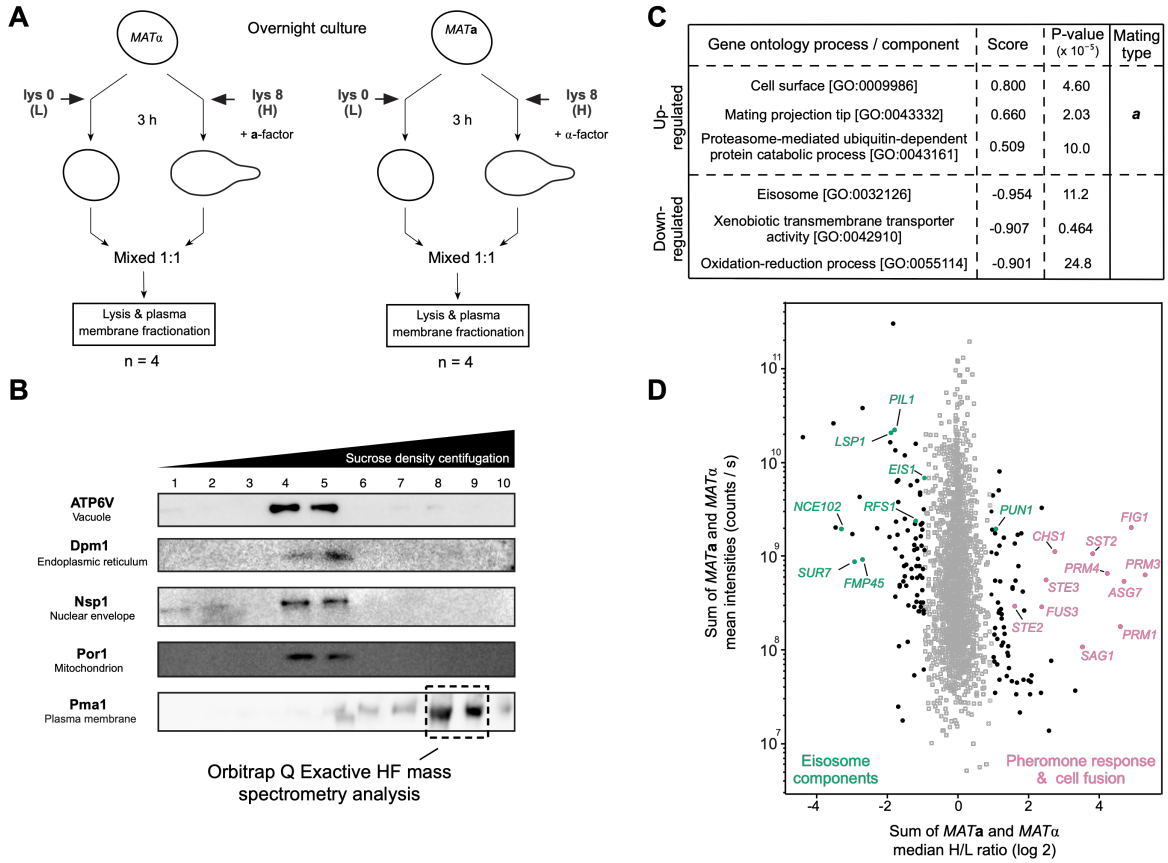

Figure 10: Yeast plasma membrane proteins are differentially expressed upon pheromone treatment. (**A**) Two equal cultures of *MAT***a** and *MATα* were differentially labelled using a Stable Isotope Labeling with amino acids in Cell culture (SILAC)-based approach. The cultures labelled with the heavy lysine isotope were treated with pheromone for 3 h while the low lysine isotope was used in vegetative cultures. The vegetative and pheromone-treated cultures of respective mating types were mixed in a 1:1 ratio before plasma membrane fraction isolation. n=4 (**B**) Membrane fractions were isolated by sucrose gradient centrifugation and the plasma membrane fraction subjected to Orbitrap Q Exactive HF mass spectrometry analysis. (**C**) Gene ontology classification according to protein function or localization was performed. (**D**) Combined expression profiles of different membrane proteins in *MAT***a** and *MATα* cells represented combined mean intensities (counts/ s) against combined median log2 H/L ratio. Data and figure provided by Matias Hernandez.

4.2 *ASG7*, *ISC1*, *PRM5* and *PUN1* are preferentially upregulated upon pheromone treatment

In order to validate the proteomics data and investigate the functional significance of the pheromone-upregulated proteins, protein expression and localization studies were performed. These two parameters functioned as initial determinants of protein function. Proteins necessary for fusion are often pheromone upregulated and localized at the cell-cell contact site or mating junction during mating ([228], [238], [266]). For the initial characterization of the novel pheromone upregulated proteins, respective genes in *MAT***a** haploid cells were either chromosomally tagged at the C-terminus or retrieved from the Yeast GFP Clone Collection ([340]). For the genes retrieved from the Yeast GFP Clone Collection, *FUS1*-GFP whose expression is pheromone-dependent and the protein localized at the shmoo tip, was used as a control protein. The remaining genes were C-terminally tagged with mNeonGreen (mNG), a stable and highly-fluorescent monomeric protein with an excitation maximum at 506 nm and an emission maximum at 517 nm ([358]). For these class of genes, a *PRM1*-mNG construct was used as a control due to the exclusive pheromone-dependent expression of *PRM1* and its localization at the shmoo tip or mating junction ([266]). The localization profile of all proteins in vegetative and pheromone-treated conditions was then determined.

Consistent with previous findings, Fus1p-GFP showed a clear pheromone-dependent expression and was localized at the shmoo tip of polarized cells (**Figure 11**). Interestingly, all the other genes including *YIL108W*, *YHR097C*, *YJL049W*, *YNR065C* and *YNR066C* showed no apparent expression in vegetative cells. Upon pheromone treatment, a mild increase in protein expression was observed in *YIL108W*-GFP and *YHR097C*-GFP expressing cells while all the other genes showed no pheromone-dependent expression. These findings therefore suggested that these genes were possibly false positives and were thus eliminated from further analysis.

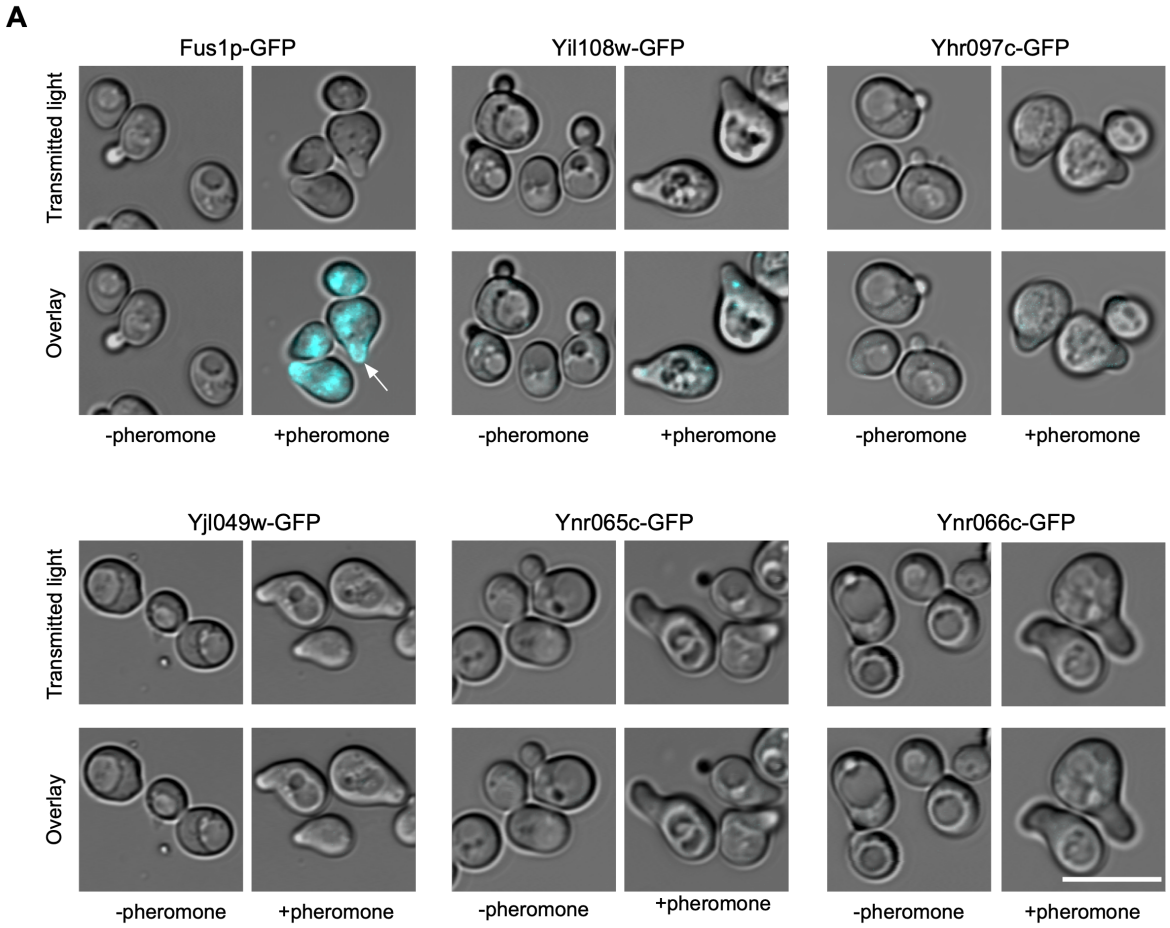

Figure 11: Verification of the pheromone- dependent expression of novel genes identified from the proteomics analysis. *MAT***a** BY4741 cells expressing either C-terminally tagged *FUS1*-GFP or uncharacterized genes retrieved from the Yeast GFP Clone Collection were grown to log phase in synthetic complete medium. Cultures were split into two equal portions and one portion was incubated with 20 µM *α*-factor for 2 h. Cells were arrested in TAF buffer and imaged. Fus1p-GFP serves as a positive control and is expressed only upon pheromone treatment and localizes at the shmoo tip (white arrow). Yil108w-GFP shows a mild increase in expression upon pheromone treatment. *YHR097C*, *YJL049W*, *YNR065C* and *YNR066C* show little to no expression in both vegetative and pheromone-treated cells. Scale bar= 5 µm.

On the other hand, proteins such as Asg7p, Isc1p, Prm5p and Pun1p showed a pheromone-dependent expression similarly to Prm1p (**Figure 12**). In comparison to the basal Asg7p-mNG expression observed in vegetative cells, Asg7p-mNG was highly expressed upon pheromone treatment and portrayed a cytoplasmic puncta-like localization. Consistent with previous findings, the Asg7p-mNG cytoplasmic puncta likely indicate sites of interactions between Asg7p and the Gβ-subunit Ste4p to promote receptor signaling inhibition during the course of the pheromone response ([359]). Similarly, Isc1p-mNG, a sphingolipid phospholipase C1 that functions in the inositol phosphosphingolipid catabolism pathway, was highly expressed in pheromone-treated cells and localized at the cortical ER. In a few cells, Isc1p-mNG was present at the shmoo tip,

suggesting a putative role in yeast mating (**Figure 12**). Additionally, Prm5p, a protein that was previously identified as a pheromone-regulated membrane protein (PRM) 5, showed a clear pheromone-dependent expression although majority of the protein was localized in the vacuole ([266]). In a few polarized cells, Prm5p-mNG was observed as a discrete puncta at the shmoo tip. Interestingly, the eisosomal protein Pun1p-mNG was highly pheromone upregulated and localized at the cell periphery as well as the shmoo tip of polarized cells, suggesting its possible role in the mating pathway. On the contrary, Ypr170w-b-mNG was expressed in both vegetative and pheromone-treated cells and portrayed a vacuolar-membrane localization pattern. The presence of a vacuolar membrane protein within a supposed PM fraction indicates the presence of possible contaminants during the preparation of PM fractions. Membrane compartments that are biochemically similar to the PM may have been carried over and analyzed together with the PM fractions. Finally, *PRM4* that encodes a previously identified pheromone-regulated membrane protein (PRM) 4, was present in the pheromone upregulated cluster. However, efforts to chromosomally tag *PRM4* at the C-terminus were not successful and the protein could not be investigated further.

Nonetheless, the three genes *ISC1*, *PRM5* and *PUN1* that demonstrated significant pheromone-upregulation and localization at the shmoo tip suggested possible yeast mating functions and were therefore ideal candidates for further analysis. As previously mentioned, *ISC1* encodes a sphingolipid phospholipase C1 that hydrolyzes inositol phosphosphingolipids to generate ceramides ([360]). However, despite the increased protein expression upon pheromone treatment, Isc1p-mNG was mainly localized at the ER, consistent with previous findings ([360], [361]). These findings therefore suggested that the protein function is possibly exerted at the ER as opposed to the PM in mating conditions. Consequently, more focus was put in characterizing *PRM5* and *PUN1* mainly because: (i) *PRM5* had been previously implicated in yeast mating but its function had not been clearly elucidated, (ii) *PUN1* was strongly pheromone upregulated and localized at the cell surface, suggestive of a putative PM-related function in yeast mating.

All in all, this two-state SILAC-based MS strategy provided new insights on the differential regulation of membrane proteins as the haploid *MAT***a** or *MATα* cell transitions from vegetative to a mating-ready state. Additionally, it revealed two novel pheromone-upregulated membrane proteins that possibly function in the yeast mating pathway.

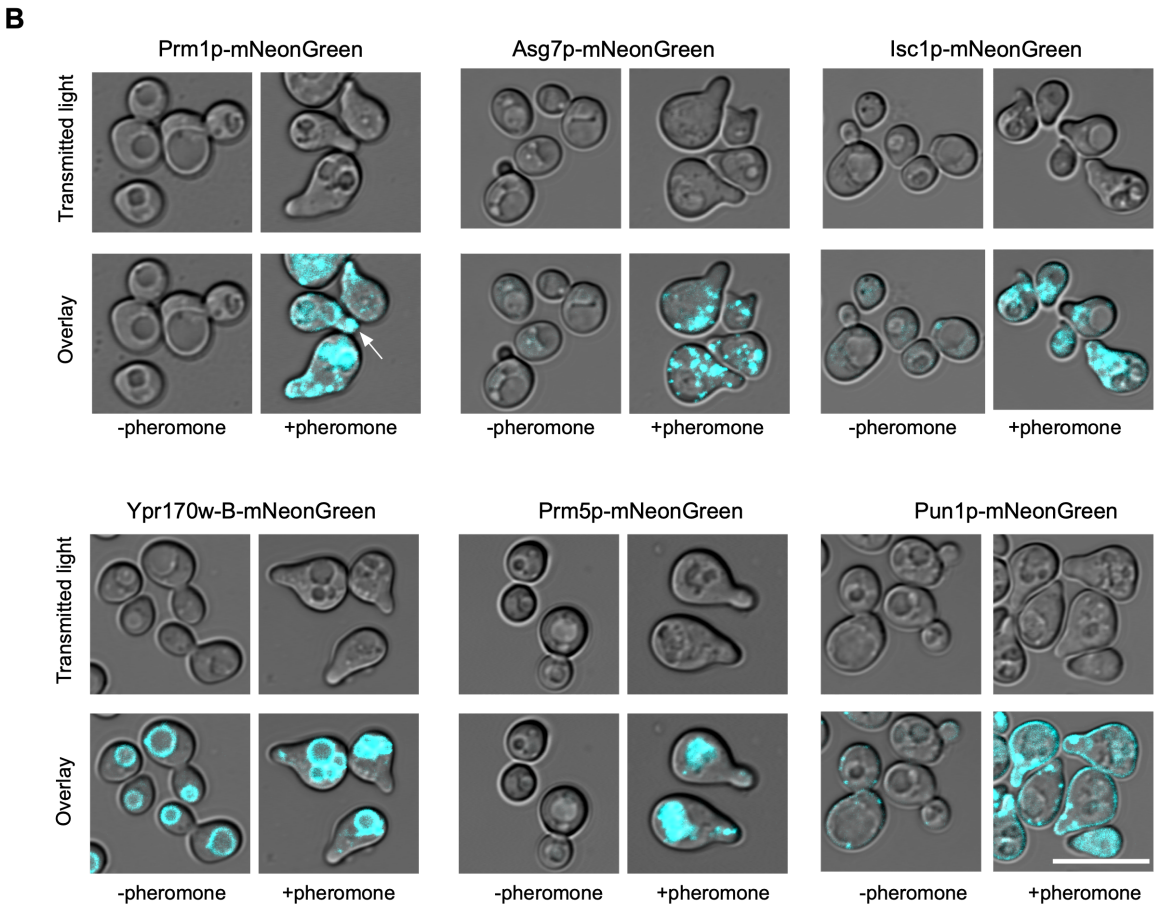

Figure 12: Expression of *ASG7*, *ISC1*, *PRM5* and *PUN1* is pheromone dependent, similar to *PRM1*. Respective genes in *MAT***a** BY4741 cells were chromosomally tagged at the C-terminus with mNeonGreen and treated with 20 µM *α*-factor for 2 h as previously described. Prm1p-mNG is exclusively expressed in pheromone treated cells and localizes at the shmoo tip (white arrow). Asg7p-mNG portrays a cytoplasmic puncta-like localization while Isc1p-mNG is localized in ER as well as shmoo tip of some polarized cells. Prm5p-mNG and Pun1p-mNG are highly expressed upon pheromone treatment with Pun1p-mNG localizing at the cell periphery as well as shmoo tip of most polarized cells. Ypr170w-B-mNG is a vacuolar membrane protein whose expression is not pheromone-dependent. Scale bar= 5 µm.

4.3 Expression of Prm5p but not its paralogous protein Ynl058cp, is pheromone- dependent

Prm5p, a 34.7kDa single-pass transmembrane protein, was initially identified as a pheromone-regulated membrane protein ([266]). In concert with the proteomics data, expression of Prm5p was pheromone-dependent with minimal Prm5p basal expression observed in vegetative cells (**Figure 13A** and **13B**). However, in contrast to Prm1p-mNG that localized at the shmoo (**Figure 13A**), Prm5p was rarely observed at the shmoo in polarized cells. Instead, the protein mainly localized at the vacuole but occasionally localized as small puncta at the shmoo tip (**Figure 13B**). The localization of Prm5p at the vacuole suggested that during pheromone response, the protein was possibly undergoing constant degradation as opposed to shmoo tip retention. This would imply that Prm5p activity is transiently exerted at the shmoo tip or that Prm5p functions upstream in the pheromone response pathway. Alternatively, functional redundancy between Prm5p and its paralogous protein Ynl058cp, would result in Ynl058cp performing a Prm5p- like function at the shmoo tip. To confirm the latter hypothesis, localization of Ynl058cp in polarized cells was assessed. Contrary to Prm5p, expression of Ynl058cp-mNG was not pheromone-dependent and the protein was constitutively expressed in both vegetative and pheromone-treated cells (**Figure 13C**) ([324], [362]). Additionally, Ynl058cp was exclusively localized at the vacuole, suggesting that the two proteins are differentially regulated.

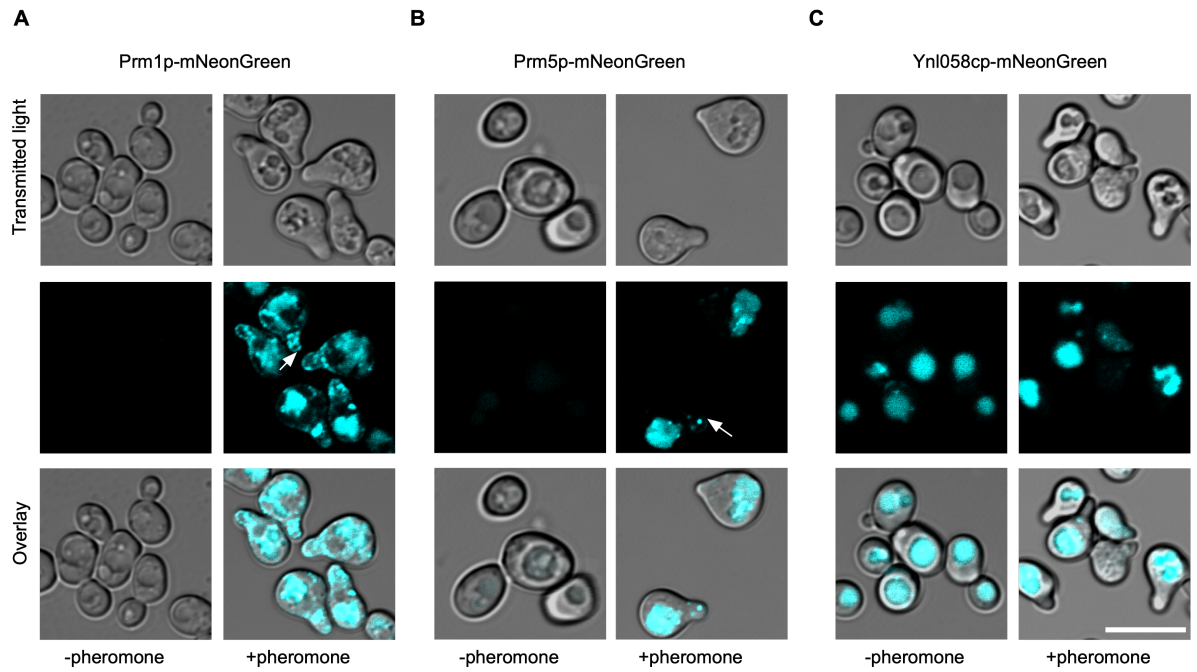

Figure 13: *PRM5* expression is pheromone dependent, similar to *PRM1*. *MAT***a** BY4741 cells expressing *PRM1, PRM5* and its paralog *YNL058C* chromosomally tagged at the C-terminus with mNeonGreen were grown to log phase in synthetic complete medium. Cultures were split into two equal portions and one portion was incubated with 20 µM *α*-factor for 2 h. Cells were arrested in TAF buffer and imaged. (**A**) Prm1p-mNG is expressed only upon pheromone treatment and is localized at the shmoo tip (white arrow). (**B**) Similarly to Prm1p, Prm5p-mNG expression is pheromone-dependent and a small percentage of the protein is localized at the shmoo tip (white arrow). Prm5p is mostly localized at the vacuole. (**C**) Ynl058cp-mNG, a Prm5p paralog is constitutively expressed in both vegetative and pheromone-treated cells. In both conditions, the protein maintains a vacuolar localization. Scale bar= 5µm.

Although the majority of Prm5p localized at the vacuole, the small percentage of Prm5p observed at the shmoo tip hinted that the protein could be playing an unknown function in mating. To confirm this hypothesis, the localization of Prm5p in mating cells was examined. As expected, the control protein Prm1p-mNG was enriched at the mating junction in unfused mating pairs and was retained at the junction of fusing cells (**Figure 14A**). Once mating was completed, Prm1p localized at the vacuole corroborating its PM fusion role after which the excess protein is transported to the vacuole for degradation. On the contrary, Prm5p-mNG was not localized at the mating junction. Instead, the protein was observed in the vacuole prior to PM fusion, suggesting that Prm5p is not directly involved in late fusion events but possibly exerts an unknown function away from the mating junction **Figure 14B**). Similarly to Prm5p, Ynl058cp-mNG was excluded from the mating junction and localized at the vacuole. Its expression was however lower than that of Prm5p (**Figure 14C**).

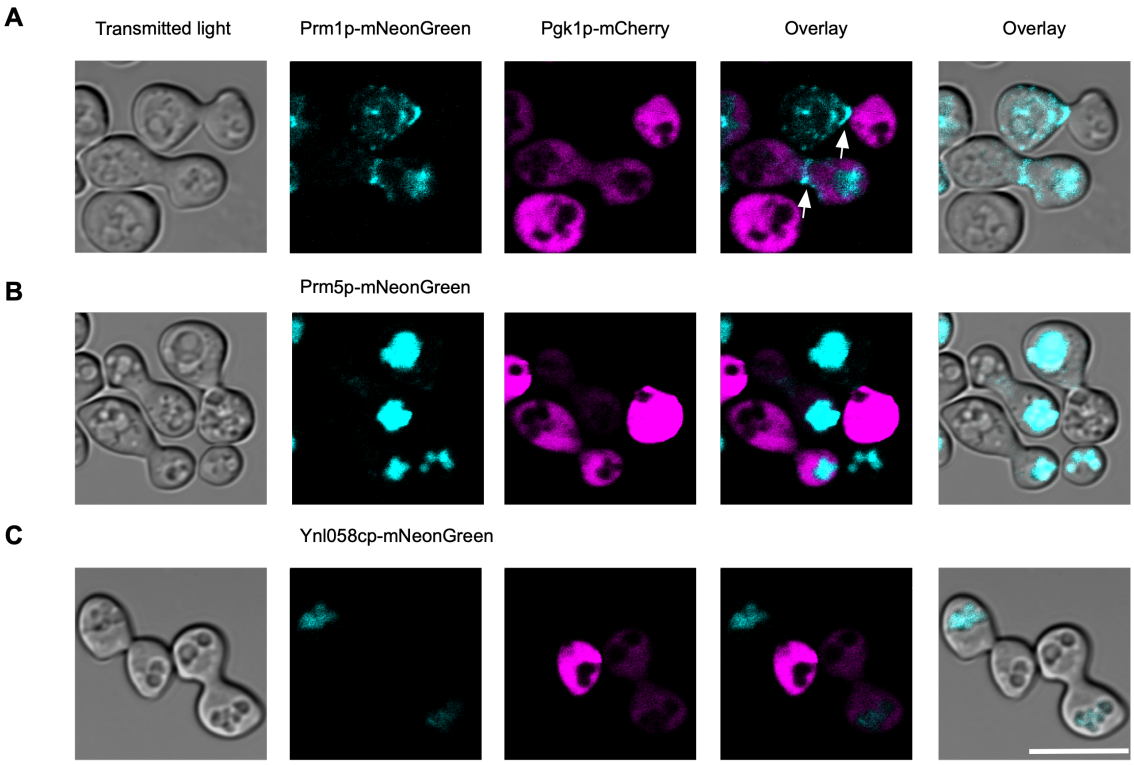

Figure 14: Prm5p is excluded from the mating junction of mating pairs. Equal amounts of cells expressing proteins in **Figure 13** were mixed with WT BY4742 *MATα* cells expressing the cytoplasmic marker Pgk1p-mCherry. Cells were incubated on filters for 90 min on YPD at 30 ºC. Mating reactions were stopped by resuspending the cells in TAF buffer at 4 ºC and thereafter cells were imaged. Transfer of Pgk1p-mCherry from one cell to the other represented PM fusion and cytoplasmic mixing. (**A**) Prm1p-mNG is recruited to the mating junction of an unfused mating pair (top white arrow) and retains its junction localization in fused cells (bottom white arrow). (**B**) Prm5p-mNG is expressed in mating conditions but is localized at the vacuole in both unfused and fused cells. (**C**) Ynl058c-mNG expression decreases in mating conditions and the protein localizes at the vacuoles. Scale bar= 5 µm.

4.3.1 Deletion of *PRM5* and its paralog presents no fusion defect

The lack of Prm5p localization at the shmoo tip and mating junction does not completely rule out its putative function in yeast mating. Indeed, proteins such as members of the polarisome (Bni1p, Spa2p and Pea2p) or proteins involved in membrane organization such as Chs5p play an indirect role in mating ([224], [259]). Chs5p, a chitin synthase III regulator, localizes in cytoplasmic patches and does not portray a clear mating junction localization. However, its null mutants exhibit a CW remodeling mating defect similar to that of *fus1Δ* and *fus2Δ* mutants ([259]). Therefore, to confirm whether Prm5p plays an indirect role in mating, *prm5Δ* and *ynl058cΔ* single deletion mutants as well as *prm5Δynl058cΔ* and *prm5Δfus1Δ* double deletion mutants were generated. The mating efficiency of the respective mutants was assessed via a GFP bimolecular fluorescence complementation (BiFC)- based flow cytometry fusion assay as described in ([348]). Fusion of *MAT***a** and *MATα* cells that harbor non-fluorescent n-GFP and c-GFP fragments results in complementation of the two fragments to form a fully functional GFP protein whose fluorescence can be quantified as a fusion event (**Figure 9**). Additionally, bilateral matings in which the respective gene is deleted in both mating types allowed a more precise analysis of all *prm5Δ* mutants. Indeed, most known cell fusion mutants including *prm1Δ*, *fus1Δ*, *fus2Δ* and *fig1Δ* have a bilateral phenotype, resulting in a greater fusion defect when the gene is absent in both mating types ([238], [266], [269], [355], [363]).

Notably, all mutants grew at WT rates with no apparent vegetative growth defects in standard growth conditions. Upon quantification, bilateral matings of *prm5Δ* and *ynl058cΔ* mutants as well as *prm5Δynl058cΔ* mutants fused with WT efficiency, suggesting that neither Prm5p nor its paralog play a role in mating. Interestingly, the *prm5Δfus1Δ* mutants fused with a lower fusion efficiency

than the *fus1Δ* mutants, indicating an additive phenotypic effect (**Figure 15**). While these findings suggested possible involvement of Prm5p in the CW remodeling step, further analyses to determine whether *PRM5* and its paralog are functionally related to *PRM1* were carried out. Notably, the bilateral matings of the *prm1Δprm5Δynl058cΔ* mutants resulted in no additive phenotype in the *prm1Δ* mutants. Instead, the *prm1Δprm5Δynl058cΔ* mutants fused similarly to the *prm1Δ* single deletion mutants, confirming that neither Prm5p nor Ynl058cp played a direct role in PM fusion (**Figure 15**).

Altogether, these findings imply that Prm5p and its paralog are not functionally involved in PM fusion. However, the additive phenotypic effect observed in the *prm5Δfus1Δ* double mutants suggests a putative Prm5p function at the CW remodeling step of yeast mating.

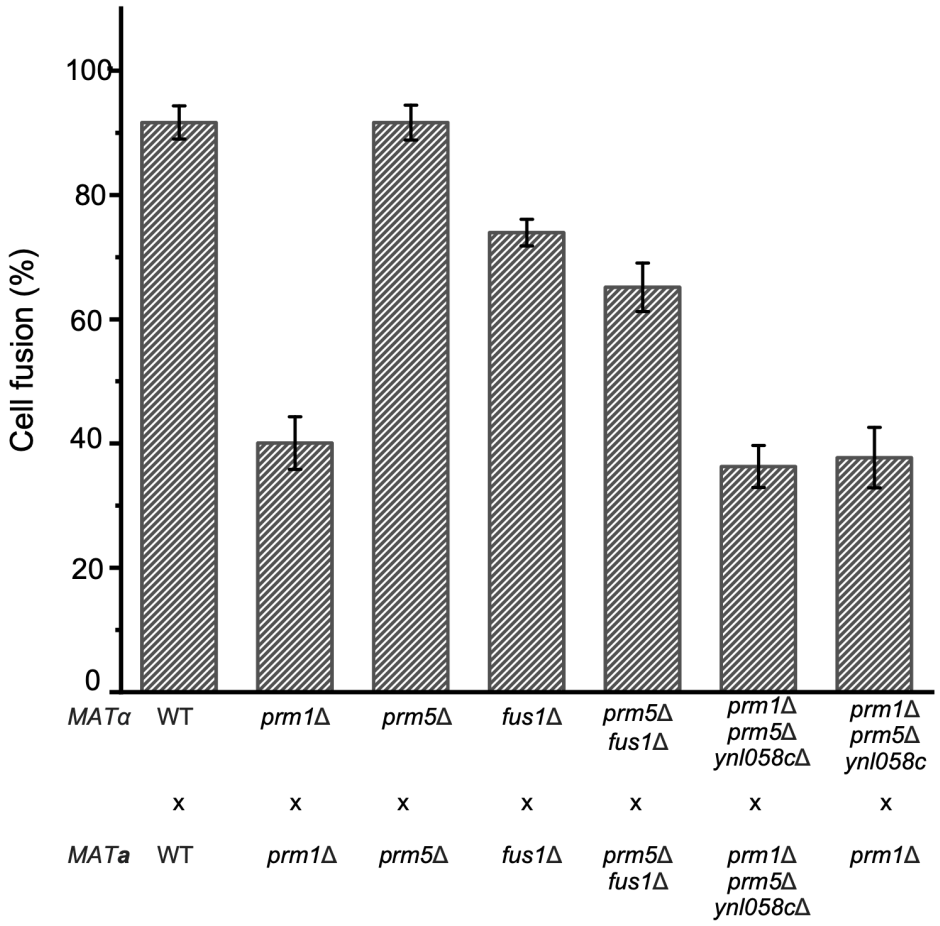

Figure 15: Deletion of *PRM5* does not affect fusion. PSAY strains of WT, *prm1*Δ, *prm5*Δ, *fus1*Δ, *prm5Δfus1Δ* and *prm1Δprm5Δynl058c*Δ triple deletion mutants were performed as described in *Materials and Methods*. Cell fusion efficiency was quantified by flow cytometry. Error bars indicate SD of three independent triplicate reactions. Scale bar= 5 µm.

4.4 Pun1p is preferentially pheromone-upregulated and localized at the mating junction

In agreement with the verified pheromone-upregulated proteins from the proteomics analysis, a second protein Pun1p, was examined. Pun1p is a PM protein upregulated during nitrogen and metal ion stress ([364], [365]). The Nitrogen and metal ion stress conditions result in increased *PUN1* transcription via activation by Kss1p kinase and Cdc28p-Cln1p, respectively, and a corresponding Pun1p localization at the cell periphery. However, no known function of *PUN1* in yeast mating has been described. Notably, Pun1p is a member of the *SUR7*-family proteins together with its paralogous proteins Sur7p, Fmp45p and Ynl194cp ([277], [278]). In addition to

their close sequence similarity, the four proteins contain four putative transmembrane domains (TMDs) and a conserved cysteine-containing claudin-like motif in their extracellular loop (ECL)1. As a result, they form part of the fungal claudin-related proteins ([254], [277], [278], [366]). In vegetative cells, all four proteins localize at the eisosomes, the immobile, stable furrow-like invaginations of the PM of about 300 nm length and 50 nm depth ([367], [368], [369]). When observed via fluorescence microscopy, eisosomes appear as stable, cortical patch structures on the yeast PM ([277]). About 20-45 eisosomes exist per mature cell with each eisosome comprising approximately 2000-5000 molecules of Pil1p and Lsp1p, the major eisosomal constituents ([369]).

Interestingly, the proteomics analysis revealed a preferential upregulation of Pun1p in pheromone-treated cells whereas all other eisosomal proteins were down-regulated (**Figure 10D**). This preferential upregulation hinted a putative Pun1p function in mating. To assess this possibility, the localization of C-terminal chromosomally tagged Pun1p-mNG was probed in pheromone-treated as well as mating conditions. Whereas a substantial basal expression was observed in vegetative cells, Pun1p was highly expressed upon pheromone treatment (**Figure 16A**). In addition, contrary to the puncta-like localization observed in vegetative cells, Pun1p was homogenously distributed along the cell periphery of polarized cells. Occasional Pun1p-containing puncta were observed at the base of the shmoo, likely corresponding to secretory vesicles ([228]). Notably, Pun1p was present at the shmoo tip of most polarized cells (**Figure 16A**). Further elucidation of the protein function in mating cells revealed that, in addition to the homogenous plasma membrane localization, Pun1p-mNG was enriched as a bright puncta at the mating junction, suggesting it may play a role in cell fusion (**Figure 16B**).

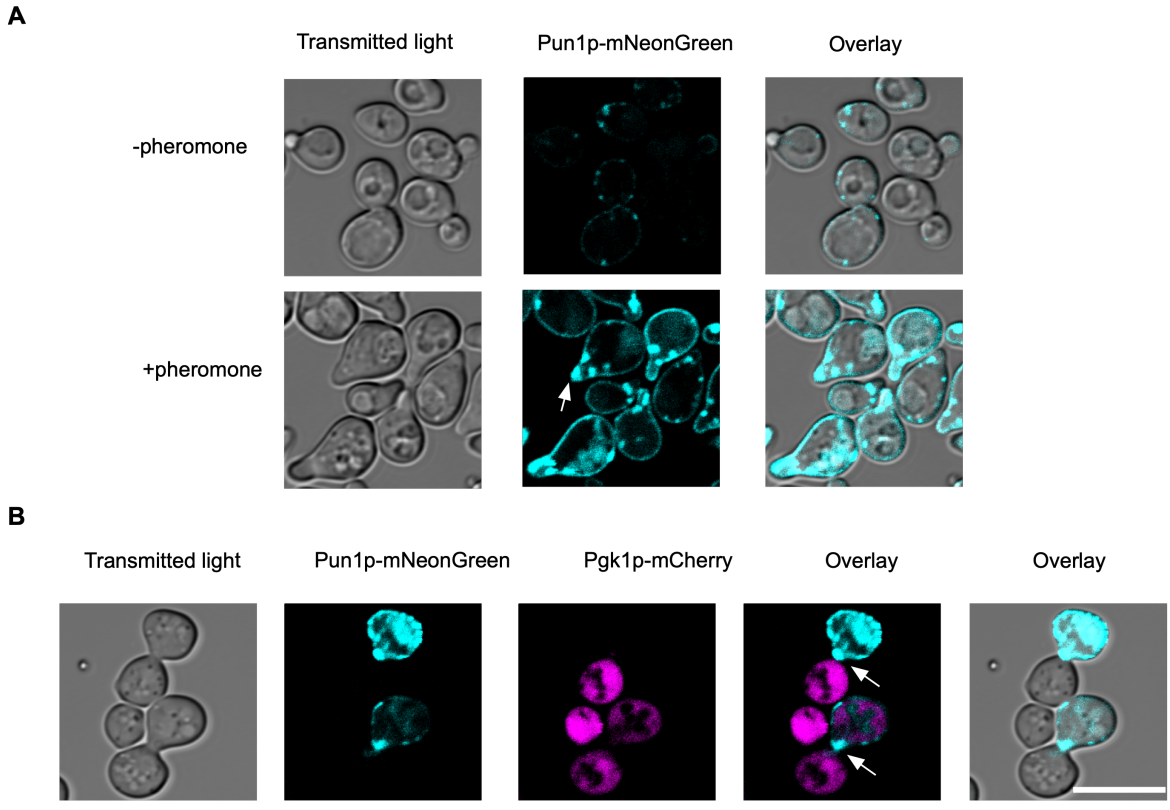

Figure 16: *PUN1* expression is preferentially upregulated upon pheromone treatment. *MAT***a** BY4741 cells expressing *PUN1::mNG* were grown to log phase in synthetic complete medium and one portion treated with 20 µM α-factor for 2 h. Cells were arrested in TAF buffer and imaged. (**A**) Pun1p-mNG is highly expressed upon pheromone treatment and localizes homogenously at the PM. In most cells, Pun1p is enriched in discrete patches at the base of the shmoo and at the shmoo tip (white arrow). (**B**) Pun1p is enriched at the mating junction. In an unfused mating pair, Pun1p is enriched at the mating junction (top white arrow) in addition to being localized to

the rest of the PM. Once PMs fuse and cytoplasmic mixing occurs, Pun1p retains its junction localization (bottom white arrow). Scale bar= 5 µm.

4.4.1 Pun1p is localized at the mating junction prior to CW remodeling and retained at the junction during PM fusion

To better dissect the localization profile of Pun1p, random prezygotes representing the different stages of cell fusion were analyzed. By combining this analysis with Concanavalin-A Alexa Fluor 647 conjugate (AF-647) CW staining, the approach permitted an in-depth dissection of the CW remodeling step from the PM fusion step. Indeed, CW staining allows a clear differentiation of late prezygotes that have undergone CW remodeling but not PM fusion from early prezygotes that contain intervening CW material at the mating junction ([228], [350]). In early prezygotes, Pun1p was homogenously distributed at the cell periphery and showed no apparent enrichment at the junction (**Figure 17A**). In some prezygotes with remodeled CW but no PM fusion, Pun1p maintained a homogenous cell surface localization (**Figure 17B**), although a considerable number of such prezygotes showed a distinct puncta-like mating junction localization like shown above (**Figure 16B**). Upon PM fusion and cytoplasmic mixing depicted by transfer of the cytoplasmic marker Pgk1p-mCherry into both mating partners, Pun1p was enriched at the junction appearing as a bright puncta while maintaining its homogenous distribution across the rest of the PM (**Figure 17C**). In late prezygotes, the protein was distributed as a collar around the neck of the zygote and later localized in the vacuoles, indicating protein degradation once the mating process is complete (**Figure S1**). These findings therefore suggested that the expression of Pun1p is mainly pheromone-dependent. The localization of Pun1p at the cell surface as well as its specific enrichment at the mating junction further indicated a Pun1p function in the late stages of yeast mating.

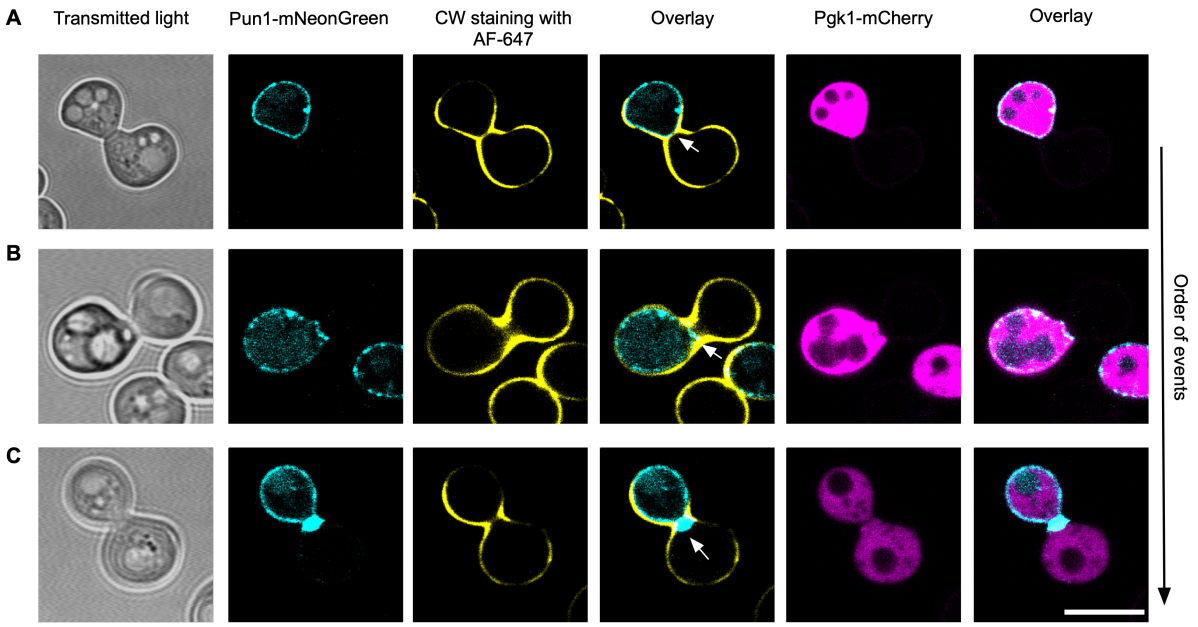

Figure 17: Pun1p is localized at the mating junction before and after CW remodeling. Mating reactions of *MAT***a** BY4741 cells expressing *PUN1::mNG* and *MATα* BY4742 cells expressing *PGK1::mCherry* were allowed to mate for 90 min on YPD at 30 ºC. Cells were arrested in TAF buffer, stained with ConA-Alexa 647 conjugate for 30 min at RT before imaging. (**A**) Pun1p-mNG is highly expressed and homogenously localized at the PM of an unfused cell including the mating junction. Fusion has not taken place as shown by presence of CW material at the mating junction (white arrow) and retention of Pgk1p-mCherry in the *MATα* cell. (**B**) Pun1p-mNG retains its junction localization once CW remodeling has occurred before PM fusion and cytoplasmic mixing (white arrow). (**C**) Pun1p-mNG remains localized at the mating junction once PM fusion and cytoplasmic mixing has taken place (white arrow). Scale bar= 5 µm.

4.4.2 Expression of other *SUR7*-family proteins is not pheromone-dependent

Pun1p and its paralogous proteins Sur7p, Fmp45p and Ynl194cp are members of the *SUR7*-family proteins ([277], [278]). The four proteins localize at the eisosomes that have been shown to co-localize with the Membrane compartment of Can1p (MCC), an arginine transporter, and together are generally referred to as MCC/eisosomes. MCC/eisosomes form a unique PM domain that is distinct from the mesh-like membrane compartment occupied by Pma1p (MCP), the H^+-ATPase ([367], [370]). Whereas the MCC domain harbors Can1p that facilitates arginine import into the cell, the exact role of eisosomes largely remains controversial. A previous study implicated eisosomes as endocytosis hotspots due to the decreased endocytosis rate in the *pil1Δ* and *lsp1Δ* mutants ([369]). However, another recent study implicated these compartments as endocytosis islands that regulate the turnover of Can1p and other proton symporters such as Fur4p and Tat2p found in the same compartment ([371]). Nonetheless, despite the localization of the *SUR7*-family proteins to the eisosomes, their role in eisosome formation and function is unclear. However, Sur7p has previously been characterized as a multi-copy suppressor of *rvs167Δ* mutation. Rvs167p is an actin-binding protein which interacts with Rvs161p to regulate actin cytoskeleton reorganization and endocytosis ([254]). Given the fact that *SUR7*, *YNL194C* and *FMP45* deletions affect the sphingolipid metabolism pathway, it has been proposed that the *SUR7*-family proteins regulate endocytic processes via sphingolipid metabolism ([254], [277], [369]).

Contrary to Pun1p, all the other *SUR7*-family proteins as well as the main eisosomal components Pil1p, Nce102p and Lsp1p, were highly down-regulated in pheromone treated cells (**Figure 10D**). This striking observation prompted the assessment of the localization of other *SUR7*-family proteins. *SUR7*, *FMP45* and *YNL194C* were chromosomally tagged at their C-termini and their localization in vegetative versus pheromone-treated cells investigated. Consistent with previous findings, Sur7p-mNG localized at distinct puncta on the PM of vegetative mother cells (**Figure 18A**). These puncta were excluded from newly-formed buds or tips of medium-sized buds ([277]). In pheromone-treated cells, Sur7p-mNG maintained a puncta-like localization at the basal cell cortex and was absent at the shmoo tip (**Figure 18A**). On the other hand, Fmp45p-mNG and Ynl194cp-mNG were not readily detectable in both vegetative and pheromone-treated cells and were expressed only in a small proportion of cells. When present, the two proteins portrayed a Sur7p-like puncta localization (**Figure 18B** and **18C**), consistent with previous findings ([277]). In summary, the Pun1p paralogs exhibit an expression and localization profile distinct from that of Pun1p. Their expression is not pheromone-dependent and the three proteins are excluded from the shmoo tip and possibly mating junction.

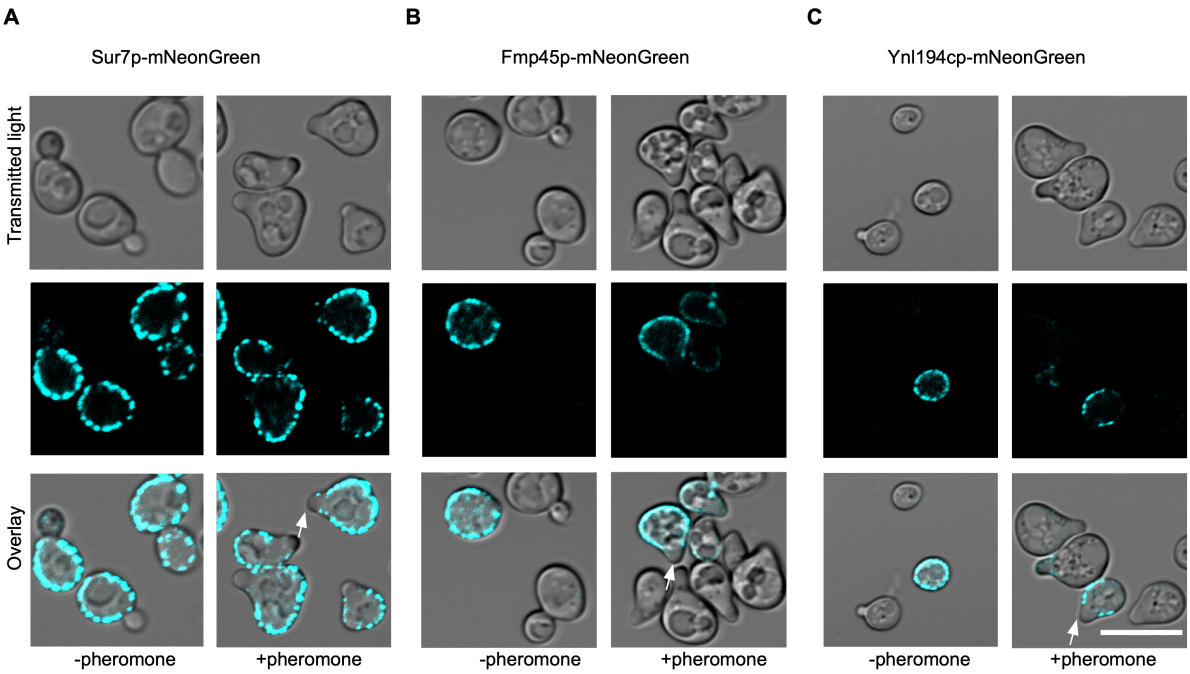

Figure 18: *SUR7, FMP45* and *YNL194C* are constitutively expressed in vegetative and pheromone treated cells. Chromosomally C-terminally tagged *SUR7, FMP45* and *YNL194C* were assessed for their localization in vegetative and pheromone-treated conditions as previously described. (**A**) Sur7p-mNG is highly expressed both in vegetative and pheromone treated cells and localizes in distinct, cortical patches. Sur7p is excluded from newly formed daughter cells and the shmoo tip of polarized cells (white arrow). (**B, C**) Fmp45p-mNG and Ynl194cp-mNG localize similarly to Sur7p in both conditions (white arrow) although the proteins are not expressed in all cells. Depicted are representative mid-sections. Scale bar= 5 µm.

To further confirm that the other *SUR7*-family proteins were excluded from the mating junction, microscopic examination of the respective mNG-tagged proteins in mating cells was carried out. *MAT***a** BY4741 cells expressing the respective mNG-tagged genes were crossed with WT BY4742 *MATα* cells and their localization examined after 90 min of mating. Contrary to Pun1p, all the *SUR7*-family proteins were excluded from the mating junction, suggesting that these proteins, and by proxy eisosomes, are preferentially excluded from the mating junction early enough before PM fusion takes place (**Figure 19**).

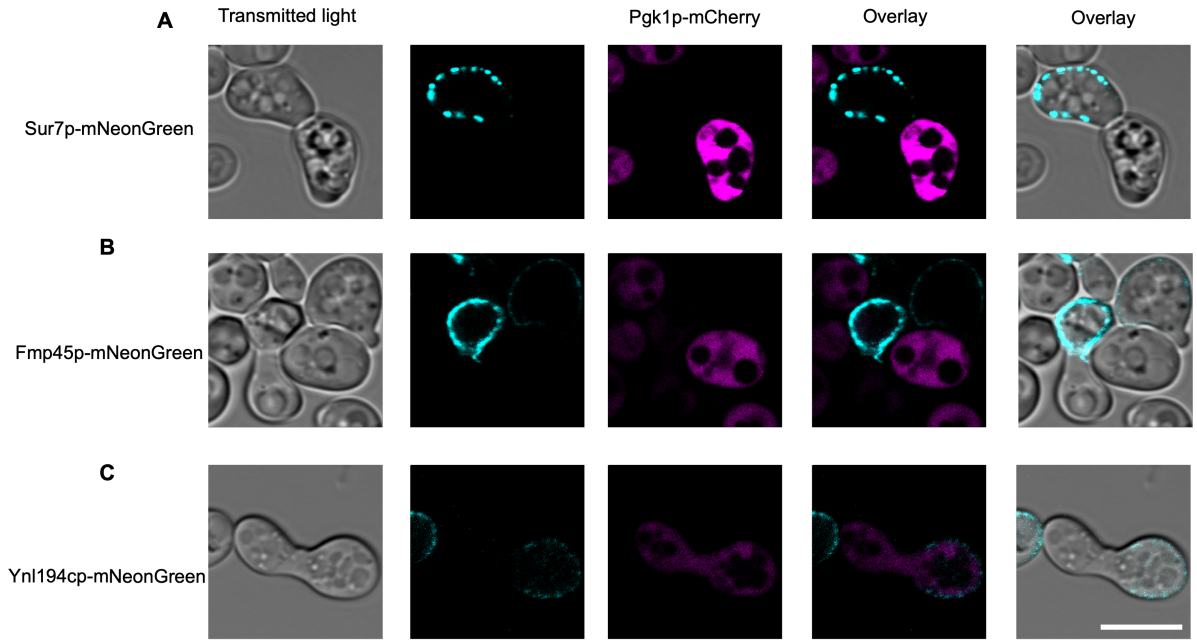

Figure 19: *SUR7*-family proteins are excluded from the mating junction. Equal amounts of *MAT***a** cells expressing *SUR7::mNG*, *FMP45::mNG* and *YNL194C::mNG* were mixed with WT *MATα* cells expressing the cytoplasmic marker Pgk1p-mCherry. Cells were incubated on filters for 90 min on YPD at 30 ºC. Mating reactions were stopped by resuspending the cells in TAF buffer at 4 ºC and thereafter cells were imaged. Transfer of Pgk1p-mCherry from the *MATα* cell to the *MAT***a** cell represents PM fusion. (**A**) Sur7p-mNG is localized at the cortical patches that are excluded from the mating junction of an unfused mating pair. (**B**) Similarly to Sur7p, Fmp45p-mNG is localized at the cortical patches that are excluded from the mating junction of an unfused mating pair. (**C**) In a fused zygote, Ynl194cp-mNG is faintly expressed and retains the patchy localization that is excluded from the zygote neck. Scale bar= 5 µm.

4.4.3 Eisosomes are preferentially excluded from the shmoo tip and mating junction

The absence of the other *SUR7*-family proteins from the shmoo of polarized cells or the mating junction has two implications: (i) it implies that Pun1p undergoes a differential regulation in mating conditions, and (ii) it suggests the preferential exclusion of eisosomes from the mating junction during yeast mating. To confirm the differential regulation of Pun1p and Sur7p, the two proteins

were C-terminally tagged with mNG and mCherry, respectively and their co-localization pattern examined. In vegetative cells, the two proteins co-localized at stable puncta in budding mother cells confirming that both proteins are present in the eisosomes. Notably, Pun1p-mNG was present in daughter cells while Sur7p-mCherry was weakly detectable, in agreement with previous findings that Sur7p is excluded from emerging buds or tips of medium-sized buds ([277]) (**Figure 20A**, upper panel). Upon pheromone treatment, Sur7p-mCherry maintained the puncta-like localization in the basal cell cortex and was excluded from the shmoo tip. On the other hand, Pun1p-mNG was homogenously distributed at the cell periphery in addition to its enrichment at the shmoo tip (**Figure 20A**, lower panel). On quantifying the fluorescence intensity along the PM, the two proteins exhibited almost similar intensities in vegetative cells indicative of similar expression and localization profiles (**Figure 20B**, upper panel). In pheromone-treated cells, Sur7p-mCherry displayed a high fluorescence intensity along the PM that significantly reduced at the shmoo consistent with a high concentration of Sur7p molecules per cell, that are mainly concentrated at the basal membrane. Pun1p on the other hand portrayed homogenous intensity levels along the PM but its intensity increased at the shmoo (**Figure 20B**, lower panel). Altogether, the exclusion of Sur7p from the shmoo in contrast to Pun1p confirmed their differential regulation upon pheromone treatment. Furthermore, the exclusion of Sur7p, an eisosomal marker, from the shmoo suggests that eisosomes are possibly excluded from the shmoo tip or mating junction and do not play a direct role in yeast mating.

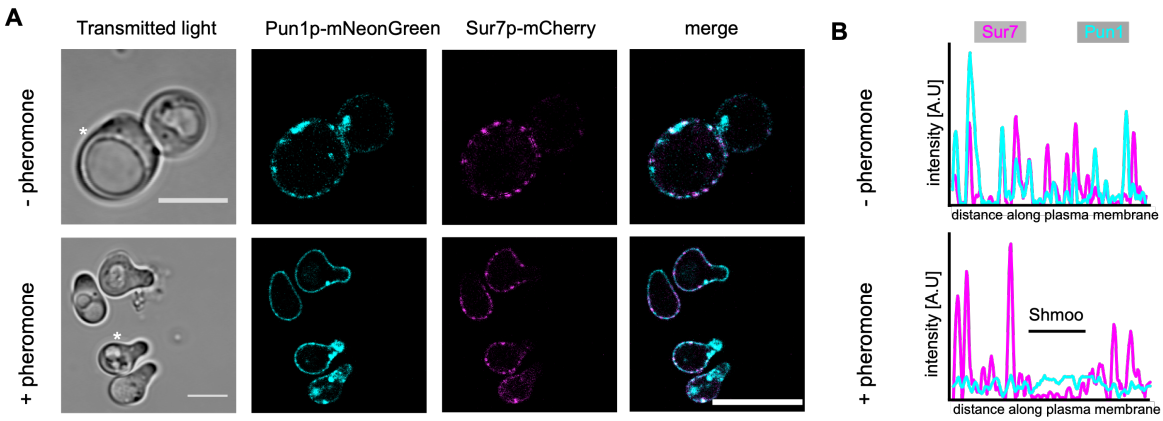

Figure 20: Pun1p dissociates from the eisosomes as the cell transitions to mating. *MAT***a** BY4741 cells expressing *PUN1::mNeonGreen* and *SUR7::mCherry* were grown to log phase in synthetic complete medium and treated with or without 20 µM *α*-factor for 2 h. Cells were arrested in TAF buffer and imaged by confocal microscopy. (**A**) Pun1p-mNG and Sur7p-mCherry co-localize at the cortical patches in a mature mother cell, but not daughter cell. In pheromone treated cells, the two proteins co-localize at the basal membrane but not at the shmoo tip. Depicted are representative mid-sections. Scale bar= 5 µm. (**B**) Fluorescence intensity plots of the respective images. For each fluorescent protein, the plot represents its intensity along the PM with the shmoo position indicated in the second plot corresponding to the pheromone treated cells.

To further elucidate the differential regulation of Pun1p and the preferential exclusion of eisosomes from the shmoo tip or mating junction, co-localization studies of Pun1p and Pil1p, the major eisosomal component, were carried out. Pil1p is a soluble protein that localizes at the cytoplasmic side of the PM of eisosomes. As a result, fluorescently-tagged Pil1p appears as distinct cortical patches, similarly to the integral membrane protein Sur7p ([369], [371]). Deletion of *PIL1* results in disassembly of eisosomes and the mislocalization of Sur7p to the cytoplasm ([369]). As expected, Pil1p was highly expressed in both vegetative and pheromone-treated cells and localized at distinct, cortical patches (**Figure 21A**). In vegetative cells, Pil1p co-localized with Pun1p although the punctate Pil1p localization was more cytoplasmic than that of Pun1p (**Figure 21A**, top panel). In pheromone-treated cells, Pil1p maintained a punctate localization but was occasionally localized at the shmoo tip. In these cells, Pun1p localized homogenously at the PM including the shmoo tip (**Figure 21A**, lower panel). On quantifying the respective fluorescence intensities, Pun1p and Pil1p

co-localized in vegetative cells whereas little to no co-localization was observed in pheromone-treated cells. Instead, Pil1p-mCherry exhibited high intensity values across the entire cell surface including the shmoo, consistent with its high expression profiles. Pun1-mNG on the other hand portrayed a homogenous intensity profile along the entire PM (**Figure 21B**). However, Pil1p was localized at the shmoo tip in few polarized cells suggesting either remnant Pil1p at the cytoplasmic leaflet of the shmoo tip PM or, that some eisosomes may be retained at the cell-cell contact site and carry out mating-related functions. To test the latter hypothesis, microscopic examination of Pil1p in mating cells was carried out. Cells expressing Pil1p-mNG were crossed with WT BY4742 *MATα* cells and the localization profile of Pil1p examined after 90 min of mating. As opposed to Pun1p, Pil1p-mNG was preferentially excluded from the mating junction of mating pairs, further suggesting that eisosomes are indeed preferentially isolated from the mating junction (**Figure 21C**). Notably, the exclusion of eisosomes from the mating junction seems to occur early enough when the two cells have not fused, suggesting that eisosomes are not required in the late events of cell fusion.

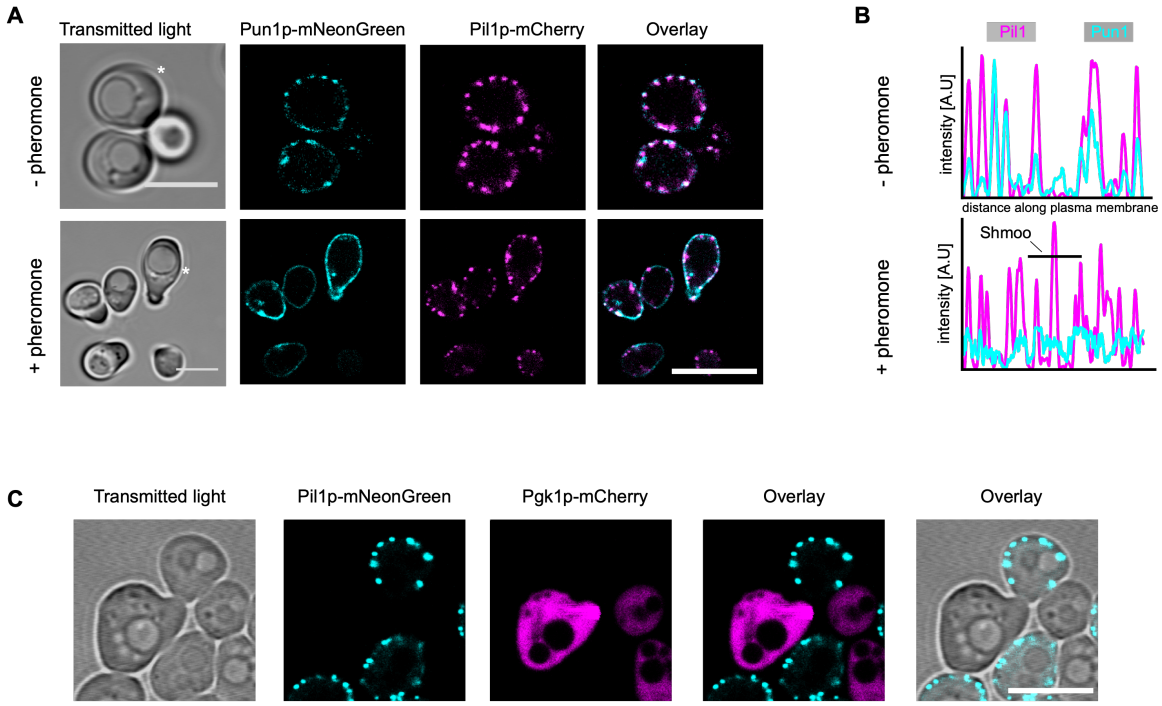

Figure 21: The eisosome organizer Pil1p is excluded from the mating junction. (**A**) Pun1p-mNG and Pil1p-mCherry co-localize at distinct cortical patches on the PM in vegetative cells. Upon pheromone treatment, Pun1p-mNG dissociates from these patches while Pil1p-mCherry is retained. The two proteins occasionally co-localize in one or two patches present at the shmoo tip. Depicted are representative mid-sections. (**B**) Fluorescence intensity plots of the respective images. For each fluorescent protein, the plot represents its intensity along the PM with the shmoo position indicated in the second plot corresponding to the pheromone treated cells. (**C**) Pil1p exhibits a Sur7p-like localization pattern in mating cells. Equal amounts of *MAT***a** cells expressing *PIL1::mNG* were crossed with WT *MATα* cells expressing the cytoplasmic marker Pgk1p-mCherry as described before. Transfer of Pgk1p-mCherry from the *MATα* cell to the *MAT***a** cell represents PM fusion. In an unfused mating pair, Pil1p-mNG is localized at the distinct, cortical patches that are absent from the mating junction. Scale bar= 5 µm.

4.4.4 Eisosome disassembly has no negative effect on yeast mating

To further confirm that eisosomes are not involved in the late steps of yeast mating, two additional approaches were explored. First, deletion mutants of *PIL1* were generated and their fusion efficiency quantified by BiFC fusion assay ([348]). Pil1p is proposed to regulate eisosome biogenesis and deletion of *PIL1* results in eisosome disassembly and a collapse of the remaining components into one or a few patches ([369]). Consistent with the proteomics data, bilateral matings of *pil1Δ* mutants fused with WT efficiencies (~93% fusion efficiency), indicating that

eisosome disassembly has no negative effect on the mating process (**Figure 22A**). Secondly, bilateral matings of deletion mutants of select eisosomal genes were carried out and examined microscopically. All the bilateral matings of the genes tested showed no apparent phenotypic defects confirming that these mutants fused effectively and that eisosomes are functionally dispensable during yeast mating (**Figure 22B**) and (**Figure S2**).

Overall, these data support the hypothesis that Pun1p has a putative function during yeast mating. While Pun1p localizes in eisosomes in vegetative cells, the protein likely dissociates from the eisosomes in mating conditions and localizes at the cell periphery including the shmoo tip. Upon cell-cell contact, Pun1p is retained at the cell periphery including the mating junction. Its concentration at the junction subsequently increases as the intervening CW is degraded and the PMs fuse to generate a fusion pore. As the mating process continues and the PM components between the two cells mix, Pun1p is localized at the neck of the mating junction and occasionally redistributed to both cells. Upon completion of fusion, Pun1p is translocated to the vacuoles for degradation. All these findings therefore prompted a further analysis of Pun1p as a novel component of the fertilization synapse and a player of cell fusion.

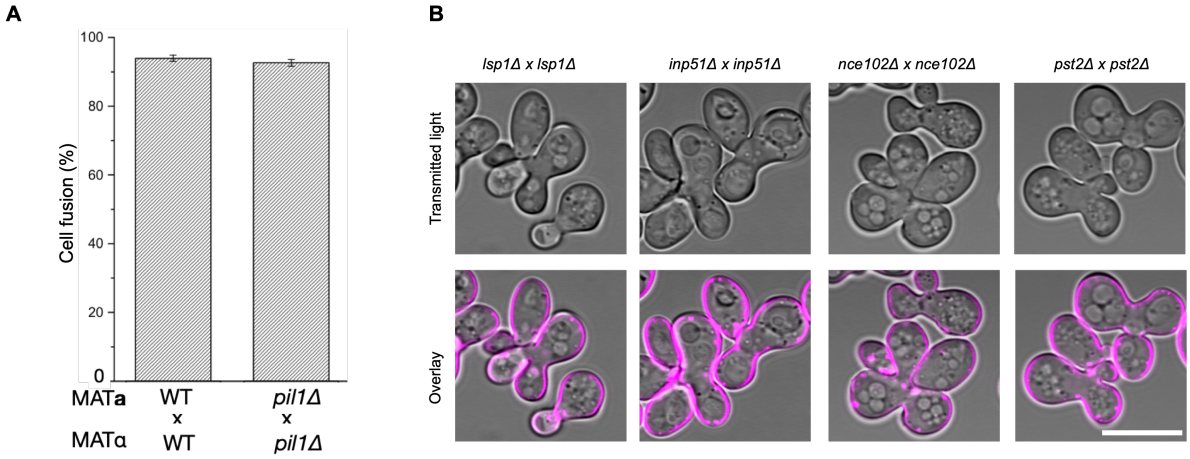

Figure 22: Eisosome disassembly has no negative effect on yeast mating. (**A**) Bilateral matings of *pil1Δ* deletion mutants fuse as efficiently as the WT cells. PSAY strains of WT and *pil1*Δ deletion mutants were performed as described in *Materials and Methods*. Cell fusion efficiency was quantified by flow cytometry. Error bars indicate SD of three independent triplicate reactions. (**B**) Representative images of the bilateral matings of deletion mutants of eisosomal genes. Gene deletion mutants of the respective genes were obtained from the standard yeast gene Knockout (YKO) library. Equal amounts of *MAT***a** and *MATα* cells were mixed and cells allowed to mate for 3.5 h. Cells were stained with the PM dye FM4-64 as described in *Materials and Methods* before imaging. The mutants show no fusion defects. Scale bar= 5 μm.

4.5 Pun1p is a four-pass transmembrane protein that structurally resembles mammalian Claudins

S. cerevisiae PUN1 encodes a 29.3kDa integral membrane protein with four transmembrane domains (TMDs), a short cytoplasmic N-terminus consisting of 6 residues, a longer extracellular loop 1 (ECL1) consisting of 116 residues and a shorter ECL2 of 30 residues (**Figure 23A**). The longer cytoplasmic C-terminal tail consists of 19 residues and a potential ubiquitylation site on lysine (K_{260}) ([372]). Additionally, Pun1p has two potential N-glycosylation sites; Asparagine (N_{100}) and Asparagine (N_{209}), that are supposedly crucial in facilitating Pun1p secretion from the ER via the Golgi to the PM ([373]). Notably, Pun1p demonstrates a few unique differences from the other *SUR7*-family proteins. Firstly, in addition to its differential regulation and localization profile, Pun1p exhibits a low sequence identity (20% identity) as opposed to the 27- 34% sequence identity, and 42- 49% similarity that exists amongst the three other proteins (Sur7p, Fmp45p and Ynl194cp) ([277], [278]). Secondly, Pun1p slightly differs from the other *SUR7*-family proteins at its ECL1

region. Contrary to the conserved cysteine-containing (WxxW/YxxC(7-10aa)C claudin-like motif present in its paralogs, the GLWxxC(8-10aa)C claudin motif present in the eukaryotic claudin family proteins is fully conserved in Pun1p ([274], [278]) (**Figure 23B**). The claudin-family proteins are major structural components of mammalian tight junctions that function as selective paracellular barriers ([280], [281], [374]). This sequence conservation therefore hints at a structural and possibly functional similarity across the eukaryotic tight junction claudins and *SUR7*-family proteins, and to a greater extent Pun1p.

To confirm the structural similarities between Pun1p and mammalian claudins, a Phyre2 modelling prediction was carried out ([375]). Interestingly, the predicted Pun1p topology adopted a left-handed model, similar to that of claudin-3 and claudin-15, except for two additional ECL1 β-strands that form the overall β-sheet structure. All the seven Pun1p β-strands adopted an anti-parallel arrangement similarly to claudin-15 ([376], [377]) (**Figure 23C**). Notably, Pun1p aligned with both claudins with >90% confidence, indicating that Pun1p is a claudin-like protein (**Figure 23D**). A HHpred search to identify additional proteins with sequence and structural homology to Pun1p revealed 9 proteins with high homology (>99% probability): *S. cerevisiae* Ina1p, Fat3p, Dcv1p, Rim9p, Ecm7p, Fig1p, *S. pombe* Dni1p, Dni2p proteins and Mac1p (**Figure S1**). Remarkably, *S. cerevisiae* Fig1p has previously been described as a fungal claudin-like protein together with its *S. pombe* orthologs Dni1p and Dni2p ([275], [282], [355], [378]). All three proteins are tetraspan membrane proteins with known roles in mating. Expression of Fig1p is pheromone-dependent and the protein localizes at the mating junction. Fig1p is proposed to play a Ca^{2+}-dependent role in PM fusion. Likewise, the *S. pombe* Dni proteins (Dni1p and Dni2p) facilitate membrane fusion by regulating PM organization and CW remodeling during mating ([355], [356], [357], [378]). Similarly to Pun1p, Fig1p and Dni proteins contain the cysteine-containing GLWxxC(8-10aa) C claudin motif at their ECL1 (**Figure 23B**). Notably, the conserved cysteine residues in the Dni proteins are crucial in protein folding and transport to the surface. Substituting these cysteine residues results in protein mis-localization to the ER instead of the specialized membrane fusion domain (MFD) that is analogous to the mating junction, and a corresponding reduction in protein function ([378]).

The high sequence similarity to mammalian claudins and the presence of the consensus motif therefore suggest that Pun1p, similarly to Fig1p and the Dni proteins, is claudin-like and is possibly necessary in cell fusion.

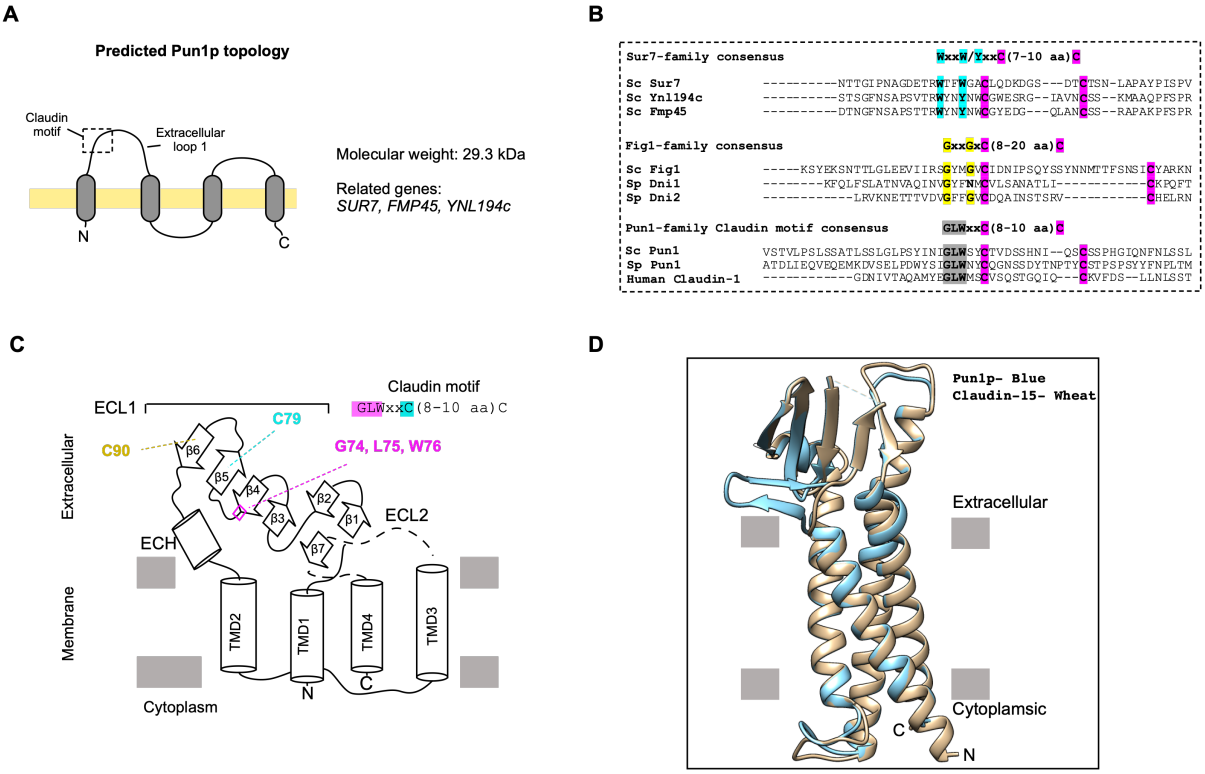

Figure 23: Pun1p is claudin-related and maintains a mCldn15-like overall structure. (**A**) Pun1p is a 4-pass membrane protein with cytoplasmic N- and C-termini. Pun1p contains three paralogs (*SUR7*, *FMP45* and *YNL194C*) and together belongs to the *SUR7*-family proteins. (**B**) Pun1p closely resembles the mammalian claudins than the *SUR7*-family and Fig1-family proteins. Multiple sequence alignment shows that Pun1p contains the exact claudin cysteine-containing consensus motif (GLWxxC(8-10 aa)C) in the first extracellular loop (ECL1). (**C**) Schematic of *S. cerevisiae* Pun1p secondary structure as predicted by Phyre2 modelling prediction. (**D**) Ribbon representation of *S. cerevisiae* Pun1p (Blue) superimposed on the structure of monomeric claudin 15 (PDB4P79) viewed parallel to the membrane. Note that Pun1p is completely superimposed on claudin-15 except for the two additional β-strands in the ECL1. Grey bars represent boundaries of outer (extracellular) and inner (cytoplasmic) leaflets of lipid bilayer.

4.6 Pun1p and the known fungal claudin-like protein Fig1p exhibit a similar PM localization pattern in mating cells

To evaluate the possible functional similarities between Pun1p and Fig1p, localization studies were carried out. First, the expression and localization profile of Fig1p was examined. As expected, Fig1p-mNG was expressed only upon pheromone treatment and localized at the shmoo tip (**Figure 24A**). Although the majority of Fig1p was enriched at the shmoo tip, some protein was localized at the base of the shmoo and its fluorescence diminished towards the basal cell cortex. In mating pairs, Fig1p-mNG was localized across the entire PM but was enriched at the mating junction of mating pairs, reminiscent of the Pun1p localization profile (**Figure 24B**). As the PMs fused and the cytoplasmic contents mixed, Fig1p was subsequently distributed as a collar at the mating bridge. Once fusion was completed, Fig1p was transported to the vacuole for degradation corroborating its involvement in the late steps of mating, as previously reported (**Figure S3**) ([271]).

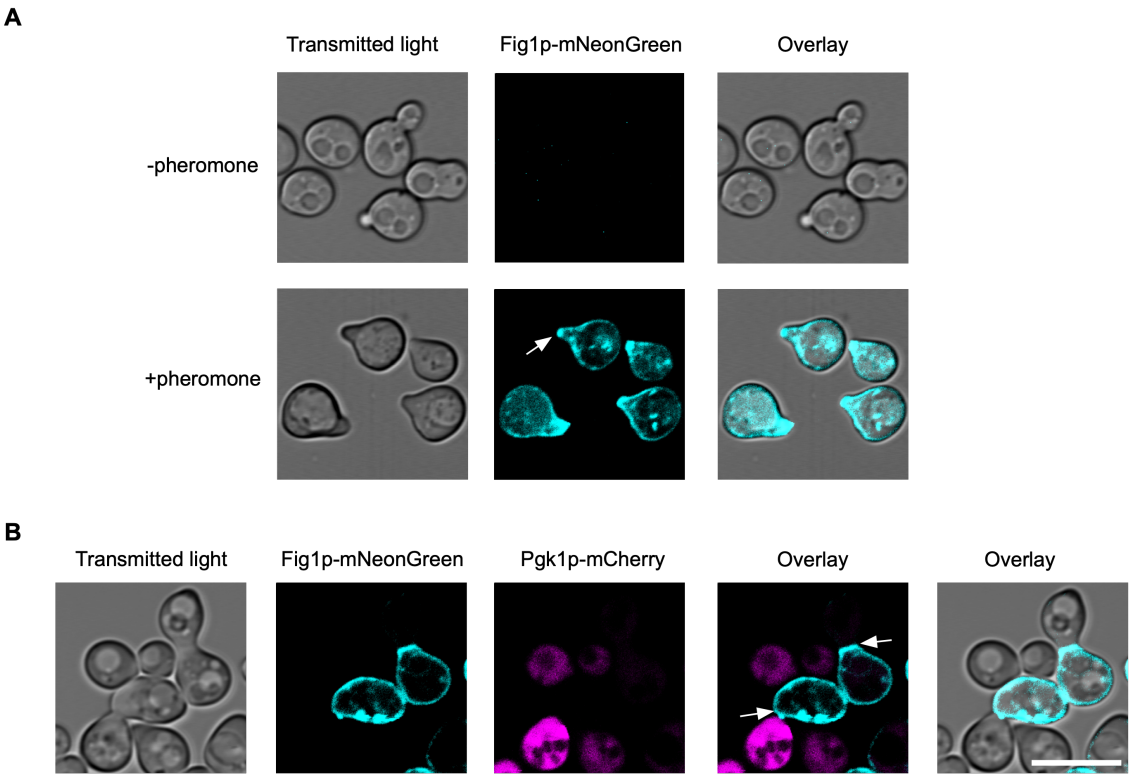

Figure 24: *FIG1* expression is pheromone-dependent and Fig1p localizes at the mating junction. (**A**) *MAT***a** BY4741 cells expressing *FIG1::mNeonGreen* were grown to log phase in synthetic complete medium and treated with or without 20 μM *α*-factor for 2 h. Cells were arrested in TAF buffer and imaged. Fig1p-mNG is expressed only upon pheromone treatment and mainly localizes at the shmoo tip (white arrow). Some Fig1p remains homogenously localized along the PM. (**B**) In mating cells, Fig1p-mNG is highly expressed and localized along

the PM including the mating junction of an unfused mating pair (bottom white arrow). Fig1p is retained at the mating junction of fused cells (top white arrow). Scale bar= 5 µm.

To examine whether Pun1p was localized similarly to Fig1p, co-localization studies of Pun1p-mNG and Fig1p-mCherry in pheromone-treated and mating cells were carried out. Similar co-localization studies with Sur7p-mCherry were also performed to further confirm the differential Pun1p localization at the mating junction. As expected, both Fig1p-mCherry and Pun1p-mNG were enriched at the shmoo tip of pheromone-treated cells as well as the rest of the PM (**Figure 25A**). In mating cells, the two proteins mainly co-localized at the mating junction of unfused cells and occasionally at the basal cell cortex (**Figure 25B**). Once the PMs fused and a fusion pore was formed, both Fig1p-mCherry and Pun1p-mNG retained their junction localization but were subsequently distributed as a collar around the neck of the zygote as the fusion pore expanded, suggesting a similar localization pattern (**Figure S3**). Conversely, Sur7p-mCherry was localized at cortical patches that were excluded from the mating junction whereas Pun1p-mNG was mainly enriched at the mating junction (**Figure 25C**). Taken together, the structural similarities between Fig1p and Pun1p as well as the similar localization pattern suggest that both proteins exist in the same membrane domain or region in pheromone-treated and mating cells. This is suggestive of putative functional similarities between the two proteins.

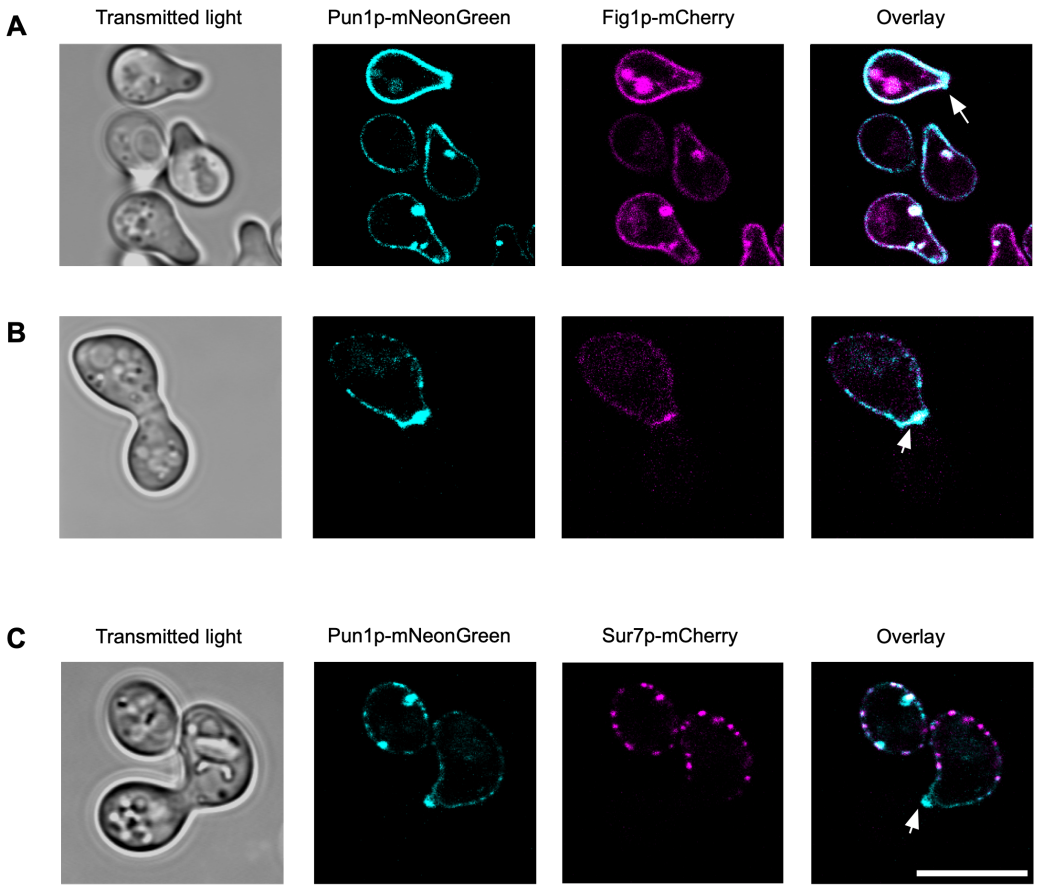

Figure 25: Pun1p and Fig1p co-localize at the PM of mating cells but not with Sur7p. (**A**) *MAT***a** BY4741 cells expressing *PUN1::mNeonGreen* and *FIG1::mCherry* were grown to log phase in synthetic complete medium and treated with 20 µM *α*-factor for 2 h. Cells were arrested in TAF buffer and imaged. Pun1p-mNG and Fig1p-mCherry are expressed in polarized cells and localized at the PM. Some protein is localized at the shmoo tip (white arrow). (**B**) Equal amounts of *MAT***a** BY4741 cells expressing *PUN1::mNeonGreen* and *FIG1::mCherry* or *SUR7::mCherry* were crossed with WT *MATα* cells and allowed to mate for 90 min. Mating was stopped by incubating the cells in TAF buffer before imaging. Pun1p-mNG and Fig1p-mCherry mainly co-localize at the

mating junction (white arrow). Both proteins are homogenously distributed across the rest of the PM. (**C**) Sur7-mCherry does not co-localize with Pun1p-mNG at the mating junction. Sur7-mCherry localizes at cortical patches that are excluded from the mating junction, while Pun1p-mNG is enriched at the mating junction (white arrow). Scale bar= 5 μm.

4.7 Deletion of *PUN1* and its paralogs does not enhance the *fig1Δ* mutants' fusion defects

The role of Fig1p in mating has been linked to its Calcium (Ca^{2+}) influx regulatory activity ([356], [357]). Similarly to the *prm1Δ* mutants, bilateral matings of *fig1Δ* mutants accumulate unfused prezygotes, 10% of which contain cytoplasmic bubbles while ~6% undergo lysis ([355]). Depletion of Ca^{2+} by chelators such as EGTA enhances the *fig1Δ* fusion defects, suggesting the cellular dependence on Ca^{2+} especially in absence of *FIG1*. Consistently, the enhanced *fig1Δ* fusion defects can be suppressed by Ca^{2+} supplementation ([355], [356]). To determine any functional relationship between Pun1p and Fig1p, single and double deletion mutants of *PUN1* and *FIG1* were generated, and their fusion efficiencies quantified via the BiFC fusion assay. Furthermore, to better deduce whether the Pun1p activity is also Ca^{2+} dependent, bilateral mating reactions of *pun1Δ*, *fig1Δ and pun1Δfig1Δ* were performed in the absence of the Ca^{2+} chelator EGTA (standard growth conditions) and in the presence of EGTA (absence of Ca^{2+}). Bilateral matings of WT and *prm1Δ* mutants were used as control reactions. In standard growth conditions, all mutants grew at WT rates with no apparent vegetative growth defects.

On quantification, the bilateral matings of *pun1Δ* fused with WT efficiencies (~90% fusion efficiency) whereas the *prm1Δ* bilateral matings exhibited ~50% fusion efficiency as previously reported ([266], [355]) (**Figure 26A**). In absence of Ca^{2+}, the WT cells fused with a slightly lower efficiency (85%) and the *pun1Δ* cells fused with ~80% fusion efficiency, comparable to the WT cells (**Figure 26B**). Bilateral matings of *fig1Δ* fused with ~80-90% fusion efficiency, but the *fig1Δ* fusion defect was enhanced by ~20% upon Ca^{2+} depletion, consistent with previous findings ([355]). Surprisingly, the *pun1Δfig1Δ* mutants fused similarly to the *fig1Δ* mutants both in the presence and absence of Ca^{2+}, with a slight insignificant increase in the fusion efficiency observed in standard conditions (**Figure 26A** and **26B**). These findings suggested the absence of an additive phenotypic effect on *fig1Δ* mutants upon *PUN1* deletion. To rule out the possibility of functional redundancy from the Pun1p paralogs, quintuple deletion mutants (5*Δ*) comprising all five genes (*PUN1*, *FIG1*, *SUR7*, *FMP45* and *YNL194C*) were generated and their fusion efficiency in both conditions determined. In presence of Ca^{2+}, the bilateral matings of 5*Δ* quintuple mutants fused similarly to the *fig1Δ* mutants, while a slightly higher but insignificant fusion efficiency was observed in absence of Ca^{2+} (**Figure 26A** and **26B**). The lack of an enhanced fusion defect in the *pun1Δfig1Δ* mutants therefore suggests that deletion of *PUN1* in *fig1Δ* mutants results in no additive phenotypic effect both in the presence and absence of Ca^{2+}, and that the Pun1p paralogs are functionally unrelated to Fig1p.

In order to have a more precise analysis of whether deletion of *PUN1* and its paralogs did not have an effect on other *fig1Δ* fusion defect phenotypes, microscopic characterization of the mating phenotypes of the respective mutants was carried out. Confocal fluorescence microscopy that combined the GFP BiFC assay and PM staining with FM4-64 dye was adopted, allowing the quantification of both the fusion efficiency as well as known and novel fusion defect phenotypes. The BiFC assay that is based on GFP fluorescence upon cell fusion of *MAT***a** and *MATα* cells expressing complementary GFP fragments, allowed a clear distinction of fused from unfused mating pairs ([348]) (**Figure 26C**). Furthermore, PM staining of the mating pairs with FM4-64, a lipophilic dye that stains the lipid bilayers, permitted exclusive PM staining and revealed various PM morphological defects ([350], [379]). Notably, mating pairs that expressed cytoplasmic GFP with no FM4-64 PM staining at the mating junction were classified as fused, indicating successful PM fusion and complementation of the GFP fragments. Mating pairs that expressed cytoplasmic GFP but exhibited PM staining at the mating junction were characterized as partially fused. This is because they represented mating pairs in which a small fusion pore had formed that allowed cytoplasmic mixing and GFP complementation, but failed to expand possibly due to incomplete degradation of the intervening CW material ([350]). Lastly, mating pairs that exhibited PM staining at the mating junction and no cytoplasmic GFP fluorescence were characterized as unfused or defective (**Figure 26C**). Following this criteria, all lysed prezygotes as well as prezygotes containing

cytoplasmic bubbles were generally quantified as defective ([269]). A minimum of 150 mating pairs were counted in each mating reaction.

Upon quantification, WT cells fused with >95% fusion efficiency and presented negligible fusion defects as expected. On the other hand, ~30% of the bilateral matings of the *prm1Δ* mutants fused successfully while ~60% were defective. Only about 10% mating pairs remained partially fused. For *fig1Δ* mutants, ~80% of mating pairs fused successfully comparable to the fusion efficiency obtained by flow cytometry assay. About 10% of all mating pairs were partially fused while the remaining 10% were defective. Notably, the bilateral matings of *pun1Δ* mutants and its paralogs fused similarly to WT cells, further corroborating the conclusion that the eisosomal components are not necessary in yeast mating. Similarly, bilateral matings of the 5Δ quintuple mutants comprising of (*pun1Δ fig1Δsur7Δfmp45Δynl194cΔ*) fused similarly to *fig1Δ* mutants, confirming that the four genes did not result in any additive phenotypic effect (**Figure 26D**).

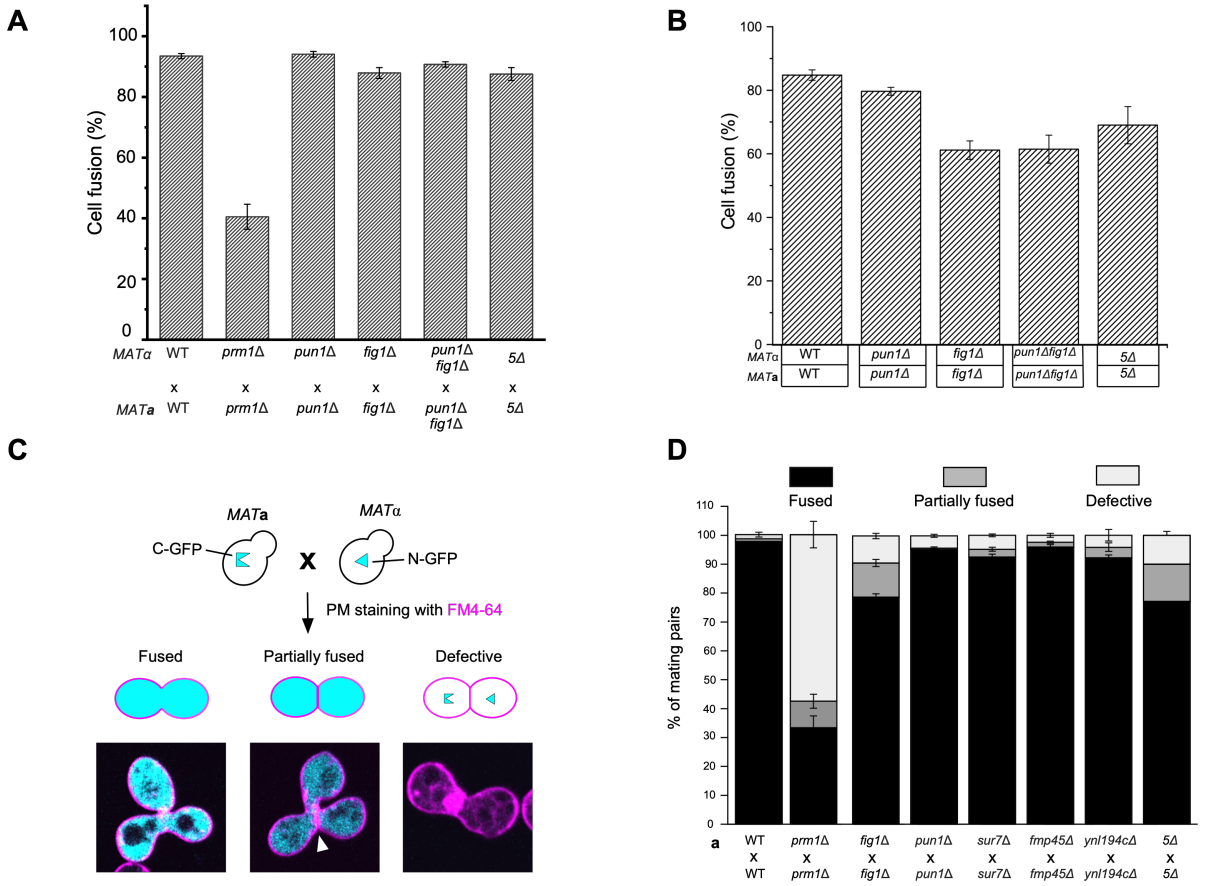

Figure 26: Deletion of *PUN1* and its paralogs does not enhance the *fig1Δ* fusion defect. Quantitative cell fusion assays of the PSAY strains of WT, *prm1*Δ, *pun1*Δ, *fig1*Δ, *pun1*Δ*fig1*Δ, *sur7*Δ, *fmp45*Δ, *ynl194c*Δ and quintuple mutants (*5Δ*) were performed as described in *Materials and Methods*. Cell fusion efficiency was assessed either by flow cytometry or microscopy. For microscopy, cells arrested in TAF buffer after 3 h of mating were stained with the PM stain, FM4-64 at 4 ºC before imaging by confocal microscopy. (**A**) Bilateral matings of *pun1*Δ*fig1*Δ and *5Δ* quintuple mutants fuse similarly to *fig1*Δ mutants in standard mating conditions. (**B**) The sensitivity of *pun1*Δ*fig1*Δ and *5Δ* quintuple mutants to Ca^{2+} depletion is due to the *FIG1* mutation. The same reactions as in (**A**) performed in media supplemented with 20mM EGTA. Neither *pun1*Δ mutants nor its paralogs are sensitive to Ca^{2+} depletion. (**C**) Representative images of the mating phenotypes observed in the bilateral matings of respective mutants. Fusion was based on Bimolecular fluorescence complementation of the complementary GFP fragments as described in *Materials and Methods*. Mating pairs expressing GFP were quantified as fused zygotes while those that expressed GFP but showed PM staining at the mating junction were quantified as partially fused zygotes. Defective prezygotes were quantified as mating pairs that do not express GFP. (**D**) Single gene deletions of *PUN1* and its paralogs are not defective. Bilateral matings of *5Δ* quintuple mutants fuse similarly to the *fig1*Δ mutants.

n>150 mating pairs in three or more independent experiments. Error bars denote SEM of three or more independent triplicate experiments.

Altogether, these findings indicate that, while a structural relationship exists between Pun1p, its paralogs and Fig1p, all the five proteins are functionally distinct. Firstly, the expression, localization profile and gene deletion studies of Pun1p paralogs suggest that they are not necessary in the mating process. Secondly, the pheromone-dependent expression of Pun1p and Fig1p, and their similar PM localization patterns suggest that the two proteins possibly localize to the same PM domain and exhibit functional similarities. However, it is evident that Fig1p performs a more direct role that is readily observed by loss-of-function analysis. The exact function of Pun1p therefore prompted further analysis.

4.8 Deletion of *PUN1* mildly enhances fusion in *prm1Δ* mutants

Pun1p has previously been implicated in the cell wall integrity (CWI) pathway during metal ion stress and nitrogen stress with the latter resulting in pseudo-hyphal growth ([364], [365]). In haploid filamentous Σ1278b cells that undergo pseudo-hyphal growth, deletion of *PUN1* resulted in a loss of surface filamentation and a corresponding decrease in mRNA transcripts of certain amino acid biosynthesis genes including *ARG1*, *ARG3*, *HIS1*, *HIS4*, *LEU1*, *LYS1* and *MET13* ([365]). Interestingly, under the same conditions, an increase in mRNA transcripts of some mating genes such as *FUS1*, *FUS3*, *STE4*, *STE3*, *GPA1* was reported with *FUS3* exhibiting the highest increase (81-fold change). While these astonishing findings did not reconcile the mechanistic relationship between *PUN1* gene deletion and the yeast mating pathway, they suggested a putative inhibitory role exerted by the filamentous growth program vis-a-vis Pun1p on the mating pathway and vice-versa.

However, so far, deletion of *PUN1* in a WT or a *fig1Δ* sensitized background did not significantly enhance fusion. Furthermore, Fig1p was correctly localized in *pun1Δ* mutants, suggesting that deletion of *PUN1* does not affect upstream events that regulate Fig1p expression and localization in mating conditions (**Figure S3**). Therefore, in order to uncover the putative Pun1p inhibitory role on the mating pathway, it was necessary to examine the effects of *PUN1* gene deletion in other more sensitized backgrounds such as *prm1Δ*, *fus1Δ* or *fus1Δfus2Δ* mutants. Fus1p, Fus2p and Prm1p are known facilitators of fusion. Fus1p and Fus2p are involved in the CW remodeling step while Prm1p is required in the PM fusion step ([238], [253], [266]). In concert with their role in CW remodeling, bilateral matings of either *fus1Δ* or *fus2Δ* mutants fuse with approximately 30-50% and 60-80% fusion efficiency, respectively. The unfused *fusΔ* mating pairs arrest as early prezygotes with intervening CW material present at the mating junction ([228], [238]). Remarkably, bilateral matings of *fus1Δfus2Δ* mutants fail to fuse (<10% fusion efficiency) and almost all mating pairs arrest as early prezygotes. This additive CW remodeling-specific phenotype suggests that the two proteins function at the CW remodeling step but on parallel pathways ([228], [238]). In addition to its role in CW remodeling, Fus1p has also been implicated in fusion pore expansion ([228], [267]).

On the other hand, Prm1p activity is exerted at the PM fusion step and bilateral matings of *prm1Δ* mutants fuse with approximately 30-60% fusion efficiency ([266], [269], [355]). Of the unfused mating pairs, the majority arrest as late prezygotes with apposed PMs but no intervening CW material. These often form cytoplasmic bubbles that emanate from the cell with higher osmotic pressure ([266], [269]) Additionally, *prm1Δ* mating pairs can undergo cell lysis, a phenotype that occurs only once the intervening CW material has been degraded ([269]). The *prm1Δ*-specific lysis is presumed to be a result of destabilized membranes during PM fusion that would otherwise be stabilized by Prm1p ([269], [355]). Notably, the similar fusion defect phenotypes observed in *prm1Δ* and *fig1Δ* mutants further corroborate the existence of at least two parallel pathways that culminate in cell-cell fusion ([271]). Cells deleted of either *FUS1*, *FUS2* or *PRM1* therefore provide a more sensitized genetic background to unravel the mechanistic relationship between *PUN1* gene deletion and the yeast mating pathway.

To begin with, the effect of *PUN1* gene deletion was assessed in *fus1Δ*, *fus2Δ* and *prm1Δ* backgrounds. Double gene deletion mutants of *prm1Δpun1Δ*, *pun1Δfus1Δ*, *pun1Δfus2Δ* and triple

pun1Δfus1Δfus2Δ were generated and their fusion efficiencies assessed by BiFC fusion assay. As controls, *prm1Δsur7Δ* and *pun1Δsur7Δ* mutants as well as a *prm1Δpun1Δsur7Δ* mutants were also generated and their fusion efficiencies assessed. Whereas WT cells fused with ~90% fusion efficiency, bilateral matings of *prm1Δ* mutants fused with ~40% fusion efficiency as expected (**Figure 27**). Bilateral matings of *pun1Δ* mutants fused with WT-like efficiency, suggesting that Pun1p does not promote fusion. However, in comparison to the *prm1Δ* mutants, bilateral matings of the *prm1Δpun1Δ* mutants fused with a slightly higher but significant fusion efficiency (48% fusion efficiency), suggesting an enhanced fusion efficiency of *prm1Δ* mutants upon *PUN1* deletion (**Figure 27**). Conversely, bilateral matings of *prm1Δsur7Δ* mutants fused similarly to the *prm1Δ* mutants, indicating that the *SUR7* deletion had no effect on the *prm1Δ* fusion defect. Lastly, whereas the bilateral matings of *pun1Δsur7Δ* fused with WT-like efficiency, bilateral matings of *prm1Δpun1Δsur7Δ* mutants fused similarly to the *prm1Δpun1Δ* mutants, corroborating the hypothesis that *SUR7* is part of a machinery that functions differently to *PUN1* (**Figure S4**).

On the other hand, bilateral matings of the *fus1Δ* mutants fused with a higher fusion efficiency (70%) than previously reported ([228], [238]). Interestingly, the *pun1Δfus1Δ* mutants fused with an efficiency comparable to the *fus1Δ* mutants, indicating no Pun1p-dependent fusion enhancement activity (**Figure 27**). Similarly, no significant difference in fusion was observed between the bilateral matings of *fus2Δ* and *pun1Δfus2Δ* mutants (data not shown). The *pun1Δfus1Δfus2Δ* mutants had little to no fusion, supporting the previous findings that Fus1p and Fus2p redundantly operate in two parallel pathways. Deletion of both genes abrogates fusion almost completely with almost all mating pairs arresting at the CW remodeling step ([228]). All in all, while no enhanced fusion was observed in the *fus1Δ*, *fus2Δ* and *fus1Δfus2Δ* mutants upon *PUN1* deletion, the enhanced fusion efficiency of the bilateral *prm1Δpun1Δ* matings suggested an inhibitory role of *PUN1* in a *prm1Δ* background.

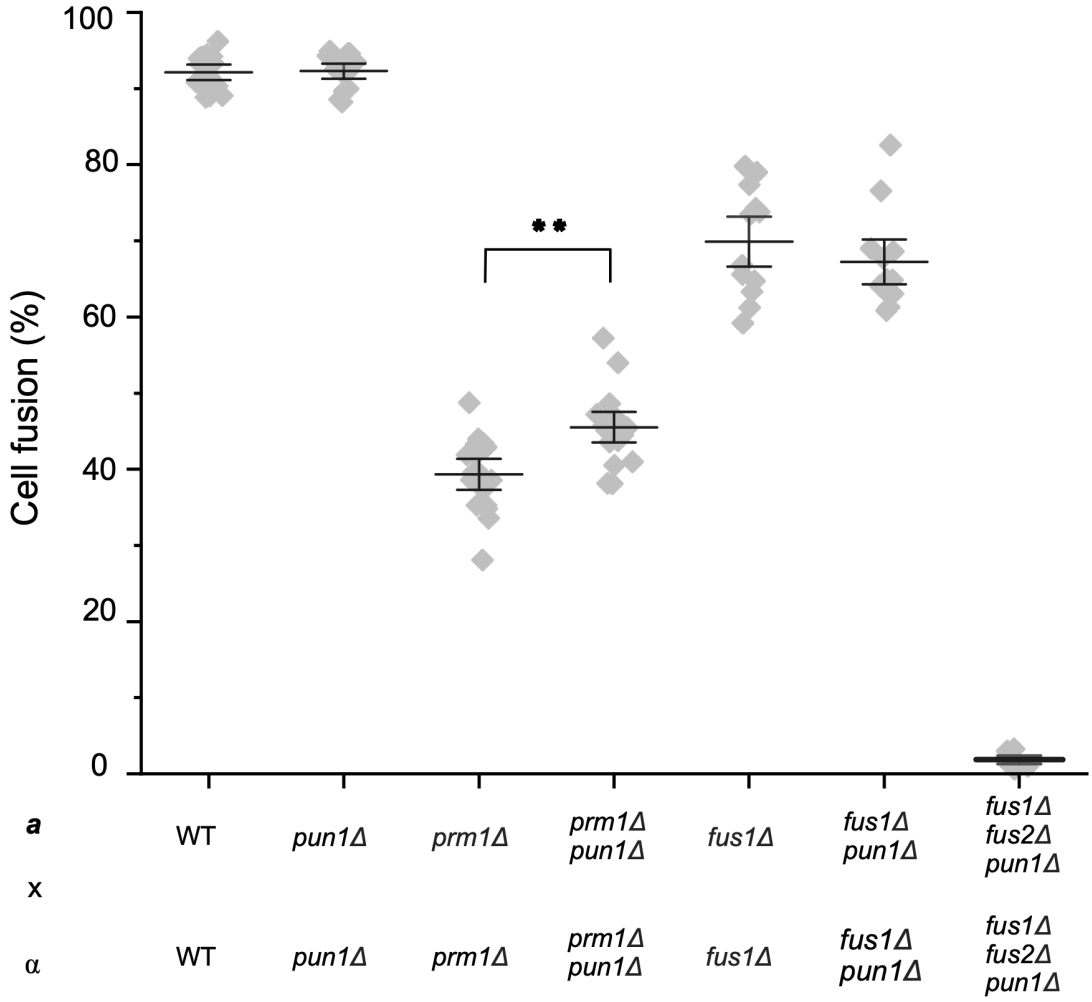

Figure 27: Deletion of *PUN1* mildly suppresses the *prm1Δ* but not *fus1Δ* fusion defect. Bilateral matings of WT, *prm1Δ, pun1Δ, prm1Δpun1Δ, fus1Δ, pun1Δfus1Δ* and *pun1Δfus1Δfus2Δ* were performed in YPD for 3 h and quantified by flow cytometry. Fusion is severely compromised in the triple *pun1Δfus1Δfus2Δ* mutants while a mild but significant enhancement of fusion is observed in *prm1Δpun1Δ* mutants. Error bars denote SEM of three or more independent triplicate experiments. **P-value <0.05.

4.9 *PUN1* overexpression inhibits fusion in *prm1Δ* and *fus1Δ* mutants

In order to test the inhibitory activity of *PUN1* and analyze any genetic interactions between *PUN1* and *PRM1*, *PUN1*-mediated high-copy suppression of fusion in *prm1Δ* and *fus1Δ* mutants was carried out. By overexpressing *PUN1* in *prm1Δ* or *fus1Δ* mutants, an enhanced fusion defect would suggest that Pun1p functionally inhibits fusion in a genetically sensitized background. To begin with, the effect of high-copy (2μ plasmid) *PUN1* expression from the constitutive *ADH1* promoter was examined. *MAT***a** and *MATα* WT cells, *pun1Δ*, *prm1Δ* and *fus1Δ* mutants were transformed with the 2μ plasmid and their fusion efficiency determined by BiFC fusion assay. *PUN1* overexpression in WT cells resulted in no significant changes in fusion efficiency when compared to the control WT cells expressing the empty vector (EV). A similar observation was made in *pun1Δ* mutants. Interestingly, *PUN1* overexpression in *prm1Δ* or *fus1Δ* mutants resulted in a decrease in fusion efficiency when compared to the respective mutants expressing the EV. Notably, the enhanced fusion defect was more pronounced in *prm1Δ* mutants than in the *fus1Δ* mutants (**Figure 28**).

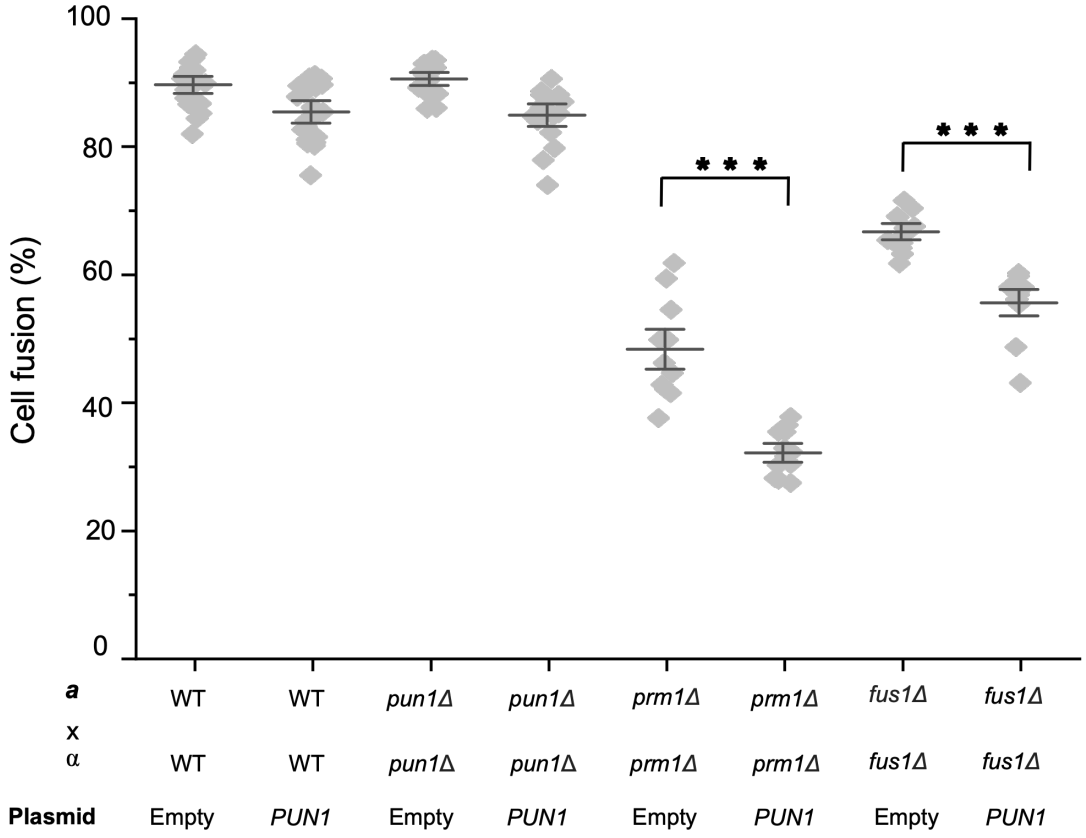

Figure 28: Overexpression of *PUN1* enhances the *prm1Δ* and *fus1Δ* fusion defects. *MAT***a** and *MATα* WT, *prm1Δ, pun1Δ and fus1Δ* mutants expressing either the empty vector (EV) or high copy *PUN1* under the *ADH1* constitutive promoter were grown in synthetic media to mid-log phase. Mating reactions were performed in YPD for 3 h and fusion quantified by flow cytometry. Error bars denote SEM of three or more independent triplicate experiments. ***P-value <0.01.

However, whilst *PUN1* overexpression in the *prm1Δ* and *fus1Δ* mutants results in enhanced fusion inhibition, these mutants contain endogenous *PUN1* whose expression is upregulated in mating conditions as previously shown (**Figure 16**). This implies that endogenous *PUN1* may have contributed to the overall Pun1p activity observed in these mutants. To eliminate this effect, *PUN1* overexpression activity was examined in *prm1Δpun1Δ* and *pun1Δfus1Δ* mutants. As expected, lower levels of fusion were observed in mutants overexpressing *PUN1* than those expressing the EV (**Figure S5**). Notably, the fusion inhibition activity was more pronounced in the *prm1Δpun1Δ* mutants than in *prm1Δfus1Δ* cells, further suggesting putative genetic interactions between *PUN1* and *PRM1*. Overall, this data demonstrates that *PUN1* overexpression in a genetically sensitized *prm1Δ* or *fus1Δ* background results in an enhanced fusion defect, inferring that *PUN1* is part of a machinery that negatively regulates fusion. Additionally, the Pun1p inhibitory activity is more pronounced in a *prm1Δ* background, suggesting that the Pun1p-dependent machinery possibly operates at the level of PM fusion as opposed to CW remodeling.

4.9.1 Pun1p displays a specific, dosage- dependent fusion inhibition activity

Up to this point, high-copy *PUN1* expression under the control of the constitutive *ADH1* promoter inhibited fusion in *prm1Δ* and *fus1Δ* mutants. However, to further confirm the fusion inhibitory activity of Pun1p, it was necessary to examine whether low-copy expression of *PUN1* in one to two copies (centromeric (CEN) plasmid) would result in a similar activity. Additionally, the promoter effect on *PUN1* expression levels was examined in both low copy (CEN) and high copy (2μ) plasmids by expressing *PUN1* from either the constitutive *ADH1* promoter or its endogenous

promoter (pr*PUN1*). All plasmids were transformed into *prm1Δpun1Δ* mutants to eliminate any leaky effects from endogenous *PUN1*. Bilateral matings of respective mutants were performed and the fusion efficiency determined. In comparison to the ~50% fusion efficiency observed in control cells expressing the high-copy EV, the Pun1p inhibition activity was dosage- dependent. Mutant cells expressing *PUN1* from the high-copy 2μ plasmids exerted higher fusion inhibition activity than those expressing *PUN1* from the low-copy, *CEN* plasmids. Notably, constitutive *PUN1* expression from the high-copy 2μ plasmid resulted in the highest fusion inhibition activity, indicating a dosage-dependent Pun1p activity (**Figure 29A**).

In order to determine the specificity of the Pun1p fusion inhibition activity, overexpression studies of the *PUN1* paralog *SUR7* were performed in parallel to *PUN1* in *prm1Δ* mutants. However, owing to the fact that *SUR7* expression is not pheromone-dependent and that about 17 000 molecules of Sur7p are present per cell during log phase ([277]), (**Figure 18A**), high-copy expression of *SUR7* under its native promoter was preferred. This approach would minimize a metabolic burden on the cells. Additionally, *prm1Δpun1Δsur7Δ* mutants were used as the ideal background to eliminate any leaky effects from the endogenously expressed proteins. Interestingly, bilateral matings of *prm1Δpun1Δsur7Δ* mutants expressing *PUN1* fused with a lower fusion efficiency (33%) than the control cells expressing the EV (42%) (**Figure 29B**). On the contrary, bilateral matings of *prm1Δpun1Δsur7Δ* mutants expressing *SUR7* fused with a higher fusion efficiency (48%) than the control cells, suggesting that overexpression of *SUR7* enhanced fusion. When *MAT***a** *prm1Δpun1Δsur7Δ* mutants expressing *PUN1* were crossed with *MATα* cells expressing *SUR7* and vice-versa, intermediate fusion efficiencies were observed that were comparable to the unilateral reactions of *prm1Δpun1Δsur7Δ* cells expressing *PUN1*. However, when *prm1Δpun1Δsur7Δ* cells expressing *SUR7* were crossed to the control cells expressing the EV, the cells fused similarly to the control cells (**Figure 29B**). These findings therefore substantiated the hypothesis that, despite their structural similarities, Pun1p exerts a different function to Sur7p. Furthermore, the unilateral *PUN1* or *SUR7* reactions imply that the two proteins do not functionally interact across the mating junction and that Sur7p does not functionally substitute Pun1p.

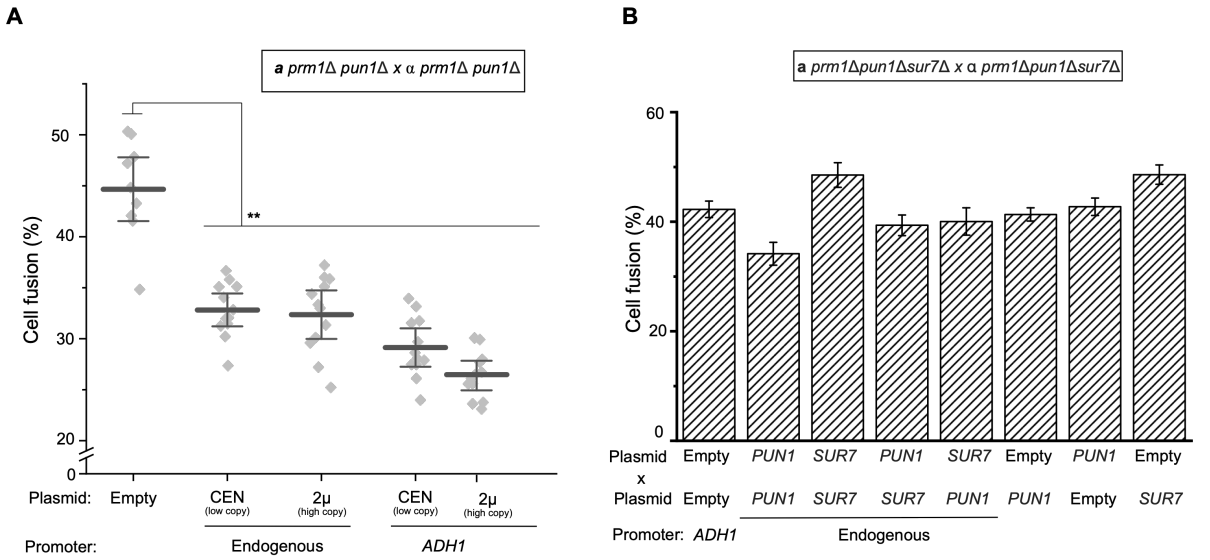

Figure 29: Pun1p fusion inhibition activity is specific and dosage- dependent. (**A**) The degree of fusion inhibition in bilateral matings of *prm1Δpun1Δ* mutants is dependent on the strength of *PUN1* expression. Mutants expressing high copy *PUN1* under the *ADH1* constitutive promoter show the least fusion efficiency. (**B**) The fusion inhibition activity is specific to *PUN1*. As opposed to *PUN1*, triple *prm1Δpun1Δsur7Δ* mutants expressing high copy *SUR7* under its endogenous promoter fuse with a higher fusion efficiency. **P-value <0.05.

4.9.2 *PUN1* overexpression enhances a flat PM interface phenotype in *prm1Δ* mutants and is Ca^{2+} independent

So far, *PUN1* overexpression in *prm1Δ* and *fus1Δ* mutants enhances the fusion defect in both mutants, but a higher fusion inhibition activity is observed in *prm1Δ* mutants. To understand the mechanistic basis of Pun1p fusion inhibition activity, it was necessary to first determine the level at which the fusion inhibition activity is exerted, particularly in *prm1Δ* mutants. As previously mentioned, bilateral matings of *prm1Δ* mutants exhibit four different phenotypes. Upon cell-cell contact, mating pairs can either undergo fusion, lysis or arrest as early or late prezygotes (**Figure 30A**) ([266], [269], [355]). Late prezygotes are characterized by unfused mating pairs that form cytoplasmic bubbles and signify a completed CW remodeling step. Consequently, these cells can bend their PMs in either direction depending on the direction of the osmotic gradient, forming bubbles or cytoplasmic fingers (**Figure 30A**) ([269], [291], [350]). On the other hand, early prezygotes are characterized by a flat PM interface at the mating junction. These are presumed to contain intervening CW material that provides structural support to the flexible PMs, thus generating a flat interface (**Figure 30A**) ([350]). Consistently, early prezygotes with a flat PM interface are common in CW remodeling mutants such as *fus1Δ* and *fus2Δ* ([228], [238], [350]).

To understand at what level of *prm1Δ* matings was the Pun1p fusion inhibition activity exerted, microscopic analysis of *prm1Δ* mutants expressing high-copy *PUN1* was performed and compared to the same mutants expressing high-copy EV. By employing FM4-64 PM staining combined with GFP-BiFC, bilateral matings of respective *prm1Δ* mutants were performed and the various phenotypes quantified (**Figure 30A**). As expected, about half (~50%) of *prm1Δ* cells expressing the EV fused successfully as demonstrated by GFP fluorescence (**Figure 30A**). Of the unfused mating pairs, ~30% lysed while ~10% were arrested as late prezygotes with cytoplasmic bubbles and the rest as prezygotes with a flat PM interface (**Figure 30B**). On the other hand, *prm1Δ* mutants expressing *PUN1* demonstrated a significant decrease in fusion efficiency (~35%). Interestingly, no change in the number of lysed mating pairs or fusion arrested prezygotes with cytoplasmic bubbles was observed. However, a corresponding increase in the number of prezygotes with a flat PM interface was observed, suggesting that Pun1p enhanced the formation of early prezygotes (**Figure 30B**).

Similarly to *fig1Δ* mutants, bilateral matings of *prm1Δ* mutants are sensitive to Ca^{2+} depletion ([355]). Removal of Ca^{2+} from the media results in a 10-fold reduction in fusion and a corresponding increase in the lysis activity of *prm1Δ* mutants. The lysis activity can however be suppressed by high extracellular Ca^{2+} supplementation as opposed to osmotic support ([269], [355]). Furthermore, the inability of *fus1Δ* mating reactions that arrest at the CW remodeling step to respond to Ca^{2+} depletion implies that the Ca^{2+} sensitivity is specific to the PM fusion step ([269], [355]). To examine whether the Pun1p fusion inhibition activity is dependent on Ca^{2+}, bilateral matings of *prm1Δpun1Δ* mutants expressing low copy *PUN1* under the constitutive *ADH1* promoter were performed in the presence and absence of Ca^{2+}. Control reactions were performed in standard mating conditions. In agreement with previous results, under standard conditions, *prm1Δpun1Δ* mutants expressing *PUN1* fused with a lower fusion efficiency than the control cells expressing the EV (52% versus 38%) (**Figure 30C**). Upon Ca^{2+} depletion via addition of the Ca^{2+} chelator EGTA to the media, fusion was completely abolished in both the control cells as well as the cells expressing *PUN1*. However, when these cells were grown in media supplemented with 1mM $CaCl_2$, fusion in both cell groups increased 1.6-fold compared to that in standard conditions. Interestingly, a corresponding 1.3-fold decrease in fusion efficiency was observed in cells expressing *PUN1* (62%) when compared to the control cells expressing the EV (80%) (**Figure 30C**). Notably, this fusion decrease was similar to that observed in standard mating conditions, suggesting that Pun1p activity in *prm1Δ* mating reactions is independent of extracellular Ca^{2+} concentration and is consistent with earlier findings that lysis is unaffected by Pun1p inhibition activity.

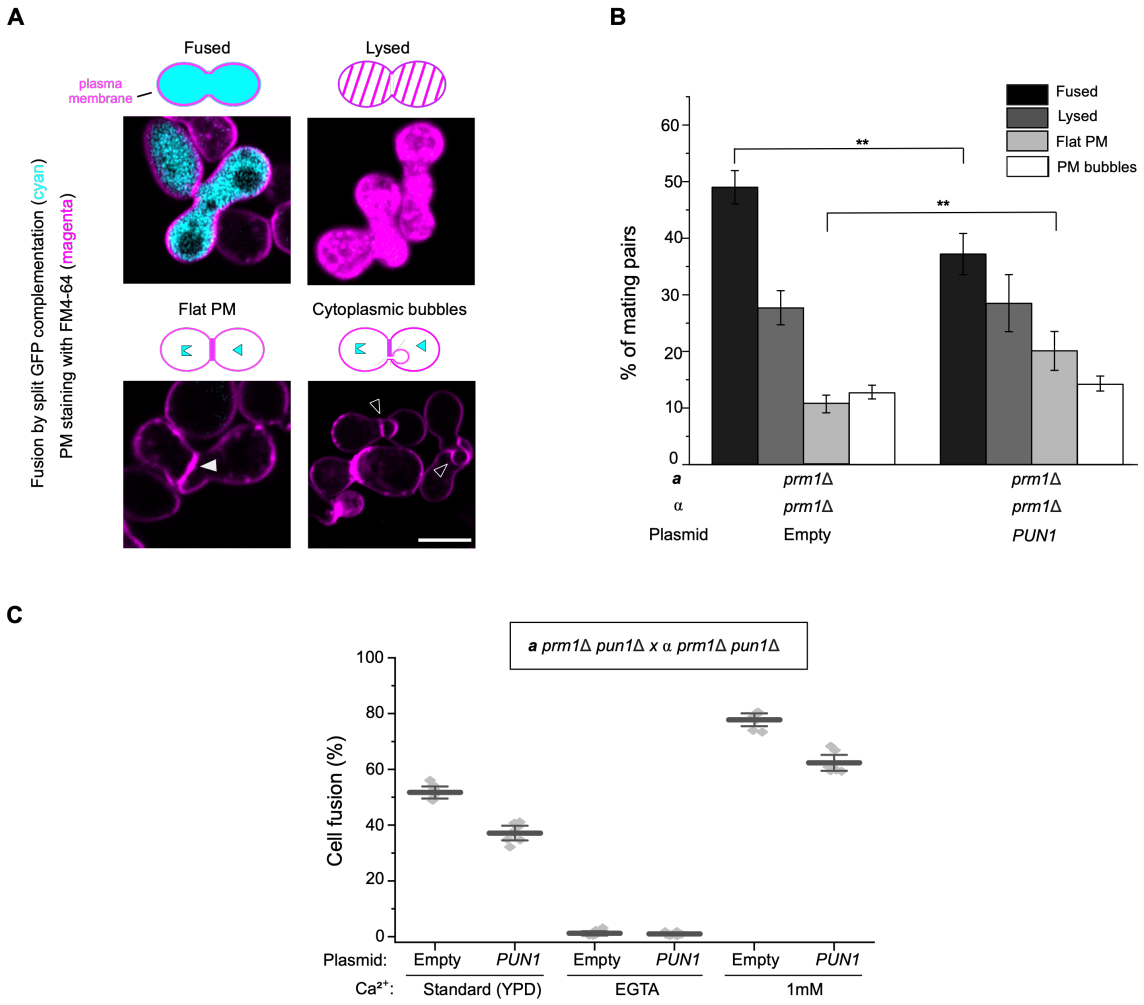

Figure 30: *PUN1* overexpression in *prm1Δ* mutants enhances the flat PM interface phenotype. (**A**) Representative images of the mating phenotypes observed in *prm1*Δ bilateral matings. Equal amounts of *MAT***a** and *MATα prm1Δ* mutants expressing either the EV or high copy *PUN1* were mixed and allowed to mate on YPD plates for 3 h. Arrested mating mixtures were stained with FM4-64 PM staining dye and then imaged by confocal microscopy. The four phenotypes: fused, lysed, flat PM or PM bubbles were quantified. (**B**) The *prm1Δ* mutants expressing high copy *PUN1* have a reduced number of fused mating pairs and a corresponding increase in the numbers of mating pairs with a flat PM interface. *n*> 300 mating pairs. Error bars denote SEM of three or more independent triplicate experiments. (**C**) Extracellular Ca^{2+} does not suppress the Pun1p fusion inhibition activity. Bilateral matings of *prm1Δpun1Δ* were performed in media supplemented with or lacking Ca^{2+} as described in *Materials and methods*. Low copy *PUN1* expression inhibits fusion of *prm1Δpun1Δ* mutants supplemented with 1mM $CaCl_2$. However, fusion is completely inhibited when these cells are mated in media supplemented with 20mM EGTA. Error bars denote SEM of three or more independent triplicate experiments. **P-value <0.05. Scale bar= 5 µm.

4.9.3 *PUN1* overexpression has no effect on the cell wall (CW) composition of *prm1Δ* mutants

High copy expression of *PUN1* in *prm1Δ* mutants inhibits fusion by enhancing the arrest of mating pairs as early prezygotes with a flat PM interface but has no effect in lysis and cytoplasmic bubble formation phenotypes (**Figure 30B**). The flat PM interface phenotype would imply a possible Pun1p function in the cell wall integrity (CWI) pathway that promotes CW synthesis, resulting in deposition of CW material at the mating junction ([364], [365]). However, a Pun1p function in the CWI pathway would result in a corresponding decrease in the lysis phenotype, similarly to a decrease in lysis that is observed in *prm1Δ* mutants upon *FUS1* deletion ([269]). This is because the lysis phenotype in *prm1Δ* mutants is PM contact- dependent, and this contact is reduced in *fus1Δ* mutants that arrest at the CW remodeling step. The fact that the lysis phenotype was unaffected upon *PUN1*

overexpression would therefore suggest that Pun1p activity is not exerted at the CW remodeling step. To confirm this hypothesis, it was necessary to examine the CW composition upon *PUN1* expression. The yeast CW is an essential organelle that functions as a protective layer against environmental conditions while offering the cell stability and shape ([380]). It is composed of the polysaccharides β-1,3-glucan, β-1,6-glucan, chitin, and various mannoproteins ([381]). Chitin makes up only a small percentage (2%) of the total CW dry weight while the β-glucans form about half of the total CW dry weight. All the four components are covalently linked forming macromolecular complexes ([382], [383]). In budding vegetative cells, chitin synthase enzymes catalyze the synthesis of chitin. Chitin is subsequently localized at the budding site where it forms a ring-like structure separating the mother and daughter cell ([259], [262], [384], [385]). Asymmetric cell division results in the majority of the chitin being retained in the mother cell bud scar, although a small percentage is also distributed throughout the rest of the CW. When budding haploid cells are stained with Calcofluor white, chitin staining mainly occurs at the bud scars that represent sites of previous budding. These sites are usually found adjacent to the new budding site. Chitin deposition can also occur at the base of the emerging bud where it forms the chitin ring. During mating, chitin is preferentially present at the base of the shmoo of polarized cells as evidenced by intense Calcofluor white staining at these regions ([257], [259]).

When *prm1Δpun1Δ* mutants expressing either the EV or *PUN1* were stained with Calcofluor White, no significant difference in the amount of synthesized chitin fluorescence was observed between the two cell populations. In haploid vegetative cells expressing the EV, intense chitin staining was observed both at the emerging bud sites and at bud scars adjacent to the new buds (**Figure 31A**). In pheromone-treated cells, chitin staining mainly occurred at the base of the shmoo, occasionally forming a fence-like structure separating the shmoo tip from the rest of the polarized cells, consistent with previous findings ([257]). Likewise, in *prm1Δpun1Δ* mutants expressing *PUN1*, a similar chitin staining pattern was observed both in haploid vegetative cells as well as pheromone-treated cells (**Figure 31B**). No apparent differences were observed in both the Calcofluor White fluorescence intensity and staining pattern. Similarly, mannoprotein staining using the ConA-AF 647 conjugate showed homogenous cellular staining in haploid vegetative cell with no significant difference in the fluorescence intensity between the two groups of cells. In pheromone-treated cells, both the control cells (EV) and cells expressing *PUN1* showed a homogenous staining at the basal cell cortex and a remarkably intense staining at the shmoo. Altogether, these findings suggest that *PUN1* overexpression has no direct effect on CW composition and by proxy the CWI pathway. Consequently, the observed flat PM interface phenotype prompted further analysis.

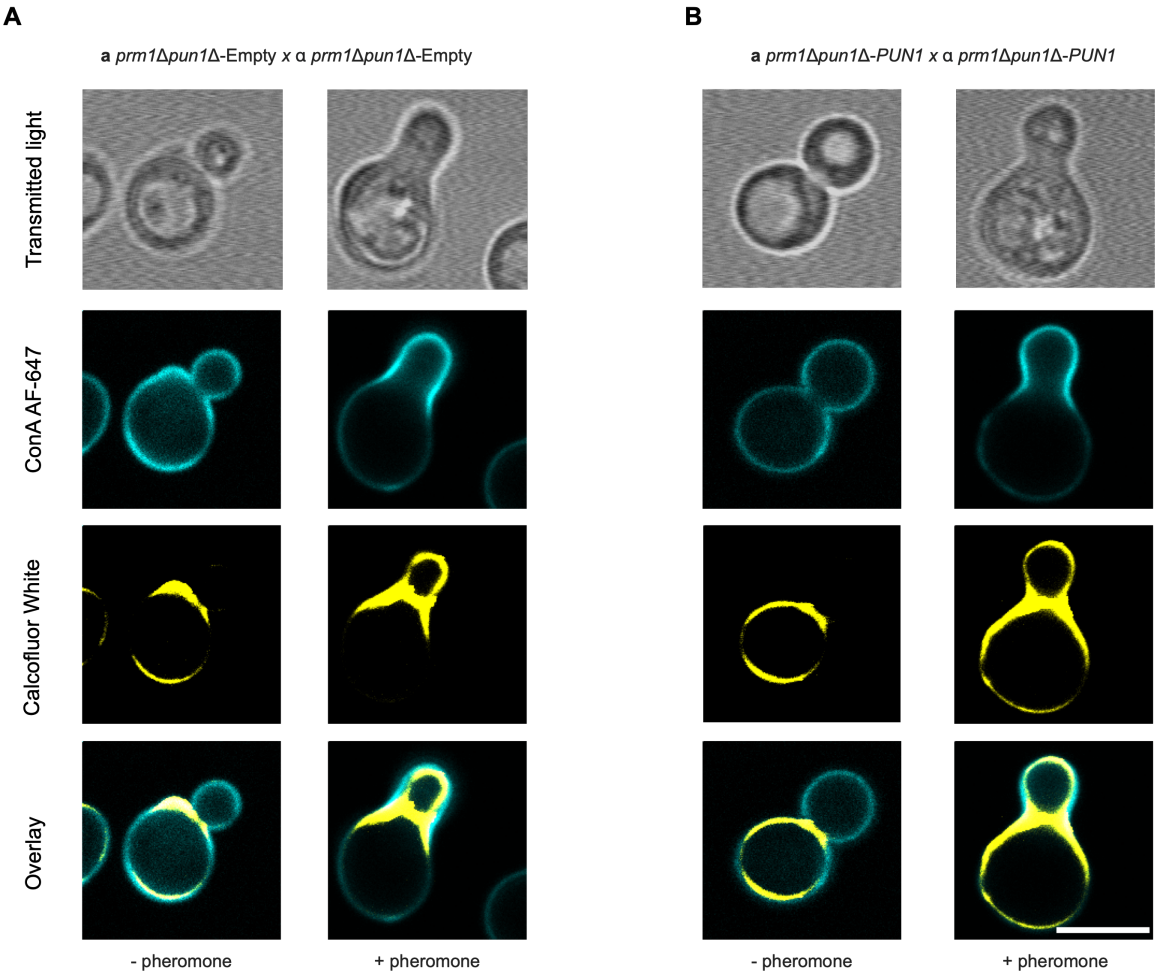

Figure 31: Overexpression of *PUN1* in *prm1Δ* mutants does not affect the CW composition. The vegetative or pheromone-treated *prm1Δpun1Δ* cells expressing either the EV or low copy *PUN1* under the *ADH1* promoter, were stained with CW dyes Calcofluor white and Concanavalin A- Alexa Fluor 647 conjugate and imaged by fluorescence microscopy. (**A**) Representative images of the vegetative and pheromone-treated *prm1Δpun1Δ* cells expressing the EV versus (**B**) low copy *PUN1* under the *ADH1* promoter. No observable differences in the staining pattern between the two groups. Scale bar= 5 µm.

4.9.4 Overexpression of *PUN1* enhances formation of a flat PM interface without intervening CW material

To assess the nature of the flat PM interface observed in *prm1Δ* mutants expressing *PUN1*, FM4-64 PM staining was coupled with CW staining using Calcofluor white, a dye that specifically binds to CW chitin. This approach allowed a deeper characterization of the flat PM interface phenotype and whether it corresponded to early prezygotes with an intervening CW material or late prezygotes in which the CW has been degraded. Bilateral matings of *pun1Δfus1Δfus2Δ* mutants known to arrest at the CW remodeling step were used as a control for early prezygotes. As expected, bilateral crosses of the *pun1Δfus1Δfus2Δ* mutant arrested as early prezygotes with nearly all mating pairs positive for both PM and CW staining at the mating junction (**Figure 32A**). Bilateral matings of *prm1Δpun1Δ* mutants expressing the EV exhibited all expected phenotypes including fusion, lysis, late prezygotes with cytoplasmic bubbles and occasionally prezygotes with a flat PM interface. Most late prezygotes with cytoplasmic bubbles portrayed only PM staining, although occasional simultaneous CW and PM staining along the mating junction was observed except at regions where the bubble emerged, indicating that these regions indeed lacked the supporting CW material (**Figure 32B)** and (**Figure S6**). Interestingly, virtually all prezygotes with a flat PM interface had an intervening CW, consistent with previous studies (**Figure 32B**) ([269], [350]). On examining the *prm1Δpun1Δ* mutants expressing *PUN1*, all the four phenotypes were also present with late

prezygotes that contained cytoplasmic bubbles similar to those observed in the control cells. Strikingly, while a majority of the prezygotes with a flat PM exhibited both PM and CW staining, a mild increase in prezygotes with a flat PM interface but no intervening CW material were observed (**Figure 32C**) and (**Figure S6**). The fact that this latter class of mating pairs was largely absent in the control cells suggests, that the Pun1p fusion inhibition activity results in the arrest of mating pairs in an intermediate stage characterized by a flat PM interface with no intervening CW material i.e. a flat late prezygote.

Overall, this data reveals that the CW remodeling step and the pathways that lead to lysis or cytoplasmic bubble formation in *prm1Δ* mutants are generally unaffected by *PUN1* overexpression. Instead, high-copy expression of *PUN1* results in the arrest of unfused mating pairs in a PM junction-like structure consisting of two closely apposed PMs with no intervening CW. The stable PMs appear flat but cannot fuse resulting in a decrease in fusion.

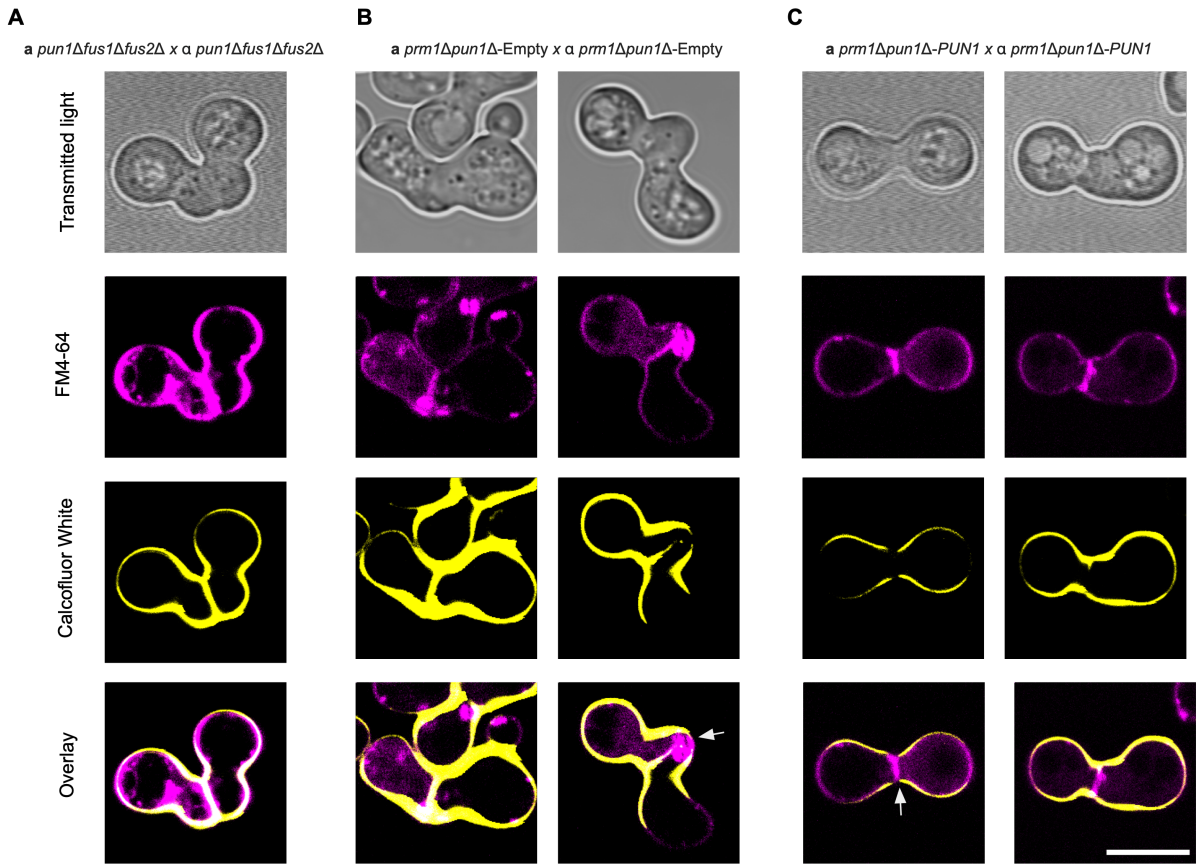

Figure 32: *PUN1* overexpression in *prm1Δpun1Δ* mutants leads to the appearance of a flat PM interface with no intervening CW material. Following mating, bilateral mating mixtures of *pun1Δfus1Δfus2* and *prm1*Δ*pun1*Δ mutants expressing either the EV or low copy *PUN1* under the *ADH1* promoter, were stained with Calcofluor white CW dye and FM4-64 PM dye and imaged by fluorescence microscopy. (**A**) Representative images of the early prezygotes observed in CW remodeling mutants. Fusion is severely compromised in bilateral matings of *pun1Δfus1Δfus2*, and mating pairs show both CW and PM staining at the mating junction. (**B**) In *prm1*Δ*pun1*Δ mutants expressing the EV, mating pairs with a flat PM interface contain intervening CW material. Late *prm1Δ* prezygotes exhibiting PM bubbles do not show CW staining at the junction (white arrow). (**C**) *PUN1* overexpression in *prm1Δpun1Δ* mutants enhances the formation of mating pairs with a flat PM interface but no intervening CW material (white arrow) in addition to those with a flat PM interface and intervening CW material. Scale bar=5 μm.

4.10 Understanding the mechanistic basis of Pun1p fusion inhibition activity

So far, deletion of *PUN1* in *prm1Δ* mutants results in a mild increase in the fusion efficiency of *prm1Δ* mutants, suggesting a putative Pun1p fusion inhibition activity. In support of that, high and low-copy expression of *PUN1* in *prm1Δ* mutants results in an enhanced fusion defect and a corresponding increase in the flat PM interface phenotype. These findings not only support the hypothesis that Pun1p is a novel negative regulator of fusion but also provide a basis to investigate the potential mechanism of Pun1p activity.

4.10.1 Pun1p fusion inhibition activity is concentration- dependent

Firstly, to understand whether the Pun1p inhibition activity was concentration- dependent, unilateral (*PUN1* expressed in one mating type) versus bilateral (*PUN1* expressed in both mating types) fusion studies in *prm1Δpun1Δ* mutants were carried out. The *prm1Δ* mutants expressing high-copy *PUN1* under the *ADH1* promoter in addition to endogenous *PUN1* levels were included, thus representing the cells with the highest *PUN1* copy number. All mating reactions were performed in standard mating conditions and the fusion efficiency determined by BiFC- fusion assay. In comparison to the ~52% fusion efficiency of control *prm1Δpun1Δ* mutants expressing the EV, *prm1Δ* single deletion mutants expressing only the endogenous *PUN1* fused with ~42% fusion efficiency. Notably, the Pun1p fusion inhibition activity increased with increasing concentration of Pun1p molecules across the mating junction, such that cells expressing high-copy *PUN1* crossed to cells expressing only the endogenous *PUN1* exhibited a higher fusion inhibition activity than the control cells (**Figure 33A**). This suggests an enhanced fusion inhibition activity when Pun1p is present in both mating partners and can form homotypic *trans* interactions. Interestingly, unilateral expression of *PUN1* in *prm1Δpun1Δ* mutants, in either mating type, resulted in ~42% fusion efficiency, comparable to *prm1Δ* mutants expressing the EV. This would suggest a *cis*-mediated Pun1p unilateral activity especially when the protein present in high copies, or a *trans* interaction with unknown components across the junction that exerts a similar effect like the *trans* interaction observed when only endogenous Pun1p is present. Remarkably, when both mating partners express high-copy *PUN1*, an increase in fusion inhibition was observed (~35% fusion efficiency), indicating an enhanced inhibition activity that possibly occurs in *trans*. Notably, the highest fusion inhibition activity was observed in bilateral matings of *prm1Δ* mutants expressing high-copy *PUN1* from the constitutive *ADH1* promoter (**Figure 33A**). Indeed, these cells express the highest concentration of Pun1p consisting of both high-copy *PUN1* as well as endogenously expressed Pun1p.

To confirm whether this progressive fusion inhibition was not due to reduced rates of fusion across the mating reactions, respective pairing efficiencies were determined. The percentage of pairing corresponds to the number of cells that obtain a mating partner, establish a strong cell-cell adhesion and undergo the upstream events of the mating pathway. This approach therefore acts as a proxy to determining the respective rates of fusion. Despite a few statistically insignificant differences, all mating reactions had ~45% pairing efficiency (**Figure 33B**), suggesting that within the 3 h mating period, all reactions proceeded roughly with the same rates of fusion.

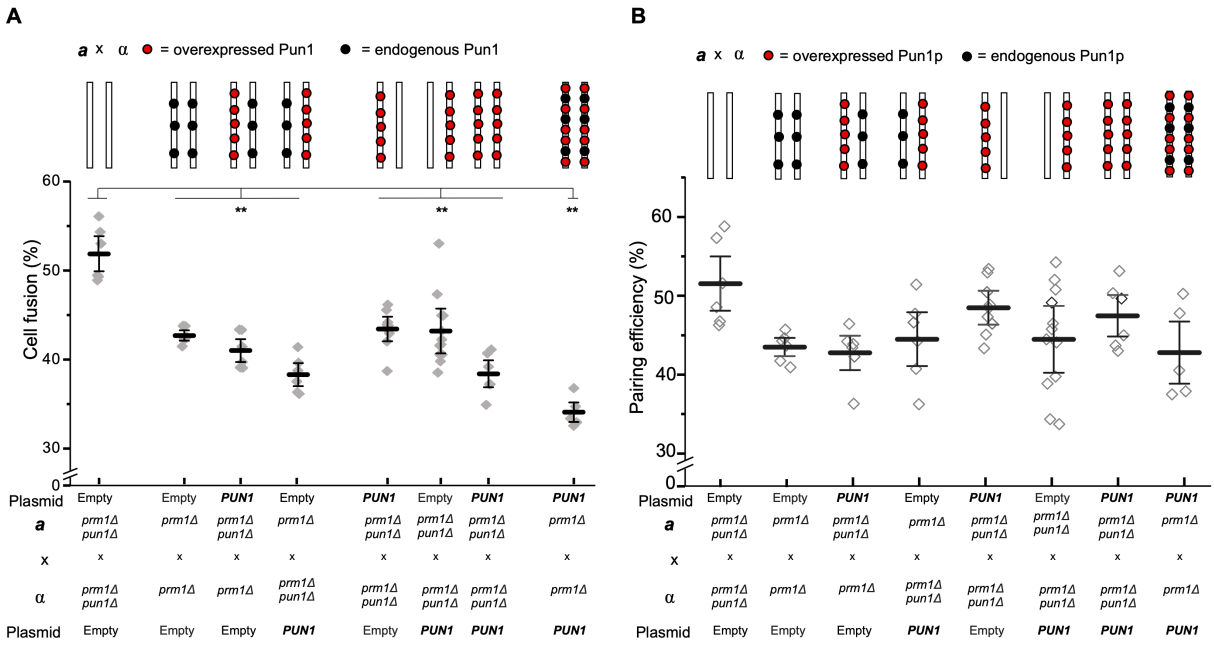

Figure 33: Pun1p fusion inhibition activity is concentration-dependent. (**A**) *prm1Δ* mutants expressing the highest Pun1p concentration exhibit the least levels of fusion. Fusion of *prm1Δ* or *prm1Δpun1Δ* mutants expressing high copy *PUN1* under the *ADH1* constitutive promoter either unilaterally (one mating type) or bilaterally (both mating types) was quantified by flow cytometry. An additional inhibition activity is present in cells expressing both endogenous *PUN1* and *PUN1* from the constitutive *ADH1* promoter. (**B**) The Pun1p fusion inhibition activity has no effect on cell pairing. Percentage of cell pairing in respective mating crosses in (**A**) was calculated by obtaining the fraction of double- stained cells to the sum total of minimum single-stained plus double-stained cell populations as described in *Materials and Methods*. All mutants pair with approximately 45% pairing efficiency. **P-value <0.05.

4.10.2 Conserved residues of the Pun1p Claudin motif are relevant for its inhibitory activity

As previously mentioned, Pun1p structurally resembles mammalian claudins and adopts a general left-handed model (**Figure 23C**). Additionally, Pun1p exhibits 100% conservation of the residues in the first extracellular loop (ECL1) that form the claudin signature motif GLWxxC(8-10 aa)C, making Pun1p a fungal claudin-like protein. Claudins are the major structural components of mammalian epithelial and endothelial Tight Junctions (TJs) that function as paracellular barriers ([280], [281], [386]). Interactions between claudins and other TJ-associated proteins such as junction adhesion molecules (JAMS), tricellulin, MarvelD3 and occludin results in the formation of paracellular barriers with occasional paracellular permeability abilities ([280], [387]). Notably, the conserved ECL1 cysteine-containing claudin signature motif GLWxxC(8-10 aa)C is the distinguishing feature of mammalian claudins. This motif plays an important structural role in stabilizing the ECL1 fold and mutations in one or all of the conserved residues results in either abolished barrier function or loss of trafficking to the tight junction ([388], [389], [390]). For instance, claudin-1 is highly expressed in liver cells and functions as a co-receptor for Hepatitis C virus (HCV) entry ([391]). Individual mutations of the claudin-1 GLW or cysteine residues to alanine result in reduced co-receptor activity and a corresponding inability of hepatocytes to bind HCV although the protein is correctly localized to the PM ([392]). Interestingly, when the three GLW residues of claudin-2 ($G_{49}L_{50}W_{51}$) are mutated to triple alanine (AAA), the protein is mis-localized and PM localization abolished. The claudin-2 AAA mutant is nevertheless able to form dimers, suggesting that the three residues are not involved in *cis*-interactions and protein polymerization ([393]). On the other hand, mutating the conserved cysteine residues in claudin-5 (C_{54} and C_{64}) results in a reduced barrier function, and similar mutations in claudin-2 result in reduced pore function ([388], [390], [392]). A stable ECL1 fold is therefore crucial for protein function and/or trafficking across the different claudins.

To study the influence of the Pun1p conserved claudin signature motif on its fusion inhibition activity, site-directed mutagenesis of the single or all conserved residues was carried out. Single cysteine residues (C_{79} and C_{90}) were mutated to serine (C79S and C90S) while the $G_{74}L_{75}W_{76}$ residues were mutated to triple alanine (AAA) (**Figure 34A**). Fusion efficiencies of the respective low-copy *PUN1* mutants expressed under the *ADH1* promoter in *prm1Δpun1Δ* mutants were quantified. As expected, overexpression of WT Pun1p resulted in a 1.6-fold reduction in fusion compared to cells expressing the EV. The single cysteine mutants (C79S and C90S) fused with efficiencies comparable to WT Pun1p although the C90S portrayed a slightly higher reduction in fusion (**Figure 34B**). This suggests that a single conserved cysteine residue is sufficient in exerting the Pun1p fusion inhibition activity. Surprisingly, the Pun1p double cysteine mutant (C79SC90S) fused similarly to the single cysteine mutants, implying that the Pun1p fusion inhibition activity is not dependent on the conserved cysteine residues. On the other hand, mutating the Pun1p GLW residues to AAA resulted in a slight reduction in the fusion inhibition activity, but fusion efficiency in these cells was still lower than that of control cells expressing the EV, suggesting that the mutant protein was still functional. Interestingly, mutating all the conserved residues of the claudin motif (AAA+C79SC90S) completely abolished the protein activity and restored fusion to levels of the control cells (**Figure 34B**). These findings therefore indicate the dependence of the Pun1p fusion inhibition activity on the claudin motif. Furthermore, mating crosses between the Pun1p AAA+C79SC90S mutant and WT Pun1p generally showed little to no fusion inhibition activity, suggesting that the interaction between a non-functional protein on one mating partner with the WT protein present in the other partner hinders the otherwise unilateral activity of the WT protein.

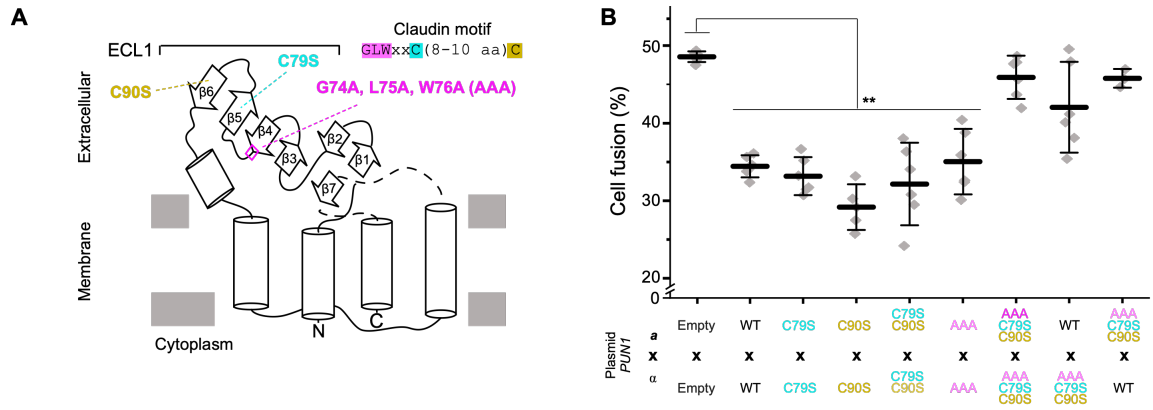

Figure 34: Pun1p fusion inhibition activity requires the conserved claudin motif residues. (**A**) Schematic showing the Pun1p protein topology and the location of the Pun1p conserved claudin motif. The conserved cysteine residues (C_{79} and C_{90}) were mutated to serine whereas the G_{74}, L_{75} and W_{76} were mutated to triple alanine (AAA). (**B**) The conserved claudin motif residues are required for Pun1p activity. Bilateral matings of *prm1Δpun1Δ* mutants expressing low-copy pr*ADH1-PUN1* in which all the all the conserved residues of the claudin motif had been mutated fused similarly to the control cells expressing the EV. **P-value <0.05.

4.10.3 The Pun1p AAA+C79SC90S mutant exhibits an unusual monomeric protein modification

In order to understand why mutating all the residues of the claudin motif i.e. (AAA+C79SC90S mutant) blocked Pun1p functionality, two approaches were adopted. First, microscopic examination of the protein localization pattern during mating was performed. WT Pun1p, Pun1p AAA, Pun1p C79SC90S as well as the Pun1p AAA+C79SC90S mutants were all C-terminally tagged with mNeonGreen. The respective genes expressed from the low-copy CEN plasmid under the *ADH1* promoter were transformed into *prm1Δpun1Δ* mutants and the bilateral matings performed. After 90 min of mating, protein localization was determined and was coupled with FM4-64 PM staining to ascertain correct protein trafficking to the PM. WT Pun1p-mNG localized uniformly at the PM

and co-localized with FM4-64, suggesting correct PM localization. Notably, WT Pun1p-mNG was present at the mating junction, consistent with previous observations (**Figure 35A**). Similarly, the Pun1p C79SC90S-mNG mutant was uniformly localized at the PM, and occasionally enriched at the mating junction where it appeared as an intense fluorescent puncta (**Figure 35A**). On the other hand, the Pun1p AAA and the AAA+C79SC90S mutants both displayed a cortical Endoplasmic Reticulum (ER)-like localization pattern (**Figure 35A**). While majority of the protein co-localized with FM4-64, some of the protein was present in the cell interior including around the nucleus, reminiscent of the localization pattern of Hmg1p, the nuclear envelope and ER marker ([350]). Despite this aberrant localization, both the Pun1p AAA and the AAA+C79SC90S mutant proteins were localized at the mating junction in at least half the mating pairs, suggesting that sufficient mutant proteins were correctly trafficked to the PM (**Figure S7**).

Finally, the expression profile of each mutant protein was analyzed by SDS-PAGE and Western blot. All Pun1p mutants were C-terminally tagged with the V5 epitope tag and their expression probed in absence or presence of pheromone to mimic mating conditions. In the absence of pheromone, all mutants including the WT Pun1p showed strong high molecular weight bands of >180kDa, corresponding to higher molecular weight protein complexes (**Figure 35B**). Additionally, distinct bands of ~30kDa, corresponding to the monomeric protein, were present in WT Pun1p, C79S, C90S, C79SC90S and the AAA mutants. However, in the Pun1p AAA+C79SC90S mutant, the monomeric band shifted to a slightly higher molecular weight and appeared as double bands (**Figure 35B**). Additionally, all mutants including the WT Pun1p showed additional low molecular weight bands that likely corresponded to degradation products due to proteolysis at the C-terminus. Importantly, similar results were obtained when cells were treated with pheromone (**Figure S7**).

The apparent accumulation of the Pun1p AAA+C79SC90S mutant in the ER would suggest possible N-glycosylation on the monomeric protein. Indeed, WT Pun1p contains two potential N-glycosylation sites; Asparagine (N_{100}) and Asparagine (N_{209}), that could be crucial in facilitating Pun1p secretion from the ER via the Golgi to the PM ([373]). To determine whether the AAA+C79SC90S mutant was undergoing N-glycosylation, treatment of cells with the N-Glycosidase PNGase F, in reducing conditions was carried out. A V5 construct of WT Prm1p that is known to undergo N-glycosylation was used as a control ([268]). In PNGase F untreated cells, Prm1p mainly existed as a glycosylated monomer of ~115kDa, although a faint band of the unglycosylated monomer of ~73kDa was also present. Additional lower MW bands were observed likely corresponding to degradation products (**Figure 35C**). Upon PNGase F treatment in reducing conditions, the glycosylated monomer band was lost while the lower bands were retained including the unglycosylated monomer of ~73kDa, thus confirming that Prm1p is indeed a glycosylated protein. In the Pun1p AAA+C79SC90S PNGase F untreated sample, the high MW band and a monomeric band were observed, consistent with previous findings (**Figure 35C**). However, upon PNGase F treatment, the high MW band was lost but no difference in the monomeric protein was observed between the PNGase F-treated and untreated sample, suggesting that the monomeric modification is likely not N-glycosylation. Additional efforts to determine the nature of this modification were incomplete during the writing process of this thesis.

Altogether, this data strongly suggests that the Pun1p fusion inhibitory activity is predominantly dependent on conserved residues in the claudin motif. Whereas mutating the two cysteine residues to serine does not have any effect on Pun1p trafficking to the membrane and function, a combined mutation of the three hydrophobic GLW residues to AAA results in protein mislocalization and decreased protein trafficking to the cell surface. This indicates that the GLW residues are critical in mediating protein trafficking along the secretory pathway. The decrease in protein localization to the surface is further corroborated by a slight decrease in Pun1p fusion inhibition activity of the Pun1p AAA mutant (**Figure 34B**). An even greater decrease in Pun1p fusion inhibition activity is observed in the Pun1p AAA+C79SC90S mutant in which about only 50% of mating pairs exhibit correct protein localization to the PM (**Figure S7**). These findings therefore suggest that Pun1p function is in part related to the correct protein localization to the cell surface. However, mutations in all residues of the claudin motif (AAA+C79SC90S) results in a modification of the monomeric protein, making this modification the likely cause of the inactivity of this mutant protein. Nevertheless, none of these mutations has an effect on protein expression and oligomerization, suggesting that protein oligomerization is dependent on other residues or segments outside the conserved claudin motif.

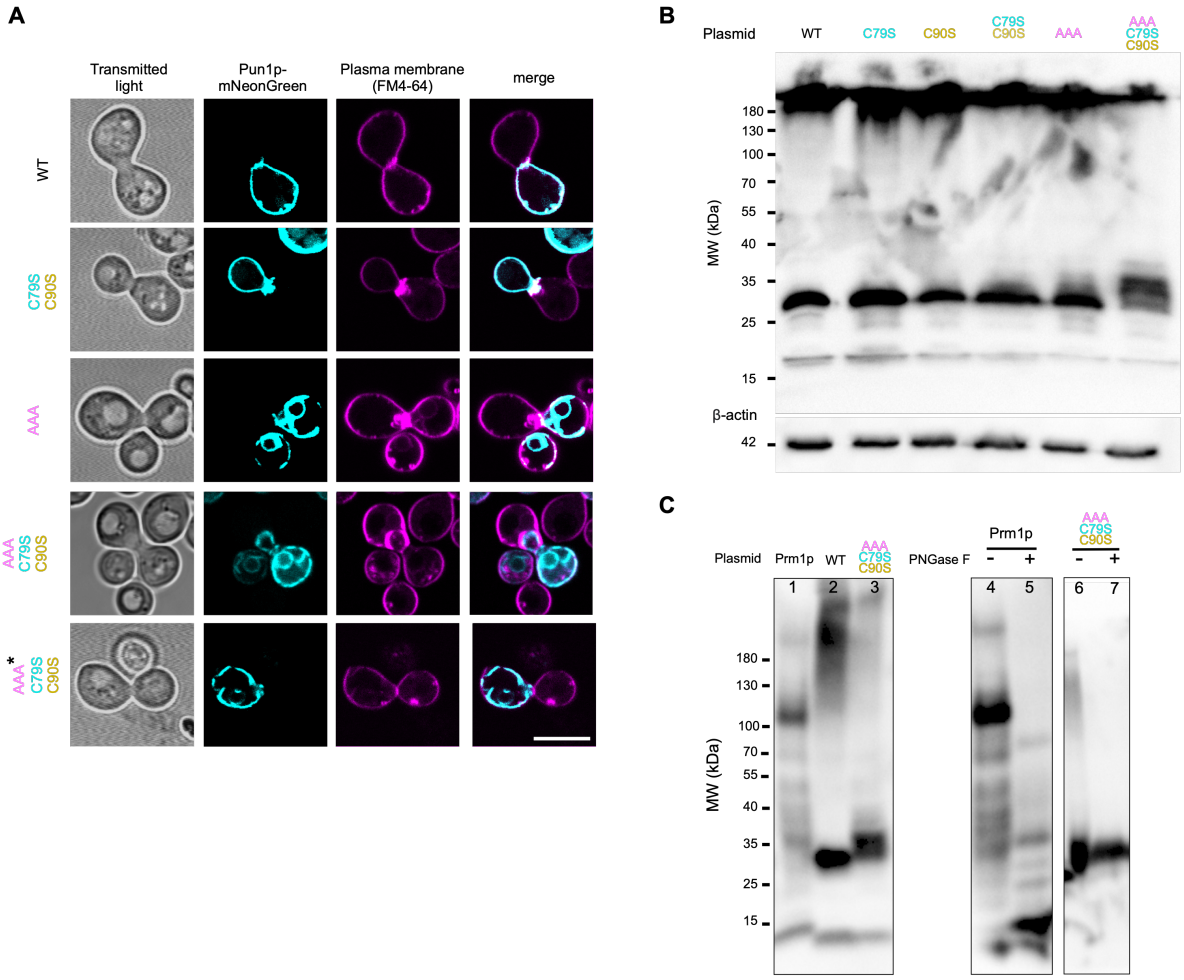

Figure 35: The GLW residues are necessary for proper protein folding and translocation to the PM. (**A**) Representative images of the bilateral matings of *prm1Δpun1Δ* mutants expressing the respective *PUN1* mutants that are C-terminally tagged with mNeonGreen. Cells were allowed to mate for 90 min before fusion was arrested and cells imaged by confocal microscopy. The AAA and the AAA+C79SC90S mutants lose the homogenous PM distribution that is observed in WT-Pun1p and C79SC90S mutants. Note the AAA+C79SC90S* mutant in which no co-localization of the mutant protein with the PM dye FM4-64 is observed. The mutant protein is in the cortical ER. (**B**) Mutating all the conserved claudin motif residues results in modification of the monomeric protein. Protein extracts from total cell lysates of vegetative cells expressing V5-tagged WT Pun1p and respective mutants were analyzed by Western blotting and detected using an anti-V5 antibody. β-actin serves as an expression control. (**C**) The monomeric AAA+C79SC90S protein does not undergo a N-glycosylation. Protein extracts from total cell lysates of vegetative cells expressing V5-tagged Prm1p, WT Pun1p and Pun1p AAA+C79SC90S mutant were treated with 50U/µL PNGase F in denaturing conditions and analyzed by Western blotting. Lanes 5 and 7 depict Prm1p-V5 and Pun1p AAA+C79SC90S-V5 samples treated with PNGase F versus the untreated ones (lanes 4 and 6). Scale bar= 5 µm.

5 Proximity labeling: a novel approach to map the yeast fertilization synapse

By employing a SILAC-based proteomics analysis of PM changes as the vegetative *MAT***a** and *MATα* cell transitions into a mating-ready state, this thesis has identified Pun1p as a putative negative regulator of PM fusion. Deletion of *PUN1* enhances fusion in *prm1Δ* mutants and its overexpression suppresses fusion in *prm1Δ* and *fus1Δ* mutants. Furthermore, the structural similarities between Pun1p and mammalian claudins suggest that Pun1p could be mediating the formation of a tight junction-like structure that anchors the fusogenic machinery while regulating proper PM fusion. Consistently with its putative function, Pun1p is pheromone-upregulated and localized at the mating junction, similarly to known key players of fusion such as Fus1p and Prm1p. However, while this approach has revealed an important and often uncharacterized arm of fusion regulation, the key players of PM fusion including the *bona fide* fusogen or fusogenic complex remain unidentified. Additionally, this approach presents a few limitations:

I. Despite its ability to intensely characterize changes across the entire PM, this approach is not specific to the PM changes that occur exclusively at the shmoo tip, where cell-cell contact and fusion eventually takes place.
II. This approach does not take into account late PM changes that occur only upon cell-cell contact such as dynamically expressed proteins that may be absent in the polarized growth stage. Consistently, cells fuse only upon contacting a mating partner, suggesting possible contact-dependent regulatory mechanisms.
III. Low-abundance proteins may remain undetected when compared to high-abundance proteins.

In order to circumvent these limitations and possibly identify unknown regulators of late steps of yeast mating, a proximity-dependent biotin labeling (PL) approach of the mating junction i.e. fertilization synapse was developed. The fertilization synapse is a short-lived, spatially limited PM junction that is generated after CW remodeling but precedes PM fusion, analogous to the mammalian claudin-mediated tight junction (**Figure 36B**) ([280], [281], [386]). At the fertilization synapse, the fusing PMs are closely apposed at about 8 nm distance, with the fusion machinery possibly anchored at either or both membranes. This machinery subsequently mediates PM fusion via dehydration and destabilization of the lipid bilayer, fusion pore formation and expansion ([3]). Indeed, a similar fusogenic synapse has been proposed during myoblast fusion between the founder cell and the fusion competent myoblast (FCM) ([7]). It therefore suffices that localized mapping of the fertilization synapse might reveal both low and high-abundance proteins that constitute the mating junction, including the components of the fusogenic machinery.

PL is a novel labeling technique that allows mapping of protein interactomes at a particular location in a cell. PL is based on the use of enzymes Biotin ligase (BirA), Ascorbate peroxidase (APEX) or Horseradish peroxidase (HRP) fused to a target protein. The enzymes catalyze the conversion of biotin or biotin derivatives into reactive radicals that react and covalently tag proteins in close proximity to the target protein ([332]). Following cell lysis, the tagged proteins are enriched and isolated using streptavidin beads. The enriched proteins are thereafter digested to generate small peptides whose mass to charge ratio (*m/z*) analysis via mass spectrometry (MS) allows the identification of the respective proteins. Recent progress has coupled PL with quantitative MS such as SILAC, in vitro chemical labeling via isobaric tags for relative and absolute quantification (iTRAQ) or tandem mass tags (TMT) ([394], [395], [396]). Notably, the low abundance of naturally biotinylated proteins and the high binding affinity and specificity of biotin to streptavidin (K_D 10^{-13}-10^{-15} M) not only reduces the background noise but increases the robustness of this approach ([397]).

At its inception, PL was based on the use of a mutant form of *E. coli* DNA-binding biotin protein ligase BirA* (R188G). BirA* permits promiscuous *in vivo* biotinylation with itself and cellular proteins in close proximity to the target protein ([398], [399]). In the presence of ATP and overnight incubation with biotin, the mutant BirA* catalyzes the conversion of biotin to biotinyl-5'-AMP (adenosine-monophosphate) mixed anhydride intermediate. Contrary to the WT BirA that

sequesters biotinyl-5'-AMP to its active site for specific biotinylation of its acetyl-CoA carboxylase substrate, mutant BirA* has a decreased affinity for biotinyl-5'-AMP. As a result, BirA* releases the biotinyl-5'-AMP intermediate from the active site facilitating its non-specific reaction with primary amines such as lysine residues and subsequent biotinylation of proximal proteins (**Figure 36A**) ([397],[398], [399]). Due to the use of a biotin substrate, BirA*- based PL is generally referred to as proximity-dependent biotin identification (BioID) and has been extensively used to map organellar proteomes including cytoplasm, mitochondria and nucleus ([332], [400]). However, due to the slow labeling kinetics (15-24 h) and high concentrations of biotin required during BioID, newer approaches of PL have been developed including a second version of BioID2 as well as HRP and APEX-mediated PL. Indeed, BioID2 exhibits a higher biotinylation activity than BioID and uses less biotin ([401]).

HRP-mediated PL is dependent on the HRP peroxidase activity. Upon activation by hydrogen peroxide (H_2O_2), HRP rapidly catalyzes the oxidation of biotin substrates such as biotin phenol (BP) or fluorescein arylazide to generate reactive, short-lived, membrane-impermeable phenoxyl radicals of about <1ms half-life ([402], [403], [404]). These radicals subsequently form covalent bonds with electron-rich residues such as tyrosine, thus biotinylating neighboring proteins ([403]). Notably, due to their short half-life, the labeling intensity of these radicals is in a nanometer scale (~10nm), similarly to BirA*, resulting in a biotinylation contour map proximal to the peroxidase active site. Intriguingly, the HRP structure contains four essential disulfide bonds and two Ca^{2+} binding sites. Consequently, HRP is inactive in reducing environments such as the cytoplasm and instead, permits proximity labeling in oxidized environments such as the ER lumen and Golgi of the secretory pathway as well as extracellular regions such as the cell surface ([405]). Recent developments have led to the generation of split HRP that permits synaptic labeling and characterization of cell-cell interactions ([405]). Similarly to HRP, APEX-mediated PL relies on an engineered soybean ascorbate peroxidase activity. Following activation by H_2O_2, APEX catalyzes the oxidation of biotin phenol (BP) into short-lived, highly reactive membrane-impermeable biotin-phenoxyl radicals that covalently tag proximal proteins via electron-rich tyrosine residues ([405], [406]). Contrary to HRP, APEX is active in reducing environments such as the cytosol and mitochondria ([406]). Notably, both HRP and APEX- mediated PL permit faster labeling kinetics with HRP-based PL taking about 5-10 min while APEX-mediated PL takes 1 min following a 30-60 min substrate incubation time ([333]). Additionally, both HRP and APEX are applicable in electron microscopy (EM) studies due to their ability to catalyze the polymerization of 3,3'-diaminobenzidine (DAB) to create an EM contrast following osmium fixation ([407]).

Interestingly, contrary to mammalian studies, the applicability of the HRP and APEX-mediated PL in yeast studies has largely been hampered by the presence of a CW that prevents the delivery of the biotin phenol substrate ([403], [408]). Consequently, high osmolarity conditions such as 1.2 M sorbitol and CW perturbations using Zymolyase reportedly enhance APEX delivery in *S. pombe* and *S. cerevisiae*, respectively ([408]). Notably, no HRP-based PL studies have been successfully carried out in yeast. All forms of PL are dependent on protein proximity to the target protein with a higher extent of biotinylation occurring ~10nm distance from the target protein. As a result, both direct and indirect interactors of the target protein are indistinguishably obtained. However, in comparison to traditional proteomic techniques, PL allows the mapping of insoluble cellular structures and the identification of weak and transient interactors that are often lost during cell disruption and organelle isolation procedures ([333], [397], [400]). Therefore, to extensively characterize the extracellular yeast fertilization synapse and identify molecular players of PM fusion, a HRP-mediated proximity labeling approach was adopted (**Figure 36B**). As a proof of principle, this thesis focused on characterizing HRP-Fus1p-dependent PL in pheromone-treated cells before applying the same approach in mating cells.

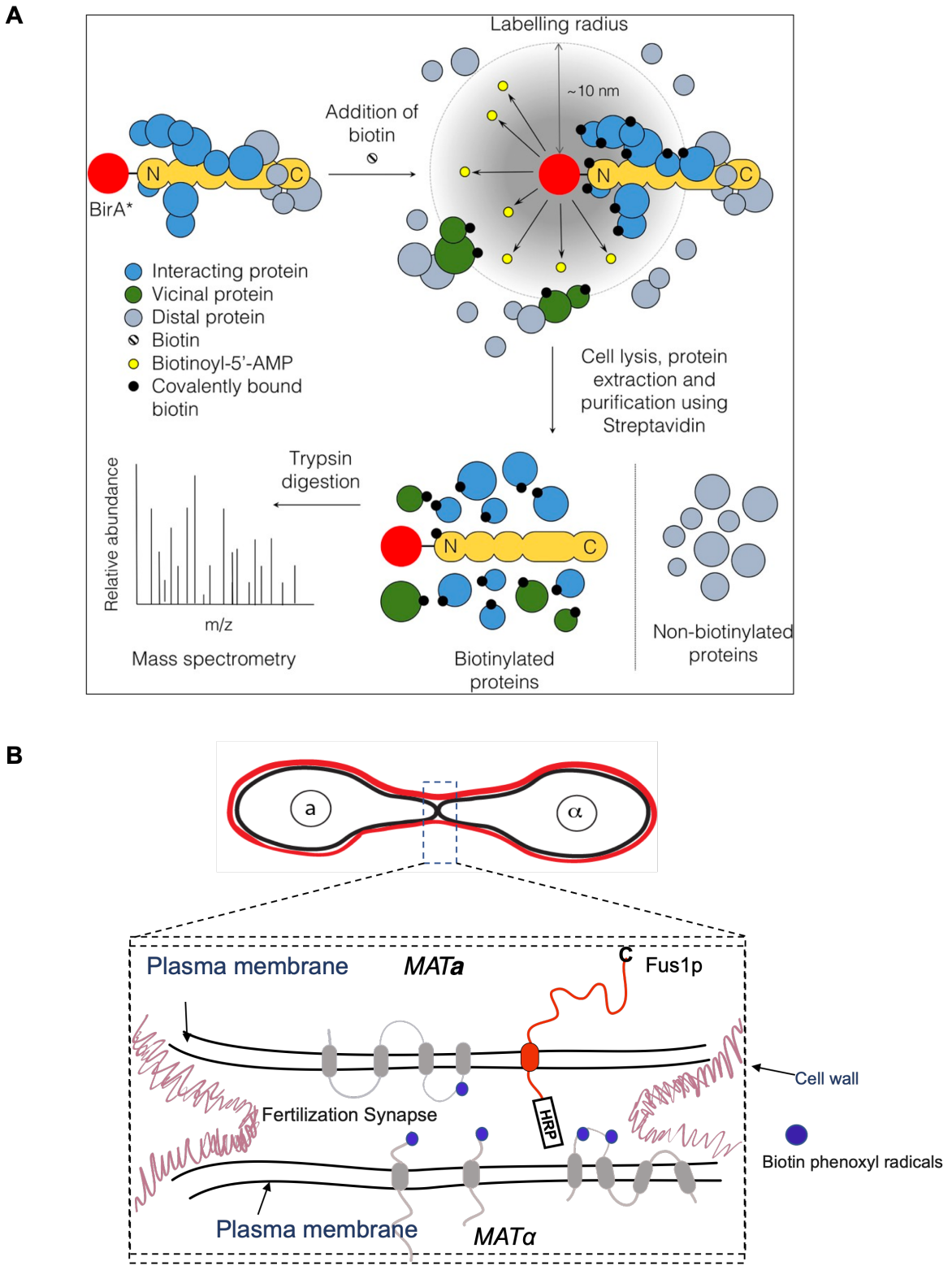

Figure 36: Model depicting application of BioID method in mapping protein-protein interactions. (**A**) BioID relies on the fusing of a target protein (pale orange) with BirA* (red). Upon incubation of cells with biotin, BirA* catalyzes the *in vivo* generation of a reactive Biotinyl-5'-AMP anhydride intermediate that promiscuously reacts and covalently tags neighboring proteins at the lysine residues. The tagged proteins can be both direct interactors (depicted in blue) or simply proximal proteins (depicted in green) of the target protein. These are subsequently isolated using Streptavidin, digested with trypsin to generate peptides that are identified via mass spectrometry using a m/z ratio. Figure adapted from ([401]). (**B**) Schematic of the HRP-Fus1p-mediated proximity labeling at the yeast fertilization synapse. HRP is introduced at the extracellular Fus1p N-terminus. Upon addition of a biotin phenol substrate in presence of H_2O_2, HRP catalyzes the oxidation of biotin phenol to generate reactive phenoxyl

radicals (depicted as blue small circles) that covalently react with electron-rich amines such as tyrosine of proximal proteins. Biotinylated proteins are then isolated using streptavidin and identified by mass spectrometry.

5.1 Generation of N-terminally tagged HRP-Fus1p recombinant protein

For the successful HRP-mediated synaptic labeling, Fus1p, a type 1 integral membrane, was chosen as the first ideal target protein. Fus1p is an O-glycosylated PM protein with an extracellular N-terminus, and a cytoplasmic C-terminus ([238], [239], [409]). Fus1p expression is exclusively pheromone-dependent and the protein localizes at the shmoo tip of polarized cells as well as the mating junction. Fus1p facilitates CW remodeling prior to PM fusion, but has also been implicated in fusion pore expansion ([238], [267]). Consequently, Fus1p is expressed and targeted to the mating junction during mating initiation and is retained at the junction until PM fusion is complete. Due to the Fus1p protein topology with an extracellular N-terminus, a yeast codon optimized HRP was introduced at the *FUS1* N-terminus using a Scarless gene tagging technique ([344]). Accordingly, a split HRP sequence with a *URA3* selection marker separating the two HRP fragments was incorporated and separated from the *FUS1* ORF by a 5X Glycine Alanine (GA) linker (**Figure 37A**). Additionally, HA tag was incorporated at the N-terminus of the HRP sequence to allow downstream HRP-Fus1p detection via SDS-PAGE and Western Blotting. Following a two-step PCR, ~300bp homology arms (H1 and H2) upstream and downstream of the *FUS1* ORF were first amplified and thereafter used to amplify and integrate the split-HRP cassette into the *FUS1* locus in *MAT***a** BY4741 cells. A colony PCR using primers specific to *FUS1* and HRP sequences confirmed the successful N-terminal *FUS1* tagging in two clones (Clone 1 and Clone 2) (**Figure 37B**). However, in order to excise the *URA3* marker and allow the reconstitution of the split HRP fragments, negative selection using 5-Fluoroorotic acid (FOA) was used ([345]). As controls, strains 4E5 containing a *URA3* gene and WT BY4741 were used as positive and negative controls, respectively. Consistently, BY4741 cells lacking the *URA3* gene grew on 5-FOA plates. On the other hand, no growth of the 4E5 strain on the 5-FOA plates was observed confirming the presence and activity of the *URA3* gene that encodes the Orotidine-5'-phosphate decarboxylase (ODCase) (**Figure S8**). Active ODCase converts 5-FOA into a toxic 5-fluorouracil compound that causes cell death ([345]). Four clones (A, B, C and D) of the *HRP-FUS1* strain were obtained following 5-FOA selection (**Figure 37B**). However, upon colony PCR, only two *HRP-FUS1* clones (C and D) were identified as correct clones in which the *URA3* selection marker had been excised and HRP spontaneously recombined (**Figure 37C**).

All in all, this approach permitted the successful N-terminal tagging of *FUS1* while preventing possible disruptions of upstream regulatory sequences such as the 5' Untranslated region (UTR) or introduction of "scars' that could otherwise result in both transcriptional and translational perturbations.

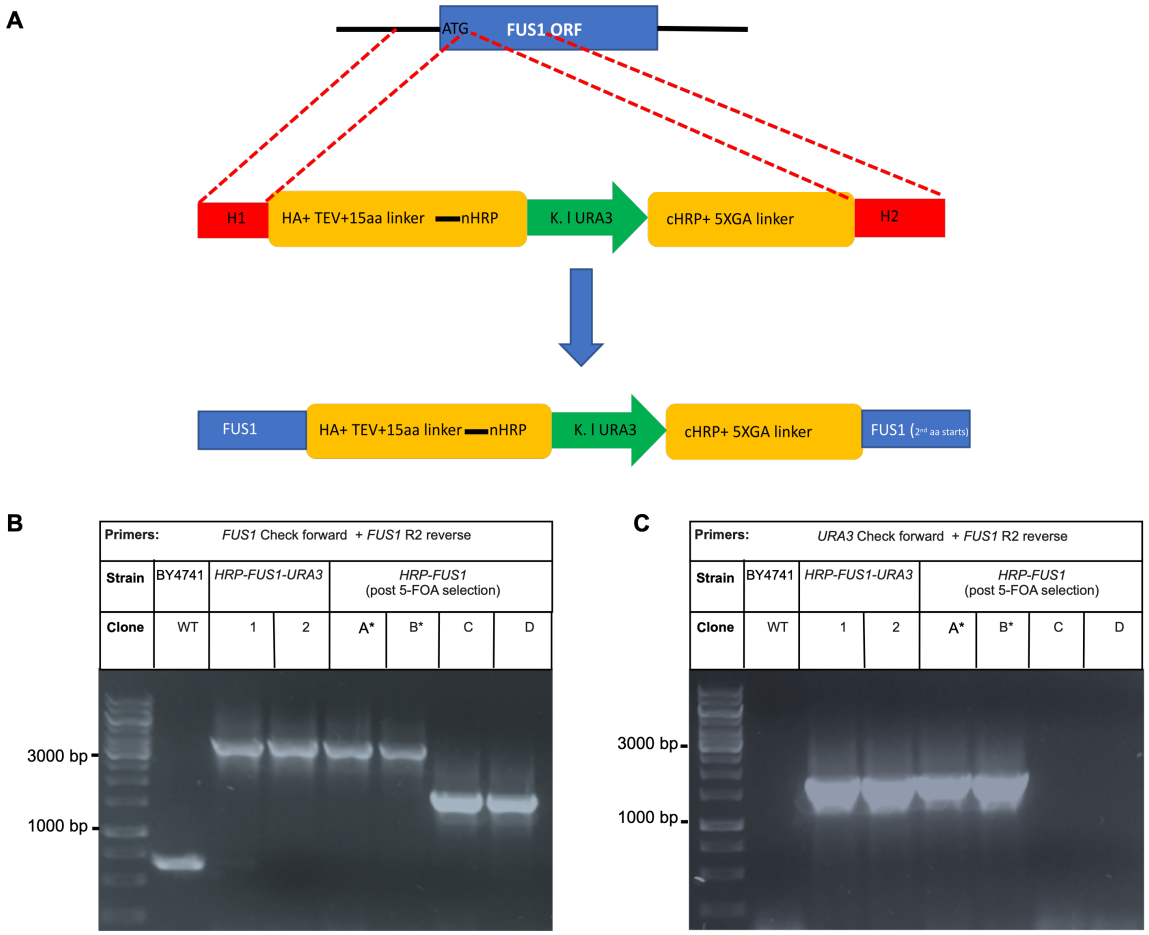

Figure 37: Scarless chromosomal N-terminal tagging of *FUS1* with yeast codon-optimized split-HRP. (**A**) Schematic of the HRP tagging design. Two homology arms H1 and H2 (depicted in red) contain 300bp upstream and downstream of the *FUS1* start codon. Using standard yeast transformation protocol, the HRP-URA3 cassette is integrated into the *FUS1* locus by homologous recombination. DNA agarose gel confirming the successful Scarless N-terminal tagging of *FUS1* with HRP. (**B**) A colony PCR using *FUS1* specific forward and reverse primers. A shift in band size upon HRP tagging is observed. *FUS1* band in WT BY4741 cells is about 661bp whereas the two clones (clone 1 and 2) contain the full HRP-*URA3* cassette of about 3652bp integrated at the *FUS1* locus. Note that following a counter-selection step using 5-FOA, two clones (clone A* and B*) contain bands similar to clones 1 and 2, indicating the presence of *URA3* marker. Clones C and D have band sizes of about 1732bp indicating *URA3* pop-out. (**C**) Colony PCR same as (**B**) except that a *URA3* specific forward primer is used in combination with a *FUS1* specific reverse primer. Note the ~1800bp band present in control clones 1 and 2, as well as clones A* and B* in which no *URA3* pop-out has taken place. WT clone as well as clones C and D have no amplification, confirming absence of the *URA3* marker.

5.2 HRP-Fus1p is correctly expressed and localized at the mating junction

In order to ascertain the functionality of the HRP-Fus1p recombinant protein, two approaches were adopted. First, its correct expression in pheromone-treated cells was confirmed via SDS-PAGE and WB using anti-HA antibody. However, in order to increase the affinity of the HA tag towards its antibody and improve the protein detection, a second HA tag (6xHA) was successfully introduced at the C-terminus generating a HA-HRP-Fus1p-6HA protein. As a positive control, WT Fus1p-6HA was generated and its pheromone-dependent expression confirmed by SDS-PAGE and WB alongside the recombinant protein. Surprisingly, vegetative cells expressing HRP-Fus1p had a slower growth rate as compared to the control cells expressing WT-Fus1p. Although the slow growth may be due to metabolic stress, it is unlikely considering HRP is under the expression of the endogenous *FUS1* promoter, and that Fus1p is exclusively expressed upon pheromone treatment. Nonetheless, both strains were grown to mid-log phase and treated with *α*-factor as previously described. As expected, both WT Fus1p-6HA and HA-HRP-Fus1p-6HA were expressed

only upon pheromone treatment, confirming the pheromone-dependent expression of Fus1p ([228], [238]) (**Figure 38A**). Of the pheromone-treated cells, the protein was detected regardless of the protein denaturation temperatures used (65 ^{o}C or 95 ^{o}C), suggesting that either denaturing condition was able to extract Fus1p from the detergent-resistant lipid rafts that associate with Fus1p at the shmoo tip ([241]). Notably, stronger bands were observed in the samples denatured at 95 ^{o}C, suggesting that higher temperatures promote better Fus1p extraction from the membrane.

Interestingly, each successful Fus1p extraction was characterized by multiple Fus1p bands. The WT Fus1p-HA appeared as two bands with a molecular weight of ~80kDa and ~110kDa (**Figure 38A**). Fus1p is an O-glycosylated membrane protein that undergoes different levels of maturation along the secretory pathway. Secreted in the ER as a precursor protein of ~57.8kDa, Fus1p is sequentially O-glycosylated during transport in the Golgi generating a fully glycosylated mature form 1 (M1) of ~80kDa that is subsequently transported to the cell surface. However, M1 supposedly undergoes additional modifications in the Golgi, generating a second mature form (M2) that migrates faster than M1, suggesting a possible proteolytic cleavage ([241], [409]). While the observed WT Fus1p-HA ~80kDa band likely corresponds to the glycosylated mature form 1 (M1), the second higher molecular weight of ~110kDa (M2*) suggests possible additional uncharacterized modifications. Indeed, the ~30kDa difference between M1 and M2 corresponds to the size of mannose oligosaccharides, thus suggesting additional Fus1p O-glycosylation ([239]). Consistently, no precursor band was observed in the WT Fus1p-HA. On the other hand, the HA-HRP-Fus1p-6HA recombinant protein appeared as three distinct bands of ~80kDa, ~110kDa and ~155kDa (**Figure 38A**). While the two lower bands were similar to those observed in the control sample, the third high molecular band (M3) corresponded to the expected size of the mature glycosylated Fus1p tagged with a 44kDa HRP protein (**Figure 38A**). Altogether, the shift in MW suggested the correct pheromone-dependent expression of the HRP-Fus1p recombinant protein.

To further confirm the correct tagging and activity of the HRP-Fus1p recombinant protein, localization studies of the recombinant protein in pheromone treated and mating cells were performed. The strain expressing *HA-HRP-FUS1* was chromosomally tagged at the C-terminus with mNeonGreen as previously described and verified by colony PCR. The localization of HA-HRP-Fus1p-mNG was subsequently assessed by confocal microscopy and WT-Fus1-GFP used as a control. Similarly to WT Fus1p, the expression of HA-HRP-Fus1p-mNG was solely pheromone dependent and the protein was enriched at the shmoo tip of polarized cells (**Figure 38B**) and (**Figure S8**). Additionally, the majority of the HA-HRP-Fus1p-mNG was localized in the vacuole suggesting constant degradation of the excess protein. In mating cells, HA-HRP-Fus1p-mNG was localized at the cell-cell contact sites, appearing as a discrete bright puncta at the mating junction of unfused cells (**Figure 38C**). Once PM fusion and cytoplasmic mixing had taken place, the recombinant protein was retained at the mating junction but later localized at the vacuole of diploid zygotes, consistent with protein degradation upon PM fusion completion.

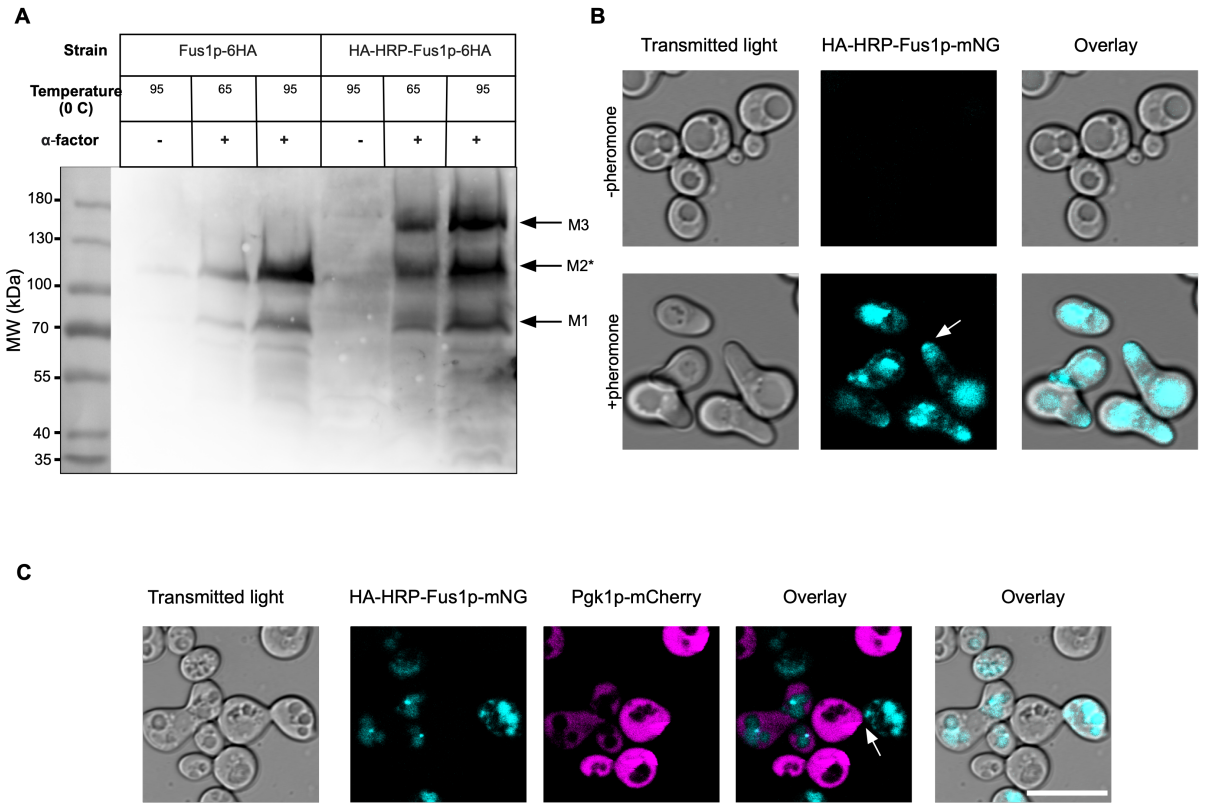

Figure 38: HA-HRP-Fus1p is correctly expressed and localized at the shmoo tip and mating junction. (**A**) Western blot analysis of HA-HRP-Fus1p-6HA expression in vegetative versus pheromone-treated cells. *MAT***a** cells expressing the control (Fus1p-6HA) or the HA-HRP-Fus1p-6HA recombinant protein were treated with 20uM α-factor for 2 h. Cells were arrested in TAF buffer and proteins extracted by TCA precipitation. Two different denaturation temperatures (65 °C and 95 °C) were used to analyze the efficacy of protein extraction. Expression of the respective Fus1p proteins was probed using anti-HA. (**B**) Expression of HA-HRP-Fus1p is pheromone-dependent. HA-HRP-Fus1p was C-terminally tagged with mNeonGreen and cells were grown to log phase in synthetic complete medium. Cultures were split into two equal portions and one portion was incubated with 20uM α-factor for 2 h. Cells were arrested in TAF buffer and imaged. HA-HRP-Fus1p-mNG is expressed only in pheromone-treated cells and localized at the shmoo tip (white arrow). (**C**) HA-HRP-Fus1p-mNG is recruited to the mating junction of an unfused mating pair (white arrow) in which cytoplasmic mixing, signified by Pgk1p-mCherry transfer, has not occurred. In fused cells, HA-HRP-Fus1p-mNG localizes at the vacuoles. Scale bar= 5 µm.

Overall, these data not only showed the correct expression and localization of HA-HRP-Fus1p recombinant protein, but also confirmed its functionality in mating conditions. Indeed, the successful fusion events observed in cells expressing HA-HRP-Fus1p-mNG confirmed the stability and suitability of this recombinant protein in subsequent PL experiments.

5.3 HA-HRP-Fus1p-6HA is correctly oriented at the PM and mediates spatial biotin labeling at the shmoo tip

Despite its localization at the shmoo tip and mating junction, a considerable proportion of HA-HRP-Fus1p was localized at the vacuole. Therefore, in order to eliminate intracellular labelling and restrict the HRP-mediated PL to the cell surface, a membrane impermeant Biotin-AEEA-Phenol substrate was used. Additionally, the presence of four structurally essential disulfide bonds in the HRP structure renders the enzyme inactive in cytosolic reduced environments. Consequently, HRP is active only when oriented to the extracellular, oxidized environment and upon activation by H_2O_2 ([405], [407]). To test whether HA-HRP-Fus1p-6HA was functional and properly localized at the

shmoo tip and that HRP was correctly oriented, vegetative and pheromone-treated cells expressing *HA-HRP-FUS1-6HA* were subjected to PL conditions using the membrane impermeant Biotin-AEEA-Phenol substrate and H_2O_2. Biotinylation was subsequently probed using Streptavidin Alexa 647 conjugate. As expected, no biotinylation was observed in vegetative cells confirming that the expression of the recombinant HA-HRP-Fus1p-6HA was pheromone-dependent (**Figure 39A**). Consistent with Fus1p localization in polarized cells, exclusive HRP-mediated labeling was observed at the tip and base of the shmoo of polarized cells (**Figure 39D**). This spatial PL is indeed consistent with Fus1p localization in which the majority of the protein is present at the shmoo tip but the protein is occasionally present at the base of the shmoo, indicative of vesicular protein trafficking to the future contact site. Furthermore, the specific labelling at the tip and base of the shmoo confirmed the correct HRP orientation and would correspond to the ~10nm contour labeling map of the reactive biotin phenoxyl radicals generated upon substrate oxidation.

Finally, to ascertain that the shmoo tip-specific PL was a result of a correctly expressed and oriented HRP, pheromone-treated cells expressing *HA-HRP-FUS1* were subjected to the same labeling conditions, except that H_2O_2 was eliminated. As expected, no biotinylation was observed in these cells despite their polarized growth, confirming that the HRP-mediated PL activity is dependent on activation by H_2O_2 (**Figure 39C**). This data therefore confirmed that the observed biotinylation was exclusively due to a functional HA-HRP-Fus1p-6HA recombinant protein that is correctly expressed and localized at the shmoo tip of polarized cells.

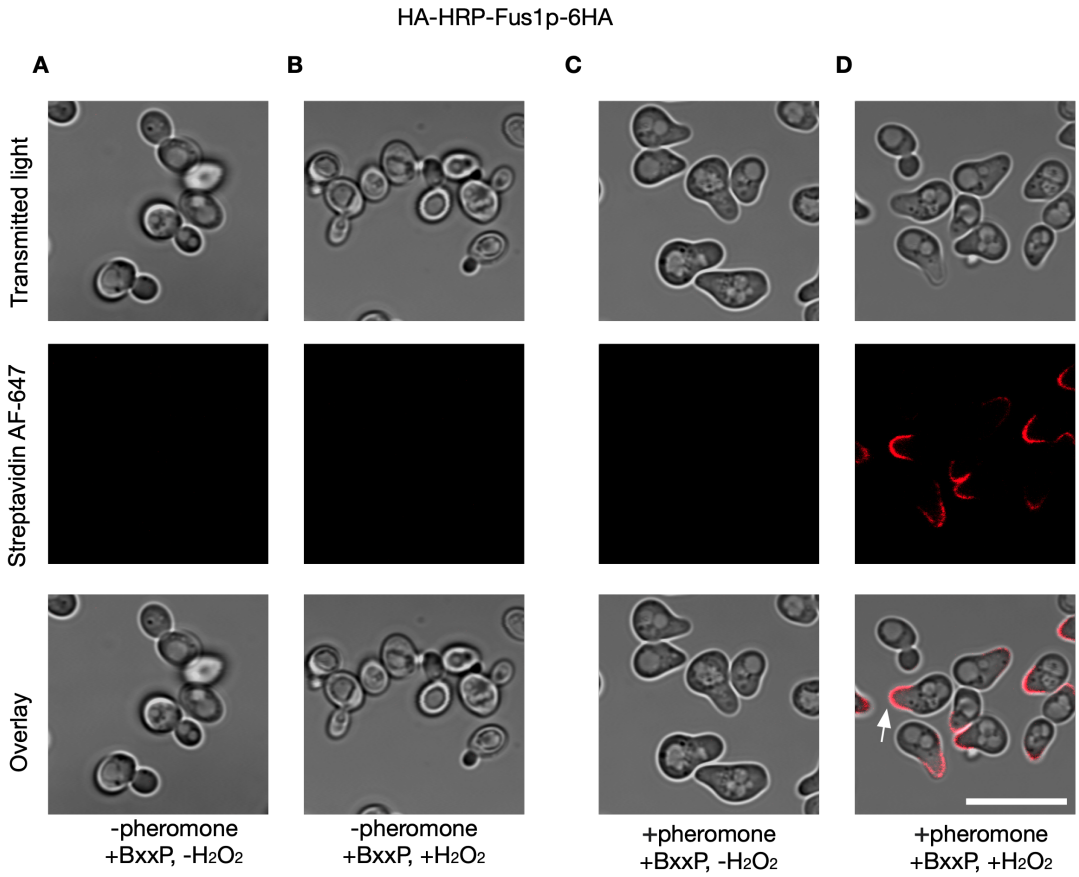

Figure 39: HA-HRP-Fus1p-6HA mediates specific HRP-mediated proximity labeling at the tip and base of the shmoo. BY4741 *MAT***a** cells expressing HA-HRP-Fus1p-6HA were grown to log phase and treated with 20 µM *α*-factor for 2 h as described before. Cells were briefly treated with 100 mM $NaCO_3$ (pH 9.4) in the presence of *α*-factor for 10 min at RT to loosen the CW. PL and biotin staining with streptavidin Alexa- 647 conjugate was then performed as described in *Methods section* before imaging. (**A** and **B**) HRP-mediated PL is dependent on Fus1p expression. No streptavidin Alexa- 647 signal is present in vegetative cells in absence or presence of H_2O_2, respectively. (**C**) HRP-mediated PL is dependent on activation by H_2O_2. No streptavidin Alexa- 647 signal is present in pheromone-treated cells in which no H_2O_2 is added. (**D**) HRP-mediated PL is dependent on activation

by H_2O_2 and presence of Fus1p. A specific streptavidin Alexa- 647 signal is observed at the shmoo tip and base of the shmoo, showing the extent of HRP-mediated labeling map. Scale bar= 5 μm.

All in all, these findings demonstrate the functionality of the HA-HRP-Fus1p recombinant protein and that HRP does not obscure Fus1p protein expression and trafficking to the shmoo tip or the mating junction. Secondly, they demonstrate the applicability of the HA-HRP-Fus1p-6HA recombinant protein in quantitative proteomic characterization of the yeast fertilization synapse. Importantly, this work is the first attempt of a specific and spatially limited HRP-mediated PL in yeast.

6 Discussion

6.1 Differential expression of membrane proteins upon pheromone treatment

Cell-cell fusion is a fundamental process in eukaryotic sexual reproduction and development. In particular, the fusion of an egg and a sperm cell during mammalian fertilization defines the creation of progeny. However, a comprehensive molecular understanding of gamete fusion and the *bona fide* fusogen(s) is still lacking. Yeast mating therefore provides a simple and genetically amenable system to study late cell fusion events. Indeed, the work in this thesis has attempted to identify the components of the yet-elusive yeast fusion machinery by: (i) exploring the PM changes as the cell transitions from a vegetative to a mating-ready state, (ii) employing a HRP-mediated proximity labeling approach to identify proteins localized at the shmoo tip or fertilization synapse.

By exploring the PM changes in both *MAT***a** and *MATα* haploid mitotic cells as they transition into a pheromone-activated mating-ready state, a comprehensive proteomic map of changes in PM composition has revealed both the pheromone upregulated and downregulated genes as well as genes that remain unchanged in both conditions (**Figure 10**). The presence of previously characterized genes such as *FUS3*, *PRM1*, *PRM3*, *FUS1* and *FIG1* in the pheromone upregulated cluster has two implications. First, it validates this approach and secondly, it demonstrates that in response to pheromone secretion, both *MAT***a** and *MATα* undergo largely conserved transcriptional changes that result in expression of similar genes. However, the presence of mating type-specific genes such as *STE2*, *STE3*, *SAG1* and *ASG7* confirms that a few mating type-specific differences such as pheromone receptors exist. Fus3p is the pheromone-responsive MAP kinase that upon pheromone secretion, activates the mating response transcription factor, Ste12p. Ste12p subsequently binds to the pheromone response elements (PREs) resulting in the downstream expression of genes necessary in the mating process [213]. Consistently, proteins such as Fus1p, Prm1p, Prm3p and Fig1p that have been implicated in mating exhibit a Ste12p-dependent transcription. Functionally, Fus1p and the cytoplasmic protein Fus2p are two proteins that mediate CW remodeling prior to PM fusion ([228], [238]). Fus1p facilitates the localization of secretory vesicles to the shmoo tip or mating junction. These vesicles presumably carry both CW remodeling enzymes as well as proteins necessary in the fusion process. An additional player and component of the polarisome, Spa2p, facilitates the clustering of these vesicles at the mating junction, an important step in increasing local protein concentration ([228]). On the other hand, Fus2p has been shown to interact with Rvs161p and Cdc42p, and together they facilitate exocytosis of these secretory vesicles to promote CW remodeling ([246]).

Once CW remodeling is completed, a short-lived and spatially-limited PM junction herein referred to as a fertilization synapse, is generated. In this junction, the two PMs are closely apposed at about 8 nm distance, with the fusion machinery possibly anchored in either or both membranes. The fusion machinery subsequently facilitates the fusion of the two membranes thus allowing cytoplasmic mixing and karyogamy. So far, a handful of proteins namely Fig1p, Prm1p, Kex2p and the proteins involved in the ergosterol biosynthesis pathway (Erg2p, Erg3p, Erg4p and Erg6p), have been implicated in PM fusion and pore formation ([271], [266], [272], [291], [294]). However, Prm1p and to a lesser extent Fig1p, are the only known proteins directly involved in the PM fusion. Consistently, bilateral matings of *prm1Δ* mutants exhibit a significant PM fusion defect with ~30-60% of *prm1Δ* mating pairs fusing successfully ([271], [266]). Of the unfused pairs, ~30% lyse while ~10% arrest as late prezygotes with cytoplasmic bubbles. The cytoplasmic bubbles are often formed when one cell with a higher osmotic pressure projects a portion of its cytoplasm into the mating partner. Importantly, both contact-dependent lysis and formation of cytoplasmic bubbles occur after the CW remodeling step is completed, corroborating a PM fusion failure ([269]). A final 5-10% arrest as late prezygotes with a flat PM interface. Previous studies by Grote *et al.,* proposed that this phenotype indicates early prezygotes in which the intervening CW material has not been degraded. Consequently, the CW material offers structural support to the rather flexible PMs, resulting in formation of a flat PM interface when the mating pairs are stained with the PM stain FM4-64 ([350]). Interestingly, such mating pairs can attempt to mate again by reorienting themselves to a different mating partner ([269]). However, a flat PM interface could also arise from cells that form very small and undetectable cytoplasmic bubbles, or cells with equal osmotic

pressure such that none is able to push its cytoplasm into the other ([269]). Indeed, this latter phenotype further supports the existence of a short-lived PM junction after CW remodeling is complete.

Bilateral matings of *fig1Δ* mutants present an ~20% fusion defect, but this defect is enhanced 4.5-fold in bilateral matings of *prm1Δfig1Δ* mutants ([271]). Additionally, bilateral matings of *fig1Δ* mutants display cytoplasmic bubbles reminiscent of the *prm1Δ* phenotypes, indicating that Fig1p exerts a PM fusion role in the mating process. Notably, the additive synthetic phenotype observed in *prm1Δfig1Δ* implies that both proteins operate at the PM fusion step on two parallel pathways. Indeed, the residual 10% fusion activity observed in these double mutants points to the existence of a third uncharacterized pathway ([271]). On the other hand, the Golgi-resident endopeptidase Kex2p has been shown to function synergistically with Prm1p, with the *MAT***a** *kex2Δprm1Δ* mutants crossed to *prm1Δ* mutants exhibiting an enhanced fusion defect when compared to bilateral *prm1Δ* matings. The synergistic effect suggests that Kex2p or its unknown substrate functions at the PM fusion step and that the Kex2p dependency is enhanced in a *prm1Δ* deletion background ([272]). Lastly, the ergosterol biosynthesis proteins (Erg2p, Erg3p, Erg4p and Erg6p) have been implicated in both upstream pheromone signaling as well as PM fusion steps. Erg6p particularly displays a *prm1Δ*-like lysis phenotype, albeit to a lesser extent. Importantly, bilateral matings of *erg3Δprm1Δ* and *erg6Δprm1Δ* mutants are highly defective in fusion and mainly accumulate as late prezygotes, consistent with the idea of at least two parallel fusion pathways ([291], [294]).

Of the newly identified proteins, Prm5p, a single-pass trans-membrane protein, displayed a pheromone-dependent expression. Consistent with other mating-responsive genes, *PRM5* contains one PRE of the sequence TGTTTCA, about 239bp upstream of the start codon. This sequence likely serves as a binding site for MAPK-Ste12p-dependent transcription activation. However, as opposed to other well characterized pheromone regulated membrane (PRM) proteins such as Prm1p and Prm4p, Prm5p was mainly localized at the vacuoles of polarized cells and mating cells ([266], [269], [410]). Despite the seldom localization at the shmoo tip and mating junction, bilateral matings of *prm5Δ* mutants presented no fusion defects and instead fuse with WT efficiency. Additionally, deletion of *PRM5* and its paralog *YNL058C* resulted in no significant mating defect suggesting that both proteins do not have a direct role in yeast mating. However, the decreased fusion efficiency observed in *prm5Δfus1Δ* mutants when compared to *fus1Δ* mutants suggests that deletion of *PRM5* enhances the *fus1Δ* fusion defect (**Figure 15**). Interestingly, Prm5p has been implicated in cell wall integrity (CWI) pathway that negatively regulates fusion ([327]).

Cellular responses to pheromone signaling involve CW remodeling and biogenesis via CW synthases and hydrolases to support polarized growth. Consistently, pheromone response events such as mating projection formation and subsequent CW remodeling result in activation of the CWI pathway ([326], [411]). This activation is executed via the CWI pathway mechano-sensors Mid2p and Wsc1p and downstream components Mkk1p and Mkk2p (MEKs), yeast Protein Kinase 1 (Pkc1p), and partly via the (MEKK) Bck1p. These components activate the CWI MAPK Mpk1p/Slt2p that facilitate the expression of CWI pathway genes involved in CW biosynthesis via the transcription factor Rlm1p ([227], [315], [320], [326], [412]). Mutants defective in the CWI pathway signaling are unable to respond to pheromone-induced morphogenesis and undergo lysis. The CWI pathway is thus necessary in maintaining cell viability ([326], [411]). Once cells establish contact at the mating junction, the intervening CW material is further remodeled to permit PM apposition and fusion while protecting the rest of the cell from lysis and death. Activation of the MAPK Slt2p during mating is therefore closely regulated to permit CW remodeling and fusion while protecting the cell from unwanted lysis. This careful remodeling at the mating junction would suggest that the CWI pathway undergoes a temporal and spatial down-regulation to permit CW removal, PM apposition and fusion ([327]). Indeed, expression of Prm5p has been previously shown to depend on the MAP kinase Slt2p, thus confirming that Prm5p is a component of the CWI pathway ([413]). However, the enhanced fusion defect observed in *prm5Δfus1Δ* mutants would suggest that Prm5p functions in another unknown pathway other than the CWI pathway, that positively regulates fusion possibly at the CW remodeling step. Consistently, *PRM5* deletion would affect fusion resulting in an additive fusion defect phenotype in *fus1Δ* mutants. Future studies to further characterize the Prm5p function in yeast mating are thus necessary.

Efforts to characterize the second pheromone upregulated protein, Prm4p, were unsuccessful and multiple attempts to chromosomally tag *PRM4* via homologous recombination failed. Nevertheless, a recent study implicated Prm4p in mating as demonstrated by a reduced mating efficiency. Intriguingly, Prm4p expression during pheromone treatment is dependent on Ecm22p and Upc2p transcription factors as opposed to Ste12p ([410]). However, its exact role in mating remains to be determined. While no further characterization was performed on genes that showed no specific pheromone regulation such as *YHR097C*, *YJL049W*, *YNR066C*, *YNR065C* and *YNL208W*, characterization of pheromone upregulated genes such as *YCR043C*, *CHS1*, *CHS3*, *TOS1*, *SCW10* and *YIL108W* revealed that, despite their apparent upregulation, respective gene deletion mutants fused with efficiencies comparable to the WT (Angela Hagemeier, personal communication). Nevertheless, their pheromone-dependent expression would suggest that they are indirect players of the mating pathway or that their functions are overridden likely through genetic redundancy. Alternatively, they could be part of other regulatory pathways whose investigation was not within the scope of this thesis.

6.2 Eisosomal proteins are dispensable in the mating process

In contrast to the pheromone-upregulated proteins, eisosomal components were highly down-regulated and represented the down-regulated protein cluster. Eisosomes are furrow-like invaginations of the PM that co-localize with the ergosterol-rich membrane compartment of the arginine permease Can1p (MCC) ([367], [414]). They appear as stable, immobile punctate patches at the cell surface, thus representing a unique MCC/eisosome PM domain ([371], [415]). Eisosomes are composed of more than twenty proteins mainly comprising of nutrient symporters such as Tat2p, Fur4p, the *SUR7*-family proteins (Sur7p, Pun1p, Fmp45p and Ynl194cp), the tetra-spanners Nce102p, Fhn1p, peripheral membrane proteins Pil1p, Lsp1, Slm1p, Slm2p, the kinases Pkh1p and Pkh2p, the flavodoxin-like proteins Pst2p, Rfs1p and Ycp4p ([277], [367], [369], [371], [368], [416], [417]). In mature vegetative cells, cytosolic proteins Pil1p and Lsp1p constitute the major eisosomal components. There exists about 115,000 and 104,000 copies per cell of Pil1p and Lsp1p, respectively ([418]). The two proteins are structurally related proteins with about 72% sequence similarity and exhibit a patchy punctate PM localization pattern ([362]). Additionally, Pil1p and Lsp1p possess the BAR domains hence are able to bind and promote membrane curvature ([419]). Consistently, Pil1p and Lsp1 are proposed to associate with the PM on the cytoplasmic inner surfaces of the invaginations ([420], [421]). Importantly, Pil1p is required for the assembly and maintenance of eisosomes and deletion of *PIL1* results in mis-localization of Lsp1p and Sur7p ([369]).

Consistent with previous findings and the proteomics analysis, the localization experiments coupled with fluorescence intensity plots confirm that Pil1p is highly expressed in vegetative cells and is localized at the eisosomes. However, while a remarked Pil1p expression is observed in pheromone-treated cells, the protein is excluded from the shmoo tip and mating junction (**Figure 21**). This expression and localization profile is indeed consistent with the observed differential downregulation of Pil1p in pheromone-treated cells as per the proteomics analysis. Additionally, it would imply that while more copies of Pil1p may be present in vegetative cells, upon pheromone response, Pil1p is preferentially downregulated in comparison to other pheromone-upregulated proteins. Indeed, similarly to Pil1p, other eisosomal proteins such as Fhn1p, Nce102p and *SUR7*-family proteins all show a differential downregulation in pheromone-treated cells as compared to vegetative cells.

The *SUR7*-family proteins consist of Sur7p, Pun1p, Fmp45p and Ynl194cp although additional members have been suggested. All four proteins are integral membrane proteins characterized by four trans-membrane domains (TMDs) and cytoplasmic N- and C-termini. The *SUR7*-family proteins exhibit a punctate, actin-independent localization in the MCC/eisosomes ([277], [367], [371]). Sur7p, Fmp45p and Ynl194cp display a great sequence homology with approximately 27-34% sequence identity and about 42- 49% similarity. A higher sequence similarity is observed in the extracellular loops than in the intracellular portions. In particular, the three proteins possess a conserved cysteine-containing (WxxW/YxxC(7-10aa)C claudin-like motif at extracellular loop 1 (ECL1), implicating them as fungal claudin-like proteins ([277]). Notably, the three proteins have been implicated in sphingolipid synthesis and to a lesser extent, sporulation ([277]). While Sur7p

was readily expressed in both vegetative and pheromone-treated cells, Fmp45p and Ynl194cp were rarely expressed and when present, their expression was not pheromone-dependent. This differential expression is likely due to the fact that the three proteins portray different expression patterns: Sur7p is constitutively expressed during late G2/M phase, Fmp45p is expressed during pseudo-hyphal growth or osmotic shock while Ynl194cp is expressed during anaerobic metabolism as well as osmotic shock conditions ([277], [422], [423]). Importantly, all three proteins were excluded from the shmoo tip (**Figure 18**).

About 17,000 copies of Sur7p exist per cell and are homogenously distributed in roughly 40 patches of eisosomes. Sur7p is proposed to occupy the upper edges of the eisosomal invaginations where it forms a ring around the perimeter of each furrow ([414], [418]). Interestingly, the Sur7p-containing immobile patches are absent in small buds and bud tips of mature cells ([277]). While this could be an indication of delayed eisosomal assembly, Sur7p localization has been correlated with the presence of mature CW, indicating that its punctate localization is likely dependent on CW interactions that are mediated by Sur7p extracellular domains ([277]). This would therefore explain its differential exclusion from the shmoo tip and in mating junctions where CW thinning and degradation occurs ([228]). While this hypothesis may apply to Fmp45p and Ynl194cp, the fact that complete PM fractions were used in the proteomics analysis suggests a general pheromone-dependent down-regulation of eisosomal genes possibly due to genetic reprogramming in favor of genes necessary in the mating process. Consistently, bilateral matings of *pil1Δ* mutants fused with WT efficiency, confirming that eisosome disassembly does not affect PM fusion.

6.3 Pun1p: An eisosomal protein with a putative function in yeast mating

Similarly to other *SUR7*-family proteins, Pun1p was constitutively expressed in vegetative cells and exhibited a punctate PM localization. However, upon pheromone treatment, there was a remarked increase in Pun1p expression with Pun1p localizing at the shmoo tip and mating junction (**Figure 16**). Its eisosomal localization in vegetative cells is consistent with previous studies whereby Pun1p co-localizes with Sur7p, albeit with lower expression levels (1660 copies per cell) ([371], [418]). On the other hand, the differential upregulation of Pun1p expression upon pheromone treatment would likely be as a result of structural and functional differences between Pun1p and the other *SUR7*-family proteins. Firstly, despite the generally conserved overall protein structure, Pun1p displays a low sequence identity of ~20% identity to the other *SUR7*-family proteins ([278]). In particular, in the extracellular loop 1 (ECL1), Pun1p contains the exact, highly conserved cysteine-containing GLWxxC(8-10aa)C claudin motif present in eukaryotic Claudin family proteins ([274], [278]). Secondly, Pun1p is functionally different from other *SUR7*-family proteins. While Sur7p, Fmp45 and Ynl194c have been implicated in sporulation and sphingolipid metabolism, Pun1p is proposedly involved in the CWI integrity pathway ([277], [424]). Interestingly, Pun1p has also been implicated in promoting pseudo-hyphal growth during nitrogen starvation conditions ([365]). During nitrogen-limited conditions, yeast cells activate an intrinsic stress response that is mainly characterized by pseudo-hyphal growth ([365]). Cells are reportedly delayed in G2/M phase with a corresponding increase in polarized growth, thickened CW and cellular attachment following cell division ([425]). The polarized growth and increased cAMP levels are characterized by cell growth into the agar likely in search for nutrients, a phenomenon referred to as invasive growth. Under these conditions, *PUN1* transcription via the activity of the Kss1p MAP kinase is enhanced and the protein localized to the cell periphery. Consistently, *pun1Δ* deletion mutants exhibit reduced filamentation, cell growth and cell-cell adhesion, all of which can be rescued upon *PUN1* overexpression ([365]). Nonetheless, no Pun1p role in yeast mating has been reported.

Several pieces of evidence suggest that Pun1p could be playing a role in yeast mating. First, contrary to the punctate-like basal expression in vegetative cells, Pun1p was highly expressed upon pheromone treatment and was homogenously localized along the PM including the shmoo tip (**Figure 16**). Consistent with the pheromone regulation, *PUN1* contains two PREs upstream of its coding sequence, hence placing *PUN1* under the activity and regulation of Ste12p transcription factor ([424]). Secondly, due to shared components of the MAPK pathway between the mating program and the pseudo-hyphal growth program, pheromone upregulation of genes involved in pseudo-hyphal growth has previously been reported ([273]). Conversely, Pun1p was localized at the mating junction prior to CW remodeling and retained at the junction during PM fusion and pore

opening, suggesting its putative function in the mating program. Consistently, Pun1p was occasionally localized in PM actin-independent micro-fingers generated prior to PM fusion in which one cell pushes its cytoplasm into the mating partner (**Figure 25**) ([269]). This further indicates that Pun1p is present at the mating junction during early PM fusion events. Once PM fusion and cytoplasmic mixing had taken place, Pun1p was preferentially localized at the neck of the mating pair after which it was translocated to the vacuole for degradation upon fusion completion (**Figure S1**). Finally, the differential Pun1p localization was corroborated by co-localization studies with Sur7p and Pil1p. In pheromone treated and mating cells, Sur7p and Pil1p retained their puncta-like localization and were excluded from the mating junction, while Pun1p was homogenously distributed along the PM and localized at the mating junction (**Figure 20**).

Regarding the question of Pun1p function in mating, a closer look at Pun1p protein sequence and topology reveals that Pun1p closely resembles mammalian tight junction claudins similar to the previously characterized claudin-like proteins Fig1p and *S. pombe* Dni1 and Dni2 proteins. Interestingly, both Fig1p and the Dni proteins have been implicated in fusion ([273], [276], [279]). Consistently, Pun1p demonstrated a Fig1p-like localization pattern and the two proteins co-localized at the mating junction, suggesting possible functional similarities (**Figure 25**). However, whereas bilateral matings of *fig1Δ* mutants result in a ~20% fusion defect, bilateral matings of *pun1Δ* mutants fuse with WT efficiencies and portray no fusion defects. Furthermore, deletion of *PUN1* in *fig1Δ* mutants results in no additive phenotype suggesting that either; (i) Pun1p does not play a Fig1p-like role in yeast mating despite their structural similarities and a similar localization profile, (ii) Pun1p function in *pun1Δfig1Δ* mutants is indirect due to functional redundancy from the Pun1p putative paralogs that otherwise obscure the true *pun1Δ* phenotype. However, the fact that the bilateral matings of *pun1Δfig1Δsur7Δfmp45Δynl194cΔ* quintuple mutants fuse similarly to *fig1Δ* mutants confirms that no synthetic additive phenotype results from deletion of *PUN1* and its paralogs (**Figure 26**). It is therefore likely that Pun1p functions in a Fig1p-independent pathway.

6.4 Pun1p negatively regulates PM fusion during yeast mating

Despite the absence of a phenotype upon *PUN1* gene deletion in a *fig1Δ* background, the pheromone-dependent expression and localization of Pun1p at the mating junction still hinted a putative Pun1p function in yeast mating and prompted the need to address whether Pun1p functions in alternative fusion pathways. Interestingly, bilateral matings of *prm1Δpun1Δ* mutants fused with a slightly higher but significant fusion efficiency than *prm1Δ* mutants (**Figure 27**). This behavior was not observed in *fus1Δ*, *fus2Δ* or *fus1Δfus2Δ* mutants, suggesting that Pun1p likely functions at the PM fusion step.

Further validating this hypothesis is that firstly, overexpression of *PUN1* in *prm1Δ* mutants results in a significant, dosage-dependent suppression of fusion and a corresponding enhancement of the *prm1Δ* fusion defect. The highest activity is observed when *PUN1* is expressed from a high copy 2μ plasmid under the activity of the constitutive *ADH1* promoter (**Figure 29**). Interestingly, *PUN1* overexpression from a low-copy centromeric plasmid under the endogenous *PUN1* promoter, in which only one or two copies of *PUN1* exist per cell, still suppresses fusion in *prm1Δ* mutants, confirming the Pun1p fusion inhibition activity. Secondly, Pun1p fusion inhibition activity increases with an increasing concentration of Pun1p molecules across the mating junction suggesting a co-operative *trans* interaction of Pun1p molecules across the mating junction. Thirdly, overexpression of *SUR7,* a putative *PUN1* paralog, exerts an opposing fusion enhancement effect in *prm1Δ* deletion mutants (**Figure 29**). Sur7p was initially identified as a multi-copy suppressor of the *rvs161Δ* and *rvs167Δ* phenotypes such as growth and cytoskeletal organization defects. Further studies implicated Sur7p in sporulation and PM organization ([254], [277]). The fact that Rvs161p has been shown to functionally interact with Fus2p and Cdc42p to facilitate vesicle exocytosis during CW remodeling renders the Sur7p suppression activity in *prm1Δ* mutants less surprising. However, it can only be speculated that Sur7p possibly regulates PM reorganization to conditions that favor fusion in a *prm1Δ* background. Finally, unilateral expression of Pun1p in *prm1Δ* mutants results in a slight decrease in Pun1p fusion inhibition activity that cannot be supplemented by *SUR7* overexpression on the opposite mating partner, thus supporting the hypothesis that *SUR7* functions differently to *PUN1*. Nevertheless, the unilateral inhibitory activity, albeit small, implies that Pun1p

can function by forming heterotypic *trans*-interactions with other unknown components. Alternatively, though unlikely, the unilateral activity would suggest a scenario whereby Pun1p is able to span across both membranes and exert its inhibitory function. A similar hypothesis has been drawn for Prm1p and its ability to unilaterally stabilize the fusion machinery during PM fusion ([269]).

6.5 Pun1p is structurally and functionally related to mammalian claudins

Claudins are key structural components of mammalian tight junctions (TJs) that function as paracellular barriers at the surface of epithelial and endothelial cells ([281]). The Claudin family is comprised of ~23kDa tetra-span proteins with four TMDs, two extracellular loops (ECL1 and ECL2) and cytoplasmic N and C-termini. There exists about 27 members of the Claudin family and are all generally characterized by a short N-terminus (~7 residues) and a longer, flexible C-terminus (21-63 residues) that contains a PDZ binding domain ([389]). This PDZ binding domain is essential in mediating claudin interactions with other cytosolic scaffold proteins such as Zona Occludens (ZO-1 and ZO-3), signaling factors and the cytoskeleton ([389], [426], [427]). Recent structural studies have revealed that claudins adopt a general left-handed model when embedded in the lipid bilayer, with the two ECLs folding into 5 anti-parallel β-strands that together form an extracellular β-sheet structure ([376], [377]). In claudin-15, interactions between extracellular helix (ECH) Methionine (Met_{68}) and the hydrophobic pocket formed by residues Phenylalanine (Phe_{146}, Phe_{147}) and Leucine (Leu_{158}) on the exposed extracellular portion of the long TMD3, facilitate side-by-side (*cis*) electrostatic interactions between claudin monomers, a process generally referred to as oligomerization (**Figure 40**) ([377]). The claudin ECL1 is longer (~52 residues) than ECL2 (16-33 residues) and harbors both the consensus cysteine-containing GLWxxC(8-10aa)C claudin motif, the variable region 1 (V1) and selective charged residues necessary in pore-forming claudins. The shorter ECL2 harbors the variable region 2 (V2) and is thought to contribute to the overall arrangement of the β-sheet structure ([377]). The proper arrangement and co-operative activity of the two extracellular loops results in formation of homotypic and heterotypic intercellular *trans*-interactions, necessary in forming either tight or selective barriers with paracellular permeability properties across the junction ([428], [429], [430]). Indeed, selective charged residues in ECL1 mediate the paracellular permeability of pore-forming claudins ([390], [431], [432], [433], [434]).

Notably, the consensus GLWxxC(8-10aa)C claudin motif is necessary in stabilizing the ECL fold. This stability is critical in overall protein expression, trafficking to the cell surface and function. Consistently, mutations in the conserved residues result in reduced pore function of claudin-2 as well as reduced barrier properties of claudin-1 and claudin-5 ([388], [390]). In addition to stabilizing the ECL fold, the conserved residues of the claudin motif have been implicated in mediating both homotypic and heterotypic side-by-side (*cis*) and head-to-head (*trans*) interactions that facilitate polymerization or barrier and pore formation, respectively ([429]). In claudin-1, mutating individual conserved residues of the claudin motif to alanine does not affect protein expression and transport to the cell surface. These mutants are capable of undergoing polymerization and form both homotypic and heterotypic *cis*-interactions within the membrane. However, despite their surface localization, these mutants are unable to form *trans*-interactions with ZO-1 at cell-cell contacts, resulting in reduced tightness ([392]). This suggests that in claudin-1, the individual claudin motif residues are not necessary in cell membrane trafficking but are rather required in mediating cell surface *trans*-interactions that favor overall protein assembly and arrangement at cell-cell contacts ([392]). Overall, claudin interactions and oligomerization result in the formation of strand-like structures along parallel TJs strands. Their interactions with other tight junction proteins such as Marvel domain-containing family (occludin, Marvel D3 and tricellulin) and the JAM IgG family further reinforces the TJ barrier properties ([389], [426], [427]).

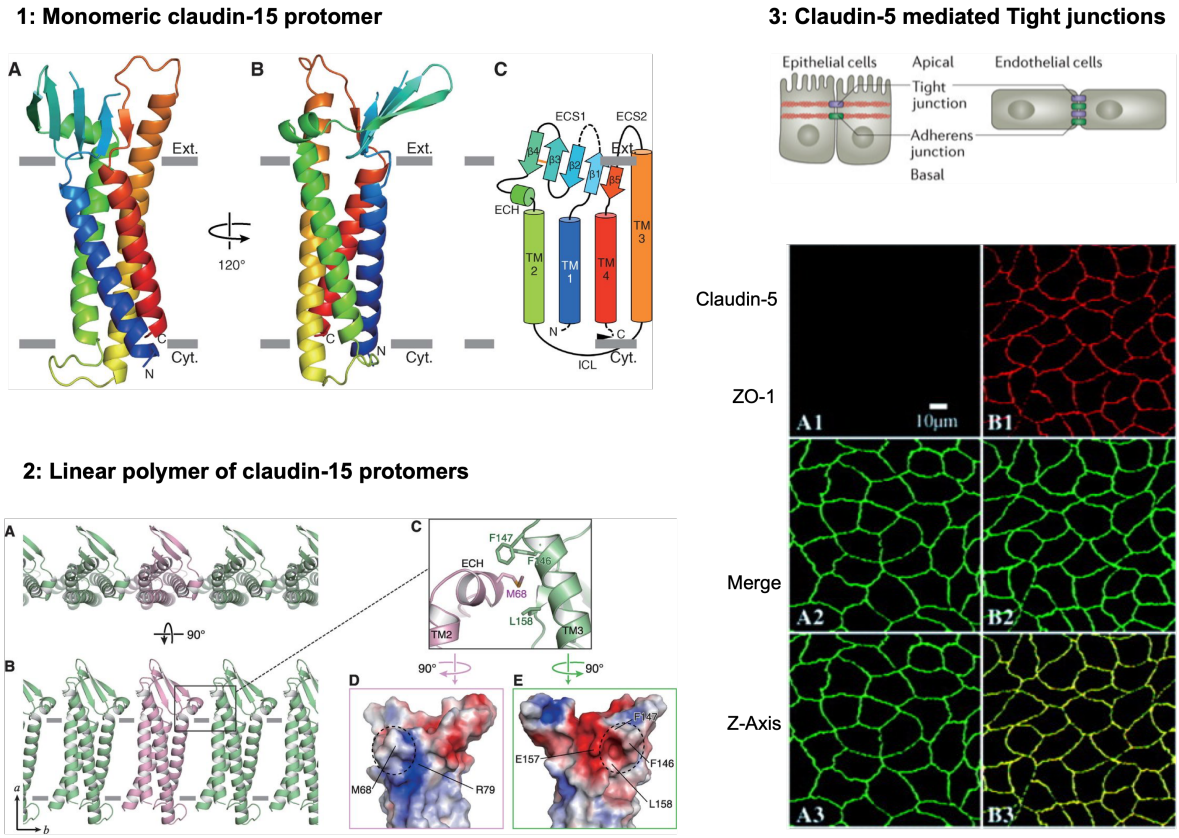

Figure 40: Mammalian claudins adopt a general left-handed model when embedded in the lipid bilayer and co-localize with Zona Occludens (ZO) at the tight junctions. (**1**) Ribbon representation of the claudin-15 crystal structure. The protein contains four transmembrane domains (TMDs) and two ECLs that fold into 5 anti-parallel β-strands, that together form an extracellular β-sheet structure. Grey bars depict boundaries of the extracellular and cytoplasmic leaflets of the bilayer. (**2**) Oligomerization of claudin-15 protomers. Interactions between extracellular helix (ECH) Methionine (Met_{68}) of one protomer (pink) and the hydrophobic pocket formed by residues Phenylalanine (Phe_{146}, Phe_{147}) and Leucine (Leu_{158}) on the exposed extracellular portion of TMD3 of a second protomer (green), facilitate side-by-side electrostatic interactions between claudin monomers to form linear polymers. (**3**) Tight junctions are apically located in epithelial cells but are intermixed with Adheren junctions in endothelial cells. Claudin-5 co-localizes with Zona Occludens (ZO-1) in epithelial cells. Figures adopted from ([377], [390], [435]).

Indeed, several indicators from this study suggest that Pun1p is an ancient fungal claudin and that structural and functional similarities between Pun1p and mammalian claudins exist. First, Pun1p is a tetra-span membrane protein with 4 TMDs and cytoplasmic N- and C-termini. Similarly to claudins, Pun1p has a longer extracellular loop 1 (ECL1) and portrays 100% sequence conservation of the cysteine-containing GLWxxC(8-10aa)C claudin motif (**Figure 23**). Secondly, Phyr2 structural modelling predictions show that Pun1p adopts a left-handed model and aligns with mammalian claudin-3 and claudin-15 with >90% confidence. However, the Pun1p β-sheet structure contains two additional β-strands in ECL1 making a total of seven β-strands. This is likely due to the fact that the Pun1p ECL1 consists of 116 residues as compared to the ~52 residues found in claudins, and that Pun1p is a larger protein (29.4kDa) than most claudins (23kDa). Thirdly, Pun1p can self-interact and form higher order oligomers that are possibly necessary for its function ([364]). Finally, similarly to claudins, adequate evidence from this thesis shows that the conserved residues of the Pun1p claudin motif are critical in mediating proper Pun1p targeting and function.

To begin with, mutating the single cysteine residues either individually (C79S or C90S) or together (C79SC90S) does not affect Pun1p expression and ability to oligomerize. Similarly to WT Pun1p, all cysteine mutants were properly expressed as monomeric proteins of ~30kDa and formed additional higher order oligomers. Furthermore, all Pun1p cysteine mutants localized correctly at the cell surface (**Figure 34**). This suggests that; (i) mutating the conserved cysteine residues does

not affect protein folding and by proxy ECL fold, and (ii) that these residues do not mediate Pun1p *cis*-interactions necessary for its oligomerization. Similarly to claudin-3 and claudin-15, it is likely that the Pun1p ECH-TMD3 interactions are responsible for *cis*-interactions ([377]). Secondly, all the Pun1p cysteine mutants functioned similarly to the WT protein. In claudin-1, single mutants of the conserved cysteine residues (C54A or C64A) are correctly expressed and transported to the PM and do not form an intramolecular disulfide bond, suggesting that the claudin-1 conserved cysteine residues are not necessary in protein folding and transport to the cell surface. However, their inability to co-localize with ZO-1 at cell-cell contacts and impede Hepatitis-C Virus (HCV) entry suggests that the claudin-1 conserved cysteine residues are important in overall protein function ([392]). Similarly in claudin-5, mutating the conserved cysteine residues (C54S or C64S) does not affect protein expression and localization at the cell surface and the mutant proteins are able to co-localize with ZO-1. Furthermore, the two cysteines do not form an intramolecular disulfide-bond. However, in comparison to WT claudin-5 protein, the respective mutants have reduced barrier activity with C64S exhibiting both reduced barrier activity and a corresponding increase in monosaccharide flux ([390]). Interestingly, the claudin-2 conserved cysteine residues form an intramolecular disulfide bond necessary for its pore function. Mutating these residues therefore affects the protein's pore function although the mutants are still capable of forming dimers and are localized at the cell surface ([388]).

It is unclear whether the two Pun1p cysteine residues form an intramolecular disulfide bond or exist as free thiol groups. Nonetheless, the ability of the Pun1p single cysteine mutants to function similarly to WT Pun1p implies that the two cysteines do not form an intramolecular disulfide bond. Alternatively, if present, its loss upon mutating the cysteine residues does not affect the overall protein function. Indeed, the Pun1p double C79SC90S mutant is properly localized at the cell surface and functions similarly to WT-Pun1p. Notably, Pun1p ECL1 contains two extra cysteine residues (C_{40} and C_{143}) that could compensate for the loss of one conserved cysteine residue in single cysteine mutants or form a novel C_{40}-C_{143} intramolecular disulfide bond. However, the fact that the fusion inhibition activity of the asymmetrical matings (C79S x C90S and vice versa) was similar to that of symmetrical matings (C79S x C79S or C90S x C90S) rules out this possibility. Additionally, mating crosses of the Pun1p double C79SC90S mutant with WT-Pun1p displayed a similar fusion inhibition activity as WT-Pun1p, further suggesting that formation of an intramolecular disulfide bond is not necessary in Pun1p function.

Thirdly, bilateral expression of *PUN1* in *prm1Δ* mutants results in enhanced fusion inhibition activity when compared to unilateral *PUN1* expression (**Figure 33**). This fusion inhibition activity increases with increasing Pun1p concentration across the mating junction, implying that increased *cis*- and *trans*-interactions between Pun1p molecules result in increased protein activity. The ability of all Pun1p cysteine mutants to function similarly to WT Pun1p or even lower (as is the case for C90S) when bilaterally expressed thus suggests that the conserved cysteine residues do not mediate *trans*-interactions. It is therefore likely that unknown residues in the extracellular β-sheet structure facilitate the head-to-head *trans*- interactions. Indeed claudin residues in the extracellular loops but outside the conserved claudin motif have been proposed to mediate *trans*- interactions ([376], [430]).

Surprisingly, mutating the Pun1p GLW residues to triple alanine (AAA) resulted in protein mis-localization into the cortical ER and other organelles including the nuclear envelope (**Figure 35**). Nevertheless, a considerable amount of the mutant protein was localized at the mating junction of most mating pairs. Furthermore, the Pun1p AAA mutant was correctly expressed as a monomeric protein and formed higher order oligomers, suggesting that the GLW residues do not mediate *cis*-interactions and subsequent oligomerization. Indeed, a similar observation has been reported in claudin-2 whereby mutating the claudin-2 GLW residues to AAA results in improper claudin-2 localization into intracellular vesicles. Consequently, claudin-2 fails to co-localize with ZO-1 at cell-cell contacts. However, the mutant claudin-2 is capable of forming dimers, suggesting that the claudin-2 dimer-forming ability is not dependent on surface localization but is instead mediated by the transmembrane domains ([393]). In claudin-15, these three hydrophobic residues are located close to the lipid bilayer hence presumed to offer a hydrophobic anchor for the extracellular β-sheet domain on the lipid bilayer ([377]). It is therefore likely that the Pun1p GLW residues are necessary in mediating a proper Pun1p fold and transport to the PM. Disruption of this hydrophobicity in Pun1p

would therefore possibly affect the overall protein fold resulting in protein retention in the cortical ER or mis-localization to other organelles.

Despite the mislocalization, a considerable amount of the Pun1p AAA mutant was localized at the mating junction in many mating pairs. Additionally, Pun1p AAA mutant functioned similarly to WT Pun1p suggesting that the protein is still functional. The fact that some protein is trafficked to the cell surface implies that the GLW residues are important but not rate-limiting in the trafficking process. The possibility that the presence of the cysteine residues in the Pun1p AAA mutant contributes to its occasional localization at the mating junction and by proxy function is unlikely because the Pun1p double C79SC90S mutant localizes at the mating junction similarly to WT Pun1p. Alternatively, the general protein fold in the Pun1p AAA mutant is not completely affected and the partial presence of the conserved residues would compensate for lack of the other. As a result, the protein can localize at the junction, albeit lower levels than WT Pun1p, and form interactions that favor activity hence restoring the protein's function. A more likely possibility is that the two additional β-strands in Pun1p ECL1 would offer a compensatory structural support to the GLW mutants therefore maintaining the protein functionality. Nevertheless, it seems plausible that sufficient Pun1p AAA molecules are trafficked to the mating junction and exert the inhibitory activity, albeit less efficiently than the WT Pun1p.

Similar observations have been made in the *S. pombe* claudin-like proteins Dni1p and Dni2p ([276]). Mutating the single conserved cysteine residues in Dni1p (C58S, C68S, C75S) does not affect protein expression and localization at the membrane fusion domain (MFD), and the single cysteine mutants function similarly to WT Dni1p. Interestingly, mutating two or all three cysteine residues in combination affects protein localization at the MFD, and the protein is mis-localized to the ER ([276]). The triple cysteine mutant exhibits the least MFD localization, suggesting putative intramolecular interactions between the cysteine residues. Even though all mutants are expressed similarly to the WT protein, the reduced Dni1p MFD localization consequently results in reduced protein function. On the contrary, single cysteine mutants of Dni2p exhibit protein mis-localization to the ER and reduced protein function, but no effect in protein expression relative to WT Dni2p is observed. It is therefore apparent that in *S. pombe*, the cysteine residues are critical in protein folding and localization at the MFD ([276]). All in all, while these findings demonstrate how different conserved residues exert different functions across the fungal claudin-like proteins, a general reduction in protein localization and concentration at the mating junction would contribute to reduced protein function.

Interestingly, mutating all the conserved residues of the Pun1p claudin motif (AAA+C79SC90S) affects both the protein expression, transport to the cell surface and function. Indeed, the Pun1p AAA+C79SC90S mutant was mis-localized to the cortical ER and other organelles, although about half the mating pairs exhibited Pun1p AAA+C79SC90S mutant localization at the PM and mating junction (**Figure 35**). Similarly to the Pun1p AAA mutant, the lack of the GLW residues would explain this mis-localization. However, the fact that some mutant protein was localized at the PM and mating junction would imply that, additional Pun1p residues or segments such as the extra ECL1 β-strands likely contribute to the general protein trafficking along the secretory pathway. Additionally, no significant difference in protein expression was observed between the Pun1p AAA+C79SC90S mutant, the WT Pun1p as well as all other mutants. The Pun1p AAA+C79SC90S mutant formed higher-order oligomers further indicating that lateral *cis*-interactions are mediated by residues outside of the claudin motif. Notably, the presence of higher-order oligomers would also suggest that oligomerization likely takes place in the ER as opposed to the cell surface. Indeed, a similar observation has been made in the *S. pombe* claudin-like proteins Dni1p and Dni2p ([276]).

Conversely to other Pun1p mutants, the Pun1p AAA+C79SC90S mutant undergoes an unknown post-translational modification that results in the formation of a monomeric protein with a slightly higher MW. The modified monomeric protein appears as double bands when analyzed by Western blotting. The absence of this modification in the Pun1p AAA or the double C79SC90S mutants suggests that it is an effect arising from a combination of both mutations. A similar modification has been reported in claudin-2 whereby mutating all the conserved cysteine residues (C54SC64S or C54AC64A) leads to the formation of multiple higher molecular weight bands that are absent in individual cysteine mutants ([388]). While the ER-based N-linked glycosylation is associated with protein fold, intracellular trafficking, stability and function, preliminary data suggests that this

modification is not a N-linked glycosylation. The presence of many serine and threonine residues in the first ECL1 of Pun1p would hint a possible O-linked glycosylation ([436], [437]). Alternatively, other modifications such as phosphorylation, ubiquitylation or formation of cleavage products cannot be overruled. However, in the latter, a modification would still be required before protein cleavage and formation of a second lower band occurs. Determining the nature of this modification may therefore help explain the lack of function in this mutant.

Finally, WT Pun1p can exert both a unilateral and bilateral fusion inhibition activity (**Figure 33**). While the unilateral *PUN1* overexpression in *prm1Δ* mutants results in an enhanced fusion inhibition activity as compared to control cells expressing the EV, bilateral *PUN1* overexpression results in an even higher fusion inhibition activity. This phenomenon suggests that WT Pun1p undergoes both homotypic and heterotypic *trans*-interactions at the mating junction. Similarly to the claudins, these interactions would result in the formation of a Pun1p-mediated PM junction-like structure that functions to inhibit PM fusion especially in a fusion-compromised background such as *prm1Δ*. Notably, the homotypic *trans*-interactions are likely favored over the heterotypic interactions resulting in a higher protein activity. Indeed, a similar observation has been reported for claudin-2 whereby homotypic interactions are favored over heterotypic ones ([388]). However, mating crosses between Pun1p AAA+C79SC90S mutant and WT Pun1p fuse similarly to the control cells (**Figure 34**), suggesting that the Pun1p AAA+C79SC90S mutant cannot compensate for the Pun1p unilateral fusion inhibition activity. The lack of Pun1p unilateral activity supports the possibility that both WT Pun1p and the Pun1p AAA+C79SC90S mutant can form homotypic *trans*-interactions. However, the modification on the Pun1p AAA+C79SC90S mutant would negatively affect the homotypic *trans*-interactions, resulting in the formation of a leaky Pun1p-mediated PM junction-like structure that fails to inhibit PM fusion and cytoplasmic content mixing.

Importantly, cell pairing in *prm1Δ* mutants expressing WT Pun1p as well as the respective Pun1p mutants remains unaffected suggesting that Pun1p does not affect upstream events of pheromone signaling and polarized growth. Consequently, the rate of fusion is generally similar across all Pun1p mutants and the differences in fusion efficiency are therefore a reflection of the magnitude of the fusion inhibition activity of the respective mutants.

6.6 The Pun1p fusion inhibition activity enhances the *prm1Δ* flat PM interface phenotype

The higher Pun1p fusion inhibition activity observed in *prm1Δ* mutants as compared to *fus1Δ* mutants points to the likelihood that the Pun1p activity is mainly exerted at the PM fusion step. Prm1p, a four-pass transmembrane protein with cytoplasmic N and C-termini, directly mediates PM fusion and localizes at the mating junction. However, *prm1Δ* mutants exhibit diverse phenotypes that characterize a PM fusion defect. While about 30-60% of *prm1Δ* mating pairs fuse successfully, the rest of the mating pairs can either lyse or arrest as late prezygotes with PM-containing cytoplasmic bubbles. These often extend from one mating partner to the other depending on the direction of the osmotic gradient. Notably, the contact-dependent lysis can be rescued by Ca^{2+} supplementation in the growth medium ([271]). Furthermore, it has been reported that some unfused mating pairs seem to exit G1 arrest and start budding or reorient towards a new mating partner ([266]). This suggests that such cells either contain pre-existing CW material or can synthesize new CW material that otherwise protects them from cell death. Consistent with this hypothesis, *prm1Δ* mutants exhibit about 5-10% unfused mating pairs that contain a flat PM interface characterized by the presence of intervening CW material ([269], [271]).

To better decipher the level at which the Pun1p fusion inhibition activity is exerted, a microscopy analysis of *prm1Δ* mutants overexpressing *PUN1* revealed that the enhanced *prm1Δ* fusion defect is as a result of a corresponding increase in the number of unfused mating pairs exhibiting the flat PM interface phenotype (**Figure 30**). In comparison to control mutants expressing the EV, *prm1Δ* mutants expressing *PUN1* do not exhibit any change in the percentage of mating pairs that undergo lysis or form cytoplasmic bubbles. This suggests that the Pun1p fusion inhibition activity does not affect either of the pathways that lead to lysis or formation of cytoplasmic bubbles. Instead, the Pun1p activity would favor formation of a flat PM interface phenotype either; (i) by slowing down the activity of CW remodeling or promoting new CW material synthesis via activation of the CWI pathway, or (ii) by arresting the unfused PMs in a junction-like structure after the CW remodeling

step. Surprisingly, further characterization of these mating pairs by combining FM4-64 PM staining and Calcofluor White CW staining revealed that, while the majority of the unfused mating pairs contained an intervening CW material, *PUN1* overexpression enhanced the formation of late prezygotes with a flat PM interface and no intervening CW material (**Figure 32** and **Figure S6**). In addition, no differences in CW composition were observed between *prm1Δ* mutants expressing *PUN1* and the control cells. These findings therefore suggest that Pun1p activity is not directly exerted at the CW remodeling step, or that Pun1p does not function in the CWI pathway that promotes CW synthesis and deposition at the mating junction. Instead, Pun1p functions in a unique, novel pathway that does not lead to lysis or cytoplasmic bubble formation but rather results in stable PM apposition resembling a tight junction-like structure. Consistently, *PUN1* overexpression does not affect the lysis phenotype that is otherwise rescued when mating pairs are arrested at the CW remodeling step either via deletion of CW remodelers *FUS1* and *FUS2*, or activation of the CWI pathway ([269], [327]). Furthermore, the Pun1p fusion inhibition activity remains unaffected by Ca^{2+} supplementation, that otherwise rescues the lysis phenotype observed in *prm1Δ* mutants ([271]). Lastly, *PUN1* overexpression in *fus1Δ* mutants resulted in a less fusion inhibition activity than in *prm1Δ* mutants. Not only do these findings confirm the Pun1p fusion inhibition activity, they also suggest that Pun1p activity is likely exerted in late prezygotes that have successfully undergone CW remodeling as opposed to early prezygotes in which CW remodeling is incomplete. Indeed, most *fus1Δ* mating pairs arrest as early prezygotes with intervening CW material at the mating junction ([238]).

Interestingly, previous studies have speculated that some unfused *prm1Δ* mating pairs can arrest as prezygotes with a flat PM interface with no intervening CW material. This is especially true if the mating pair contains cytoplasmic bubbles that are too small to be detected, or both cells exhibit equal osmotic pressure such that neither cell pushes its cytoplasm against the other ([269]). While this has not been previously demonstrated, the current findings indeed suggest a similar phenomenon in which cells arrest as late prezygotes with a flat PM interface and no cytoplasmic bubbles.

6.7 Why regulate PM fusion?

So far, compelling evidence suggests that Pun1p overexpression negatively regulates fusion in *prm1Δ* mutants and to a lesser but significant extent in *fus1Δ* mutants. Additionally, deletion of *PUN1* enhances fusion in *prm1Δ* mutants, further corroborating this hypothesis. During yeast mating, PM fusion is preceded by closely apposed fusion-competent membranes with an intervening CW material. Localized CW removal and engagement of the fusion machinery results in fusion of the juxtaposed PMs. However, if no fusion occurs after CW remodeling such as in PM fusion mutants *prm1Δ* and *fig1Δ*, the cells lyse or form cytoplasmic bubbles ([271], [269]). Interestingly, lysis and fusion pore opening occur with similar kinetics, suggesting that lysis events seem to occur in mating pairs that attempt to fuse ([269]). Furthermore, the lysis phenotype is enhanced in absence of extracellular Ca^{2+}, suggesting that Ca^{2+} ions are necessary in mediating membrane repair and stability especially in absence of Prm1p ([271]). In support of lysis events occurring only after CW removal, lysis does not occur in *fus1Δ* mutants that are arrested at the CW remodeling step, and even when present in CWI pathway mutants such as *pkc1-2*, lysis can be rescued by osmotic stabilizers such as 1 M sorbitol ([271]). Notably, the contact-dependent lysis as well as fusion events observed in *prm1Δ* mutants are reportedly preceded by formation of small cytoplasmic bubbles or microfingers (<1 μm in length) that push into the opposite mating partner. Although these microfingers can grow up to a length of 5 μm to form large cytoplasmic bubbles, it is likely that cytoplasmic bubble formation is the major default pathway in delayed PM fusion ([269], [271]). Further characterization of fusion arrested *prm1Δ* mating pairs show that a few unfused mating pairs arrest as early prezygotes with a flat PM interface and intervening CW material at the mating junction ([269]). Consistently, *prm1Δ* mutants that attempt to mate with a new mating partner or exit the G1 arrest and start budding have been reported, ([266]). This suggests that such mating pairs either contain undissolved CW material or are able to synthesize new CW material before exiting the fusion process.

It is therefore plausible that in a fusion compromised background such as *prm1Δ*, Pun1p negatively regulates fusion by functioning in a novel 'corrective' pathway that results in close PM apposition

without leading to dead-end lysis or cytoplasmic bubble formation. Further supporting this observation is that the Pun1p fusion inhibition activity is not dependent on extracellular Ca^{2+} concentration that otherwise rescues the lysis phenotype in *prm1Δ* mutants (**Figure 30**) ([271]). As part of the novel 'corrective' pathway, Pun1p enhances the formation of a flat PM interface phenotype without intervening CW material. Consistent with its claudin-like structure and function, the conserved residues of the Pun1p claudin motif would mediate Pun1p localization at the cell surface and enrichment at the mating junction. At the junction, Pun1p would form homotypic and heterotypic *trans*-interactions between Pun1p molecules and other proteins. These interactions would in turn establish an intercellular protein layer or tight junction-like structure that holds the merging membranes in close apposition, herein seen as a flat PM interface without intervening CW material, while providing an anchorage for the fusion machinery. Analogous to the mammalian barrier-forming claudins, the Pun1p-mediated tight junction-like structure would act as a barrier that prevents content mixing and ensuring fusion fidelity. Unavoidably, this barrier would function as a PM fusion fine-tuning checkpoint that is mainly activated in the presence of a defective fusion machinery such as in *prm1Δ* deletion mutants. In such cases, activation of the fine-tuning checkpoint would result in either; (i) arrest of the unfused cells in a flat PM interface as seen in a few *prm1Δ* mating pairs (**Figure 32** and **Figure 41**), or (ii) downstream signaling and activation of repair mechanisms such as the CWI pathway that activates CW biosynthesis (**Figure 41**). Indeed, this would explain why the Pun1p activity is detectable in a *prm1Δ* and *fus1Δ* deletion background as opposed to the WT conditions, and the observed increase in percentage of *prm1Δ* mating pairs with a flat PM interface upon *PUN1* overexpression.

Notably, the low amount of unfused cells with a flat PM interface and no intervening CW material suggests that this is a rare intermediate stage that would result either in fusion once a Prm1p-independent fusion pathway is engaged, or revert back to a less lethal pre- CW remodeling stage. While both events result in a 'corrective' outcome, reverting back to a less lethal pre- CW remodeling stage would suggest possible CW regeneration and reorienting of the mating cells to find new mating partners or exit from G1 phase to reenter budding ([266]). While it is unclear how quickly such mating pairs would revert, it is likely that the Pun1p-mediated tight junction-like structure functions as signaling platform for downstream activation of the CWI pathway. Although Pun1p has been implicated in the CWI pathway due to its upregulation upon metal ion stress, it is unlikely that Pun1p performs a CWI role during mating. Consistently, no differences in CW composition of *prm1Δ* mutants were observed upon *PUN1* overexpression, suggesting that Pun1p does not activate the CWI pathway, an observation that does not agree with previous reports (**Figure 31**) ([364]). it is therefore conceivable that Pun1p promotes the formation of a stable tight junction-like structure that promotes downstream signaling to activate 'rescue' pathways including the CWI pathway. Indeed, mammalian tight junctions function as signaling networks that transmit information to and from the cytoskeleton and the rest of the cell via the claudins and other tight junction associated proteins ([435]).

Additionally, the rare phenotype would imply that Pun1p is part of a machinery that negatively regulates fusion, such that a more readily observed phenotype would be possible when more components of this machinery are perturbed. Consistently, only a slight but significant increase in fusion was observed when *PUN1* was deleted in *prm1Δ* mutants (**Figure 27**). Additionally, a unilateral fusion inhibition activity is observed when *PUN1* is expressed in one mating type, suggesting that other components of tight junction-like structure exist that interact with Pun1p (**Figure 33**). Indeed, additional proteins such as Ina1p, Fat3p, Dcv1p, Rim9p and Ecm7p, that show high sequence homology to Pun1p exist (**Figure S1**). While proteins such as Ina1p and its paralog Fat3p are localized to the PM although their exact function is unknown, Ecm7p has been implicated in the high affinity Ca^{2+} influx system (HACS) that is activated upon pheromone response. However, in contrast to other proteins involved in high affinity Ca^{2+} influx such as Mid1p, Cch1p and the low affinity Ca^{2+} influx system (LACS) regulator Fig1p, the *ecm7Δ* mutants fuse efficiently suggesting that Ecm7p likely performs roles other than Ca^{2+} influx. Notably, Ecm7p contains the highly conserved claudin-like motif in ECL1 suggesting that it could interact with Pun1p to regulate fusion ([438]). Future studies to determine possible Pun1p interactors will therefore shed more light on the Pun1p fusion inhibition activity.

Taken together, these data suggest that Pun1p is a component of a previously undescribed negative regulatory network that specifically operates at the PM fusion step. During mating, Pun1p

and other unknown components mediate the formation of a tight junction-like structure that acts as a fine-tuning checkpoint to ensure fusion fidelity especially in a fusion-compromised background such as *prm1Δ*. However, this model leaves many unanswered questions such as: the molecular mechanism of Pun1p as a negative regulator of PM fusion, whether Pun1p interacts with other *SUR7*-family proteins or novel proteins such as Ecm7p, and how these interactors are affected in the respective mutants. Lastly, it remains unknown whether the Pun1p-mediated tight junction-like fine-tuning checkpoint results in activation of the general CWI pathway, implicating Pun1p as a bridge between PM fusion step and the CWI pathway.

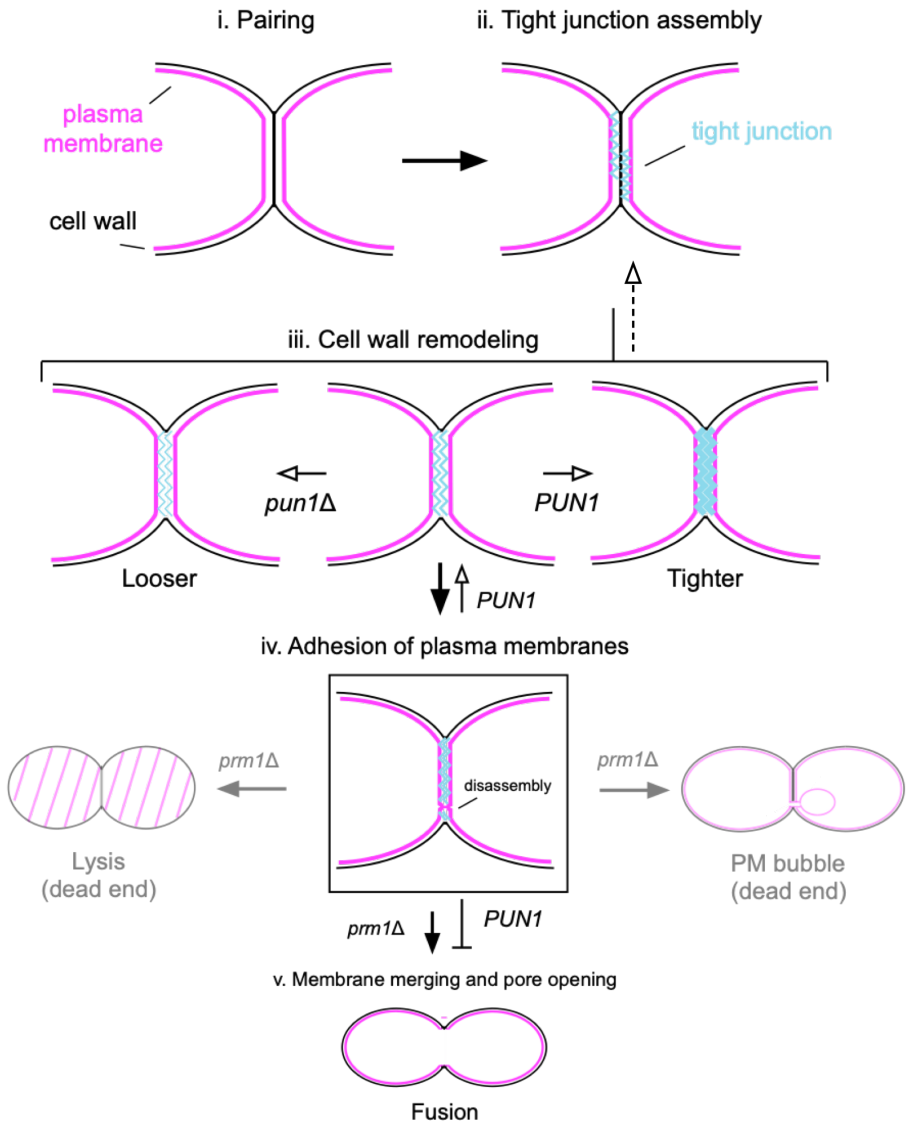

Figure 41: Proposed mechanism of Pun1p fusion inhibition activity. During mating, Pun1p is expressed and localized at the mating junction. At the junction, Pun1p forms both homotypic and heterotypic intercellular *trans*-interactions resulting in the formation of a tight junction-like structure that holds the PMs in close apposition prior to PM fusion. In presence of a functional fusion machinery such as in WT conditions, the junction structure is disassembled to facilitate PM fusion. In presence of a defective fusion machinery such as *prm1Δ* deletion mutants, the tight junction-like structure is reversibly reinforced via recruitment of additional junction molecules, generating a tighter assembly. Dotted arrow indicates the reversible CW remodeling step. The Pun1p-mediated tight junction-like structure pathway is distinct from the lysis and cytoplasmic bubble formation pathways that are activated in presence of a defective fusion machinery.

7 CONCLUDING REMARKS

Cell-cell fusion is a fundamental process in eukaryotic development. The merging of two membranes is a critical step in all cell fusion events. Yeast mating provides a genetically amenable system to understand the molecular mechanisms of membrane fusion during sexual reproduction. The work herein aimed at identifying and characterizing novel players of PM fusion during yeast mating. By employing a range of molecular approaches, Pun1p was identified as a component of the yeast fertilization synapse that negatively regulates cell fusion.

Pun1p, a *SUR7*-family protein that constitutes the MCC/ eisosome PM domain, undergoes differential regulation during yeast mating. Pun1p is highly pheromone-upregulated and localizes at the cell surface and is enriched at the shmoo tip and mating junction. Notably, Pun1p is retained at the mating junction before and after PM fusion, suggesting that it plays a role in the fusion process. Once PM fusion is complete and cytoplasmic mixing occurs, Pun1p is redistributed to the neck of the mating bridge before re-localization to the vacuoles for degradation. By employing a combination of yeast genetics tools, compelling evidence indicates that Pun1p negatively regulates PM fusion. Similarly to mammalian claudins, the conserved residues of the Pun1p extracellular claudin motif facilitate its localization at the mating junction where it possibly forms heterotypic and homotypic *trans*-interactions, resulting in the formation of a putative tight junction-like structure consisting of two closely apposed membranes. It is plausible that this junction-like structure not only anchors the fusion machinery, but also forms a barrier that prevents unwanted PM fusion especially in the presence of a compromised fusion machinery. Importantly, the Pun1p-mediated tight junction-like structure represents a novel pathway which appears to operate in the absence of a functional fusion machinery such as in *prm1Δ* mutants.

Further work is needed to ascertain Pun1p activity in other CW remodeling and PM fusion-related mutants such as *FUS1, FUS2*, *KEX2* and the ergosterol biosynthesis genes *ERG6*, *ERG4* and *ERG3*. Such studies will help clarify the role and stage of Pun1p activity. Secondly, studies to identify and characterize putative Pun1p interactors will not only reinforce the proposed hypothesis but will also reveal additional players of the yeast fusion machinery. Thirdly, this study has unveiled a new function of *S. cerevisiae* Pun1p. The question of whether Pun1p function is conserved in other fungi remains open. Nonetheless, this study provides a roadmap that can be applied in identifying Pun1p-like proteins in other fungal species and possibly in mammalian sperm-egg fusion studies. Importantly, unregulated PM fusion has been proposed as a positive regulator of cancer progression especially following viral infection ([439]). Formation of hybrid cells with metastatic functions result in cancer progression. Identification of Pun1p-like proteins or proteins with claudin-like barrier properties may prove necessary in cancer therapies.

Secondly, *ISC1*, encoding the inositol phosphosphingolipid phospholipase C protein, was identified as another novel player of PM fusion. Isc1p is pheromone upregulated and localized at the shmoo of polarized cells. Although less effort was put in characterizing this protein, preliminary findings show that *isc1Δ* mutants mate with about 80% fusion efficiency. These findings suggest that Isc1p is a putative component of the fusion machinery, possibly via the sphingolipid catabolism pathway. Future work will help shed more light on the role of sphingolipids in yeast mating.

Finally, this thesis has demonstrated the applicability of HRP-mediated proximity labeling in identifying novel components of the yeast cell fusion machinery. Using N-terminally tagged HRP-Fus1p, the recombinant protein is expressed and localized at the shmoo tip and mating junction. Notably, HRP-Fus1p mediates a specific and localized labeling at the tip and base of the shmoo. While this approach remains to be adopted in mating cells, it has sufficiently demonstrated the possibility of employing a HRP-mediated proximity labeling approach in mapping yeast extracellular or oxidized environments. Additionally, the use of the membrane-impermeant Biotin-AEEA-Phenol allows the exclusive labeling of the extracellular environment. This is the first of its kind in yeast and opens avenues for future proximity labeling studies in other fertilization systems.

8 REFERENCES

1. Aguilar, P.S., et al., *Genetic basis of cell-cell fusion mechanisms.* Trends Genet, 2013. **29**(7): p. 427-37.
2. Chen, E.H. and E.N. Olson, *Towards a molecular pathway for myoblast fusion in Drosophila.* Trends Cell Biol, 2004. **14**(8): p. 452-60.
3. Podbilewicz, J.M.H.a.B., *The hallmarks of cell-cell Fusion.* Developmental Cell, 2017. **144**: p. 4481-4495.
4. Brukman, N.G., et al., *How cells fuse.* J Cell Biol, 2019. **218**(5): p. 1436-1451.
5. L. D. Hernandez, L.R.H., T. G. Wolfsberg, and J. M. White, *Virus-cell and Cell-cell fusion.* Annu Rev. Cell. Dev. Biol, 1996. **12**: p. 627-661.
6. Südhof, R.J.a.T.C., *Membrane fusion and exocytosis.* Annu Rev Biochem, 1999. **68**: p. 863-911.
7. Kim, J.H. and E.H. Chen, *The fusogenic synapse at a glance.* J Cell Sci, 2019. **132**(18).
8. Reinhard Jahn, T.L., and Thomas C. Südhof, *Membrane Fusion.* Cell, 2003. **112**: p. 519-533.
9. Sergey L. Leikin, M.M.K., Leonid V. Chernomordik, Vladislav S. Markin And Yuri A. Chizmadzhev, *Membrane Fusion: Overcoming of the Hydration Barrier and Local Restructuring.* Journal of theoretical biology, 1987. **129**(4): p. 411-425.
10. Shemer, G., et al., *EFF-1 is sufficient to initiate and execute tissue-specific cell fusion in C. elegans.* Curr Biol, 2004. **14**(17): p. 1587-91.
11. Chernomordik, L.V. and M.M. Kozlov, *Membrane hemifusion: crossing a chasm in two leaps.* Cell, 2005. **123**(3): p. 375-82.
12. Chernomordik, L.V. and M.M. Kozlov, *Protein-lipid interplay in fusion and fission of biological membranes.* Annu Rev Biochem, 2003. **72**: p. 175-207.
13. Zaitseva, E., et al., *Class II fusion protein of alphaviruses drives membrane fusion through the same pathway as class I proteins.* J Cell Biol, 2005. **169**(1): p. 167-77.
14. Reese, C., F. Heise, and A. Mayer, *Trans-SNARE pairing can precede a hemifusion intermediate in intracellular membrane fusion.* Nature, 2005. **436**(7049): p. 410-4.
15. George W. Kemble, T.D., and Judith M. White, *Lipid-Anchored Influenza Hemagglutinin Promotes Hemifusion, Not Complete Fusion.* Cell, 1994. **76**: p. 383-391.
16. Xu, Y., et al., *Hemifusion in SNARE-mediated membrane fusion.* Nat Struct Mol Biol, 2005. **12**(5): p. 417-22.
17. Reese, C. and A. Mayer, *Transition from hemifusion to pore opening is rate limiting for vacuole membrane fusion.* J Cell Biol, 2005. **171**(6): p. 981-90.
18. Kozlov, Y.K.a.M.M., *Stalk Model of Membrane Fusion: Solution of Energy Crisis.* Biophysical Journal, 2002. **82**: p. 882-895.
19. Aditya Mittal, E.L., Leonid V. Chernomordik, and Joe Bentz, *Kinetically Differentiating Influenza Hemagglutinin Fusion and Hemifusion Machines.* Biophysical Journal, 2003. **85**: p. 1713-1724.
20. Rand, N.F.a.R.P., *The Influence of Lysolipids on the Spontaneous Curvature and Bending Elasticity of Phospholipid Membranes.* Biophys J, 2001. **81**: p. 243-254.
21. Leonid V. Chernomordik, V.A.F., Eugenia Leikina, Peter Bronk, and Joshua Zimmerberg, *The Pathway of Membrane Fusion Catalyzed by Influenza Hemagglutinin- Restriction of Lipids, Hemifusion, and Lipidic Fusion Pore Formation.* Journal of Cell Biology, 1998. **140**(6): p. 1369-1382.
22. Eric Grote, M.B., Yoshinori Ohsumi, and Peter J. Novick, *Geranylgeranylated SNAREs Are Dominant Inhibitors of Membrane Fusion.* Journal of Cell Biology, 2000. **151**(2): p. 453-465.
23. Podbilewicz, B., *Virus and cell fusion mechanisms.* Annu Rev Cell Dev Biol, 2014. **30**: p. 111-39.
24. Mi, S., et al., *Syncytin is a captive retroviral envelope protein involved in human placental morphogenesis.* Nature, 2000. **403**(6771): p. 785-9.
25. William A. Mohler, G.S., Jacob J. del Campo, Clari Valansi, Eugene Opoku-Serebuoh, Victoria Scranton, Nirit Assaf, John G. White, and Benjamin Podbilewicz, *The Type I Membrane Protein EFF-1 Is Essential for Developmental Cell Fusion.* Developmental Cell, 2002. **2**: p. 355-362.

26. Sapir, A., et al., *AFF-1, a FOS-1-regulated fusogen, mediates fusion of the anchor cell in C. elegans.* Dev Cell, 2007. **12**(5): p. 683-98.
27. Millay, D.P., et al., *Myomaker is a membrane activator of myoblast fusion and muscle formation.* Nature, 2013. **499**(7458): p. 301-5.
28. Zhang, Q., et al., *The microprotein Minion controls cell fusion and muscle formation.* Nat Commun, 2017. **8**: p. 15664.
29. Liu, Y., et al., *The conserved plant sterility gene HAP2 functions after attachment of fusogenic membranes in Chlamydomonas and Plasmodium gametes.* Genes Dev, 2008. **22**(8): p. 1051-68.
30. White, J.M., et al., *Structures and mechanisms of viral membrane fusion proteins: multiple variations on a common theme.* Crit Rev Biochem Mol Biol, 2008. **43**(3): p. 189-219.
31. Lazebnik, D.D.a.Y., *Cell-to-cell fusion as a link between viruses and cancer.* Nature, 2007. **7**: p. 968-976.
32. Kim, D.M.E.a.P.S., *Mechanisms of viral membrane fusion and its inhibition.* Annu Rev Biochem, 2001. **70**: p. 777-810.
33. Ivanovic, T., et al., *Influenza-virus membrane fusion by cooperative fold-back of stochastically induced hemagglutinin intermediates.* Elife, 2013. **2**: p. e00333.
34. Kim, Y.H., et al., *Capture and imaging of a prehairpin fusion intermediate of the paramyxovirus PIV5.* Proc Natl Acad Sci U S A, 2011. **108**(52): p. 20992-7.
35. Tsafi Danieli, S.L.P., Yoav I. Henis, and Judith M. White, *Membrane Fusion Mediated by the Influenza Virus Hemagglutinin Requires the Concerted Action of at Least Three Hemagglutinin Trimers.* Journal of Cell Biology, 1996. **133**(3): p. 559-569.
36. Per A. Bullough, F.M.H., John J. Skehelt, and Don C. Wiley, *Structure of influenza haemagglutinin at the pH of membrane fusion.* nature, 1994. **371**: p. 37-43.
37. Kim, C.M.C.a.P.S., *A Spring-Loaded Mechanism for the Conformational Change of Influenza Hemagglutinin.* Cell, 1993. **73**: p. 823-832.
38. Harris, A., et al., *Influenza virus pleiomorphy characterized by cryoelectron tomography.* Proc Natl Acad Sci U S A, 2006. **103**(50): p. 19123-7.
39. I. A. Wilson, J.J.S.D.C.W., *Structure of the haemagglutinin membrane glycoprotein of influenza virus at 3 A resolution.* Nature, 1981. **289**: p. 366-373.
40. Harrison, S.C., *Viral membrane fusion.* Nat Struct Mol Biol, 2008. **15**(7): p. 690-8.
41. Jue Chen, K.H.L., David A. Steinhauer, David J. Stevens, John J. Skehel and Don C. wiley, *Structure of the Hemagglutinin Precursor Cleavage Site, a Determinant of Influenza Pathogenicity and the Origin of the Labile Conformation.* Cell, 1998. **95**: p. 409-417.
42. Wiley, J.J.S.a.D.C., *Receptor Binding and Membrane Fusion in Virus Entry_ The Influenza Hemagglutinin.* Annu Rev Biochem, 2000. **69**: p. 531-569.
43. Skehel, D.C.W.a.J.J., *The structure and function of the Hemagglutinin membrane glycoprotein of Influenza virus.* Annu Rev Biochem, 1987. **56**: p. 365-394.
44. Jue Chen, J.J.S., and Don C. Wiley, *N- and C-terminal residues combine in the fusion-pH influenza hemagglutinin HA2 subunit to form an N cap that terminates the triple-stranded coiled coil.* Proc Natl Acad Sci U S A, 1999. **96**: p. 8967-8972.
45. Akihiko Yoshimura, K.K., Kazunori Kawasaki, Shohei Yamashina, Toyozo Maeda, and Shun-Ichi Ohnishi, *Infectious Cell Entry Mechanism of Influenza Virus.* Journal of Virology, 1982. **43**(1): p. 284-293.
46. Weber, T., et al., *Evidence for H(+)-induced insertion of influenza hemagglutinin HA2 N-terminal segment into viral membrane.* Journal of Biological Chemistry, 1994. **269**(28): p. 18353-18358.
47. Suren A.Tatulian, P.H., Gwen Baber and Lukas K.Tamm, *Influenza hemagglutinin assumes a tilted conformation during membrane fusion as determined by attenuated total reflection FTIR spectroscopy.* EMBO J, 1995. **14**(22): p. 5514-5523.
48. Tsurudome, M., et al., *Lipid interactions of the hemagglutinin HA2 NH2-terminal segment during influenza virus-induced membrane fusion.* Journal of Biological Chemistry, 1992. **267**(28): p. 20225-20232.
49. Durell, S.R., et al., *What studies of fusion peptides tell us about viral envelope glycoprotein-mediated membrane fusion (review).* Mol Membr Biol, 1997. **14**(3): p. 97-112.
50. Gruenke, J.A., et al., *New insights into the spring-loaded conformational change of influenza virus hemagglutinin.* J Virol, 2002. **76**(9): p. 4456-66.
51. Calder, L.J. and P.B. Rosenthal, *Cryomicroscopy provides structural snapshots of influenza virus membrane fusion.* Nat Struct Mol Biol, 2016. **23**(9): p. 853-8.

52. Lee, K.K., *Architecture of a nascent viral fusion pore.* EMBO J, 2010. **29**(7): p. 1299-311.
53. V. A. Frolov, A.Y.D.-B., A. V. Samsonov, and J. Zimmerberg, *Membrane Permeability Changes at Early Stages of Influenza Hemagglutinin-Mediated Fusion.* Biophys J, 2003. **85**: p. 1725-1733.
54. Chlanda, P., et al., *The hemifusion structure induced by influenza virus haemagglutinin is determined by physical properties of the target membranes.* Nat Microbiol, 2016. **1**(6): p. 16050.
55. Harrison, S.C., *Viral membrane fusion.* Virology, 2015. **479-480**: p. 498-507.
56. S. A. Wharton, R.B.B., J. J. Skehel and A. J. Hay *Role of virion M2 protein in influenza virus uncoating- specific reduction in the rate of membrane fusion between virus and liposomes by amantadine.* Journal of General Virology, 1994. **75**: p. 945-948.
57. Ofer Nussbaum, M.L., and Abraham Loyter, *Reconstitution of Functional Influenza Virus Envelopes and Fusion with Membranes and Liposomes Lacking Virus Receptors.* Journal of Virology, 1987. **61**(7): p. 2245-2252.
58. Judy White, A.H.a.M.-J.G., *Haemagglutinin of influenza virus expressed from a cloned gene promotes membrane fusion.* Nature, 1982. **300**: p. 658-659.
59. Martens, S. and H.T. McMahon, *Mechanisms of membrane fusion: disparate players and common principles.* Nat Rev Mol Cell Biol, 2008. **9**(7): p. 543-56.
60. Rizo, J. and C. Rosenmund, *Synaptic vesicle fusion.* Nat Struct Mol Biol, 2008. **15**(7): p. 665-74.
61. Jahn, R. and R.H. Scheller, *SNAREs--engines for membrane fusion.* Nat Rev Mol Cell Biol, 2006. **7**(9): p. 631-43.
62. Thomas Söllner, M.K.B., Sidney W. Whiteheart, Richard H. Scheller, and James E. Rothman, *A Protein Assembly-Disassembly Pathway In Vitro That May Correspond to Sequential Steps of Synaptic Vesicle Docking, Activation, and Fusion.* Cell, 1993. **75**: p. 409-418.
63. Rizo, J. and T.C. Sudhof, *SNAREs and Munc18 in synaptic vesicle fusion.* Nat Rev Neurosci, 2002. **3**(8): p. 641-53.
64. Scheller, R.C.L.a.R.H., *Structural Organization of the Synaptic Exocytosis Core Complex.* Neuron, 1997. **19**: p. 1087-1094.
65. Phyllis I Hanson, J.E.H.a.R.J., *Neurotransmitter release -four years of SNARE complexes.* Current Opinion in Neurobiology, 1997. **7**: p. 310-315.
66. Montecucco, C., G. Schiavo, and S. Pantano, *SNARE complexes and neuroexocytosis: how many, how close?* Trends Biochem Sci, 2005. **30**(7): p. 367-72.
67. Patrick Brennwald, B.K., Kathy Champion, Sirkka Keränen, Vytas Bankaitis, and Peter Novick, *Sec9 Is a SNAP-25-like Component of a Yeast SNARE Complex That May Be the Effector of Sec4 Function in Exocytosis.* Cell, 1994. **79**: p. 245-258.
68. Markku K. Aalto, H.R.a.S.K., *Yeast syntaxins Ssolp andSso2p belong to a family of related membrane proteins that function in vesicular transport.* EMBO J, 1993. **12**(11): p. 4095-4104.
69. Tobias H. Kloepper, C.N.K., and Dirk Fasshauer, *An Elaborate Classification of SNARE Proteins Sheds Light on the Conservation of the Eukaryotic Endomembrane System.* Molecular Biology of the Cell, 2007. **18**: p. 3463-3471.
70. Brunger, A.T., *Structure and function of SNARE and SNARE-interacting proteins.* Q Rev Biophys, 2005. **38**(1): p. 1-47.
71. Michael Veit, T.H.S., James E. Rothman, *Multiple palmitoylation of synaptotagmin and the t-SNARE SNAP-25.* FEBS Letters, 1996. **385**: p. 119-123.
72. Douglas T. Hess, T.M.S., Michael C. Wilson, and J. H. Pate Skene, *The 25 kDa Synaptosomal-associated Protein SNAP-25 Is the Major Methionine-Rich Polypeptide in Rapid Axonal Transport and a Major Substrate for Palmitoylation in Adult CNS.* The Journal of Neuroscience, 1992. **12**(12): p. 4634-4641.
73. Zwilling, D., et al., *Early endosomal SNAREs form a structurally conserved SNARE complex and fuse liposomes with multiple topologies.* EMBO J, 2007. **26**(1): p. 9-18.
74. Antonin, W., et al., *Crystal structure of the endosomal SNARE complex reveals common structural principles of all SNAREs.* Nat Struct Biol, 2002. **9**(2): p. 107-11.
75. R. Bryan Sutton, D.F., Reinhard Jahn & Axel T. Brunger, *Crystal structure of a SNARE complex involved in synaptic exocytosis at 2.4 A ˚ resolution.* Nature, 1998. **395**: p. 347-353.

76. Tetsuya Hayashi, S.Y., Sonja Nauenburg, Thomas Binz and Heiner Niemann, *Disassembly of the reconstituted synaptic vesicle membrane fusion complex in vitro.* EMBO J, 1995. **14**(10): p. 2317-2325.
77. Michelle A. Poirier, W.X., Jed C. Macosko, Charles Chan, Yeon-Kyun Shin and Mark K. Bennett, *The synaptic SNARE complex is a parallel fourstranded helical bundle.* Nature Structural Biology, 1998. **5**(9): p. 765-769.
78. Luba Katz, P.I.H., John E. Heuser and Patrick Brennwald, *Genetic and morphological analyses reveal a critical interaction between the C-termini of two SNARE proteins and a parallel four helical arrangement for the exocytic SNARE complex.* EMBO J, 1998. **17**(21): p. 6200-6209.
79. Sorensen, J.B., et al., *Sequential N- to C-terminal SNARE complex assembly drives priming and fusion of secretory vesicles.* EMBO J, 2006. **25**(5): p. 955-66.
80. Li, Y., G.J. Augustine, and K. Weninger, *Kinetics of complexin binding to the SNARE complex: correcting single molecule FRET measurements for hidden events.* Biophys J, 2007. **93**(6): p. 2178-87.
81. Stein, A., et al., *Helical extension of the neuronal SNARE complex into the membrane.* Nature, 2009. **460**(7254): p. 525-8.
82. Javier M. Hernandez, A.S., Elmar Behrmann, Dietmar Riedel,Anna Cypionka, and P.J.W. Zohreh Farsi, Stefan Raunser, Reinhard Jahn, *Membrane Fusion Intermediates via Directional and Full Assembly of the SNARE Complex.pdf>.* Science, 2012. **336**: p. 1581-1584.
83. Lu, X., et al., *Membrane fusion induced by neuronal SNAREs transits through hemifusion.* J Biol Chem, 2005. **280**(34): p. 30538-41.
84. Jackson, M.B. and E.R. Chapman, *The fusion pores of Ca2+ -triggered exocytosis.* Nat Struct Mol Biol, 2008. **15**(7): p. 684-9.
85. Fesce Riccardo, F.G., Flavia Valtorta, and Jacopo Meldolesi, *Neurotransmitter release: fusion or 'kiss-and-run'?* Trends in Cell Biology, 1994. **4**(1): p. 1-4.
86. Thomas Weber, B.V.Z., James A. McNew, Benedikt Westermann, Michael Gmachl, Francesco Parlati, Thomas H. Söllner, and James E. Rothman, *SNAREpins: Minimal Machinery for Membrane Fusion.* Cell, 1998. **92**: p. 759-772.
87. Dyer, R.B. and M.W. Eller, *Dynamics of hemagglutinin-mediated membrane fusion.* Proceedings of the National Academy of Sciences, 2018. **115**(35): p. 8655-8657.
88. Jackson, M.B. and E.R. Chapman, *Fusion pores and fusion machines in Ca2+-triggered exocytosis.* Annu Rev Biophys Biomol Struct, 2006. **35**: p. 135-60.
89. James C. Cross, Z.W., Susan J. Fisher, *Implantation and the Placenta- Key Pieces of the Development Puzzle.* Science, 1994. **266**: p. 1508-1517.
90. Chang, C., et al., *Functional characterization of the placental fusogenic membrane protein syncytin.* Biol Reprod, 2004. **71**(6): p. 1956-62.
91. David H. Munn, M.Z., John T. Attwood, Igor Bondarev, Simon J. Conway, Brendan Marshall, Corrie Brown, Andrew L. Mellor, *Prevention of Allogeneic Fetal Rejection by Tryptophan Catabolism.* Science, 1998. **281**(5380): p. 1191-1193.
92. Hamilton, P.K.L.a.G.S., *Growth Factors, Proteases and Protease Inhibitors in the Maternal-fetal Dialogue.* Placenta, 1996. **17**: p. 545-555.
93. E. Alsat, V.M., C. Fondacci, M. Dodeur, And D. Evain-Brion, *Parathyroid Hormone Increases Epidermal Growth Factor Receptors in Cultured Human Trophoblastic Cells from Early and Term Placenta.* Journal of Clinical Endocrinology and Metabolism, 1991. **73**(2): p. 288-295.
94. Jean-Luc Blond, D.L., Valérie Cheynet, Olivier Bouton, Guy Oriol, Sylvie Chapel-Fernandes, Bernard Mandrand,1 François Mallet and rançois-Loïc Cosset, *An Envelope Glycoprotein of the Human Endogenous Retrovirus HERV-W Is Expressed in the Human Placenta and Fuses Cells Expressing the Type D Mammalian Retrovirus Receptor.* Journal of Virology, 2000. **74**(7): p. 3321-3329.
95. Jean-Luc Blond, F.B., Laurent Duret, Olivier Bouton, Frédéric Bedin, Hervé Perron, Bernard Mandrand, and François Mallet, *Molecular Characterization and Placental Expression of HERV-W, a New Human Endogenous Retrovirus Family.* Journal of Virology, 1999. **73**(2): p. 1175-1185.
96. Huang, Q., et al., *Epigenetic and non-epigenetic regulation of syncytin-1 expression in human placenta and cancer tissues.* Cell Signal, 2014. **26**(3): p. 648-56.

97. Gimenez, J., et al., *Comparative methylation of ERVWE1/syncytin-1 and other human endogenous retrovirus LTRs in placenta tissues.* DNA Res, 2009. **16**(4): p. 195-211.
98. Matouskova, M., et al., *CpG methylation suppresses transcriptional activity of human syncytin-1 in non-placental tissues.* Exp Cell Res, 2006. **312**(7): p. 1011-20.
99. Pamela L. Strissel, M.R., Falk Thiel, David Wachter, Arif B. Ekici, Friedericke Wolf, Franziska Thieme, Klemens Ruprecht, Matthias W. Beckmann, Reiner Strick, *Reactivation of codogenic endogenous retroviral (ERV) envelope genes in human endometrial carcinoma and prestages: Emergence of new molecular targets.* Oncotarget, 2012. **3**(10): p. 1204-1219.
100. Laura Menendez, B.B.B.a.J.F.M., *L1 and HERV-W retrotransposons are hypomethylated in human ovarian carcinomas.* Molecular Cancer, 2004. **3**(12).
101. Frendo, J.L., et al., *Direct involvement of HERV-W Env glycoprotein in human trophoblast cell fusion and differentiation.* Mol Cell Biol, 2003. **23**(10): p. 3566-74.
102. Guy Keryer1, E.A., Kjetil Taskén and Danièle Evain-Brion, *Cyclic AMP-dependent protein kinases and human trophoblast cell differentiation in vitro.* Journal of Cell Science, 1998. **111**: p. 995-1004.
103. Strick, R., et al., *Proliferation and cell-cell fusion of endometrial carcinoma are induced by the human endogenous retroviral Syncytin-1 and regulated by TGF-beta.* J Mol Med (Berl), 2007. **85**(1): p. 23-38.
104. Bjerregaard, B., et al., *Syncytin is involved in breast cancer-endothelial cell fusions.* Cell Mol Life Sci, 2006. **63**(16): p. 1906-11.
105. Colman, P.M. and M.C. Lawrence, *The structural biology of type I viral membrane fusion.* Nat Rev Mol Cell Biol, 2003. **4**(4): p. 309-19.
106. Lavillette, D., et al., *The envelope glycoprotein of human endogenous retrovirus type W uses a divergent family of amino acid transporters/cell surface receptors.* J Virol, 2002. **76**(13): p. 6442-52.
107. Tailor, C.S., et al., *Truncated forms of the dual function human ASCT2 neutral amino acid transporter/retroviral receptor are translationally initiated at multiple alternative CUG and GUG codons.* J Biol Chem, 2001. **276**(29): p. 27221-30.
108. Compans, C.Y.a.R.W., *Analysis of the Cell Fusion Activities of Chimeric Simian Immunodeficiency Virus-Murine Leukemia Virus Envelope Proteins- Inhibitory Effects of the R Peptide.* Journal of Virology, 1996. **70**(1): p. 248-254.
109. Blaise, S., et al., *Genomewide screening for fusogenic human endogenous retrovirus envelopes identifies syncytin 2, a gene conserved on primate evolution.* Proc Natl Acad Sci U S A, 2003. **100**(22): p. 13013-8.
110. Esnault, C., et al., *A placenta-specific receptor for the fusogenic, endogenous retrovirus-derived, human syncytin-2.* Proc Natl Acad Sci U S A, 2008. **105**(45): p. 17532-7.
111. Mangeney, M., et al., *Placental syncytins: Genetic disjunction between the fusogenic and immunosuppressive activity of retroviral envelope proteins.* Proc Natl Acad Sci U S A, 2007. **104**(51): p. 20534-9.
112. Moller, A.M., J.M. Delaisse, and K. Soe, *Osteoclast Fusion: Time-Lapse Reveals Involvement of CD47 and Syncytin-1 at Different Stages of Nuclearity.* J Cell Physiol, 2017. **232**(6): p. 1396-1403.
113. Soe, K., et al., *Involvement of human endogenous retroviral syncytin-1 in human osteoclast fusion.* Bone, 2011. **48**(4): p. 837-46.
114. Redelsperger, F., et al., *Genetic Evidence That Captured Retroviral Envelope syncytins Contribute to Myoblast Fusion and Muscle Sexual Dimorphism in Mice.* PLoS Genet, 2016. **12**(9): p. e1006289.
115. Heidmann, O., et al., *Identification of an endogenous retroviral envelope gene with fusogenic activity and placenta-specific expression in the rabbit: a new "syncytin" in a third order of mammals.* Retrovirology, 2009. **6**: p. 107.
116. Dupressoir, A., et al., *Syncytin-A and syncytin-B, two fusogenic placenta-specific murine envelope genes of retroviral origin conserved in Muridae.* Proc Natl Acad Sci U S A, 2005. **102**(3): p. 725-30.
117. William A. Mohler, J.S.S., Ellen M. Williams-Masson, Jeffrey D. Hardin and John G. White, *Dynamics and ultrastructure of developmental cell fusions in the Caenorhabditis elegans hypodermis.* Current Biology, 1998. **8**: p. 1087-1090.
118. Benjamin Podbilewicz, J.G.W., *Cell Fusions in the Developing Epithelia of C. elegans.* Dev Biol, 1994. **161**: p. 408-424.

119. Podbilewicz, G.S.a.B., *LIN-39:Hox triggers cell division and represses EFF-1:fusogen-dependent vulval cell fusion.* Genes & Development, 2002. **16**: p. 3136-3141.
120. del Campo, J.J., et al., *Fusogenic activity of EFF-1 is regulated via dynamic localization in fusing somatic cells of C. elegans.* Curr Biol, 2005. **15**(5): p. 413-23.
121. Avinoam, O., et al., *Conserved eukaryotic fusogens can fuse viral envelopes to cells.* Science, 2011. **332**(6029): p. 589-92.
122. Avinoam, O. and B. Podbilewicz, *Eukaryotic cell-cell fusion families.* Curr Top Membr, 2011. **68**: p. 209-34.
123. Podbilewicz, B., et al., *The C. elegans developmental fusogen EFF-1 mediates homotypic fusion in heterologous cells and in vivo.* Dev Cell, 2006. **11**(4): p. 471-81.
124. Kontani, K. and J.H. Rothman, *Cell fusion: EFF is enough.* Curr Biol, 2005. **15**(7): p. R252-4.
125. Smurova, K. and B. Podbilewicz, *RAB-5- and DYNAMIN-1-Mediated Endocytosis of EFF-1 Fusogen Controls Cell-Cell Fusion.* Cell Rep, 2016. **14**(6): p. 1517-1527.
126. Perez-Vargas, J., et al., *Structural basis of eukaryotic cell-cell fusion.* Cell, 2014. **157**(2): p. 407-419.
127. Valansi, C., et al., *Arabidopsis HAP2/GCS1 is a gamete fusion protein homologous to somatic and viral fusogens.* J Cell Biol, 2017. **216**(3): p. 571-581.
128. Okamoto, M., et al., *Two HAP2-GCS1 homologs responsible for gamete interactions in the cellular slime mold with multiple mating types: Implication for common mechanisms of sexual reproduction shared by plants and protozoa and for male-female differentiation.* Dev Biol, 2016. **415**(1): p. 6-13.
129. Cole, E.S., et al., *Function of the male-gamete-specific fusion protein HAP2 in a seven-sexed ciliate.* Curr Biol, 2014. **24**(18): p. 2168-2173.
130. Hirai, M., et al., *Male fertility of malaria parasites is determined by GCS1, a plant-type reproduction factor.* Curr Biol, 2008. **18**(8): p. 607-13.
131. Mori, T., et al., *GENERATIVE CELL SPECIFIC 1 is essential for angiosperm fertilization.* Nat Cell Biol, 2006. **8**(1): p. 64-71.
132. von Besser, K., et al., *Arabidopsis HAP2 (GCS1) is a sperm-specific gene required for pollen tube guidance and fertilization.* Development, 2006. **133**(23): p. 4761-9.
133. Johnson, M.A., et al., *Arabidopsis hapless mutations define essential gametophytic functions.* Genetics, 2004. **168**(2): p. 971-82.
134. Wong, J.L. and M.A. Johnson, *Is HAP2-GCS1 an ancestral gamete fusogen?* Trends Cell Biol, 2010. **20**(3): p. 134-41.
135. Liu, Y., et al., *The cytoplasmic domain of the gamete membrane fusion protein HAP2 targets the protein to the fusion site in Chlamydomonas and regulates the fusion reaction.* Development, 2015. **142**(5): p. 962-71.
136. Fedry, J., et al., *The Ancient Gamete Fusogen HAP2 Is a Eukaryotic Class II Fusion Protein.* Cell, 2017. **168**(5): p. 904-915 e10.
137. Pinello, J.F., et al., *Structure-Function Studies Link Class II Viral Fusogens with the Ancestral Gamete Fusion Protein HAP2.* Curr Biol, 2017. **27**(5): p. 651-660.
138. Feng, J., et al., *Fusion surface structure, function, and dynamics of gamete fusogen HAP2.* Elife, 2018. **7**.
139. Michael J. Misamore, S.G., and William J. Snell, *The Chlamydomonas Fus1 Protein Is Present on the Mating Type plus Fusion Organelle and Required for a Critical Membrane Adhesion Event during Fusion with minus Gametes.* Molecular Biology of the Cell, 2003. **14**: p. 2530-2542.
140. Melissa R. van Dijk, C.J.J., Joanne Thompson, Andrew P. Waters, Joanna A. M. Braks, Huub J. Dodemont, Henk G. Stunnenberg, Geert-Jan van Gemert, Robert W. Sauerwein, and Wijnand Eling, *A Central Role for P48:45 in Malaria Parasite Male Gamete Fertility.* Cell, 2001. **104**: p. 153-164.
141. Stefanie Sprunck, S.R., Frank Vogler, Jacqueline Gheyselinck, Ueli Grossniklaus, Thomas Dresselhaus, *Egg Cell–Secreted EC1 Triggers Sperm Cell Activation During Double Fertilization.* Science, 2012. **338**(6110): p. 1093-1097.
142. Okabe, M., *The cell biology of mammalian fertilization.* Development, 2013. **140**(22): p. 4471-9.
143. Paul M. Wassarman, L.J.a.E.S.L., *A profile of fertilization in mammals.* Nature, 2001. **3**: p. 59-64.

144. Hirohashi, N. and R. Yanagimachi, *Sperm acrosome reaction: its site and role in fertilization.* Biol Reprod, 2018. **99**(1): p. 127-133.
145. João Ramalho-Santos, G.S., and Ricardo D. Moreno, *Control of Membrane Fusion During Spermiogenesis and the Acrosome Reaction.* Biology of Reproduction, 2002. **67**: p. 1043-1051.
146. Evans, J.P., *Preventing polyspermy in mammalian eggs-Contributions of the membrane block and other mechanisms.* Mol Reprod Dev, 2020. **87**(3): p. 341-349.
147. Bianchi, E., et al., *Juno is the egg Izumo receptor and is essential for mammalian fertilization.* Nature, 2014. **508**(7497): p. 483-7.
148. Wong, J.L. and G.M. Wessel, *Defending the Zygote: Search for the Ancestral Animal Block to Polyspermy*. 2005. p. 1-151.
149. Bianchi, E. and G.J. Wright, *Find and fuse: Unsolved mysteries in sperm-egg recognition.* PLoS Biol, 2020. **18**(11): p. e3000953.
150. Seals, D.F. and S.A. Courtneidge, *The ADAMs family of metalloproteases: multidomain proteins with multiple functions.* Genes Dev, 2003. **17**(1): p. 7-30.
151. Blobel, J.S.n.a.C.P., *Metalloprotease-disintegrins- modular proteins capable of promoting cell-cell interactions and triggering signals by protein-ectodomain shedding.* Journal of Cell Science, 1999. **112**: p. 3603-3617.
152. Carl P. Blobel, T.G.W., Christoph W. Turck, Diana G. Myles, Paul Primakoff & Judith M. White, *A potential fusion peptide and an integrin ligand domain in a protein active in sperm-egg fusion.* Nature, 1992. **356**.
153. Tyra G. Wolfsberg, P.D.S., Robyn L. Gerena, Ari-Pekka J. Huovila, Paul Primakoff, Diana G. Myles and Judith M. White, *ADAM, a Widely Distributed and Developmentally Regulated Gene Fmaily Encoding Membrane Proteins with A Disintegrin And Metalloprotease Domain.* Developmental Biology, 1995. **169**: p. 378-383.
154. White, W.J.S.a.J.M., *The Molecules of Mammalian Fertilization.* Cell, 1996. **85**: p. 629-637.
155. Diana G. Myles, L.H.K., Carl P. Blobel, Judith M. White, and Paul Primakoff, *Identification of a binding site in the disintegrin domain of fertilin required for sperm-egg fusion.* Proc Natl Acad Sci U S A, 1994. **91**: p. 4195-4198.
156. Chunghee Cho, D.O.D.B., Jean-Emmanuel Faure, Eugenia H. Goulding, Edward M. Eddy, Paul Primakoff, Diana G. Myles, *Fertilization Defects in Sperm from Mice Lacking Fertilin b.* Science, 1998. **281**: p. 1857-1859.
157. Kim, E., et al., *Mouse sperm lacking ADAM1b/ADAM2 fertilin can fuse with the egg plasma membrane and effect fertilization.* J Biol Chem, 2006. **281**(9): p. 5634-9.
158. Naokazu Inoue, M.I., Ayako Isotani, & Masaru Okabe, *The immunoglobulin superfamily protein Izumo is required for sperm to fuse with eggs.* Nature, 2005. **434**: p. 234-238.
159. Ellerman, D.A., et al., *Izumo is part of a multiprotein family whose members form large complexes on mammalian sperm.* Mol Reprod Dev, 2009. **76**(12): p. 1188-99.
160. Satouh, Y., et al., *Visualization of the moment of mouse sperm-egg fusion and dynamic localization of IZUMO1.* J Cell Sci, 2012. **125**(Pt 21): p. 4985-90.
161. Yamaguchi, T., et al., *Control of immune responses by antigen-specific regulatory T cells expressing the folate receptor.* Immunity, 2007. **27**(1): p. 145-59.
162. Inoue, N., et al., *Oocyte-triggered dimerization of sperm IZUMO1 promotes sperm-egg fusion in mice.* Nat Commun, 2015. **6**: p. 8858.
163. Nishimura, K., et al., *The structure of sperm Izumo1 reveals unexpected similarities with Plasmodium invasion proteins.* Curr Biol, 2016. **26**(14): p. R661-2.
164. Aydin, H., et al., *Molecular architecture of the human sperm IZUMO1 and egg JUNO fertilization complex.* Nature, 2016. **534**(7608): p. 562-5.
165. Ohto, U., et al., *Structure of IZUMO1-JUNO reveals sperm-oocyte recognition during mammalian fertilization.* Nature, 2016. **534**(7608): p. 566-9.
166. Jean, C., et al., *JUNO, the receptor of sperm IZUMO1, is expressed by the human oocyte and is essential for human fertilisation.* Hum Reprod, 2019. **34**(1): p. 118-126.
167. Inoue, N., et al., *Molecular dissection of IZUMO1, a sperm protein essential for sperm-egg fusion.* Development, 2013. **140**(15): p. 3221-9.
168. Keisuke Kaji, S.O., Tomohide Shikano, Tatsuya Ohnuki, Yoshikatsu Uematsu, Junko Sakagami, Norihiro Tada, Shunichi Miyazaki, & Akira Kudo, *The gamete fusion process is defective in eggs of Cd9-deficient mice.* Nature Genetics, 2000. **24**: p. 279-282.
169. Tomlinson, M.D.W.a.M.G., *The ins and outs of the transmembrane4 superfamily.* Immunology, 1994. **15**(12): p. 588-594.

170. Umeda, R., et al., *Structural insights into tetraspanin CD9 function.* Nat Commun, 2020. **11**(1): p. 1606.
171. Stipp, C.S., T.V. Kolesnikova, and M.E. Hemler, *EWI-2 is a major CD9 and CD81 partner and member of a novel Ig protein subfamily.* J Biol Chem, 2001. **276**(44): p. 40545-54.
172. Kenji Miyado, G.Y., Shuichi Yamada, Hidetoshi Hasuwa, Yasuhiro Nakamura, Fuminori Ryu, Kentaro Suzuki, Kenichiro Kosai, Kimiko Inoue, Atsuo Ogura, Masaru Okabe, Eisuke Mekada, *Requirement of CD9 on the Egg Plasma Membrane for Fertilization.* Science, 2000. **287**(5451): p. 321-324.
173. Eric Rubinstein, F.L.N., Martine Billard, Michel Prenant and Claude Boucheix, *CD9 antigen is an accessory subunit of the VLA integrin complexes*.* European Journal of Immunology, 1994. **24**(12): p. 3005-3013.
174. Charrin, S., et al., *The major CD9 and CD81 molecular partner. Identification and characterization of the complexes.* J Biol Chem, 2001. **276**(17): p. 14329-37.
175. Runge, K.E., et al., *Oocyte CD9 is enriched on the microvillar membrane and required for normal microvillar shape and distribution.* Dev Biol, 2007. **304**(1): p. 317-25.
176. Holden T. Maecker, S.C.T., and Shoshana Levy, *The tetrasapanin superfamily: molecular facilitators.* The FASEB journal, 1997. **11**(6): p. 428-442.
177. Shaw, A.R., et al., *Ectopic expression of human and feline CD9 in a human B cell line confers beta 1 integrin-dependent motility on fibronectin and laminin substrates and enhanced tyrosine phosphorylation.* J Biol Chem, 1995. **270**(41): p. 24092-9.
178. Rubinstein, E., et al., *Reduced fertility of female mice lacking CD81.* Dev Biol, 2006. **290**(2): p. 351-8.
179. Jegou, A., et al., *CD9 tetraspanin generates fusion competent sites on the egg membrane for mammalian fertilization.* Proc Natl Acad Sci U S A, 2011. **108**(27): p. 10946-51.
180. Ravaux, B., et al., *A specific flagellum beating mode for inducing fusion in mammalian fertilization and kinetics of sperm internalization.* Sci Rep, 2016. **6**: p. 31886.
181. Ravaux, B., et al., *Egg CD9 protein tides correlated with sperm oscillations tune the gamete fusion ability in mammal.* J Mol Cell Biol, 2018. **10**(6): p. 494-502.
182. Benammar, A., et al., *Tetraspanins and Mouse Oocyte Microvilli Related to Fertilizing Ability.* Reprod Sci, 2017. **24**(7): p. 1062-1069.
183. Inoue, N., T. Saito, and I. Wada, *Unveiling a novel function of CD9 in surface compartmentalization of oocytes.* Development, 2020. **147**(15).
184. François Le Naour, E.R., Claude Jasmin, Michel Prenant, Claude Boucheix, *Severely Reduced Female Fertility in CD9-Deficient Mice.* Science, 2000. **287**(5451): p. 319-321.
185. Barbaux, S., et al., *Sperm SPACA6 protein is required for mammalian Sperm-Egg Adhesion/Fusion.* Sci Rep, 2020. **10**(1): p. 5335.
186. Lorenzetti, D., et al., *A transgenic insertion on mouse chromosome 17 inactivates a novel immunoglobulin superfamily gene potentially involved in sperm-egg fusion.* Mamm Genome, 2014. **25**(3-4): p. 141-8.
187. Noda, T., et al., *Sperm proteins SOF1, TMEM95, and SPACA6 are required for sperm-oocyte fusion in mice.* Proc Natl Acad Sci U S A, 2020. **117**(21): p. 11493-11502.
188. Lamas-Toranzo, I., et al., *TMEM95 is a sperm membrane protein essential for mammalian fertilization.* Elife, 2020. **9**.
189. Pausch, H., et al., *A nonsense mutation in TMEM95 encoding a nondescript transmembrane protein causes idiopathic male subfertility in cattle.* PLoS Genet, 2014. **10**(1): p. e1004044.
190. Fujihara, Y., et al., *Spermatozoa lacking Fertilization Influencing Membrane Protein (FIMP) fail to fuse with oocytes in mice.* Proc Natl Acad Sci U S A, 2020. **117**(17): p. 9393-9400.
191. Shetty, J., et al., *SAMP14, a novel, acrosomal membrane-associated, glycosylphosphatidylinositol-anchored member of the Ly-6/urokinase-type plasminogen activator receptor superfamily with a role in sperm-egg interaction.* J Biol Chem, 2003. **278**(33): p. 30506-15.
192. Sarah Herberg, K.R.G., Alexander Schleiffer, Andrea Pauli, *The Ly6/uPAR protein Bouncer is necessary and sufficient for species-specific fertilization.* Science, 2018. **361**(6406): p. 1029-1033.
193. Charles Saginario, H.S., Cornelius Beckers, Ruji Kobayashi, Michele Solimena, Elisabetta Ullu, and Agnès Vignery, *MFR, a Putative Receptor Mediating the Fusion of Macrophages.* Mol Cell Biol, 1998. **18**(11): p. 6213-6223.

194. Han, X., et al., *CD47, a ligand for the macrophage fusion receptor, participates in macrophage multinucleation.* J Biol Chem, 2000. **275**(48): p. 37984-92.
195. Cui, W., et al., *The intracellular domain of CD44 promotes the fusion of macrophages.* Blood, 2006. **107**(2): p. 796-805.
196. Elion, E.A., *Pheromone response, mating and cell biology.* Current Opinion in Microbiology, 2000. **3**: p. 573-581.
197. Malcolm S. Whiteway, C.W., Thomas Leeuw, Karen Clark, Anne Fourest-Lieuvin, David Y. Thomas, and Ekkehard Leberer, *Association of the Yeast Pheromone Response G Protein Ay Subunits with the MAP Kinase Scaffold Ste5p.* Science, 1995. **269**(5230): p. 1572-1575.
198. Garrenton, L.S., S.L. Young, and J. Thorner, *Function of the MAPK scaffold protein, Ste5, requires a cryptic PH domain.* Genes Dev, 2006. **20**(14): p. 1946-58.
199. Winters, M.J., et al., *A membrane binding domain in the ste5 scaffold synergizes with gbetagamma binding to control localization and signaling in pheromone response.* Mol Cell, 2005. **20**(1): p. 21-32.
200. Wang, Y., et al., *Cdc24 regulates nuclear shuttling and recruitment of the Ste5 scaffold to a heterotrimeric G protein in Saccharomyces cerevisiae.* J Biol Chem, 2005. **280**(13): p. 13084-96.
201. Marie-Noëlle Simon, C.D.V., Brian Souza, John R. Prlngle, Arle Abo & Steven I. Reed, *Role for the Rho-family GTPase Cdc42 in yeast mating-pheromone signal pathway.* Nature, 1995. **376**: p. 702-705.
202. John J. Moskow, A.S.G., Rachel E. Lamson, Peter M. Pryciak, and Daniel J. Lew, *Role of Cdc42p in Pheromone-Stimulated Signal Transduction in Saccharomyces cerevisiae.* Molecular and Cellular Biology, 2000. **20**(20): p. 7559-7571.
203. Jesse G. Zalatan, S.M.C., Saravanan Rajan, Sachdev S. Sidhu, Wendell A. Lim, *Conformational Control of the Ste5 Scaffold Protein Insulates Against MAP Kinase Misactivation.* Science, 2012. **337**(6099): p. 1218-1222.
204. Zhuo-Shen Zhao, T.L., Edward Manser, and Louis Lim, *Pheromone Signalling in Saccharomyces cerevisiae Requires the Small GTP-Binding Protein Cdc42p and Its Activator CDC24.* Molecular and Cellular Biology, 1995. **15**(10): p. 5246-5257.
205. Arkowitz, A.N.R.A., *A GTP-exchange factor required for cell orientation.* Nature, 1998. **9**: p. 195-198.
206. Elion, E.A., *The Ste5p scaffold.* Journal of Cell Science, 2001. **114**: p. 3967-3978.
207. Jeanette Gowen Cook, L.B.J.T., *Inhibitory and activating functions for MAPK Kss1 in the S. cerevisiae filamentous growth signalling pathway.* Nature, 1997. **390**: p. 85-88.
208. Kerry Tedford, S.K., Danne Sa, Ken Stevens and Mike Tyers, *Regulation of the mating pheromone and invasive growth responses in yeast by two MAP kinase substrates.* Current Biology, 1997. **7**: p. 228-238.
209. Anne-Christine Butty, P.M.P., Linda S. Huang, Ira Herskowitz, Matthias Peter, *The Role of Far1p in Linking the Heterotrimeric G Protein to Polarity Establishment Proteins During Yeast Mating.* Science, 1998. **282**(5393): p. 1511-1516.
210. Anton Gartner, A.J., Doo-Il Jeoung, Sarah Bourlat, Frederick R. Cross, and Gustav Ammerer, *Pheromone-Dependent G1 Cell Cycle Arrest Requires Far1 Phosphorylation, but May Not Involve Inhibition of Cdc28-Cln2 Kinase, In Vivo.* Molecular and Cellular Biology, 1998. **18**(7): p. 3681-3691.
211. Matthias Peter, A.G., Joe Horecka, Gustav Ammerer, and Ira Herskowitz, *FAR1 Links the Signal Transduction Pathway to the Cell Cycle Machinery in Yeast.* Cell, 1993. **73**: p. 747-760.
212. Matheos, D., et al., *Pheromone-induced polarization is dependent on the Fus3p MAPK acting through the formin Bni1p.* J Cell Biol, 2004. **165**(1): p. 99-109.
213. E. Bucking-Throm, W.D., L. H. Hartwell and T. R. Manney, *<REVERSIBLE ARREST OF HAPLOID YEAST CELLS AT THE INITIATION OF DNA SYNTHESIS BY A DIFFUSIBLE SEX FACTOR.pdf>.* Experimental Cell Research, 1973. **76**: p. 99-110.
214. Bruckner, S., et al., *Differential regulation of Tec1 by Fus3 and Kss1 confers signaling specificity in yeast development.* Curr Genet, 2004. **46**(6): p. 331-42.
215. Smith, G.R., et al., *GTPase-activating proteins for Cdc42.* Eukaryot Cell, 2002. **1**(3): p. 469-80.
216. Juliane P. Caviston, M.L., John R. Pringle, and Erfei Bi, *The Role of Cdc42p GTPase-activating Proteins in Assembly of the Septin Ring in Yeast.* Molecular Biology of the Cell, 2003. **14**: p. 4051-4066.

217. Zheng, Y., R. Cerione, and A. Bender, *Control of the yeast bud-site assembly GTPase Cdc42. Catalysis of guanine nucleotide exchange by Cdc24 and stimulation of GTPase activity by Bem3.* Journal of Biological Chemistry, 1994. **269**(4): p. 2369-2372.
218. Anne-Christine Butty, N.P., Audrey Petit, Malika Jaquenoud, Jeffrey E.Segall, Kay Hofmann, Catherine Zwahlen and Matthias Peter, *A positive feedback loop stabilizes the guanine-nucleotide exchange factor Cdc24 at sites of polarization.* EMBO J, 2002. **21**(7): p. 1565-1576.
219. John Chant, K.C., John R. Pringle, and Ira Herskowitz, *Yeast BUD5, Encoding a Putative GDP-GTP Exchange Factor, Is Necessary for Bud Site Selection and Interacts with Bud Formation Gene BEM1.* Cell, 1991. **65**: p. 1213-1224.
220. Valeria Brizzio, A.E.G., * Gaby Nijbroek,* Susan Michaelis,* and Mark D. Rose*, *Cell fusion requires high levels of pheromones.* Journal of Cell Biology, 1996. **135**(6, Part 2): p. 1727-1739.
221. Gulli, M.P. and M. Peter, *Temporal and spatial regulation of Rho-type guanine-nucleotide exchange factors: the yeast perspective.* Genes Dev, 2001. **15**(4): p. 365-79.
222. Nicole Valtz, M.P., and Ira Herskowitz, *FAR1 Is Required for Oriented Polarization of Yeast Cells in Response to Mating Pheromones.* Journal of Cell Biology, 1995. **131**(4): p. 863-873.
223. Russell Dorer, P.M.P., and Leland H. Hartwell, *Saccharomyces cerevisiae Cells Execute a Default Pathway to Select a Mate in the Absence of Pheromone Gradients.* Journal of Cell Biology, 1995. **131**(4): p. 845-861.
224. Russell Dorer, C.B., Tyler Kimbrough, Joshua Kim and Leland H. Hartwell, *Genetic Analysis of Default Mating Behavior in Saccharomyces cerevisiae.* Genetics, 1997. **146**: p. 39-55.
225. Marie Evangelista, K.B., Mark S. Longtine, Clinton J. Chow, Neil Adames, John R. Pringle, Matthias Peter, Charles Boone, *Bni1p, a Yeast Formin Linking Cdc42p and the Actin Cytoskeleton During Polarized Morphogenesis.* Science, 1997. **276**(5309): p. 118-122.
226. Misuzu Baba, N.B., Yoshunori Ohsumi, Koichi Kanaya and Masako Osumi *Three-dimensional analysis of morphogenesis induced by mating pheromone a factor in Saccharomyces cerevisiae.pdf.* Journal of Cell Science, 1989. **94**: p. 207-216.
227. Snyder, S.G.a.M., *The SPA2 Gene of Saccharomyces cerevisiae Is Important for Pheromone-induced Morphogenesis and Efficient Mating.* Journal of Cell Biology, 1990. **111**: p. 1451-1464.
228. Alison E. Gammie, V.B., and Mark D. Rose, *Distinct Morphological Phenotypes of Cell Fusion Mutants.* Mol Biol Cell, 1998. **9**: p. 1395-1410.
229. Amit Roy, C.F.L., Donna L. Marykwas, Peter N. Lipke, and Janet Kurjan, *The AGA1 Product Is Involved in Cell Surface Attachment of the Saccharomyces cerevisiae Cell Adhesion Glycoprotein a-Agglutinin.* Molecular and Cellular Biology, 1991. **11**(8): p. 4196-4206.
230. Corinna Cappellaro, C.B., Reinhard Rachel and Widmar Tanner, *Mating type-specific cell-cell recognition of Saccharomyces cerevisiae- cell wall attachment and active sites of a- and alpha-agglutinin.* EMBO J, 1994. **13**(20): p. 4737-4744.
231. Shen, Z.M., et al., *Delineation of functional regions within the subunits of the Saccharomyces cerevisiae cell adhesion molecule a-agglutinin.* J Biol Chem, 2001. **276**(19): p. 15768-75.
232. Chen, M.H., et al., *Structure of Saccharomyces cerevisiae alpha-agglutinin. Evidence for a yeast cell wall protein with multiple immunoglobulin-like domains with atypical disulfides.* J Biol Chem, 1995. **270**(44): p. 26168-77.
233. Donald Wojciechowicz, C.-F.L., Janet Kurjan, and Peter N. Lipkel, *Cell Surface Anchorage and Ligand-Binding Domains of the Saccharomyces cerevisiae Cell Adhesion Protein alpha-Agglutinin, a Member of the Immunoglobulin Superfamily.* Molecular and Cellular Biology, 1993. **13**(4): p. 2554-2563.
234. Zhao, H., et al., *Interaction of alpha-agglutinin and a-agglutinin, Saccharomyces cerevisiae sexual cell adhesion molecules.* J Bacteriol, 2001. **183**(9): p. 2874-80.
235. Suzuki, K., *Roles of sexual cell agglutination in yeast mass mating.* Genes Genet Syst, 2003. **78**(3): p. 211-9.
236. Frans M. Klis, P.M., Klaas Hellingwerf, Stanley Brul, *Dynamics of cell wall structure in Saccharomyces cerevisiae.* FEMS Microbiology Reviews, 2002. **26**: p. 239-256.

237. Alexander E. Smith, Z.Z., Colin R. Thomas, Kennith E. Moxham, and Anton P. J. Middelberg, *The mechanical properties of Saccharomyces cerevisiae.* PNAS, 2000. **97**(18): p. 9871-9874.
238. Joshua Trueheart, J.D.B.a.G.R.F., *Two Genes Required for Cell Fusion during Yeast Conjugation- Evidence for a Pheromone-Induced Surface Protein.pdf>.* Mol Biol Cell, 1987: p. 2316-2328.
239. Fink, J.T.a.G.R., *The yeast cell fusion protein FUS1 is 0-glycosylated and spans the plasma membrane.* Proc Natl Acad Sci U S A, 1989. **86**: p. 9961-9920.
240. Bryce Nelson, A.B.P., Marie Evangelista, Karen Schaefer, Kathy Kennedy, Steven Ritchie, Tracey L. Petryshen and Charles Boone, *Fus1p Interacts With Components of the Hog1p Mitogen-Activated Protein Kinase and Cdc42p Morphogenesis Signaling Pathways to Control Cell Fusion During Yeast Mating.* Genetics, 2003. **166**.
241. Simons, M.B.a.K., *Cell surface polarization during yeast mating.* PNAS, 2002. **99**(22): p. 14183-14188.
242. Grote, E., *Secretion is required for late events in the cell-fusion pathway of mating yeast.* Journal of Cell Science, 2010. **123**: p. 1902-1912.
243. Kurihara, L.J., *Nuclear congression and membrane fusion: two distinct events in the yeast karyogamy pathway.* The Journal of Cell Biology, 1994. **126**(4): p. 911-923.
244. Misuzu Baba, N.B., Yoshunori Ohsumi, Koichi Kanaya and Masako Osumi <*Three-dimensional analysis of morphogenesis induced by mating pheromone a factor in Saccharomyces cerevisiae.pdf>.* Journal of Cell Science, 1989. **94**: p. 207-216.
245. M.Osumi, *Mating Reaction in Saccharomyces cerevisiae V. Changes in the Fine Structure during the Mating Reaction.* Microbiology, 1974. **97**: p. 27-38.
246. Valeria Brizzio, A.E.G., and Mark D. Rose, <*Rvs161p Interacts with Fus2p to Promote Cell Fusion in Saccharomyces cerevisiae.pdf>.* Journal of Cell Biology, 1998. **141**: p. 567-584.
247. Richard A. Stein, J.A.S., and Mark D. Rose, *An Amphiphysin-Like Domain in Fus2p Is Required for Rvs161p Interaction and Cortical Localization.* G3 (Bethesda), 2015. **6**: p. 337-349.
248. Rose, J.A.S.a.M.D., *Kel1p Mediates Yeast Cell Fusion Through a Fus2p- and Cdc42p-Dependent Mechanism.* Genetics, 2016. **202**: p. 1421-1435.
249. Jean A. Smith, A.E.H., and Mark D. Rose, *Membrane curvature directs the localization of Cdc42p to novel foci required for cell–cell fusion.* Journal of Cell Biology, 2017. **216**(12): p. 3971-3980.
250. Joanna Mathis Paterson , C.A.Y., and Mark D. Rose, *Dynamic localization of yeast Fus2p to an expanding ring at the cell fusion junction during mating.* Journal of Cell Biology, 2008. **181**(4): p. 697-709.
251. **Herskowitz, J.P.a.I.**, *Identification of Kel1p, a Kelch Domain-containing Protein Involved in Cell Fusion and Morphology in Saccharomyces cerevisiae.* Journal of Cell Biology, 1998. **143**(2): p. 375-389.
252. Josephine Adams, R.K.a.L.C., *The kelch repeat superfamily of proteins: propellers of cell function.* Trends Cell Biol, 2000. **10**: p. 17-24.
253. Elion, E.A., Trueheart, J and Fink, G., *Fus2 localizes near the site of cell fusion and is required for both cell fusion and nuclear alignment during zygote formation.* The Journal of Cell Biology, 1995. **130**(6): p. 1283-1296.
254. Pierre Sivadon, M.-F.P., Francois Doignon, Michle Aigle and Marc Crouzet, *Cloning of the Multicopy Suppressor Gene SUR7- Evidence for a Functional Relationship between the Yeast Actin-binding Protein Rvs167 and a Putative Membranous Protein.pdf>.* Yeast, 1997. **13**: p. 747-761.
255. Rose, A.E.H.a.M.D., *Cell Fusion in Yeast is Negatively Regulated by Components of the Cell Wall Integrity Pathway.* Journal of Cell Biology, 2018.
256. Lori B. Huberman, A.W.M., *A Model for Cell Wall Dissolution in Mating Yeast Cells: Polarized Secretion and Restricted Diffusion of Cell Wall Remodeling Enzymes Induces Local Dissolution.* PLoS ONE, 2014. **9**(10): p. e109780.
257. Brawley, R.S.a.V., *Localized deposition of chitin on the yeast cell surface in response to mating pheromone.* PNAS, 1979. **76**(2): p. 645-649.
258. Won-Ja choi, B.S., Angel Duran, and Enrico Cabib, *Are Yeast Chitin Synthases Regulated at the Transcriptional or the PosttranslationalLevel?* Mol Cell Biol, 1994. **14**(12): p. 7685-7694.

259. Beatriz Santos, A.D.a.M.H.V., *CHS5, a Gene Involved in Chitin Synthesis and Mating in Saccharomyces cerevisiae.* Molecular and Cellular Biology, 1997. **17**(5): p. 2485-2496.
260. Snyder, B.S.a.M., *Targeting of Chitin Synthase 3 to Polarized Growth Sites in Yeast Requires Chs5p and Myo2p.* Journal of Cell Biology, 1997. **136**(1): p. 95-110.
261. J. Andrew Shaw, P.M., Blair Bowers, Sanford J.Silverman, M .Henar Valdivieso, Angel Durdn, and Enrico Cabib, *The Function of Chitin Synthases 2 and 3 in the Saccharomyces cerevisiae Cell Cycle.* Journal of Cell Biology, 1991. **114**(1): p. 111-123.
262. M .Henar Valdivieso, P.C.M., J.Andrew Shaw, Enrico Cabib, and Angel Durán, *CAL1, A Gene Required for Activity of Chitin Synthase 3 in Saccharomyces cerevisiae.* Journal of Cell Biology, 1991. **114**(1): p. 101-109.
263. ACHSTETTER, U.A.a.T., *Hormone-inducedexpression of the CHSl gene from Saccharomyces cerevisiae.* Eur. J.Biochem, 1989. **181**: p. 243-247.
264. Kevin Redding, C.H., and Robert S. Fuller, *Immunolocalization of Kex2 Protease Identifies a Putative Late Golgi Compartment in the Yeast Saccharomyces cerevisiae.* Journal of Cell Biology, 1991. **113**(3): p. 527-538.
265. Alex Franzusoff, K.R., Jeff Crosby, Robert S. Fuller, and Randy Schekman, *Localization of Components Involved in Protein Transport and Processing through the Yeast Golgi Apparatus.* Journal of Cell Biology, 1991. **112**(1): p. 27-37.
266. Walter, M.G.H.a.P., *Prm1p, a Pheromone-regulated Multispanning Membrane Protein, Facilitates Plasma Membrane Fusion during Yeast Mating.* Journal of Cell Biology, 2000. **151**(3): p. 719-730.
267. Nolan, S., et al., *FUS1 regulates the opening and expansion of fusion pores between mating yeast.* Mol Biol Cell, 2006. **17**(5): p. 2439-50.
268. Olmo, V.N. and E. Grote, *Prm1 functions as a disulfide-linked complex in yeast mating.* J Biol Chem, 2010. **285**(4): p. 2274-83.
269. Jin, H., et al., *Prm1 prevents contact-dependent lysis of yeast mating pairs.* Eukaryot Cell, 2004. **3**(6): p. 1664-73.
270. Curto, M.A., et al., *Membrane organization and cell fusion during mating in fission yeast requires multipass membrane protein Prm1.* Genetics, 2014. **196**(4): p. 1059-76.
271. Pablo S. Aguilar, A.E., and Peter Walter, *The Plasma Membrane Proteins Prm1 and Fig1 Ascertain Fidelity of Membrane Fusion during Yeast Mating.* Mol Biol Cell, 2007. **18**: p. 547-556.
272. Heiman, M.G., A. Engel, and P. Walter, *The Golgi-resident protease Kex2 acts in conjunction with Prm1 to facilitate cell fusion during yeast mating.* J Cell Biol, 2007. **176**(2): p. 209-22.
273. Erdman, S., et al., *Pheromone-regulated Genes Required for Yeast Mating Differentiation.* The Journal of Cell Biology, 1998. **140**(3): p. 461-483.
274. Van Itallie, C.M., and James Melvin Anderson., *The molecular physiology of tight junction pores.* Physiology, 2004. **19**(6): p. 331-338.
275. Clemente-Ramos, J.A., et al., *The tetraspan protein Dni1p is required for correct membrane organization and cell wall remodelling during mating in Schizosaccharomyces pombe.* Mol Microbiol, 2009. **73**(4): p. 695-709.
276. Curto, M.A., et al., *The ancient claudin Dni2 facilitates yeast cell fusion by compartmentalizing Dni1 into a membrane subdomain.* Cell Mol Life Sci, 2018. **75**(9): p. 1687-1706.
277. Young, M.E., et al., *The Sur7p Family Defines Novel Cortical Domains in Saccharomyces cerevisiae, Affects Sphingolipid Metabolism, and Is Involved in Sporulation.* Molecular and Cellular Biology, 2002. **22**(3): p. 927-934.
278. Francisco J. Alvarez, L.M.D., Adam Rosebrock, and James B. Konopka, *The Sur7 Protein Regulates Plasma Membrane Organization and Prevents Intracellular Cell Wall Growth in Candida albicans.pdf>.* Mol Biol Cell, 2008. **19**: p. 5214-5225.
279. Eric M. Muller, N.A.M., Scott E. Erdman, and Kyle W. Cunningham, *<Fig1p Facilitates Ca2+ Influx and Cell Fusion During Mating of Saccharomyces cerevisiae.pdf>.* J Biol Chem, 2003.
280. Gunzel, D. and A.S. Yu, *Claudins and the modulation of tight junction permeability.* Physiol Rev, 2013. **93**(2): p. 525-69.
281. Mikio Furuse, K.F., Takashi Hiiragi, Kazushi Fujimoto and Shoichiro Tsukita, *Claudin-1 and -2: Novel Integral Membrane Proteins Localizing at Tight Junctions with No Sequence Similarity to Occludin.* Journal of Cell Biology, 1998. **141**(7): p. 1539-1550.

282. Nan-Nan Zhang, D.D.D., Saurabh Paliwal, Andre Levchenko, Eric Grote, and Kyle W. Cunningham, *Multiple Signaling Pathways Regulate Yeast Cell Death during the Response to Mating Pheromones.* Molecular Biology of the Cell, 2006. **17**: p. 3409-3422.
283. David Julius, A.B., Lindley Blair, Riyo Kunisawa, and Jeremy Thorner, *Isolation of the Putative Structural Gene for the Lysine-Arginine-Cleaving Endopeptidase Required for Processing of Yeast Prepro-alpha-Factor.* Cell, 1984. **37**: p. 1075-1089.
284. Robert S. Fuller, A.B.a.J.T., <*Yeast prohormone processing enzyme (KEX2 gene product) is a Ca2+-dependent serine protease.pdf*>. Proc Natl Acad Sci U S A, 1988. **86**: p. 1434-1438.
285. Bussey, A.C.a.H., *Yeast Kex1p Is a Golgi-associated Membrane Protein- Deletions in a Cytoplasmic Targeting Domain Result in Mislocalization to the Vacuolar Membrane.* Journal of Cell Biology, 1992. **119**(6): p. 1459-1468.
286. Yves Bourbonnais, D.G., Lilian Latchinian-Sadek, Guy Boileau, David Y. Thomas, *Prohormone Processing by Yeast Proteases.* Enzyme, 1991. **45**: p. 244-256.
287. Schneiter, R., et al., *Electrospray Ionization Tandem Mass Spectrometry (Esi-Ms/Ms) Analysis of the Lipid Molecular Species Composition of Yeast Subcellular Membranes Reveals Acyl Chain-Based Sorting/Remodeling of Distinct Molecular Species En Route to the Plasma Membrane.* The Journal of Cell Biology, 1999. **146**(4): p. 741-754.
288. Meer, G.v., *Lipids of the Golgi membrane.* Trends in Cell Biology, 1998. **8**: p. 29-33.
289. Günther Daum, N.D.L., Martin Bard and Robert Dickson, *Biochemistry, Cell Biology and Molecular Biology of Lipids of Saccharomyces cerevisiae.* Yeast, 1998. **14**: p. 1471-1510.
290. Jorge Cerbón, V.C., *Generation, modulation and maintenance of the plasma membrane asymmetric phospholipid composition in yeast cells during growth: their relation to surface potential and membrane protein activity.* Biochimica et Biophysica Acta, 1995. **1235**: p. 100-106.
291. Jin, H., J.M. McCaffery, and E. Grote, *Ergosterol promotes pheromone signaling and plasma membrane fusion in mating yeast.* J Cell Biol, 2008. **180**(4): p. 813-26.
292. Erwin Zinser, F.P., And Günther Daum, *Sterol Composition of Yeast Organelle Membranes and Subcellular Distribution of Enzymes Involved in Sterol Metabolism.* Journal of Bacteriology, 1993. **175**(10): p. 2853-2858.
293. Hancock, J.F., *Lipid rafts- contentious only from simplistic standpoints.* Nature, 2006. **7**: p. 456-462.
294. Aguilar, P.S., et al., *Structure of sterol aliphatic chains affects yeast cell shape and cell fusion during mating.* Proc Natl Acad Sci U S A, 2010. **107**(9): p. 4170-5.
295. Tiedje, C., et al., *Proteins involved in sterol synthesis interact with Ste20 and regulate cell polarity.* J Cell Sci, 2007. **120**(Pt 20): p. 3613-24.
296. Woodman, S., et al., *Yeast membrane lipid imbalance leads to trafficking defects toward the Golgi.* Cell Biol Int, 2018. **42**(7): p. 890-902.
297. Weliky, W.Q.a.D.P., *HIV Fusion Peptide and Its Cross-Linked Oligomers- Efficient Syntheses, Significance of the Trimer in Fusion Activity, Correlation of Strand Conformation with Membrane Cholesterol, and Proximity to Lipid Headgroups.* Biochemistry, 2009. **48**: p. 289-301.
298. Chang, J., et al., *Fusion step-specific influence of cholesterol on SNARE-mediated membrane fusion.* Biophys J, 2009. **96**(5): p. 1839-46.
299. Czub, J. and M. Baginski, *Comparative molecular dynamics study of lipid membranes containing cholesterol and ergosterol.* Biophys J, 2006. **90**(7): p. 2368-82.
300. Jean-Philippe Richard, E.L., Ralf Langen, William Mike Henne, Margarita Popova, Tamas Balla, Harvey T. MCmahon, Michael M. Kozlov andd Leonid V. Chernomordik, *Intracellular curvature-generating proteins in cell-to-cell fusion.* Biochem J, 2011. **440**: p. 185-193.
301. Thorner, H.G.D.a.J.W., *Regulation of G protein–initiated signal transduction in yeast-Paradigms and Principles.* Annu Rev Biochem, 2001. **70**: p. 703-754.
302. Hiten D. Madhani, a.G.R.F., *The riddle of MAP kinase signaling specificity.* Trends in Genetics, 1998. **14**(4): p. 151-155.
303. Tim Köhler, S.W., Naimeh Taheri, Gerhard H. Braus, and Hans-Ulrich Mösch, *Dual Role of the Saccharomyces cerevisiae TEA:ATTS Family Transcription Factor Tec1p in Regulation of Gene Expression and Cellular Development.* Eukaryot Cell, 2002. **1**(5): p. 673-686.
304. L. Oehlen, F.R.C., *The mating factor response pathway regulates transcription of TEC1, a gene involved in pseudohyphal di¡erentiation of Saccharomyces cerevisiae.* FEBS Letters, 1998. **429**: p. 83-88.

305. Hiten D. Madhani, C.A.S., and Gerald R. Fink, *MAP Kinases with Distinct InhibitoryFunctions Impart Signaling Specificity during Yeast Differentiation.* Cell, 1997. **91**: p. 673-684.
306. Walid Sabbagh, J., Laura J. Flatauer, A. Jane Bardwell, and Lee Bardwell, *Specificity of MAP Kinase Signaling in Yeast Differentiation Involves Transient versus Sustained MAPK Activation.* Molecular Cell, 2001. **8**: p. 683-691.
307. Julia Zeitlinger, I.S., Christopher T. Harbison, Nancy M. Hannett, Thomas L. Volkert, Gerald R. Fink, and Richard A. Young, *Program-Specific Distribution of a Transcription Factor Dependent on Partner Transcription Factor and MAPK Signaling.* Cell, 2003. **113**: p. 395-404.
308. Ashton Breitkreutz, L.B.a.M.T., *MAPK specificity in the yeast pheromone response independent of transcriptional activation.* Current Biology, 2001. **11**: p. 1266-1271.
309. Bao, M.Z., et al., *Pheromone-dependent destruction of the Tec1 transcription factor is required for MAP kinase signaling specificity in yeast.* Cell, 2004. **119**(7): p. 991-1000.
310. Fink, R.L.R.a.G.R., *Elements of a single MAP kinase cascade in Saccharomyces cerevisiae mediate two developmental programs in the same cell type- mating and invasive growth.* Genes & Development, 1994. **8**: p. 2974-2985.
311. Hans-Ulrich Mösch, R.L.R., and Gerald R. Fink, *Ras2 signals via the Cdc42:Ste20:mitogen-activated protein kinase module to induce filamentous growth in Saccharomyces cerevisiae.* Proc Natl Acad Sci U S A, 1996. **93**: p. 5352-5356.
312. Philip, B. and D.E. Levin, *Wsc1 and Mid2 are cell surface sensors for cell wall integrity signaling that act through Rom2, a guanine nucleotide exchange factor for Rho1.* Mol Cell Biol, 2001. **21**(1): p. 271-80.
313. James Verna, A.L., Kyunghee Lee, Alicia Vagts, and Roymarie Ballester, *A family of genes required for maintenance of cell wall integrity and for the stress response in Saccharomyces cerevisiae.* Proc Natl Acad Sci U S A, 1997. **94**: p. 13804-13809.
314. Troy Ketela, R.G., and Howard Bussey, *Saccharomyces cerevisiae Mid2p Is a Potential Cell Wall Stress Sensor and Upstream Activator of the PKC1-MPK1 Cell Integrity Pathway.* Journal of Bacteriology, 1999. **181**(11): p. 3330-3340.
315. Mathumathi Rajavel, B.P., Benjamin M. Buehrer, Beverly Errede, and David E. Levin, *Mid2 Is a Putative Sensor for Cell Integrity Signaling in Saccharomyces cerevisiae.* Molecular and Cellular Biology, 1999. **19**(6): p. 3969-3976.
316. Levin, D.E., *Cell wall integrity signaling in Saccharomyces cerevisiae.* Microbiol Mol Biol Rev, 2005. **69**(2): p. 262-91.
317. Hutzler, F., et al., *Protein N-glycosylation determines functionality of the Saccharomyces cerevisiae cell wall integrity sensor Mid2p.* Mol Microbiol, 2008. **68**(6): p. 1438-49.
318. Vay, H.A., B. Philip, and D.E. Levin, *Mutational analysis of the cytoplasmic domain of the Wsc1 cell wall stress sensor.* Microbiology (Reading), 2004. **150**(Pt 10): p. 3281-8.
319. Kumi Ozaki, K.T., Hiroshi Imamura, Taro Hihara, Takaaki Kameyama, Hidetaro Nonaka, Hisanobu Hirano,Yoshiharu Matsuura and Yoshimi Takai, *Rom1p and Rom2p are GDP:GTP exchange proteins (GEPs) for the Rhoip small GTP binding protein in Saccharomyces cerevisiae.* EMBO J, 1996. **15**(9): p. 2196-2207.
320. David E. Levin, F.O.F., Riyo Kunisawa, J. Michael Bishop, and Jeremy Thorner, *A Candidate Protein Kinase C Gene, PKC1, Is Required for the S. cerevisiae Cell Cycle.* Cell, 1990. **62**: p. 213-224.
321. Levin, K.S.L.a.D.E., *Dominant mutations in a gene encoding a Putative Protein Kinase (BCKI) bypass the requirement for a Saccharomyces cerevisiae Protein Kinase C Homolog.* Molecular and Cellular Biology, 1992. **12**(1): p. 172-182.
322. Kenji Irie, M.T., Kyung S.Lee, David E.Levin, Hiroyuki Araki, Kunihiro Matsumoto, and Yasuji Oshima, *MKK1 and MKK2, which encode Saccharomyces cerevisiae Mitogen-Activated Protein Kinase-Kinase Homologs, function in the pathway mediated by Protein Kinase C.* Molecular and Cellular Biology, 1993. **13**(5): p. 3076-3083.
323. Yasuyuki Watanabe, G.T., Masatoshi Hagiwara, Kenji Irie, and Kunihiro Matsumoto, *Characterization of a Serum Response Factor-Like Protein in Saccharomyces cerevisiae, Rlm1, Which Has Transcriptional Activity Regulated by the Mpk1 (Slt2) Mitogen-Activated Protein Kinase Pathway.* Molecular and Cellular Biology, 1997. **17**(5): p. 2615-2623.
324. Levin, U.S.J.a.D.E., *Genome-wide analysis of gene expression regulated by the yeast cell wall integrity signalling pathway.pdf>.* Molecular Microbiology, 1999. **34**(5): p. 1049-1057.

325. Hidetaro Nonaka, K.T., Hisanobu Hirano, Takeshi Fujiwara, Hideshi Kohno, Masato Umikawa, Akihisa Mino and Yoshimi Takai, *A downstream target of RHO1 small GTP-binding protein is PKC1, a homolog of protein kinase C, which leads to activation of the MAP kinase cascade in Saccharomyces cerevisiae.* EMBO J, 1995. **14**(23): p. 5931-5938.
326. Errede, B.M.B.a.B., *Coordination of the Mating and Cell Integrity Mitogen-Activated Protein Kinase Pathways in Saccharomyces cerevisiae.* Molecular and Cellular Biology, 1997. **17**(11): p. 6517-6525.
327. Hall, A.E., and Mark D. Rose, *Cell fusion in yeast is negatively regulated by components of the cell wall integrity pathway.* Molecular biology of the cell, 2019. **30**(4): p. 441-452.
328. Hidetoshi Iida, H.N., Tomoko Ono, Makiko S. Okumura, And Yasuhiro Anraku, *MID1, a Novel Saccharomyces cerevisiae Gene Encoding a Plasma Membrane Protein, Is Required for Ca^{2+} Influx and Mating.* Molecular and Cellular Biology, 1994. **14**(12): p. 8259-8271.
329. Tomoko Ono, T.S., Yasuhiro Anraku and Hidetoshi Iida, *The MID2 gene encodes a putative integral membrane protein with a Ca^{2+}-binding domain and shows mating pheromone-stimulated expression in Saccharomyces cerevisiae.* Gene, 1994. **151**(1-2): p. 203-208.
330. Philips, J. and I. Herskowitz, *Osmotic Balance Regulates Cell Fusion during Mating in Saccharomyces cerevisiae.* The Journal of Cell Biology, 1997. **138**(5): p. 961-974.
331. Laura Merlini, O.D.a.S.G.M., *Mate and fuse: how yeast cells do it.pdf.* Open Biology, 2013. **3**.
332. Roux, K.J., et al., *A promiscuous biotin ligase fusion protein identifies proximal and interacting proteins in mammalian cells.* J Cell Biol, 2012. **196**(6): p. 801-10.
333. Chen, C.L. and N. Perrimon, *Proximity-dependent labeling methods for proteomic profiling in living cells.* Wiley Interdiscip Rev Dev Biol, 2017. **6**(4).
334. Sikorski, R.S., and Philip Hieter., *A system of shuttle vectors and yeast host strains designed for efficient manipulation of DNA in Saccharomyces cerevisiae.* Genetics, 1989. **122**(1): p. 19-27.
335. Carsten Janke, M.M.M., Nicole Rathfelder, Christof Taxis, Simone Reber,, A.M.-B. Hiromi Maekawa, Georg Doenges, Etienne Schwob, Elmar Schiebel, and a.M. Knop, *A versatile toolbox for PCR-based tagging of yeast genes: new fluorescent proteins, more markers and promoter substitution cassettes.* Yeast, 2004. **21**: p. 947-962.
336. Longtine, M.S., et al., *Additional modules for versatile and economical PCR-based gene deletion and modification in Saccharomyces cerevisiae.* Yeast, 1998. **14**(10): p. 953-961.
337. Houseley, J. and D. Tollervey, *Repeat expansion in the budding yeast ribosomal DNA can occur independently of the canonical homologous recombination machinery.* Nucleic acids research, 2011. **39**(20): p. 8778-8791.
338. Brachmann, C.B., Adrian Davies, Gregory J. Cost, Emerita Caputo, Joachim Li, Philip Hieter, and Jef D. Boeke. , *Designer deletion strains derived from Saccharomyces cerevisiae S288C: a useful set of strains and plasmids for PCR-mediated gene disruption and other applications.* Yeast, 1998. **14**(2): p. 115-132.
339. Giaever, G., et al., *Functional profiling of the Saccharomyces cerevisiae genome.* nature, 2002. **418**(6896): p. 387-391.
340. Howson, R., et al., *Construction, verification and experimental use of two epitope-tagged collections of budding yeast strains.* Comp Funct Genomics, 2005. **6**(1-2): p. 2-16.
341. Coulson, F.S.a.A.R., *A Rapid Method for Determining Sequences in DNA by Primed Synthesis with DNA Polymerase.* J Mol Biol, 1975. **94**: p. 441-448.
342. Knop, M., Katja Siegers, Gislene Pereira, Wolfgang Zachariae, Barbara Winsor, Kim Nasmyth, and Elmar Schiebel., *Epitope Tagging of Yeast Genes using a PCR-based Strategy: More Tags and Improved Practical Routines.* Yeast, 1999. **15**(10B): p. 963-972.
343. Blount, B.A., M.R. Driessen, and T. Ellis, *GC Preps: Fast and Easy Extraction of Stable Yeast Genomic DNA.* Sci Rep, 2016. **6**: p. 26863.
344. Landgraf, D., et al., *Scarless Gene Tagging with One-Step Transformation and Two-Step Selection in Saccharomyces cerevisiae and Schizosaccharomyces pombe.* PLoS One, 2016. **11**(10): p. e0163950.
345. Jef D. Boeke, J.T., Georges Natsoulis, and Gerald R. Fink, *5-Fluoroorotic Acid as a Selective Agent in Yeast Molecular Genetics.* Methods in enzymology, 1987. **154**: p. 164-175.

346. Achim Wach, A.B., Rainer Pohlmann and Peter Philippsen, *New Heterologous Modules for Classical or PCR-based Gene Disruptions in Saccharomyces cerevisiae.* Yeast, 1994. **10**: p. 1793-1808.
347. Bilinski, C.A. and J.J. Miller, *Induction of normal ascosporogenesis in two-spored Saccharomyces cerevisiae by glucose, acetate, and zinc.* Journal of bacteriology, 1980. **143**(1): p. 343-348.
348. Salzman, V., et al., *Quantitation of yeast cell-cell fusion using multicolor flow cytometry.* Cytometry A, 2015. **87**(9): p. 843-54.
349. McCullagh, E., et al., *Coordinate control of gene expression noise and interchromosomal interactions in a MAP kinase pathway.* Nature cell biology, 2010. **12**(10): p. 954-962.
350. Grote, E., *Cell Fusion Assays for Yeast Mating Pairs.* Methods in Molecular Biology, 2008. **475**.
351. Laemmli, U.K., *Cleavage of Structural Proteins during the Assembly of the Head of Bacteriophage T4* Nature, 1970. **227**: p. 680-685.
352. Tsirigos, K.D., et al., *The TOPCONS web server for consensus prediction of membrane protein topology and signal peptides.* Nucleic acids research, 2015. **43**(W1): p. W401-W407.
353. Hildebrand, A., et al., *Fast and accurate automatic structure prediction with HHpred.* Proteins: Structure, Function, and Bioinformatics, 2009. **77**(S9): p. 128-132.
354. Pettersen, E.F., et al., *UCSF Chimera—a visualization system for exploratory research and analysis.* Journal of computational chemistry, 2004. **25**(13): p. 1605-1612.
355. Pablo S. Aguilar, A.E.a.P.W., *The Plasma Membrane Proteins Prm1 and Fig1 Ascertain Fidelity of Membrane Fusion during Yeast Mating.* Molecular Biology of the Cell, 2007. **18**: p. 547-556.
356. Eric M. Muller, N.A.M., Scott E. Erdman, and Kyle W. Cunningham, *Fig1p Facilitates Ca2+ Influx and Cell Fusion During Mating of Saccharomyces cerevisiae.pdf.* J Biol Chem, 2003.
357. Scott Erdman, L.L., Michael Malczynski, and Michael Snyder, *Pheromone-regulated Genes Required for Yeast Mating Differentiation.* Journal of Cell Biology, 1998. **140**(3): p. 461-483.
358. Shaner, N.C., et al., *A bright monomeric green fluorescent protein derived from Branchiostoma lanceolatum.* Nat Methods, 2013. **10**(5): p. 407-9.
359. Jinah Kim, E.B., Hualin Zhong, Thomas Leeuw, Ekkehard Leberer, Andrew K. Vershon, and Jeanne P. Hirsch, *Localization and Signaling of Gb Subunit Ste4p Are Controlled by a-Factor Receptor and the a-Specific Protein Asg7p.* Molecular and Cellular Biology, 2000. **20**(23): p. 8826-8835.
360. Sawai, H., et al., *Identification of ISC1 (YER019w) as inositol phosphosphingolipid phospholipase C in Saccharomyces cerevisiae.* J Biol Chem, 2000. **275**(50): p. 39793-8.
361. Vaena de Avalos, S., Y. Okamoto, and Y.A. Hannun, *Activation and localization of inositol phosphosphingolipid phospholipase C, Isc1p, to the mitochondria during growth of Saccharomyces cerevisiae.* J Biol Chem, 2004. **279**(12): p. 11537-45.
362. Won-Ki Huh, J.V.F., Luke C. Gerke, Adam S. Carroll, Russell W. Howson, Jonathan S. Weissman & Erin K. O'Shea, *Global analysis of protein localization in budding yeast.pdf.* Nature, 2003. **425**: p. 686-691.
363. Valeria Brizzio, A.E.G., and Mark D. Rose, *Rvs161p Interacts with Fus2p to Promote Cell Fusion in Saccharomyces cerevisiae.pdf.* Journal of Cell Biology, 1998. **141**: p. 567-584.
364. Hosiner, D., et al., *Pun1p is a metal ion-inducible, calcineurin/Crz1p-regulated plasma membrane protein required for cell wall integrity.* Biochim Biophys Acta, 2011. **1808**(4): p. 1108-19.
365. Xu, T., et al., *A profile of differentially abundant proteins at the yeast cell periphery during pseudohyphal growth.* J Biol Chem, 2010. **285**(20): p. 15476-88.
366. Guido Grossmann, M., J.M. Opekarova´, and I.W.-M.a.W. Tanner, *Membrane potential governs lateral segregation of plasma membrane proteins and lipids in yeast.pdf>.* EMBO, 2007. **26**: p. 1-7.
367. Malínská, K., Jan Malínský, Miroslava Opekarová, and Widmar Tanner., *Visualization of protein compartmentation within the plasma membrane of living yeast cells.* Molecular biology of the cell, 2003. **14**(11): p. 4427-4436.
368. Grossmann, G., Miroslava Opekarova, Jan Malinsky, Ina Weig-Meckl, and Widmar Tanner, *Membrane potential governs lateral segregation of plasma membrane proteins and lipids in yeast.* The EMBO journal, 2007. **26**(1): p. 1-8.

369. Walther, T.C., Jason H. Brickner, Pablo S. Aguilar, Sebastián Bernales, Carlos Pantoja, and Peter Walter. , *Eisosomes mark static sites of endocytosis.* Nature, 2006. **439**(7079): p. 998.
370. Malinska, K., et al., *Distribution of Can1p into stable domains reflects lateral protein segregation within the plasma membrane of living S. cerevisiae cells.* J Cell Sci, 2004. **117**(Pt 25): p. 6031-41.
371. Grossmann, G., Jan Malinsky, Wiebke Stahlschmidt, Martin Loibl, Ina Weig-Meckl, Wolf B. Frommer, Miroslava Opekarová, and Widmar Tanner, *Plasma membrane microdomains regulate turnover of transport proteins in yeast.* J Cell Biol, 2008. **183**(6): p. 1075-1088.
372. Starita, L.M., et al., *Sites of ubiquitin attachment in Saccharomyces cerevisiae.* Proteomics, 2012. **12**(2): p. 236-40.
373. Kung, L.A., et al., *Global analysis of the glycoproteome in Saccharomyces cerevisiae reveals new roles for protein glycosylation in eukaryotes.* Mol Syst Biol, 2009. **5**: p. 308.
374. Mikio Furuse, H.S., Kazushi Fujimoto and Shoichiro Tsukita, *A Single Gene Product, Claudin-1 or -2, Reconstitutes Tight Junction Strands and Recruits Occludin in Fibroblasts.* Journal of Cell Biology, 1998. **143**(2): p. 391-401.
375. Kelley, L.A., et al., *The Phyre2 web portal for protein modeling, prediction and analysis.* Nat Protoc, 2015. **10**(6): p. 845-58.
376. Nakamura, S., et al., *Morphologic determinant of tight junctions revealed by claudin-3 structures.* Nat Commun, 2019. **10**(1): p. 816.
377. Hiroshi Suzuki, T.N., Kazutoshi Tani, Yuji Yamazaki, Atsushi Tamura, Ryuichiro Ishitani, Naoshi Dohmae, Sachiko Tsukita, Osamu Nureki and Yoshinori Fujiyoshi, *Crystal Structure of a Claudin Provides Insight into the Architecture of Tight Junctions.pdf.* Science, 2014. **344**: p. 304-306.
378. Curto, M.-Á., Sandra Moro, Francisco Yanguas, Carmen Gutiérrez-González, and M-Henar Valdivieso., *The ancient claudin Dni2 facilitates yeast cell fusion by compartmentalizing Dni1 into a membrane subdomain.* Cellular and molecular life sciences, 2017. **75**(9): p. 1687-1706.
379. Emr, T.A.V.a.S.D., *A New Vital Stain for Visualizing Vacuolar Membrane Dynamics and Endocytosis in Yeast.* Journal of Cell Biology, 1995. **128**(5): p. 779-792.
380. V´ictor J. Cid, A.D.n., Francisco Del Rey, Michael P. Snyder, Ce´sar Nombela, and Miguel Sa´nchez, *Molecular Basis of Cell Integrity and Morphogenesis in Saccharomyces cerevisiae.* Microbiological Reviews, 1995. **59**(3): p. 345-386.
381. Lagorce, A., et al., *Genome-wide analysis of the response to cell wall mutations in the yeast Saccharomyces cerevisiae.* J Biol Chem, 2003. **278**(22): p. 20345-57.
382. Kollar, R., et al., *Architecture of the yeast cell wall. Beta(1-->6)-glucan interconnects mannoprotein, beta(1-->)3-glucan, and chitin.* J Biol Chem, 1997. **272**(28): p. 17762-75.
383. Gertien J Smits, J.C.K., Herman van den Ende and Frans M Klis, *Cell wall dynamics in yeast.* Current Opinion in Microbiology, 1999. **2**: p. 348-352.
384. Christine E. Bulawa, M.S., Enrico Cabib, Janice Au-Young, Adriana Sburlati, W. Lee Adair, Jr., and Phillips W. Robbins, *The S. cerevisiae Structural Gene for Chitin Synthase Is Not Required for Chitin Synthesis In Vivo.* Cell, 1986. **46**: p. 213-225.
385. Jesus Molano, B.B., and Enrico Cabib, *Distribution of chitin in the yeast cell wall- An Ultrastructural and Chemical Study.* Journal of Cell Biology, 1980. **85**: p. 199-212.
386. Morita, K., Mikio Furuse, Kazushi Fujimoto, and Shoichiro Tsukita, *Claudin multigene family encoding four-transmembrane domain protein components of tight junction strands.* Proceedings of the National Academy of Sciences 96, 1999. **2**: p. 511-516.
387. Cording, J., et al., *In tight junctions, claudins regulate the interactions between occludin, tricellulin and marvelD3, which, inversely, modulate claudin oligomerization.* J Cell Sci, 2013. **126**(Pt 2): p. 554-64.
388. Li, J., et al., *Claudin-2 pore function requires an intramolecular disulfide bond between two conserved extracellular cysteines.* Am J Physiol Cell Physiol, 2013. **305**(2): p. C190-6.
389. Van Itallie, C.M. and J.M. Anderson, *Claudins and epithelial paracellular transport.* Annu Rev Physiol, 2006. **68**: p. 403-29.
390. Wen, H., et al., *Selective decrease in paracellular conductance of tight junctions: role of the first extracellular domain of claudin-5.* Mol Cell Biol, 2004. **24**(19): p. 8408-17.
391. Evans, M.J., Thomas von Hahn, Donna M. Tscherne, Andrew J. Syder, Maryline Panis, Benno Wölk, Theodora Hatziioannou, Jane A. McKeating, Paul D. Bieniasz, and Charles

M. Rice., *Claudin-1 is a hepatitis C virus co-receptor required for a late step in entry.* Nature, 2007. **446**(7137): p. 801.
392. Cukierman, L., et al., *Residues in a highly conserved claudin-1 motif are required for hepatitis C virus entry and mediate the formation of cell-cell contacts.* J Virol, 2009. **83**(11): p. 5477-84.
393. Van Itallie, C.M., L.L. Mitic, and J.M. Anderson, *Claudin-2 forms homodimers and is a component of a high molecular weight protein complex.* J Biol Chem, 2011. **286**(5): p. 3442-50.
394. Ong, S.E., et al., *Stable isotope labeling by amino acids in cell culture, SILAC, as a simple and accurate approach to expression proteomics.* Mol Cell Proteomics, 2002. **1**(5): p. 376-86.
395. Ross, P.L., et al., *Multiplexed protein quantitation in Saccharomyces cerevisiae using amine-reactive isobaric tagging reagents.* Mol Cell Proteomics, 2004. **3**(12): p. 1154-69.
396. Andrew Thompson, J.S., Karsten Kuhn, Stefan Kienle, Josef Schwarz, Günter Schmidt, Thomas Neumann, and Christian Hamon, *Tandem Mass Tags- A Novel Quantification Strategy for Comparative Analysis of Complex Protein Mixtures by MS/MS.* Anal. Chem, 2003. **75**: p. 1895-1904.
397. Cronan, J.E., *Targeted and proximity-dependent promiscuous protein biotinylation by a mutant Escherichia coli biotin protein ligase.* J Nutr Biochem, 2005. **16**(7): p. 416-8.
398. Choi-Rhee, E., H. Schulman, and J.E. Cronan, *Promiscuous protein biotinylation by Escherichia coli biotin protein ligase.* Protein Sci, 2004. **13**(11): p. 3043-50.
399. Anne Chapman-Smith and John E. Cronan, J., *Molecular Biology of Biotin Attachment to Proteins.* The Journal of Nutrition, 1999. **129**(2): p. 477S-484S.
400. Kim, D.I. and K.J. Roux, *Filling the Void: Proximity-Based Labeling of Proteins in Living Cells.* Trends Cell Biol, 2016. **26**(11): p. 804-817.
401. Varnaite, R. and S.A. MacNeill, *Meet the neighbors: Mapping local protein interactomes by proximity-dependent labeling with BioID.* Proteomics, 2016. **16**(19): p. 2503-2518.
402. Han, S., J. Li, and A.Y. Ting, *Proximity labeling: spatially resolved proteomic mapping for neurobiology.* Curr Opin Neurobiol, 2018. **50**: p. 17-23.
403. Rees, J.S., et al., *Selective Proteomic Proximity Labeling Assay Using Tyramide (SPPLAT): A Quantitative Method for the Proteomic Analysis of Localized Membrane-Bound Protein Clusters.* Curr Protoc Protein Sci, 2015. **80**: p. 19 27 1-19 27 18.
404. Jiang, S., et al., *A proteomics approach to the cell-surface interactome using the enzyme-mediated activation of radical sources reaction.* Proteomics, 2012. **12**(1): p. 54-62.
405. Martell, J.D., et al., *A split horseradish peroxidase for the detection of intercellular protein-protein interactions and sensitive visualization of synapses.* Nat Biotechnol, 2016. **34**(7): p. 774-80.
406. Hyun-Woo Rhee, P.Z., Namrata D. Udeshi, Jeffrey D. Martell, Vamsi K. Mootha, Steven A. Carr, Alice Y. Ting, *Proteomic Mapping of Mitochondria in Living Cells via Spatially Restricted Enzymatic Tagging.* Science, 2013. **339**(6125): p. 1328-1331.
407. Colin Hopkins, A.G., Jane Stinchcombe, and Clare Futter *Chimeric Molecules Employing Horseradish Peroxidase as Reporter Enzyme for Protein Localization in the Electron Microscope.* Methods in enzymology 2000. **327**: p. 35-45.
408. Hwang, J. and P.J. Espenshade, *Proximity-dependent biotin labelling in yeast using the engineered ascorbate peroxidase APEX2.* Biochem J, 2016. **473**(16): p. 2463-9.
409. Tomasz J. Proszynski, K.S., and Michel Bagnat, *O-Glycosylation as a Sorting Determinant for Cell Surface Delivery in Yeast.* Molecular Biology of the Cell, 2004. **15**: p. 1533-1543.
410. Hofken, T., *Ecm22 and Upc2 regulate yeast mating through control of expression of the mating genes PRM1 and PRM4.* Biochem Biophys Res Commun, 2017. **493**(4): p. 1485-1490.
411. Beverly Errede, R.M.C., Beverly M. Yashar, Yoshiaki Kamada, David E. Levin, Kenji Irie And Kunihiro Matsumot0, *Dynamics and Organization of MAP Kinase Signal Pathways.* Molecular Reproduction and Development, 1995. **42**: p. 477-485.
412. Janet Chenevert, N.V.a.I.H., *Identification of Genes Required for Normal Pheromone-Induced Cell ~ Polarization in Saccharomyces cerevisiae.* Genetics, 1994. **136**: p. 1287-1297.
413. Garcia, R., et al., *A novel connection between the Cell Wall Integrity and the PKA pathways regulates cell wall stress response in yeast.* Sci Rep, 2017. **7**(1): p. 5703.

414. Stradalova, V., et al., *Furrow-like invaginations of the yeast plasma membrane correspond to membrane compartment of Can1.* J Cell Sci, 2009. **122**(Pt 16): p. 2887-94.
415. Malinsky, J., M. Opekarova, and W. Tanner, *The lateral compartmentation of the yeast plasma membrane.* Yeast, 2010. **27**(8): p. 473-8.
416. Walther, T.C., et al., *Pkh-kinases control eisosome assembly and organization.* EMBO J, 2007. **26**(24): p. 4946-55.
417. Zhang, X., R.L. Lester, and R.C. Dickson, *Pil1p and Lsp1p negatively regulate the 3-phosphoinositide-dependent protein kinase-like kinase Pkh1p and downstream signaling pathways Pkc1p and Ypk1p.* J Biol Chem, 2004. **279**(21): p. 22030-8.
418. Sina Ghaemmaghami, W.-K.H., Kiowa Bower, Russell W. Howson, Archana Belle, Noah Dephoure, Erin K. O'Shea & Jonathan S. Weissman, *Global analysis of protein expression in yeast.* Nature, 2003. **425**: p. 737-741.
419. Zimmerberg, J. and S. McLaughlin, *Membrane curvature: how BAR domains bend bilayers.* Curr Biol, 2004. **14**(6): p. R250-2.
420. Olivera-Couto, A., et al., *The eisosome core is composed of BAR domain proteins.* Mol Biol Cell, 2011. **22**(13): p. 2360-72.
421. Ziolkowska, N.E., et al., *Eisosome-driven plasma membrane organization is mediated by BAR domains.* Nat Struct Mol Biol, 2011. **18**(7): p. 854-6.
422. Pérez-Ortín, S.P.A.J.E., *Stress response and expression patterns in wine fermentations of yeast genes induced at the diauxic shift.* Yeast, 2000. **16**: p. 139-148.
423. Paul T. Spellman, G.S., Michael Q. Zhang, Vishwanath R. Iyer, Kirk Anders, Michael B. Eisen, Patrick O. Brown, David Botstein, and Bruce Futcher, *Comprehensive Identification of Cell Cycle–regulated Genes of the Yeast Saccharomyces cerevisiae by Microarray Hybridization.* Molecular Biology of the Cell, 1998. **9**: p. 3273-3297.
424. Rodríguez-Peña, J.M., Rosa M. Pérez-Díaz, Sara Alvarez, Clara Bermejo, Raúl García, Catalina Santiago, Cesar Nombela, and Javier Arroyo, *The 'yeast cell wall chip' – a tool to analyse the regulation of cell wall biogenesis in Saccharomyces cerevisiae.* Microbiology, 2005. **151**(7): p. 2241-2249.
425. Conway, M.K., D. Grunwald, and W. Heideman, *Glucose, nitrogen, and phosphate repletion in Saccharomyces cerevisiae: common transcriptional responses to different nutrient signals.* G3 (Bethesda), 2012. **2**(9): p. 1003-17.
426. Gonzalez-Mariscal, L., R. Tapia, and D. Chamorro, *Crosstalk of tight junction components with signaling pathways.* Biochim Biophys Acta, 2008. **1778**(3): p. 729-56.
427. Chiba, H., et al., *Transmembrane proteins of tight junctions.* Biochim Biophys Acta, 2008. **1778**(3): p. 588-600.
428. Angelow, S., R. Ahlstrom, and A.S. Yu, *Biology of claudins.* Am J Physiol Renal Physiol, 2008. **295**(4): p. F867-76.
429. Krause, G., J. Protze, and J. Piontek, *Assembly and function of claudins: Structure-function relationships based on homology models and crystal structures.* Semin Cell Dev Biol, 2015. **42**: p. 3-12.
430. Daugherty, B.L., et al., *Regulation of heterotypic claudin compatibility.* J Biol Chem, 2007. **282**(41): p. 30005-13.
431. Suzuki, H., et al., *Model for the architecture of claudin-based paracellular ion channels through tight junctions.* J Mol Biol, 2015. **427**(2): p. 291-7.
432. Oscar R. Colegio, C.M.V.I., Heather J. Mccrea, Christoph Rahner, and James Melvin Anderson, *Claudins create charge-selective channels in the paracellular pathway between epithelial cells.pdf.* Am J Physiol Cell Physiol, 2002. **283**: p. C142-C147.
433. Konrad, M., et al., *Mutations in the tight-junction gene claudin 19 (CLDN19) are associated with renal magnesium wasting, renal failure, and severe ocular involvement.* Am J Hum Genet, 2006. **79**(5): p. 949-57.
434. Amasheh, S., et al., *Claudin-2 expression induces cation-selective channels in tight junctions of epithelial cells.* J Cell Sci, 2002. **115**(Pt 24): p. 4969-76.
435. Zihni, C., et al., *Tight junctions: from simple barriers to multifunctional molecular gates.* Nat Rev Mol Cell Biol, 2016. **17**(9): p. 564-80.
436. Varki, A., *Biological roles of oligosaccharides: all of the theories are correct.* Glycobiology, 1993. **3**(2): p. 97-130.
437. M. A. Kukuruzinska, M.L.E.B., and B. J. Jackson, *Protein Glycosylation In Yeast.* Annu Rev Biochem, 1987. **56**: p. 915-944.

438. Martin, D.C., et al., *New regulators of a high affinity Ca2+ influx system revealed through a genome-wide screen in yeast.* J Biol Chem, 2011. **286**(12): p. 10744-54.
439. Lazebnik, D.D.a.Y., *Cell-to-cell fusion as a link between viruses and cancer.* Nature Reviews Cancer, 2007. **7**(12): p. 968-976.

9 SUPPLEMENTARY INFORMATION

Table S1

Gene	Protein function according to the Saccharomyces Genome Database (SGD)
ASG7	*MAT***a** specific gene. Protein regulates pheromone response signalling via the G protein beta subunit Ste4p.
CHS1	Pheromone regulated gene encoding Chitin synthase 1. Required in chitin septum repair during cytokinesis.
FIG1	Factor- Induced gene 1 protein required in regulation of low affinity Ca2+ influx (LAC) system. Involved in PM fusion.
FUS3	Mitogen-activated serine/threonine protein kinase (MAPK) required in mating.
ISC1	Inositol phosphosphingolipid lipase C involved in sphingolipid catabolism.
PRM1	Pheromone-regulated membrane protein involved in PM fusion during mating.
PRM3	Pheromone-regulated membrane protein required in nuclear envelope fusion during karyogamy.
PRM4	Pheromone-regulated membrane protein proposed to function in yeast mating.
PRM5	Pheromone-regulated membrane protein involved in the cell integrity signaling.
PUN1	Plasma membrane protein upregulated during nitrogen stress. Protein co-localizes with Sur7p in punctate patches and is part of the cell wall integrity (CWI) pathway.
SAG1	Alpha-agglutinin expressed on *MATα* cells. Involved in agglutination by binding to Aga1p on *MAT***a** cells.
SST2	GTPase-activating protein involved in regulating desensitization to α-factor pheromone.
STE13	A Golgi-integral membrane Dipeptidyl aminopeptidase required for maturation of α-factor pheromone.
STE2	A seven Transmembrane G-protein coupled receptor (GPCR) protein for α-factor pheromone. Expressed in *MAT***a** cells.
YCR043C	Putative protein of unknown function.
YHR097C	Protein involved in clathrin-mediated endocytosis. Protein localizes to the cytoplasm and nucleus.
YIL108W	Putative metalloendopeptidase that form cytoplasmic foci during DNA replication stress.
YJL049W	Charged multivesicular body protein that localizes to the ER presumably as part of an ESCRT-III like complex.
YML131W	Protein of unknown function. Expression increases during osmotic shock or DNA replication stress.
YMR315W	Protein with NADP(H) oxidoreductase activity. Expression increases with increased DNA replication stress.
YNL208W	Protein of unknown function.
YNR065C	Protein of unknown function. Possible role in actin patch formation.
YNR066C	Putative membrane protein of unknown function.
YPR170W-B	Putative non-essential component of the vacuolar ATPase. Localizes to the vacuole membrane.

A

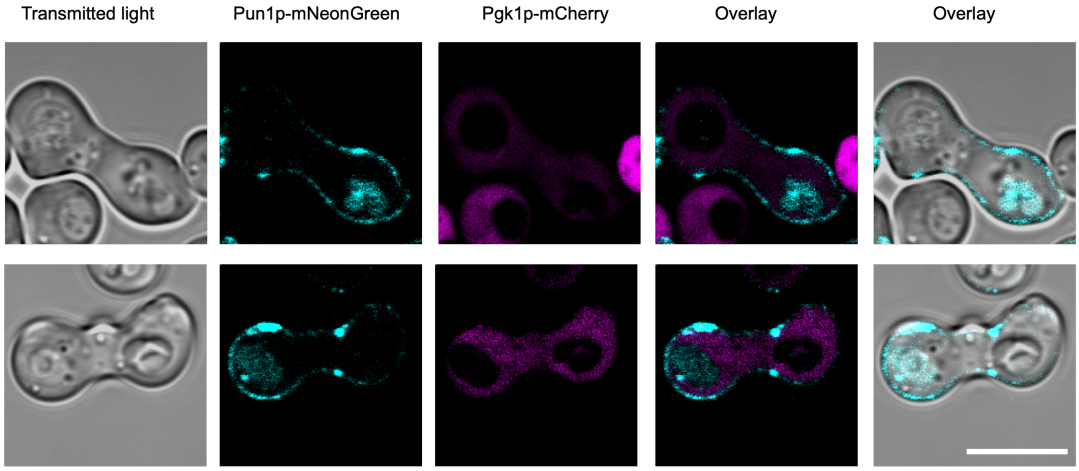

B

```
Command       hhsearch -cpu 8 -i ../results/full.a3m -d /cluster/toolkit/production/databases/hh-suite/mmcif70/pdb70 -d /clust

 No Hit                             Prob E-value P-value  Score    SS Cols Query HMM  Template HMM
  1 NP_013518.3 Pun1p [Saccharomyc 100.0 1.3E-33   2E-38  234.9  32.7  263    1-263     1-263 (263)
  2 NP_594296.1 SUR7 family protei 100.0 5.1E-29 7.6E-34  209.9  29.1  237    2-245     8-280 (288)
  3 NP_010059.1 Fmp45p [Saccharomy 100.0   3E-27 4.4E-32  199.8  26.9  207    3-245     4-210 (309)
  4 NP_013660.1 Sur7p [Saccharomyc 100.0   3E-27 4.5E-32  199.7  26.8  222    2-261     5-229 (302)
  5 NP_013548.1 Ecm7p [Saccharomyc 100.0 3.8E-26 5.7E-31  201.7  28.5  246    3-262    21-333 (448)
  6 NP_013517.1 Ina1p [Saccharomyc  99.9 1.5E-25 2.2E-30  203.7  24.8  244   14-260   399-650 (675)
  7 NP_014205.1 hypothetical prote  99.9 1.9E-24 2.8E-29  182.6  26.7  224    1-259     2-225 (301)
  8 NP_012734.1 Fat3p [Saccharomyc  99.9 5.8E-22 8.7E-27  185.6  22.8  227   17-261   428-665 (750)
  9 NP_116667.1 Dcv1p [Saccharomyc  99.9 1.1E-20 1.6E-25  151.3  17.1  196    1-257     2-202 (202)
 10 NP_594007.2 tetraspan protein   99.9 6.5E-20 9.7E-25  149.6  19.7  212    1-260     3-216 (234)
 11 NP_593706.1 membrane anchored   99.9 4.7E-20 7.1E-25  164.5  17.5  184    1-259     1-185 (756)
 12 NP_013779.1 Rim9p [Saccharomyc  99.8 1.8E-18 2.7E-23  141.8  20.4  190    3-261     1-193 (239)
 13 NP_588418.1 conserved fungal p  99.8 1.8E-18 2.7E-23  145.8  17.6  187    1-263     1-192 (336)
 14 NP_595474.1 tetraspan protein   99.8 3.8E-16 5.7E-21  128.0  22.2  200    7-262    25-231 (248)
 15 NP_009596.1 Fig1p [Saccharomyc  99.7 1.1E-15 1.6E-20  129.0  21.4  242    2-260    11-280 (298)
 16 NP_014623.1 hypothetical prote  99.7 4.4E-15 6.6E-20  132.5  19.4  183    2-258     4-197 (551)
 17 6JPA_E Voltage-dependent calci  99.4 1.4E-10 2.1E-15   93.2  19.1  216    1-261     3-220 (222)
 18 7KP4_A Claudin-4; Claudin, Ent  99.3 1.2E-09 1.7E-14   88.1  18.8  192    1-261     1-200 (214)
 19 6OV2_A Claudin-9; Claudin, Ent  99.3 1.6E-09 2.3E-14   87.5  19.4  192    1-261     1-200 (217)
 20 4P79_A Claudin-15; cell adhesi  99.2 6.7E-09   1E-13   82.3  19.0  186    1-257     4-198 (198)
 21 7LDD_H Voltage-dependent calci  99.1 8.1E-09 1.2E-13   92.0  15.0  202    1-258    15-240 (423)
 22 3X29_A Claudin-19; TOXIN-CELL   99.0 3.5E-08 5.2E-13   77.6  15.8  176    1-244     1-185 (185)
 23 6C14_B LHFPL tetraspan subfami  99.0 7.2E-08 1.1E-12   79.0  16.0  194    1-261    27-224 (228)
```

Figure S1: (**A**) Pun1p is localized at the collar of the mating bridge and in vacuoles in fused cells. Scale bar= 5µm. **(B)** Pun1p hits with >99% probability are mainly *SUR7*-family proteins and previously characterized tetraspan proteins including mammalian claudins.

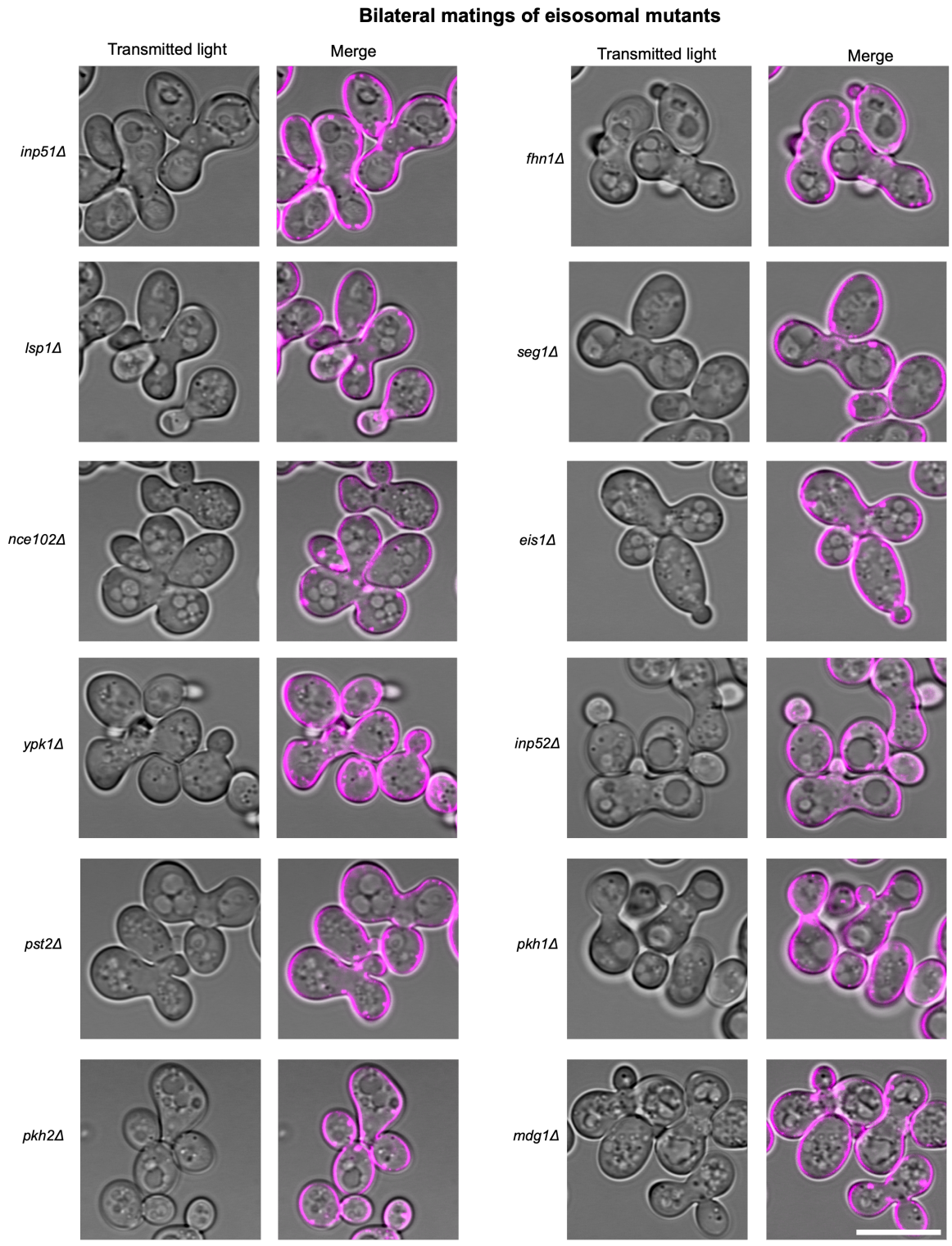

Figure S2: Deletion mutants of eisosomal proteins fuse similarly to WT cells. PM is stained with FM4-64 and cells mated for 3.5 h in YPD. Scale bar= 5 µm. Adapted from: manuscript in preparation.

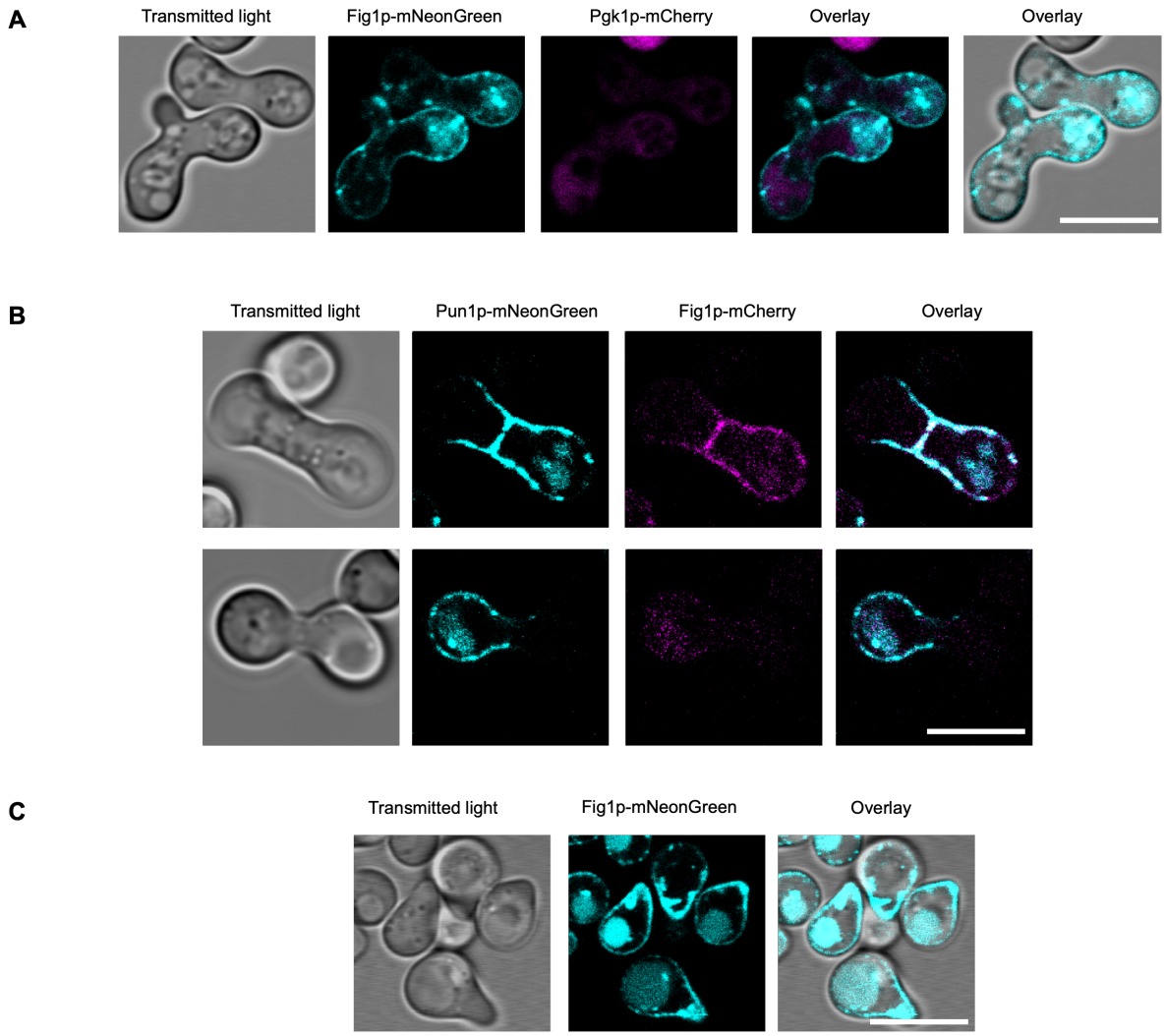

Figure S3: Fig1p is localized at the collar of the mating bridge and vacuoles in fused cells, similarly to Pun1p. Scale bar= 5 µm.

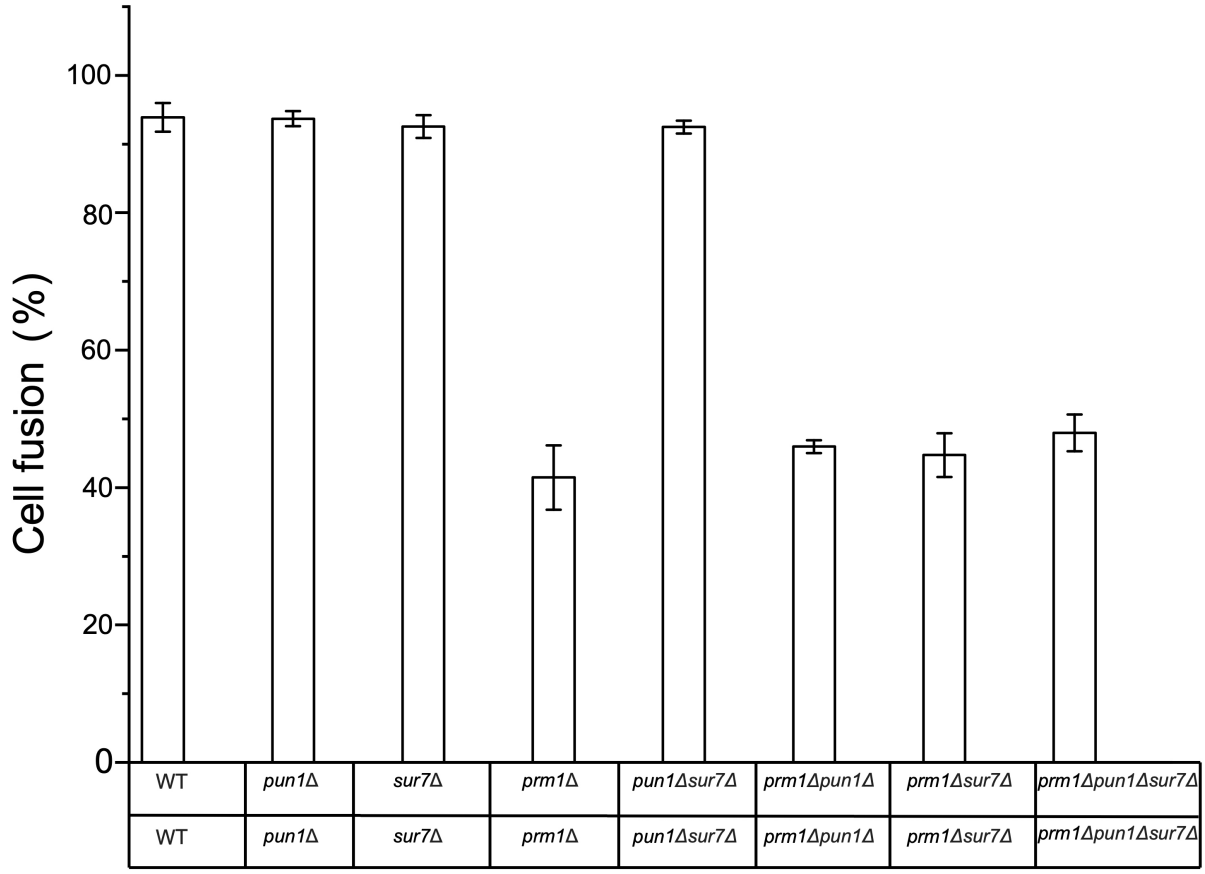

Figure S4: Deletion of *SUR7* does not suppress the *prm1Δ* fusion defect. The mild suppression observed in the *prm1Δpun1Δsur7Δ* mutants is due to *PUN1*. Error bars denote SEM of three independent experiments.

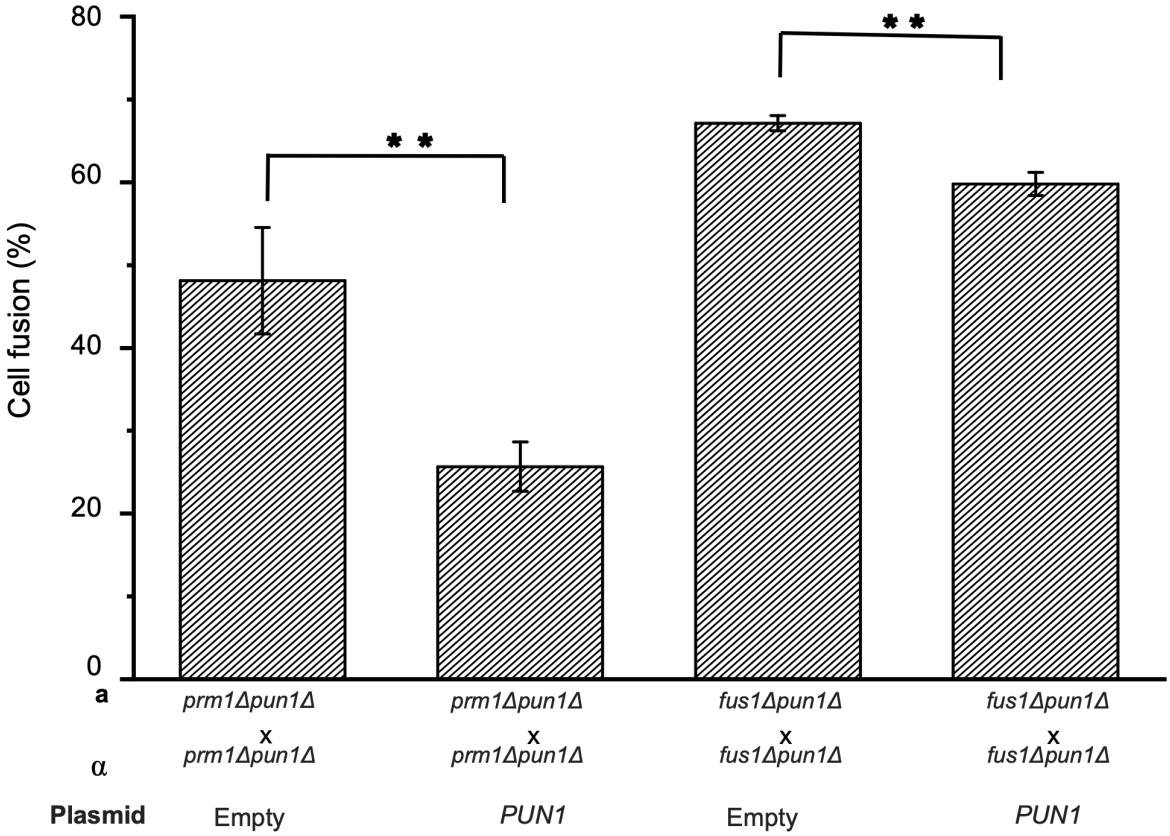

Figure S5: Overexpression of *PUN1* enhances the *prm1Δpun1Δ* and *pun1Δfus1Δ* fusion defects. A higher fusion inhibition activity was observed in the *prm1Δpun1Δ* than the *pun1Δfus1Δ* mutants. Error bars denote SEM of three or more independent experiments.

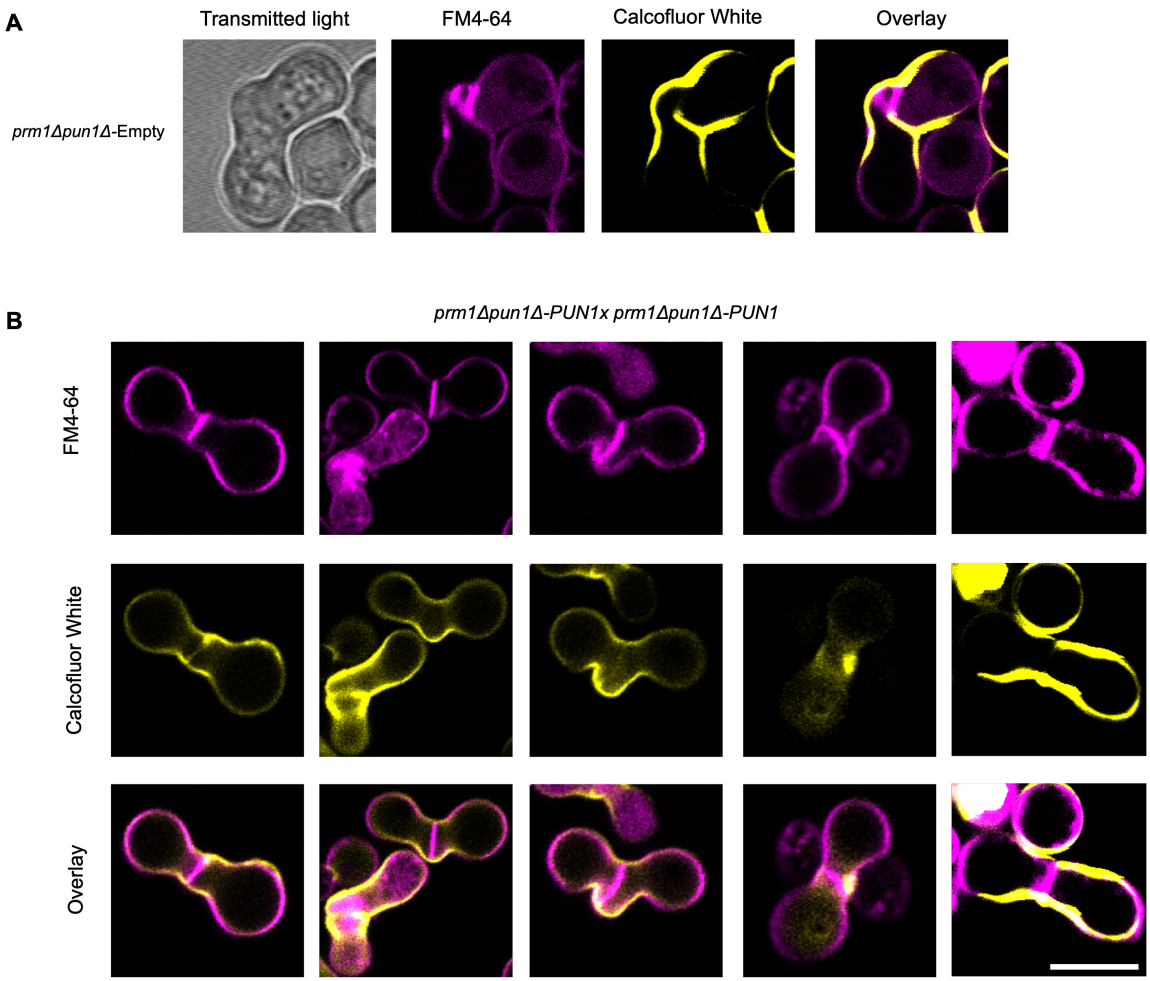

Figure S6: *PUN1* overexpression in *prm1Δpun1Δ* mutants leads to the appearance of a flat PM interface with no intervening CW material. (**A**) A late *prm1Δpun1Δ*- EV prezygote with a cytoplasmic bubble in which no CW material is observed. (**B**) Representative images of the flat PM interface with no intervening CW material phenotype upon *PUN1* overexpression. Scale bar= 5 µm. Adapted from: manuscript in preparation.

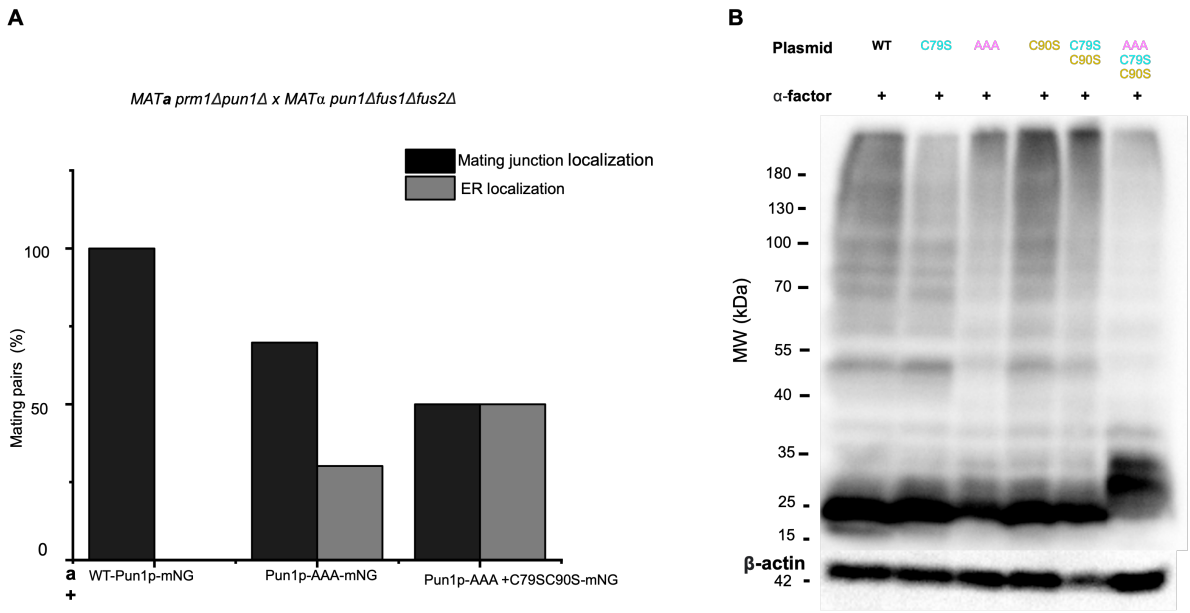

Figure S7: Mutating all the conserved claudin motif residues results in modification of the monomeric protein and a reduction in junction localization. (**A**) About 50% of the AAA+C79SC90S mutant protein is present at the PM, suggesting that the modified protein (**B**) is still localized at the mating junction. Cells expressing WT-Pun1p-mNG or the mutant proteins were mated to *pun1Δfus1Δfus2Δ* mutants to slow down the fusion process and allow sufficient mating pairs to localize the Pun1p proteins at the junction before PM fusion after 90 min of mating. Adapted from: manuscript in preparation.

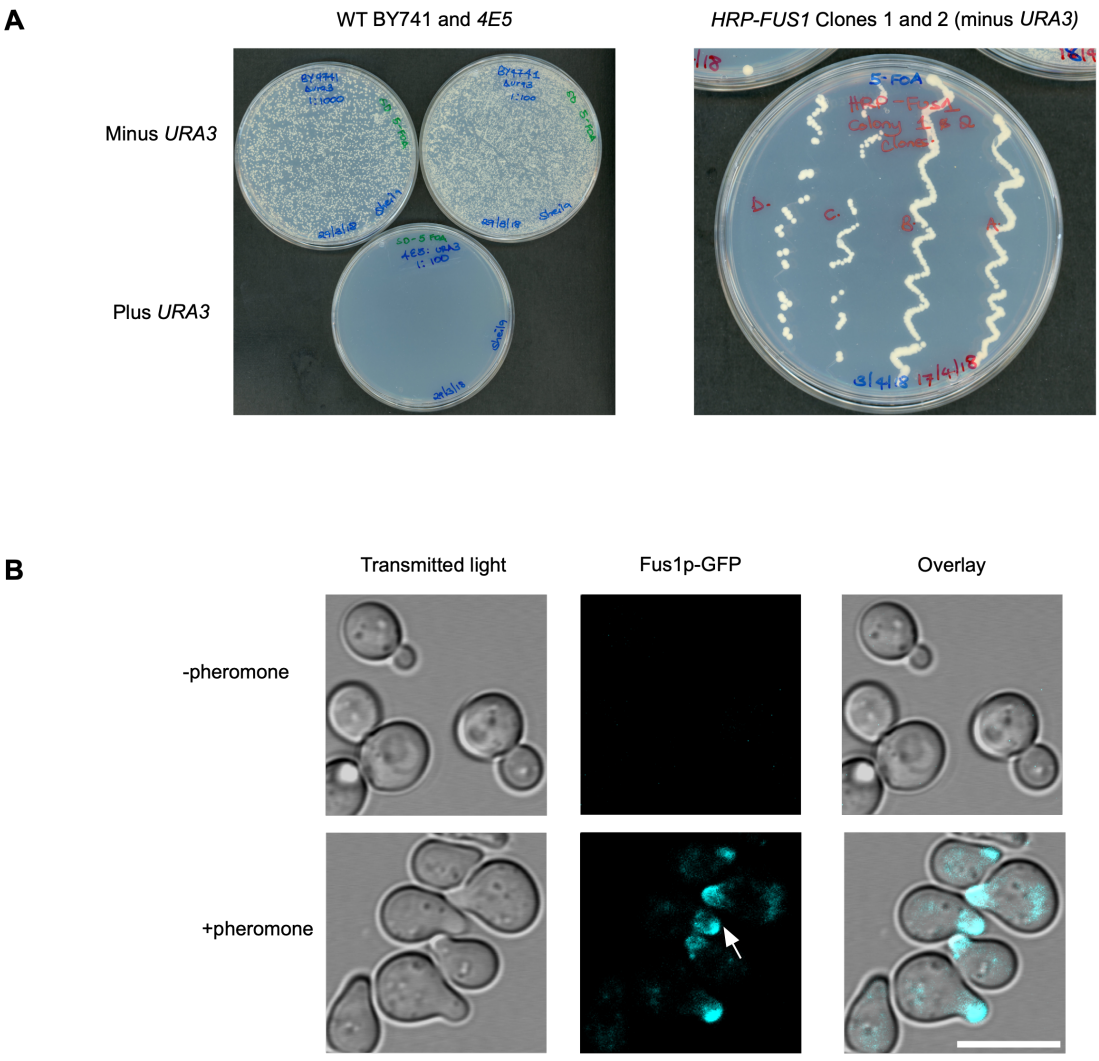

Figure S8: (**A**) Generation of *HRP-FUS1* using the 5-FOA negative selection approach. Strains harboring a *URA3* gene do not grow on 5-FOA-containing media. (**B**) WT Fus1p-GFP is expression only upon pheromone treatment and is localized at the shmoo tip (white arrow). Scale bar= 5 µm

10 ACKNOWLEDGMENTS

First, I express my utmost gratitude to my advisor Dr. Matias Hernández, who believed in my potential and gave me the opportunity to be part of his research group. As his first PhD student, he has been a great mentor and supervisor and has given me the freedom to explore new scientific ideas, make mistakes and learn from them. I am immensely grateful for this privilege.

Secondly, I would like to thank Prof. Dr. Stefan Raunser for not only being my referee, but also my advisor as head of the Structural Biochemistry Department. I acknowledge the financial support, the technical and administration support but even more importantly for his constant concern of my 'well-being' whenever he visited our office.

Many thanks to Prof. Dr. Roland Winter for accepting to be my second referee despite a short notice.

I also extend my gratitude to Dieter Schmidt, MPI-Gottingen who provided me with strains as well as lots of scientific input on sporulation and tetrad dissection. I thank Pablo Aguilar who provided us with the PSAY strains and took part in various scientific discussions. I also thank Dr. Michal Skruzny (MPI-Marburg) for providing us with the mNeonGreen plasmid.

I thank my lab mates in the AG-Hernandez as well as the Structural Biochemistry Department. Special thanks to Anson Shek who helped generate some of the strains used in this thesis and for the continuous lab discussions and jokes. I also thank Angela Hagemeier for her help with microscopy and for being a colleague and a sister. I don't forget our lab technician Diana Ludwig for her help in generating some of the strains used in this thesis and for always ensuring a smooth running of the lab. Through her, I also had the opportunity to supervise Azubis. My sincere thanks to Dr. Alexander Belly and Dr. Tobias Raisch who have been the 'unseen Postdocs' of the group.

I would like to thank other members of the institute including Dr. Stefano Maffini, Dr. Petra Janning, Amal Alex, Dr. Richard Cardoso, Dr. Neha Jain, Dr. Martin Spinck, Dr. Jan-Erik Hoffmann and many more who through their help made this journey a success.

Last but not least, I am sincerely grateful to the IMPRS coordinators Dr. Lucia Sironi and Christa Hornemann who have been a phone-call away be it matters pertaining the PhD program or personal.

I will not forget to thank my friends outside the institute who have made my PhD time so much fun. Thank you Dr. Kitso, Dr. Peter Njenga, Maria, Velma, Alex, Violet.

Lastly, special thanks to Samuel and my family in Kenya for being the support system that has kept me going even in the most difficult times. This achievement is for all of us, for our strength, our common belief in hard work and our resilience.

11 PUBLICATIONS AND CONFERENCES

Publications

Mainye S, Shek A, Hagemeier A, Aguilar P, Hernandez M, Raunser S. The tight junction-like protein Pun1 regulates the transition between adhesion and cell fusion in yeast mating. Manuscript in preparation.

Conferences

2019- Conference**: poster** presentation

Poster title: “Role of Eisosomal proteins in yeast mating”.

29th Conference of Yeast Genetics and Molecular Biology-Gothenburg, Sweden.

2019- MPI-SAB Meeting**: poster** and **oral** presentation

Poster title: “Molecular mechanisms of cell-cell fusion in yeast mating”.

MPI-Dortmund, Germany.

2018- EMBO workshop meeting**: oral** presentation

Talk title: “Identification and characterization of proteins at the yeast fertilization synapse”.

EMBO Workshop- Membrane Fusion in Health and Disease- Cambridge, United Kingdom.

2018- IMPRS Student’s symposium**: oral** presentation

Talk title: “Identification and characterization of the yeast fertilization synapse proteins”.

IMPRS Student’s symposium- MPI-Dortmund, Germany.

2017- Ruhr symposium**: oral** presentation

Talk title: “Cell-cell fusion in budding yeast: what are the key players?”

Ruhr Forum: Chromosomes and Cytoskeleton- Essen, Germany.